

Sun shading of the future

A next generation workflow for applying the performative computational architecture framework to sun shading design, based on an example sun shading system for high-rise office buildings with all-glass exteriors in tropical climates optimised on visual and thermal comfort

Author:
Shane Prins
(4225171)

Mentors:
Dr. Michela Turrin
Dr.ir. Martin Tenpierik

Studios:
Design informatics
Building physics

Abstract

This thesis is about improving the workflow for applying the Performative Computational Architecture (PCA) framework to sun shading design. The PCA framework is a design approach consisting of three phases; form-finding, performance evaluation and optimisation. The conventional workflow in regard to sun shading design is defined as a combination of tools for each of the PCA framework phases. The feasibility of this conventional workflow is explored based on an example case. This example case refers to a fictional office high-rise building in a tropic climate with an all-glass exterior, which is optimised on visual and thermal comfort. The selected sun shading system is an adaptation of the egg-crate system, which has an increased potential over other shading systems for this specific building typology in tropic climates. All further assumptions for the fictional example case are based on common trends in architectural design. Based on the optimisation results of the example case using the conventional workflow, the challenges limiting the feasibility of the workflow are identified. Proposals for overcoming these challenges resulted in the development of the next generation workflow. The core concept of this next generation workflow is to split up the workflow in three parts; preparation, execution and interpretation. First tests using the next generation workflow indicated it significantly faster on a single high-end computer, compared to the conventional workflow. In addition, the next generation workflow offers a solution to some limitations in running sun shading optimisations in grid- and render farm environments.

Acknowledgements

After a year of hard work, completing this thesis will mark the first step of my professional career as a building technologist. In this paragraph I would like to thank some people for helping me to achieve this milestone.

First of all, I want to thank Michela Turrin for being my main mentor and Martin Tenpierink for being my secondary mentor during this graduation project. Your expertise on the fields of respectively Design Informatics and Building Physics was a very valuable source of information and has guided me throughout the thesis. In addition, I want to thank Steffen Nijhuis for acting as the delegate of the board of examiners during all evaluation moments regarding this thesis.

Secondly, I want to thank Hans Hoogenboom for helping out with running optimisations in the VR-lab and Aytaç Balci for helping out with running optimisations on the BK Renderfarm. I hope my results will help future research to utilize the available computational power as efficient as possible.

Thirdly, I want to thank the developer team of ESTECO, for their active response on updating the Grasshopper custom myNode to accommodate the needs for this research.

Finally, I want to thank all of my family and friends for supporting me on a personal level during this graduation project and all prior semesters of studying at the TU Delft.

Table of contents

1. Introduction	8
1.1 - Personal background	10
1.2 - Problem statement	10
1.3 - Research objectives & design assignments	13
1.4 - Research questions	13
1.5 - Research output	15
1.6 - Research methodology	17
2. Literature review	18
2.1 - Fundamentals of visual comfort	20
2.1.1 - Definition	20
2.1.2 - Contributing factors	21
2.1.3 - Calculation methods	28
2.1.4 - Relation to sun shading	32
2.1.5 - References	33
2.2 - Fundamentals of thermal comfort	34
2.2.1 - Definition	34
2.2.2 - Contributing factors	35
2.2.3 - Calculation methods	43
2.2.4 - Relation to sun shading	47
2.2.5 - References	49
2.3 - Fundamentals of performative computational architecture	51
2.3.1 - Principles of PCA	51
2.3.2 - The form-finding phase of PCA for sun shading design	54
2.3.3 - The performance evaluation phase of PCA for sun shading design	56
2.3.4 - The optimization phase of PCA sun shading design	62
2.3.5 - References	67
2.4 - Fundamentals of sun shading in contemporary high-rise	69
2.4.1 - The relevance	69
2.4.2 - Technical requirements	72
2.4.3 - Local climate	77
2.4.4 - The potential for PCA implementation	78
2.4.5 - References	80

2.5 - State of the art: PCA use in sun shading design	82
2.5.1 - Case studies	82
2.5.2 - Typology analysis	89
2.5.3 - References	92
2.6 - State of the art: Sun shading in high-rise	93
2.6.1 - Case studies	93
2.6.2 - Typology analysis	101
2.6.3 - References	103
3. Practical research	104
3.1 - Conceptual sun shading design	106
3.1.1 - Eggcrate shading as start point	106
3.1.2 - Parameterization	109
3.1.3 - Free-form perimeter buildings	114
3.1.4 - Shading & building parameters	117
3.2 - Test set-up design	118
3.2.1 - Office zone set-up	118
3.2.2 - Double skin facade set-up	119
3.2.3 - Material parameters	121
3.2.4 - Occupancy, HVAC systems, Internal loads & Ventilation parameters	122
3.3 - Performance evaluation	123
3.3.1 - Analysis input parameters	123
3.3.2 - UDI evaluation	124
3.3.3 - PMV evaluation	125
3.3.4 - DGP evaluation	126
3.3.5 - Graphic presentation of results	128
3.4 - Optimisation	130
3.4.1 - Workflow definition	130
3.4.2 - Input parameters	131
3.4.3 - Objectives	132
3.4.4 - Design of experiments	133
3.4.5 - Algorithms	133
3.4.6 - Results overview	134
3.4.7 - Conclusions on optimisation results	138
3.4.8 - The final assessment and design choice	141

3.5 - Comparison	144
3.5.1 - Definition of alternative shading concepts	144
3.5.2 - Comparison of alternatives in three climates	146
3.6 - Challenge identification	148
3.6.1 - The stepped approach	148
3.6.2 - Grid based optimisation approach	150
3.7 - Developing the next generation workflow	152
3.7.1 - The first conceptual setup: Separating the Grasshopper script	152
3.7.2 - The lighting schedule issue	154
3.7.3 - Analysis numbering (custom node)	156
3.7.4 - Delocalizing the EPW-file	156
3.7.5 - Preparing the Energyplus simulation (custom node)	156
3.7.6 - Suppressing the Grasshopper multi-save pop-up (custom node)	156
3.7.7 - Updating the Grasshopper custom MyNode	157
3.7.8 - Finalizing the next generation workflow	157
3.7.9 - Testing on the BK Renderfarm	158
3.7.10 - Testing in the VR lab	159
3.8 - Analysing the next generation workflow	160
3.8.1 - Comparing the feasibility to the conventional workflow	160
3.8.2 - Comparing the results to the conventional workflow	161
3.8.3 - Conclusions on the next generation workflow	162
3.9 - Automated physical models	164
3.9.1 - Automatized workflow	164
3.9.2 - Physical test models	165
3.9.3 - Relation to the commercial design process	166
3.10 - Automated VR rendering	167
3.10.1 - Automatized workflow	167
3.10.2 - VR renderings	168
3.10.3 - Relation to the commercial design process	169

4. Conclusions	170
4.1 - Literature review conclusions	172
4.1.1 - Conclusions on visual comfort	172
4.1.2 - Conclusions on thermal comfort	172
4.1.3 - Conclusions on performative computational architecture	173
4.1.4 - Conclusions on sun shading in contemporary high-rise	174
4.1.5 - Conclusions on the state of the art: PCA use in sun shading design	175
4.1.6 - Conclusions on the state of the art: Sun shading design in high-rise	176
4.2 - Practical research conclusions	177
4.2.1 - Conclusions on the example case	177
4.2.2 - Conclusions on the next generation workflow	179
4.2.3 - Conclusion on the main research question	180
4.3 - Recommendations & further development	182
4.3.1 - Broadening future research	182
4.3.2 - Deepening future research	182
4.4 - Reflection	184
4.4.1 - Relationship between research & design	184
4.4.2 - Relationship between the topic, building technology track & Msc program	185
4.4.3 - Research method & approach in relation to BT inquiry & scientific relevance	185
4.4.4 - The research in wider frameworks & transferability	187
4.4.5 - Ethical issues & dilemmas	187
5. Appendices	190
5.1 - Appendix I: Complete results of compared evaluations	192
5.2 - Appendix II: GH scripts contemporary workflow	198
5.3 - Appendix III: GH scripts next generation workflow	212

1. Introduction





1.1 - Personal background

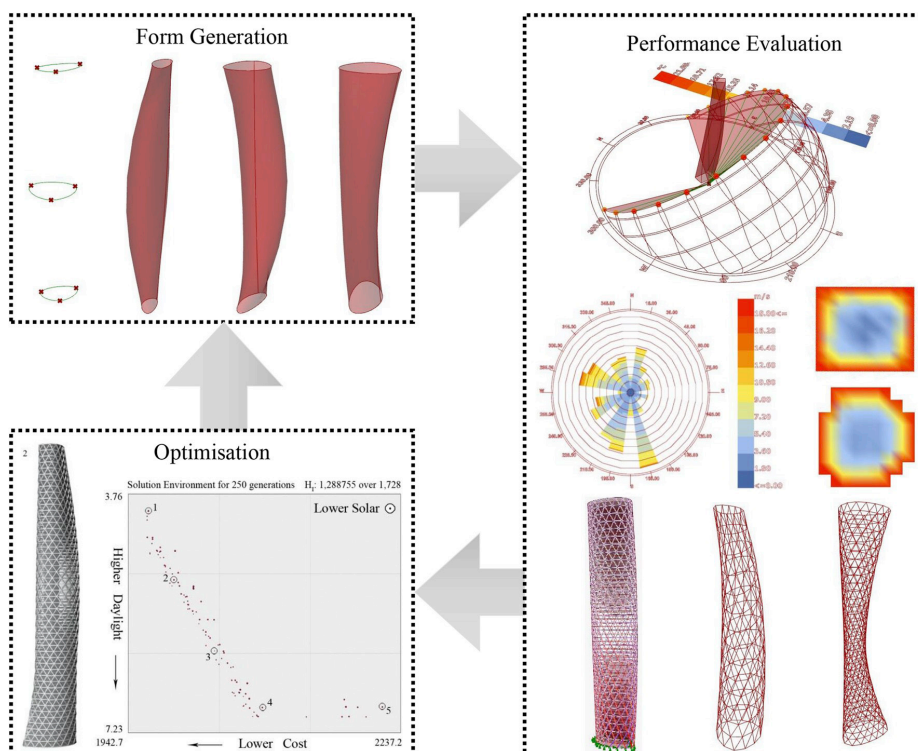
As a future building technology engineer, I am observing and embracing the evolution of emerging technologies and their potential for popular trends in contemporary and future architecture. Especially the technologies of parametric modeling and performance simulation driven design have my interest. In the future I want to be part of the next generation building engineers, who use parametric design tools to create healthier, more comfortable buildings. This will also result in more sustainable building usage, due to the decrease in energy demand for artificially created comfort by mechanical installations. I believe this parametric approach and healthier buildings to be important cornerstones of the future of architectural design.

1.2 - Problem statement

The first part of this paragraph contains the problem statement as found in the graduation plan delivered at the P2 evaluation. The final part does contain some revisions which were added to the research problem statement based on preliminary findings after the P2 evaluation.

The PCA method

Over the recent years there has been a great evolution in performative computational architecture (PCA) as shown in the literature review of Ekici, Cubukcuoglu, Turrin, and Sariyildiz (2019) in which one hundred researches between 1998 and 2018 involving the PCA method are evaluated. Performative computational architecture is based on a three-phase cycle which is iteratively looped until the best solution is found. The first step is generating geometry, based on input parameters. The second step is about evaluating the performance of the geometry using digital simulations. The third step uses a search method to find the most desirable performance by altering the input parameters. This is often done by using an evolutionary algorithm. (Ekici et al., 2019). The PCA method is shown in the figure below.



The performative computational architecture framework (Ekici et al., 2019)

The research of Ekici et al. (2019) indicates the PCA method offers potential for sun shading design. This is confirmed by Eltaweel & Yuehong (2017) in their literature review about parametric design and daylight, which includes nine in-depth researches on the relation between parametric design, visual- and thermal comfort. The review concludes the following:

“The use of parametric design within daylight can improve the performance of buildings’ design, daylighting and energy saving in the early stages of design. Link with buildings’ thermal performance simulation and visual comfort will be an attractive direction for parametric design in daylighting for future research.” (Eltaweel & Yuehong, 2017, p. 1102)

Increased risk of visual and thermal discomfort in high-rise office buildings with all-glass exteriors

One of the most iconic building typologies for our era is the high-rise building. The number of high-rise buildings has increased fast since 2000 and the most common functionality is office use (CTBUH, 2019). It is commonly stated that all-glass exteriors are a trend in contemporary architecture, with office buildings in particular. (Chow & Lin, 2010; Nicholson-Cole, 2016; MacErlean, 2018). However, buildings with large glazed facades are vulnerable to visual and thermal discomfort (Evola, Gullo, & Marletta, 2017). Especially in the tropics, where solar radiation levels are relatively high, the risks of visual and thermal discomfort as a result of overheating and intense solar radiatio are high. (Al-Tamimi & Fadzil, 2011) After comparing various sun shading principles for all glazed buildings, Evola, Gullo, & Marletta, (2017) drew the following conclusions:

“The results discussed in this paper show that the adoption of suitable shading devices in highly-glazed office buildings is of the uttermost importance, as it allows to significantly reduce the energy needs for space cooling and to improve thermal comfort while limiting indoor overheating. Moreover, the indoor daylight illuminance keeps suitable levels to allow visual tasks” (Evola, Gullo, & Marletta, 2017, p.354)

“The present study suggests that the design of highly glazed office buildings must be tackled through dynamic simulations involving both visual and thermal comfort, and must be optimized case by case.” (Evola, Gullo, & Marletta, 2017, p.355)

The dynamic simulations and case by case optimization refer to the PCA method. The review on one hundred PCA researches by Ekici et al. (2019) contains 36 papers on the applications of PCA for sun shading design and 6 papers which focus on the applications of PCA for high-rise building design. However, none of the papers in the review addresses sun shading in high-rise buildings.

Sun shading in contemporary high-rise office buildings in extreme climates

Al-Masrani, Al-Obaidib, Zalina & Ismaa (2018) reviewed a total of 72 different researches on optimization of sun shading systems for buildings in tropical climates, in order to define challenges and future trends, with an emphasis on high-rise buildings. The motive for this review was the stated as following:

“Most high-rise office buildings in the tropics, particularly in Malaysia and Singapore, exceed the required level of the energy efficiency index.” (Al-Masrani et al., 2018, p.849)

The researches in the literature review are categorized according to their ability to move; passive, active and hybrid. Many of researches included an approach similar to the PCA method. The review states conclusions about the challenges and future trends of each of the three defined categories:

Passive sun shading for high-rise office buildings in tropical climates:

“The majority of shading studies in the tropics adopted fixed shading devices, and most literature has identified egg-crate devices as the best device to improve daylight and thermal performance.” (Al-Masrani et al., 2018, p.869)

Active sun shading for high-rise office buildings in tropical climates:

“Performance and the applicability of intelligent building systems, this design faces many criticisms due to its complexity, cost and high operational energy.” (Al-Masrani et al., 2018, p.869)

Hybrid sun shading for high-rise office buildings in tropical climates:

“The performances of dynamic complex geometries and shape morphing shading systems have not yet been explored in the tropics. Consequently, studies must urgently assess the performance of more adaptive geometries in addition to biomimetic approaches represented by hybrid shading systems in a tropical climate.” (Al-Masrani et al., 2018, p.869)

The contemporary PCA workflow (revised paragraph)

The principles of the PCA method can be applied through various different workflows. Analysis of multiple precedences (Turrin et al., 2011 & Yang et al., 2018) has led to a typology definition of the PCA workflows. One workflow in particular seems very promising in regard to sun shading design; the model-dependent workflow, using Grasshopper for the form-finding phase, Radiance & Daysim (via Ladybug/Honeybee) for the performance evaluation on visual comfort, Energyplus & Openstudio (via Ladybug/Honeybee) for the performance evaluation on thermal comfort and ModeFRONTIER for the optimisation phase. This will be referred to as the contemporary workflow or conventional workflow throughout this report. Although this workflow shows a lot of potential, it is still under development. Currently, the integration of Grasshopper is not an integration node provided with standard modeFRONTIER installations, but only supported through a custom myNode. This custom node is developed by ESTECO, the company behind modeFRONTIER, especially for academic use at the TU Delft. Due to this reason, the custom Grasshopper MyNode is not implemented to cover all the possible use cases, resulting in some limitations for developing more advanced workflows.

Summary (partly revised paragraph)

As stated above, performative computational architecture has made a big leap forward over the past few decades and has proven to have potential for designing sun shading systems which improve visual and thermal comfort. (Ekici et al., 2019; Eltaweel & Yuehong, 2017). A common building type of contemporary architecture is the high-rise office building with an all-glass exterior. (Chow & Lin, 2010; Nicholson-Cole, 2016; MacErlean, 2018; CTBUH, 2019). However, buildings with all-glass exteriors are at increased risk to visual and thermal discomfort and a well-designed sun shading system is essential to control the levels of visual and thermal comfort. (Evola, Gullo, & Marletta, 2017). This problem is especially present in tropic climates, where many high-rise office buildings don't meet the required energy efficiency requirements. (Al-Tamimi & Fadzil, 2011; Al-Masrani et al., 2018).

This failure to meet energy usage requirements is mainly caused by poor sun shading strategies being applied to these high-rise office buildings with all-glass exteriors, resulting in high energy consumption by building installations, which are used to artificially ensure visual and thermal comfort. This problem can be solved by improving the performance of sun shading systems in high-rise office buildings with all-glass exteriors in tropical climates by implementing new design methods, such as the promising PCA method. This evolution is encouraged by multiple research conclusions on the matter (Eltaweel & Yuehong, 2017; Evola, Gullo, & Marletta, 2017; Al-Masrani et al., 2018).

There are many different workflows for implementing the PCA method. (Turrin et al., 2011 & Yang et al., 2018). One workflow in particular, has shown to have a lot of potential in regard to sun shading design. According to the PCA method typology which was defined during the literature research, this workflow fits the model-based typology and is based on a conjunction between Grasshopper, Radiance/Energy plus (via Ladybug/Honeybee) and ModeFRONTIER. However, this workflow is based on the integration of Grasshopper in modeFRONTIER, which is currently only available through a custom myNode, developed by ESTECO especially for academic use at the TUDelft. Due to this integration still being in an unofficial beta phase, some limitations are still present in regard to the development of more advanced workflows.

1.3 - Research objectives & design assignments

The contemporary PCA workflow for sun shading optimisation on visual and thermal comfort performance in high-rise buildings is still under development. This research aims to explore this methodology using a relatively complex example case. Designing this example case will be the first design assignment for this thesis. The design will be based on common trends within the building typology of high-rise office buildings with all-glass exteriors in tropic climates. The starting point will be an existing shading system, which has increased potential in contrast to other systems. The choice for this existing system will be made based on findings in literature. The existing system will be customized in regard to the principles of the form-finding phase of the PCA framework and optimised using the contemporary workflow. Based on the optimisation results, the research aims to compare the performance of the optimised example case shading to other available systems, various façade orientations and various climates.

In addition, the results of the optimisation using the contemporary workflow will be used to identify the challenges still present in the workflow. This will initiate the second design assignment of this thesis; improving the contemporary workflow to overcome the identified challenges. This will result in an improved workflow. Thereafter, the research aims to compare this improved workflow to the contemporary workflow and reflect on the extent to which the challenges have been resolved and which challenges remain to be overcome in future research.

1.4 - Research questions

This paragraph contains the research main and sub-questions. The main question has been revised based on preliminary research results and a shift in focus, targeting the research more on improving the contemporary workflow mentioned in the revised paragraphs of the problem statement.

The research contains a lot of sub-questions which are to be answered by literature research. They are grouped, corresponding to the section index within the literature review chapter of the report. The sub-questions regarding the practical research are shown at the end of this list. These questions have been extended with some additional questions after the P2 evaluation and are split into two groups, corresponding with the two research objectives and design assignments mentioned in the previous paragraph. In addition, the grouping and relations of sub-questions is also graphically explained in figure 1.

Main question (original)

How can sun shading systems for high-rise office buildings with all-glass exteriors in tropical climates be improved by using performative computational architecture methods to optimize the performance on visual and thermal comfort?

Main question (revised)

How can the contemporary Performative Computational Architecture (PCA) workflow for optimising sun shading designs on visual and thermal comfort in high-rise office buildings with all-glass exteriors be advanced to the next generation?

Sub questions

Fundamentals of visual and thermal comfort:

1. How are visual and thermal comfort defined?
2. What factors are responsible for the level of visual and thermal comfort?
3. How can visual and thermal comfort be calculated?
4. How are visual and thermal comfort related to shading systems?

Fundamentals of the performative computational architecture method used for sun shading design

5. What are the principles of the performative computational architecture method?
6. How can the form-finding phase of the performative computational architecture method be used to design sun shading systems?
7. How can the performance evaluation phase of the performative computational architecture method be used to design sun shading systems?
8. How can the optimization phase of the performative computational architecture method be used to design sun shading systems?

Fundamentals of sun shading in contemporary high-rise:

9. What is the relevance of sun shading in contemporary high-rise buildings?
10. What are the technical requirements for sun shading systems in high rise office buildings with all-glass exteriors?
11. How does the local climate influence sun shading design in contemporary high-rise office buildings with all-glass exteriors?
12. How can PCA be used to improve sun shading systems in contemporary high-rise office buildings in extreme climates with all-glass exteriors?

State of the art: PCA methods for designing sun shading systems:

13. What projects have been important to the development of PCA methods for designing sun shading?
14. How would PCA methods for designing sun shading be categorized based on typology?

State of the art: Sun shading in contemporary high-rise office buildings in extreme climates:

15. What projects have been important to the development of sun shading in contemporary high-rise office buildings in extreme climates?
16. How would designs for sun shading in contemporary high-rise office buildings in extreme climates be categorized based on typology?

Research by design questions (involving the example case, revised):

17. Can the performance on visual and thermal comfort of current state-of-the-art sun shading systems with potential for high-rise office buildings be improved using the common contemporary PCA workflow?
18. How does the possibly improved sun shading system perform in comparison to currently available systems for high-rise office buildings with all glass facades?
19. How do the possibly improved sun shading system perform for different façade orientations of the building envelope?
20. How do the possibly improved sun shading system perform in various tropic climates around the world?

Research by design questions (involving the next generation workflow, revised):

21. What are the challenges of the of the contemporary PCA workflow in regard to sun shading design?
22. How can the workflow be altered in order to overcome these challenges?

1.5 - Research output

The main output of this thesis will be a next generation PCA workflow for sun shading design, which enables designers to overcome the challenges still present in the contemporary workflow. The novelty of this next generation PCA workflow will increase the potential of the PCA framework as an interesting design approach for sun shading systems in the architectural design process of the future.

As a secondary product, an optimised sun shading system will be generated. This sun shading is based on existing shading systems and the assumptions of the example case. The main purpose of this example case is to identify the challenges of the contemporary workflow. However, the comparison with other available shading systems will also give insight in the feasibility of applying the shading system in practice.

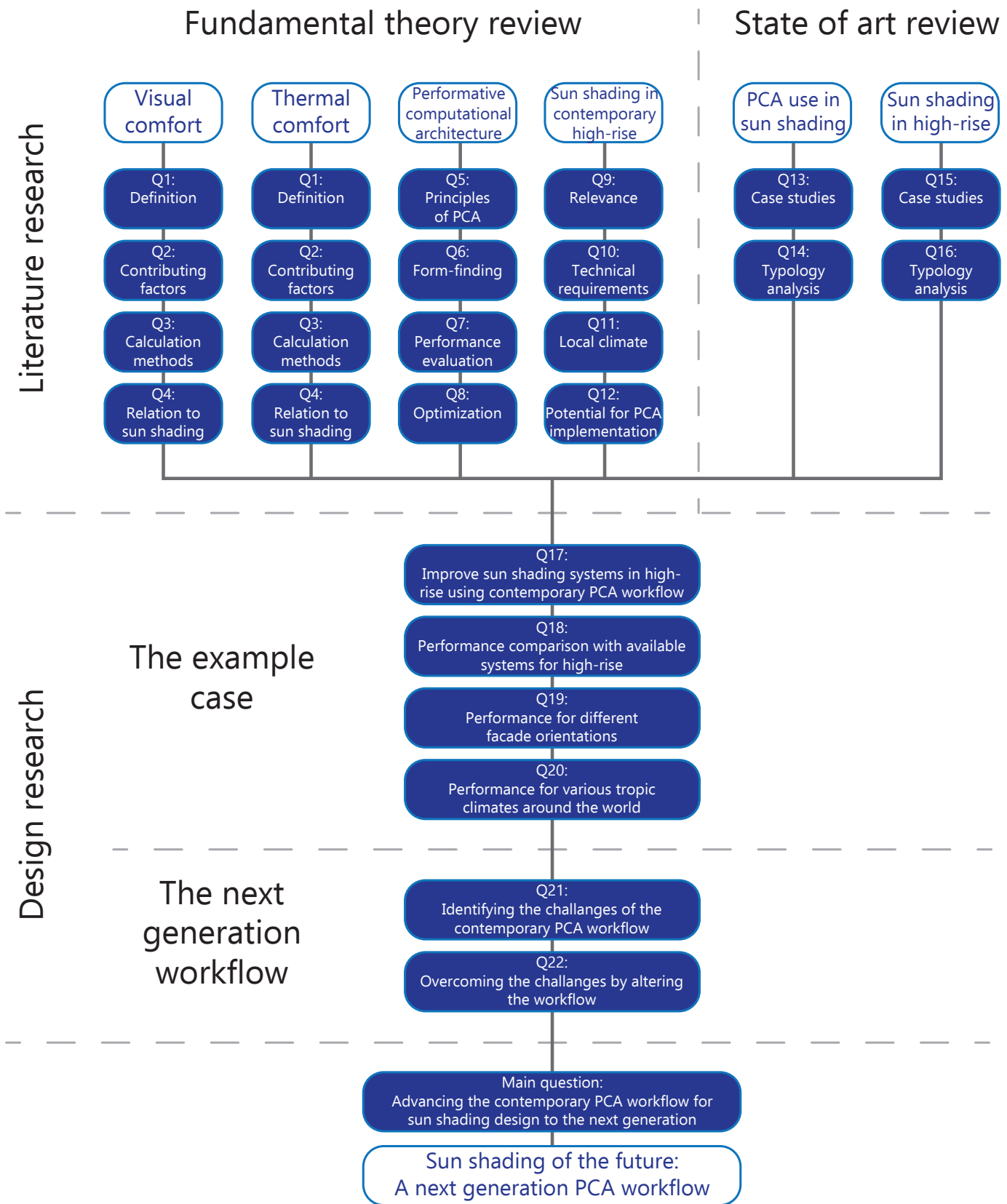


Figure 1. Relation scheme of sub-questions and literature review sections (by author)

1.6 - Research methodology

This paragraph describes the methods that will be utilized for answering the research questions. As stated before, a majority of the research sub-questions will be answered by literature research. The research by design phase of this graduation project applied four different methods; the selection method, PCA method, comparison method and exploration method. A textual elaboration can be found in the graduation plan, although minor changes have been implemented due to preliminary research results. A graphic overview of the updated methodology used for the practical research is given in the scheme below in figure 2.

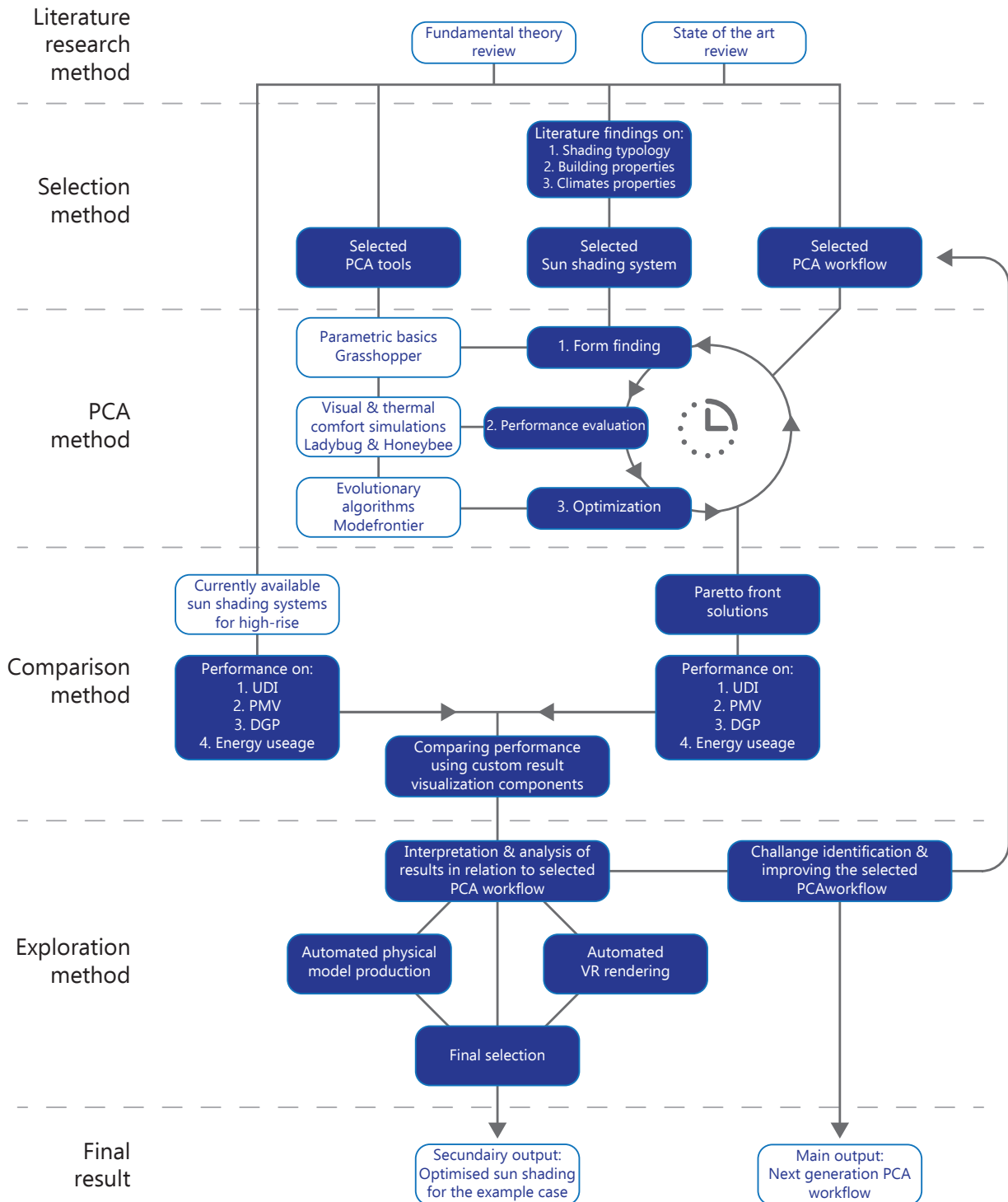


Figure 2. Methodology scheme (by author)

2. Literature review





2.1 - Fundamentals of visual comfort

2.1.1 - Definition

Visual comfort is defined in the European standard NEN-EN-12665 as a:

“Subjective condition of visual well-being induced by the luminous environment” (CEN, 2018, p.9)

Visual comfort is subjective because it is depending on the physiology of the human, the physical amount and distribution of light in a room and the spectral emission on the light source. (Carlucci, 2015). This means the perception of comfort at the same conditions will vary for person to person, making it hard to quantify the level of visual comfort. However, Carlucci (2015) distinguishes four factors which help describe the relationship between the observer and the light environment;

1. The amount of light
2. The uniformity of light
3. The quality of light in rendering colors
4. The prediction of the risk of glare for occupants

The correlation and dependency between those factors are not that clear. This resulted in various indexes for visual comfort throughout the history of building physics. The following graph shows the number of indices available for quantifying the different factors of visual comfort. However, non of the available indices can quantify visual comfort in a single value. Visual comfort always has to be described as a combination of multiple quantities. (Carlucci, 2015).

The next few paragraphs will elaborate on the four contributing factors of visual comfort as stated above. This will be followed by a common quantification method and the appurtenant physical measuring methods.

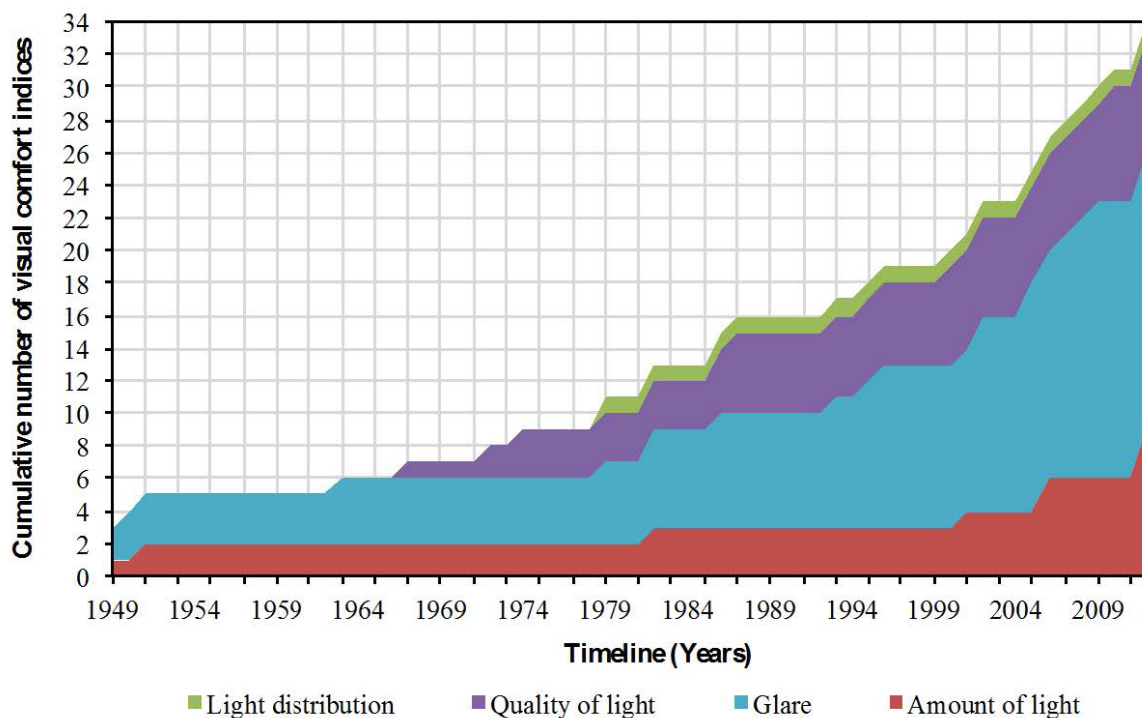


Figure 3. Amount of indices for visual comfort over time (Carlucci, 2015)

2.1.2 - Contributing factors

Amount of light

Visual comfort can be described as the situation where a building occupant can accomplish all required tasks. For this the occupant needs an adequate amount of light. Discomfort can be experienced by either too high or too low levels of light. (Carlucci, 2015) The amount of light can be described as four different physical quantities;

1. Luminous flux
2. Luminous intensity
3. Illuminance
4. Luminance

Zumtobel (2017) gives the following definitions for these quantities. Figure 4 shows the relationships between the different light amount qualities.

Luminous flux:

"The luminous flux describes the quantity of light emitted by a light source. The luminous efficiency is the ratio of the luminous flux to the electrical power consumed (lm/W). It is a measure of a light source's economic efficiency." (Zumtobel, 2017)

Abbreviation: Φ Phi Unit: Lumen (lm)

Luminous intensity:

"The luminous intensity describes the quantity of light that is radiated in a particular direction. This is a useful measurement for directive lighting elements such as reflectors. It is represented by the luminous intensity distribution curve (LDC)." (Zumtobel, 2017)

Abbreviation: I Unit: Candela (cd)

Illuminance:

"Illuminance describes the quantity of luminous flux falling on a surface. Relevant standards specify the required illuminance (e.g. EN 12464 "Lighting of indoor workplaces")." (Zumtobel, 2017)

Abbreviation: E Unit: Lux (lx)

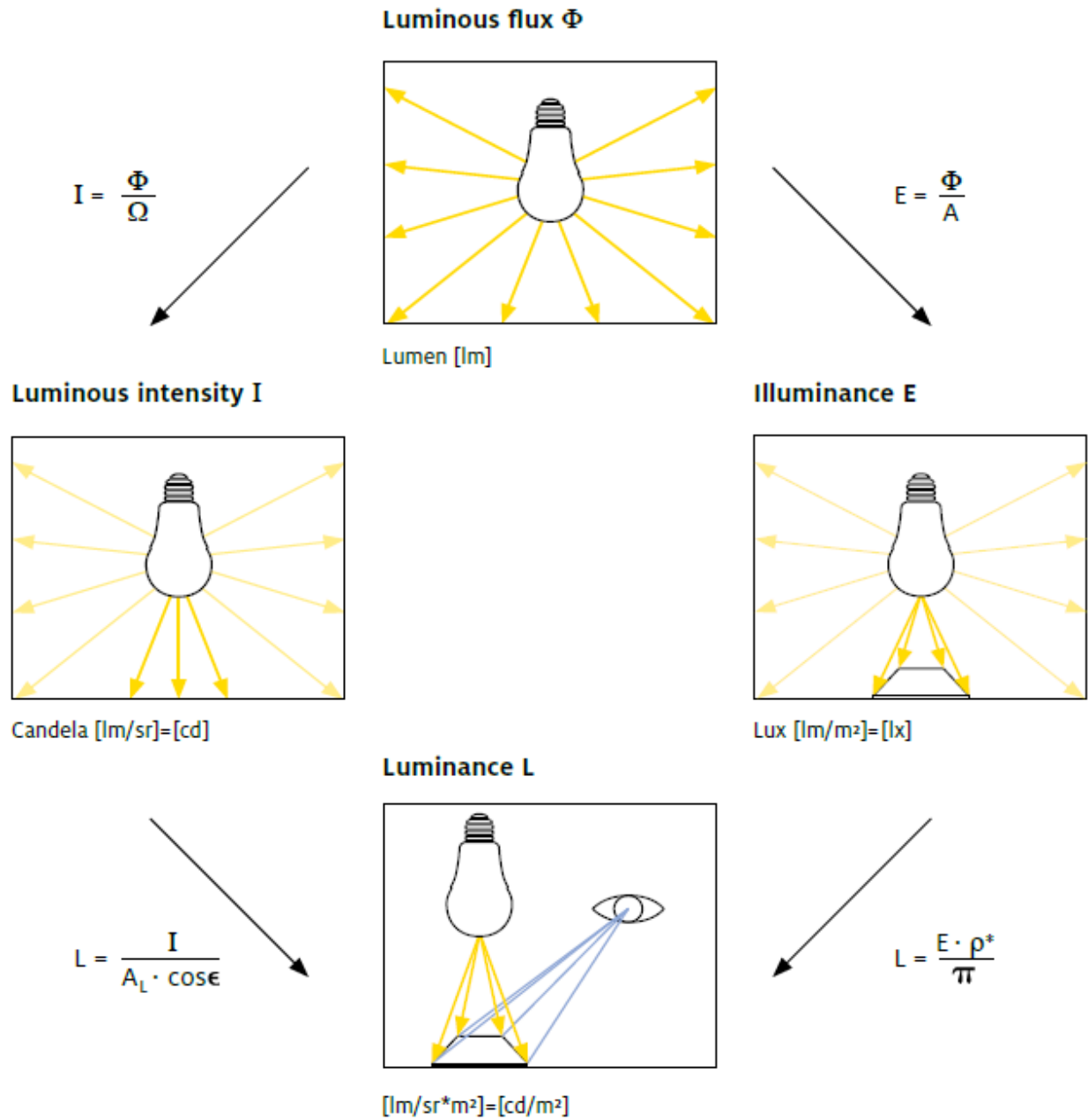
Formula: $E(\text{lx}) = \text{luminous flux (lm)} / \text{area (m}^2\text{)}$

Luminance:

"Luminance is the only basic lighting parameter that is perceived by the eye. It describes on the one hand a light source's impression of brightness, and on the other, a surface and therefore depends to a large extent on the degree of reflection (colour and surface)." (Zumtobel, 2017). In other words, luminance is the amount of luminous flux emitted by a small surface in a particular direction.

Abbreviation: L Unit: cd/m²

Formula: $L(\text{cd/m}^2) = d\Phi^2 / (d\Omega^2 * dA)$



- Ω = solid angle into which luminous flux is emitted
- A = area hit by luminous flux
- $A_L \cdot \cos \epsilon$ = visible areas of light source
- ρ = reflectance of area
- π = 3.14
- * = for diffuse surface areas

Figure 4. *Mathematical relationship between the four main quantities of light (Zumtobel, 2017)*

Uniformity of light

The uniformity of light is defined as how evenly light is distributed over a task area. Sufficient levels of uniformity avoid visual stress caused certain over-lit or under-lit areas within the visual field, and therefore increase the level of visual comfort. (Carlucci, 2015). In other words, humans tend to favor a uniformly distributed amount of light, because this reduces stress on our eyes. In reality this can be hard to realize, because the natural light is often coming from one single direction; the façade side of the room. Zumtobel (2017) Defines two quantities revolving the uniformity of light, the Illuminance maintenance value and the Uniformity, as following:

Illuminance maintenance value \bar{E}_m :

This is the lowest illuminance value that is allowed to occur, if illuminance values drop below this threshold, visual comfort will most likely be experienced. (Zumtobel, 2017)

Uniformity U_o :

“Uniformity U_o is the ratio between the lowest (E_{min}) and the mean illuminance level (\bar{E}) in the area to be evaluated. The result is a minimum level. In order to perform visual tasks in illuminated areas, there should not be any great differences in brightness so that uniformity should not fall below.” (Zumtobel, 2017).

$$U_o = E_{min}/\bar{E}.$$

Both the illuminance maintenance value and the uniformity can be applied to an entire room or a specific task area. For an office building, which is the scope of this graduation, a typical task area can be defined as a desk at working height including the surrounding space for the chair (see the figure below). Both these values can often be found in tables regarding daylight requirements. These values often vary according to the program.

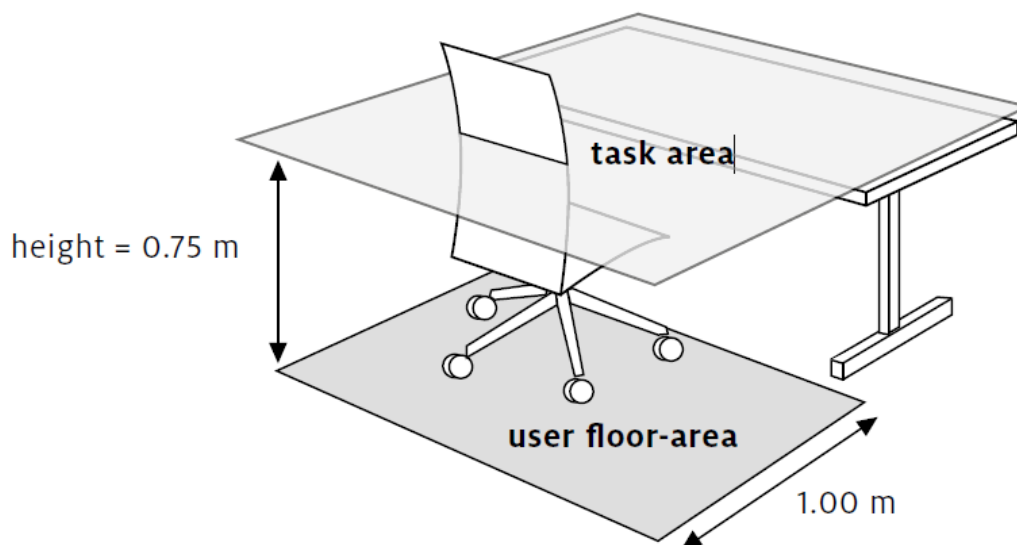


Figure 5. Definition of a task area (Zumtobel, 2017)

Quality of light in rendering colors

“According to several studies, people are prone to preferring natural light in the living and working spaces. It implies great benefits both for health and wellbeing of occupants, by involving perceptive, physiological, psychological, and also economic aspects.”

Several studies have shown humans tend to prefer natural light over artificial light. Larger amounts of natural light correlate with health and wellbeing of the building occupants regarding psychological, physiological and even work efficiency. (Carlucci, 2015). This indicates there is a difference between natural and artificial light. To gain insight in this difference a spectral power distribution (SPD) graph can be drawn. A SPD graph can be defined as following:

“A spectral power distribution is simply a plot, or table of a radiometric quantity as a function of wavelength. Since the overall power level of light sources can vary over many orders of magnitude, spectral power distributions are often normalized to facilitate comparisons of color properties.” (Fairchild, 2013, p.60)

In other words, the graphs show the relative presence of different colors within the spectrum of the light source. The figure below shows the SPD's of several artificial light sources compared to natural daylight. It can immediately be concluded that natural light has a more even distribution of different frequencies/light colors, which is better for human comfort. (Carlucci, 2015).

After determining the difference between natural and artificial light, there is a need to quantify those differences in quality of light source. The quality of the spectral power distribution graph is identified by the colour rendering index (CRI).

Colour rendering describes the difference in color perception compared to the same color under perfect lighting conditions. This can be measured using 8 default test colours; R_1 to R_8 . (Zumtobel, 2017). In order to quantify the quality of the color distribution, the light is tested for the presence of eight reference colors, shown in the figure below. The best colour rendering is $R_a = 100$, whereas $R_a > 90$ is regarded as very good rendering and $R_a > 80$ is the minimum requirement for workplaces.

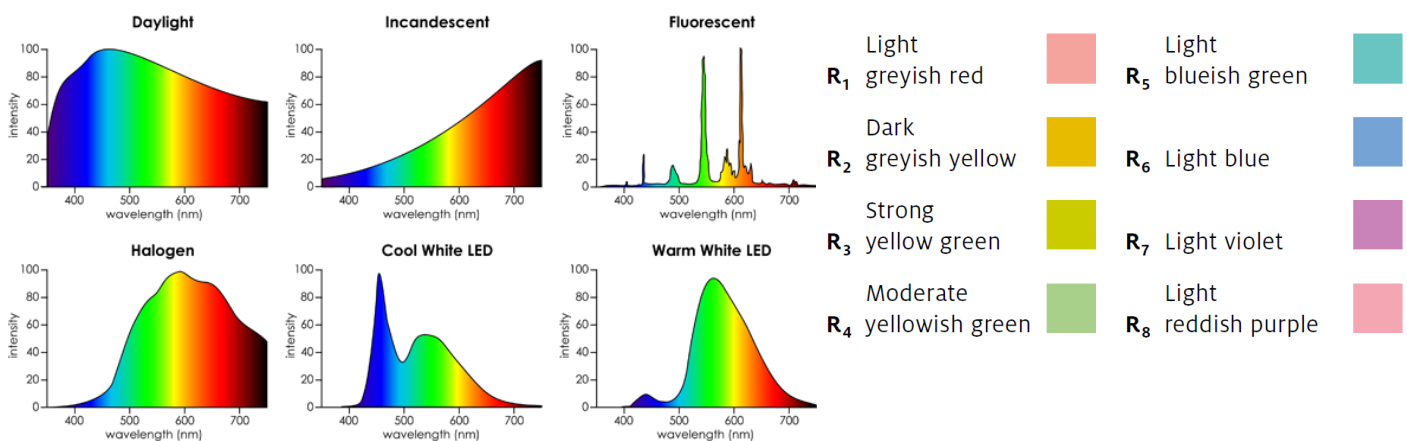


Figure 6. Spectral power distribution graphs of various light sources (ELS - European Lighting School, 2019) Figure 7. Colour rendering reference colors (Zumtobel, 2017)

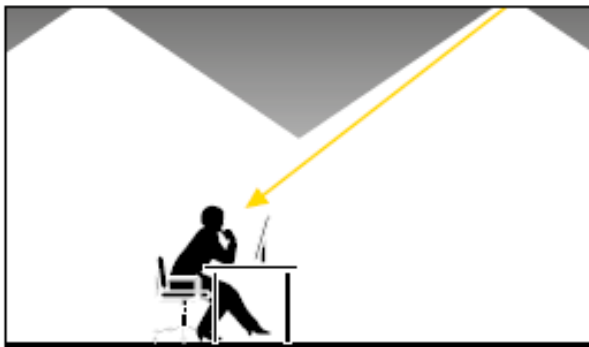
Glare

Glare is a phenomenon caused by light where humans experience visual discomfort as a result of too bright natural or artificial lighting. The luminance within the visual field is higher than human eyes can process, causing a loss of visibility. (Carlucci, 2015). The International Commission on Illumination (CIE) defines glare as:

“Visual conditions in which there is excessive contrast or an inappropriate distribution of light sources that disturbs the observer or limits the ability to distinguish details and objects”. (CIE, 2002).

In other words, glare is the effect of being blinded by an unwanted light source within the visual field. This can happen both directly and indirectly as Zumtobel (2017) shows in the figure below.

Direct glare



Cause

- Luminaires without glare control
- Very bright surfaces

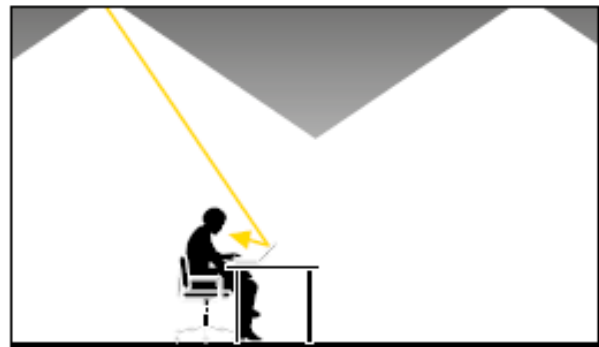
Effect

- Loss of concentration
- More frequent mistakes
- Fatigue

Remedy

- Luminaires with limited luminance levels
- Blinds on windows

Reflected glare



Cause

- Reflective surfaces
- Incorrect luminaire arrangement
- Incorrect workstation position

Effect

- Loss of concentration
- More frequent mistakes
- Fatigue

Remedy

- Matching luminaire to workstation (layout)
- Indirect lighting
- Matt surfaces

Figure 8. Differences between direct and indirect glare (Zumtobel, 2017)

As stated in the introduction of this chapter there are many indices for quantifying glare. Since this research is scoped to developing a sun shading, only glare indices for daylight glare will be elaborated. Indexes for quantifying glare from artificial light sources will be disregarded, because there are developed to aid lighting manufacturers and designers. Two types of glare can be distinguished; disability glare and discomfort glare. The types can be defined as following:

Disability glare

“Glare that impairs the vision of objects without necessarily causing discomfort” (CEN, 2018, p.9)

Discomfort glare

“Glare that causes discomfort without necessarily impairing the vision of objects” (CEN, 2018, p.9)

Four methods for describing daylight glare will be shortly elaborated. In essence both methods describe the difference in background luminance and glare source luminance. These values are altered taking several other factors into account in order to approximate a certain glaring situation. Both methods are developed using physical testing in a laboratory.

First of all the DGI method, also known as the Cornell glare equation. The method is derived from the British glare index and is adapted to situation with large light sources such as windows. The equation is based on experiments using fluorescent lamps behind an opal-diffusing screen. (Wienold, 2006). This is very similar to the situation to be tested later on in this research. The equation is expressed as following:

$$GI = 10 \log_{10} 0.48 \sum_{i=1}^n \frac{L_s^{1.6} \Omega_s^{0.8}}{L_b + 0.07 \omega_s^{0.5} L_s}$$

Where:

GI = Daylight Glare Index

ω_s = Solid angle subtended by the source

Ω_s = Solid angle subtended by the glare source modified by the position of the source with respect to field of view and Guth’s position index.

L_b = Background luminance (cd/m²)

L_s = Glare source luminance (cd/m²)

Figure 9. DGI formula (Wienold, 2006)

Whereas the DGI method focuses on calculating physical quantities on glare, it does not reveal enough insight in the human experience of glare. The DGP method is based on the probability an occupant experiences visual discomfort by the glare instead of the physical magnitude of the glare. In order to do so, the DGP method takes the vertical eye illuminance into account, as well as the luminance of the glare source, the solid angle and the position index. (Wienold, 2006). In essence this method is derived from the DGI method, with two key alterations.

Firstly, the background luminance is replaced by the vertical eye illumination. Instead of the luminance level of the background, the luminance level perceived by a virtual eye is compared to the glare source luminance. This already satisfies the need of developing insight in the human experience of glare.

Secondly, various factors are added to predict a level of comfort experienced by the observer. This is done by adding constant four parameters to the formula. "For optimizing the parameters c_1, \dots, c_4 all detected glare sources for each of the 349 cases were written into a file and merged with the subject's glare rating. Using a random optimization algorithm, thousands of different parameter settings were tested. Highest correlation with subjective glare rating were found with the following:

$$DGP = c_1 E_v + c_2 \log \left(1 + \sum_i \frac{L_{s,i}^2 \omega_{s,i}}{E_v^{c_4} P_i^2} \right) + c_3$$

$$DGP = 5.87 \cdot 10^{-5} \cdot E_v + 9.18 \cdot 10^{-2} \cdot \log \left(1 + \sum_i \frac{L_{s,i}^2 \cdot \omega_{s,i}}{E_v^{1.87} \cdot P_i^2} \right) + 0.16$$

Where:

- E_v = Vertical eye illuminance (lux)
- L_s = Luminance of source (cd/m²)
- ω_s = Solid angle of source (sr)
- P = Guth position index

Figure 10. *DGP formula with the four parameters (Wienold, 2006)*

Figure 11. *Optimized DGP formula (Wienold, 2006)*

Thirdly, the unified glare rating (UGR) formula, which is also prescribed by the European Committee for standardization in standard NEN-EN-12665. The UGR method is used to quantify psychological glare. In essence this formula is the logarithm of the glare from all light sources combined, divided by the background luminance. The formula for the UGT method is shown in the figure below:

$$UGR = 8 \log_{10} \left(\frac{0,25}{L_B} \sum \frac{L^2 \omega}{p^2} \right)$$

Where:

- L_B = Background luminance (cd/m²)
- L = Luminance of sources (cd/m²)
- ω = Solid angles of sources (sr)
- P = Guth position indices

Figure 12. *UGR method (CEN, 2011)*

The fourth and final explained quantification for glare is the use of luminance ratio's. This does is a very quick method for accessing the amount of glare. However, it only supplies the magnitude of glare, not the human perception. The luminance ratio is the maximum luminance divided by the average luminance. An example of the luminance ratio method is given in the next paragraph.

2.1.3 - Calculation methods

As stated in the introduction it is difficult to quantify the overall level of visual comfort, since it's based on multiple factors, whose comprehensive relation is not always that easy to describe. However, there is a need for the building industry to quantify the level of visual comfort in order to design a healthy indoor environment. Dubois (2001) conducted a research on the impact of shading devices on the daylighting quality in typical south-oriented office rooms. In this study Dubois (2001) defined five performance indicators. These performance indicators are based on a review of literature, various building codes and guides for workspace lighting. (AFNOR, 1990; ISO, 2000; IES, 1993; CIE, 1986; CIBSE, 1994; NUTEK, 1994). These five performance indicators are shown in the figure below. The table also shows the values which are interpreted as levels of acceptance.

Each of the five performance indicators will be elaborated separately below. Depending on the aim of the research, the requirements can be used for both a specific task area, entire room of even and entire floor in an open office work environment.

#	Performance indicator	Interpretation
1	DAYLIGHT FACTOR < 1 % 1-2 % 2-5 % > 5 %	unacceptable acceptable preferable ideal for paper work / too bright for computer work
2	WORK PLANE ILLUMINANCE < 100 lx 100-300 lx 300-500 lx > 500 lx	too dark for paper and computer work too dark for paper work / acceptable for computer work acceptable for paper work / ideal for computer work ideal for paper work / too bright for computer work
3	ILLUMINANCE UNIFORMITY ON THE WORK PLANE $E_{min}/E_{max} > 0.5$ $E_{min}/E_{max} > 0.7$ $E_{min}/E_{av} > 0.8$	acceptable ideal ideal
4	ABSOLUTE LUMINANCE > 2000 cd/m ² > 1000 cd/m ² < 500 cd/m ² < 30 cd/m ²	too bright, anywhere in the room too bright, in the normal visual field* preferable unacceptably dark
5	LUMINANCE RATIOS $0.33 < L_{paper_task}/L_{VDT} < 3$ $0.33 < L_{paper_task}/L_{adjacent_wall} < 3$ $0.33 < L_{VDT}/L_{adjacent_wall} < 3$ $(L_{paper_task}/L_{VDT} < 0.33 \text{ or } > 3$ $(L_{paper_task}/L_{adjacent_wall} < 0.33 \text{ or } > 3$ $(L_{VDT}/L_{adjacent_wall} < 0.33 \text{ or } > 3$	acceptable acceptable acceptable unacceptable) unacceptable) unacceptable)

*The normal visual field is the area that extends 90° each side horizontally, 50° upwards and 70° down from the horizon (NUTEK, 1994).

Figure 13. *The five performance indicators and their requirement values (Wienold, 2006)*

Daylight factor

The daylight factor can be defined as following:

“The total horizontal interior illuminance E_{vi} without interreflections divided by the total exterior illuminance E_{vh} under the absolutely unobstructed overcast sky with uniform unity luminance preliminarily” (Kittler, Kocifaj and Darula, 2012, p.213)

The daylight factor is expressed in formula below. In essence the daylight factor describes the ratio between the interior and exterior absolute illuminance. This means it will primarily be influenced by the façade openings when put in a building physical context.

$$DF(1 : 1) = \frac{E_{vi}}{E_{vh}}$$

Where:

DF = Daylight factor (%)

E_{vi} = Illuminance interior (lx)

E_{vh} = Illuminance exterior (lx)

Figure 14. *The formula for calculating the daylight factor (Kittler, Kocifaj and Darula, 2012)*

In his handbook, Watt (2016) describes methods for environmental analysis. The image belows shows a typical daylight factor study. This specific study compares two different façade opening typologies. It is to be noted that the daylight factor varies across the room. Height values can be found close to the façade and lower values at the core of the floorplan layout. The daylight factor referred to in requirements always considers an average of either the task area or the entire room

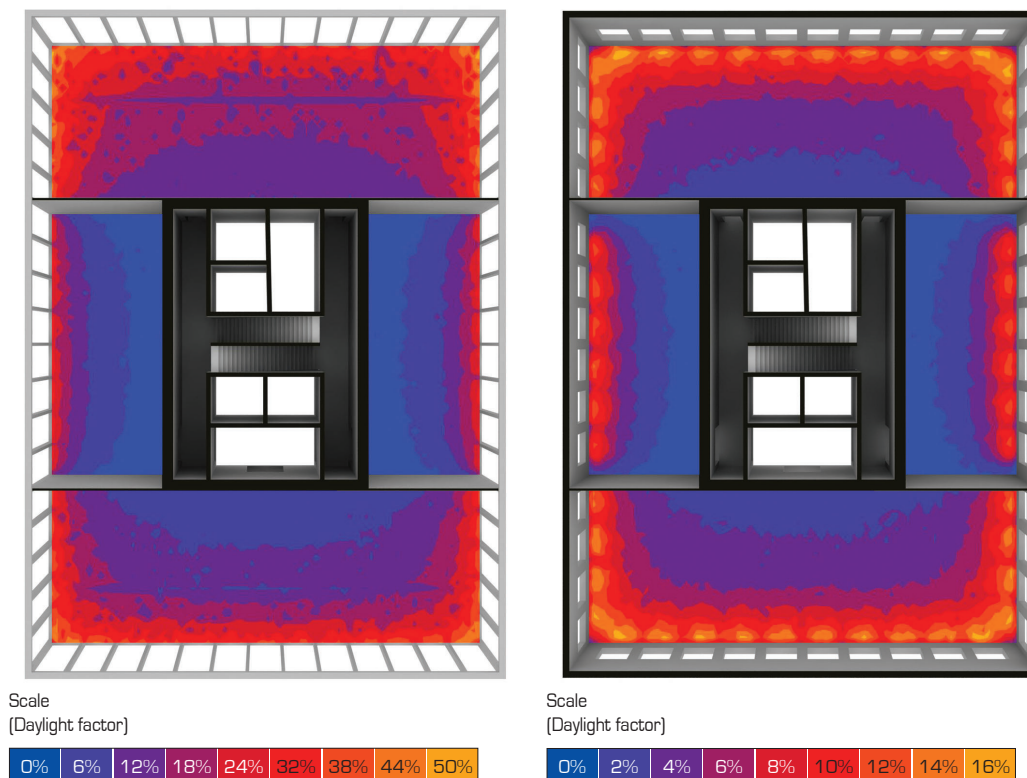


Figure 15. *Example of a daylight factor analysis (Watt, 2016)*

Work plane illuminance

The work plane illuminance describes the absolute illuminance as elaborated previously. In contrast to the daylight factor this does not regard an average but specifies absolute minimum and maximum values. The illuminance is measured at work plane/desk height. When put in a building physical context, this means a desk close to the façade can be too bright and far from the façade can be too dark. Dubois (2001) only defines workplane illuminance requirements for office paper- and computer work. However, over the past few decades various standards have come up with different work plane illuminance requirements based on more specific activities. Shown below are requirements tables from ASHRAE (2010) and the European Committee for Standardization (CEN). The second table only shown minimum work plane illumination levels.

Activity	Illuminance (lx, lumen/m ²)
Public areas with dark surroundings	20 - 50
Simple orientation for short visits	50 - 100
Areas with traffic and corridors - stairways, escalators and travelators - lifts - storage spaces	100
Working areas where visual tasks are only occasionally performed	100 - 150
Warehouses, homes, theaters, archives, loading bays	150
Coffee break room, technical facilities, ball-mill areas, pulp plants, waiting rooms,	200
Easy office work	250
Class rooms	300
Normal office work, PC work, study library, groceries, show rooms, laboratories, check-out areas, kitchens, auditoriums	500
Supermarkets, mechanical workshops, office landscapes	750
Normal drawing work, detailed mechanical workshops, operation theaters	1000
Detailed drawing work, very detailed mechanical works, electronic workshops, testing and adjustments	1500 - 2000
Performance of visual tasks of low contrast and very small size for prolonged periods of time	2000 - 5000
Performance of very prolonged and exacting visual tasks	5000 - 10000
Performance of very special visual tasks of extremely low contrast and small size	10000 - 20000

Figure 16. *Illuminance requirements per activity (ASHRAE, 2010)*

Ref. no.	Type of area, task or activity	\bar{E}_m lx	UGR_L	U_o	R_a	Specific requirements
5.26.1	Filing, copying, etc.	300	19	0,40	80	
5.26.2	Writing, typing, reading, data processing	500	19	0,60	80	DSE-work, see 4.9.
5.26.3	Technical drawing	750	16	0,70	80	
5.26.4	CAD work stations	500	19	0,60	80	DSE-work, see 4.9.
5.26.5	Conference and meeting rooms	500	19	0,60	80	Lighting should be controllable.
5.26.6	Reception desk	300	22	0,60	80	
5.26.7	Archives	200	25	0,40	80	

Figure 17. *Illuminance requirements per activity (CEN, 2011)*

Illuminance uniformity

The illuminance uniformity describes the difference ratio between the minimum and average illuminance very as similar as elaborated previously. In addition to the definition of uniformity as $U_O = E_{\min}/E_{av}$, Dubois (2001) also reviews uniformity in terms of $U_O = E_{\min}/E_{\max}$. These uniformities in illumination are commonly caused by glare.

Absolute luminance

The absolute luminance describes the brightness of the surrounding environment as perceived by the eye, as elaborated previously. This can regard both direct light sources or indirect light reflected from surfaces. However, these requirements for absolute values focus primarily on the direct light sources, which may not be too bright in order to achieve comfort. Dubois (2001) makes a difference in absolute luminance's inside and outside the normal visual area. This area is defined as shown in the image below.

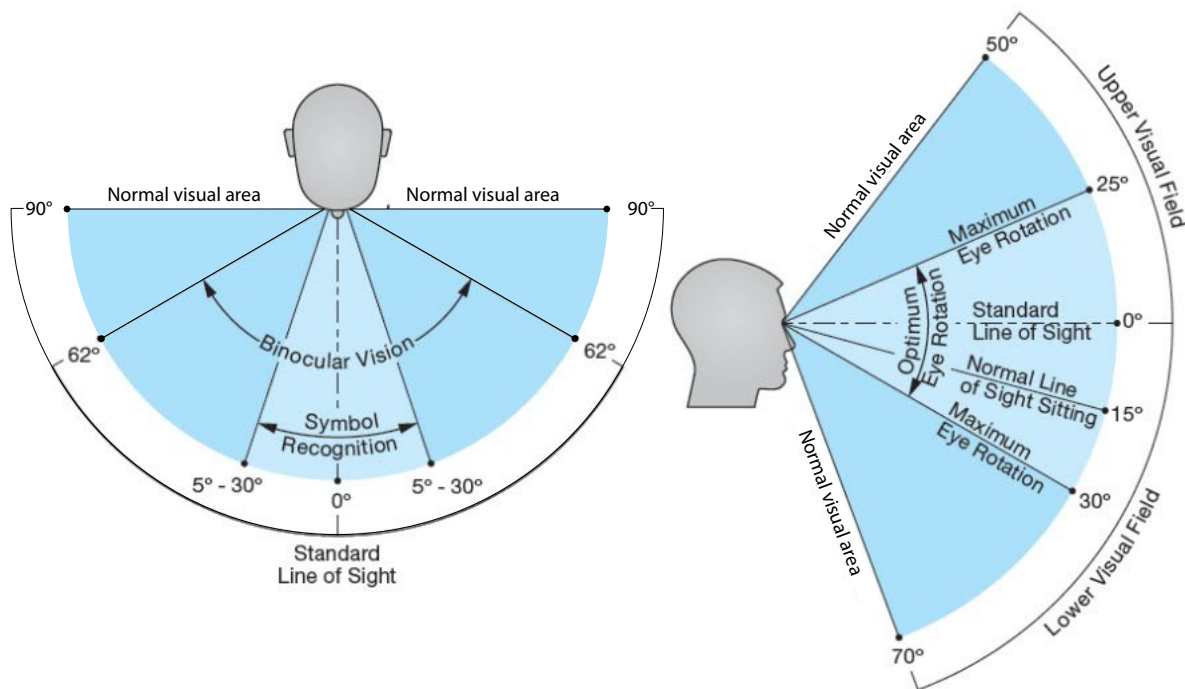


Figure 18. Normal visual area (www.quora.com, edited by author)

Luminance ratio's

Luminance ratio's, in contrast to the absolute luminance, focus more on the luminance of area's within the field caused by indirect, reflected light. It regards the luminance of the desk where paperwork happens ($L_{\text{paper_task}}$), the computer screen (L_{VDT}) and the area behind the computer screen which is usually a wall ($L_{\text{adject_wall}}$). M.C. Dubois (2001) states that the luminance of these areas may not differ more than a factor 3. If this ratio is exceeded, discomfort glare is likely to appear.

2.1.4 - Relation to sun shading

As stated in the previous paragraph, Dubois (2001) conducted a research on the impact of shading devices on the daylighting quality in typical south-oriented office rooms. The study contained a field experiment where the performance on visual comfort of multiple interior roller screens and venetian blinds were tested. All shading devices used in the study are manually operable by the occupant. Dubois (2001) concluded all shading devices could be grouped based on their darkness. If the window is within the field of vision and the occupant is doing computer tasks, darker shading devices are needed to keep the amount of discomfort glare within requirement boundaries. However, as a result artificial lighting might be needed to compensate for the loss of absolute illumination levels. When the window was not within the field of view, brighter sun shading devices were preferred. This results in a blockage of direct sunlight and gives pleasant diffuse light instead. Dubois (2001).

From the results of this study it can be concluded that shading is primarily needed to reduce glare. The most common source for this glare is the direct sun light. The secondary goal of the shading is to allow indirect daylight to enter the room in order to keep absolute illuminance levels within the requirement boundaries as well

2.1.5 - References

1. ASHRAE Standard 55-2010 (2010). Thermal Environment Standards for Human Occupancy. American Society of Heating, Refrigerating and Air-Conditioning Engineers. Atlanta,GA.
2. Carlucci, S. (2015). A review of indices for assessing visual comfort with a view to their use in optimization processes to support building integrated design. *Renewable and Sustainable Energy Reviews*, 47, pp.1016-1033.
3. Fairchild, M. (2013). *Color appearance models*. Chichester, West Sussex, U.K.: Wiley.
4. Dubois M.C. (2001), *Impact of Solar Shading Devices on Daylight Quality: Measurements in Experimental Office Rooms*, Department of Construction and Architecture, Lund University, Lund.
5. ELS - European Lighting School. (2019). 2. Understanding the light. [online] Available at: <http://www.lightingschool.eu/portfolio/understanding-the-light/> [Accessed 3 Jan. 2019].
6. European Committee for Standardization (CIE). (2002). CIE equations for disability glare. *Color Research & Application*, 2002 27(6): p. 457-458.
7. European Committee for Standardization (CEN). (2018). NEN-EN-12665: Light and lighting - Basic terms and criteria for specifying lighting requirements.
8. European Committee for Standardization (CEN). (2011). NEN-EN-12464: Light and lighting - Lighting of work places - Part1: Indoor work places
9. Kittler, R., Kocifaj, M. and Darula, S. (2012). *Daylight science and daylighting technology*. New York, NY: Springer.
10. Watts, A. (2016). *Modern construction handbook*. Retrieved from <https://ebookcentral-proquest-com.tudelft.idm.oclc.org>
11. Wienold, J. and Christoffersen, J. (2006). Evaluation methods and development of a new glare prediction model for daylight environments with the use of CCD cameras. *Energy and Buildings*, 38(7), pp.743-757.
12. Zumtobel Lighting GmbH (2017). *The Lighting Handbook*. 5th ed.
13. AFNOR (1990). *Ergonomical Principles Applicable to the Lighting of Workplaces for Visual Comfort*. French code NF X 35-103. AFNOR (Association française de normalisation). Paris (France).
14. ISO (2000). *Ergonomic Requirements for Office Work with Visual DisplayTerminals (VDTs) – Part 6: Guidance on the Work Environment*. French,European and International code NF EN ISO 9241-6:1999. AFNOR (Association française de normalisation). Paris (France).
15. CIE (1986). *Guide on Interior Lighting*. Second Edition. Publication No 29.2. Commission Internationale de l'Éclairage (CIE). Vienna (Austria).
16. CIBSE (1994). *Code for Interior Lighting*. CIBSE (Chartered Institution of Building Services Engineers). London (UK).
17. NUTEK (1994). *Programkrav: belysning på kontor*. Programkrav för god och energieffektiv belysning på kontor. 1994-11. Utgåva 2. Näringsoch teknikutvecklingsverket (NUTEK). Stockholm (Sweden).

2.2 - Fundamentals of thermal comfort

2.2.1 - Definition

Thermal comfort is defined by the International Organization for Standardization (ISO) NEN-EN-ISE-7730 standard as:

“That condition of mind which expresses satisfaction with the thermal environment” (ISO, 2005).

In the review on thermal comfort indices, Carlucci (2013) reviewed the evolution of indices over time, like shown in the image below. Many of the proposed thermal comfort indices involve physiological, psychological, medical, climatological and engineering aspects. (Carlucci, 2013).

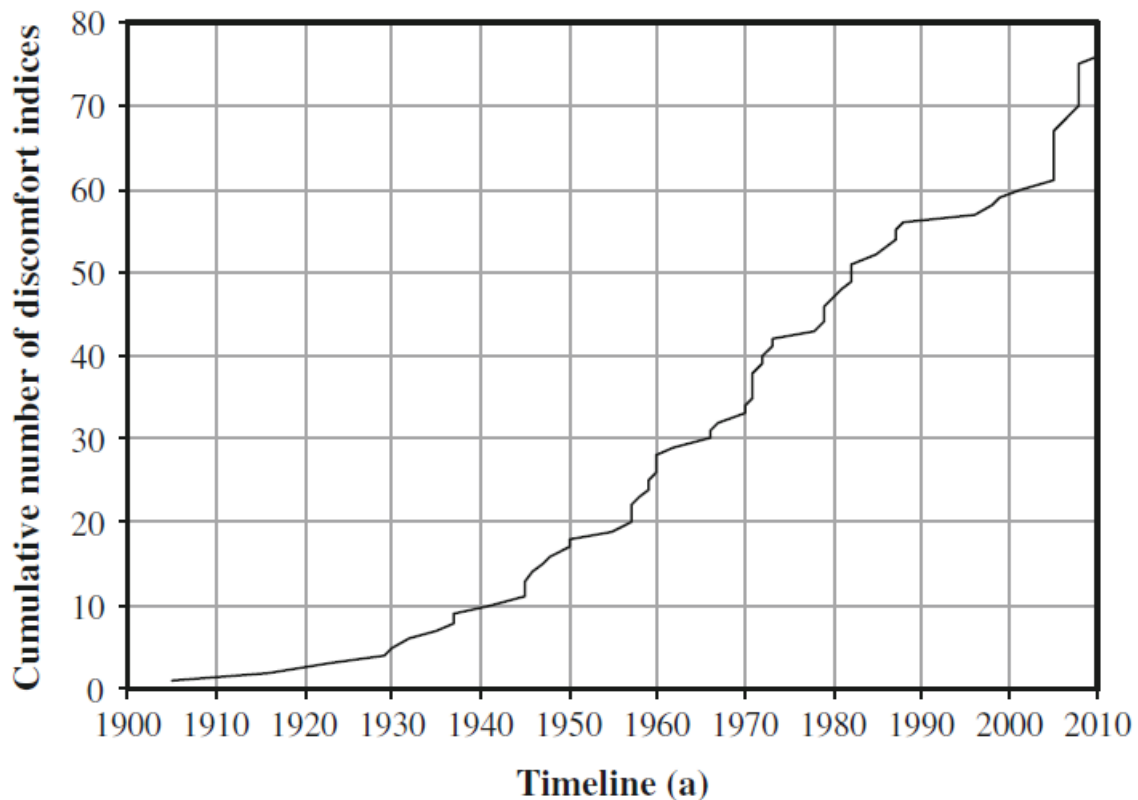


Figure 19. Amount of indices for thermal comfort over time (Carlucci, 2013)

2.2.2 - Contributing factors

Creating a classification for these different indices will gain insight in the various components that make up the level of thermal comfort experienced by the building user. MacPherson (1962) reviewed 19 of the at the time available thermal comfort indicators and concluded the indices can be grouped into the following three categories:

1. Those which are based on the physical factors in the environment,
2. Those which are based on a measurement of the physiological strain produced by the environment,
3. Those based on the calculation on the heat exchange between the body and its environment

However, Carlucci (2013) noticed there has been developing a fourth category; indices for assessing long-term comfort. The most of present studies regard this new category. The four comfort index categories can be defined as following:

Physical factors in the environment indices:

It can be argued this is the most simple category of thermal indices. They are based on:

“Direct measurements of the physical parameters characterizing a thermal environment, generally analyzed through a linear regression model. The physiological effects are usually not taken into account.” (Carlucci, 2013, p.3).

Three indices which are quite common include the equivalent temperature, the globe thermometer temperature and the operative temperature. (Carlucci, 2013).

Physiological strain indices:

Indices based on physiological strain try to quantify thermal comfort by using a large dataset of actual human ratings of indoor climate conditions which is usually gathered through surveys. Carlucci (2013) defines this category as following:

“These metrics were generally developed by correlating a wide range of environmental conditions and behavioral parameters with the thermal strain produced on individuals.” (Carlucci, 2013, p.3).

MacPherson (1962) defined the principle behind this category to be that conditions of equal environmental stress are those which produce an equal physiological strain. Which means level of thermal comfort is equal to the physiological strain experienced by the environmental conditions. This physiological strain can vary along individuals, but the average of many people's strain provides a prediction from an average individual. Some indices within this category are the effective temperature, the corrected effective temperature, the equatorial comfort index, the index of physiological effect, the predicted four-hour sweat rate and the thermal strain index. (Carlucci, 2013).

Heat exchange indices:

Carlucci (2013) defines this category as following:

“These indices generally combine physiological parameters (e.g., the value of skin wetness and mean skin temperature), behavioral parameters (e.g., metabolic rate connected to activity and thermal resistance of clothing) and parameters of the thermal environment (e.g., dry-bulb air temperature, mean radiant temperature evaluated in a representative position of a room, relative humidity or wet-bulb temperature, air velocity, etc.)” (Carlucci, 2013, p.2-3).

These indices try to quantify the most important parameters of a situation of actual building usage by individuals. Many of the indices in this category are developed by correlating the level of thermal comfort of people in climate chambers and a variety of environmental parameters; air temperature, humidity, air speed and mean radiant temperature. (Carlucci, 2013). This already defines six important parameters for this category of thermal format indices; clothing, activity, air temperature, humidity, air speed and the mean radiant temperature (MRT). Two of the most commonly used heat exchange indices are the Predicted mean vote (PMV) and Predicted percentage of dissatisfied (PPD) proposed by Fanger (1970). The PPD and PMV method are very commonly used nowadays and provide the guideline for the NEN-EN-ISO-7730 standard. ISO (2005), states the following about the PMV method:

“The PMV index takes into account the influence of all 6 thermal parameters (clothing, activity, air- and mean radiant temperature, air velocity and humidity) and can be directly used as criteria.” (ISO, 2005)

Those six parameters correspond with the ones Carlucci (2013) defined. The PMV method will be elaborated in the next paragraph as a main quantification method for thermal comfort.

Long-term thermal comfort:

More recently the focus of thermal comfort indices shifted toward quantifying long-term thermal comfort. Many of those indices include mutations of the previously mentioned PPD and PMV methods, taking into account extra long-term factors. Some of the long-term indices are shown in the figure below. However, Carlucci (2013) concluded the following about the long-term thermal comfort indices:

“None of the reviewed indices showed to be fully suitable for the long-term evaluation of the general thermal comfort conditions in a building.” (Carlucci, 2013, p. 33)

This conclusion does not implicate the irrelevance of thermal comfort indices, but addresses future improvement opportunities to more closely resemble actual building usage, which in generally often for longer periods of times. Carlucci (2013) defines the his improvement opportunities as cited below.

- *That is applicable for both free-running and mechanically cooled buildings and can be used with both the adaptive and the Fanger comfort models (e.g., Percentage outside range).*
- *That reflects the nonlinear relationship between perception of discomfort and the exceedance from the theoretical comfort temperature (e.g., Averaged PPD and Nicol’s overheating risk).*
- *That, in case of multi-zone buildings, weights the zone indices by the number of occupants inside each zone, rather than by buildings features such as net volume, or net floor area (e.g., ExceedanceM).*
- *That is applicable to the evaluation of both summer and winter discomfort.*
- *That is symmetric, i.e., able to estimate possible discomfort due to the upper and lower exceedance from the theoretical comfort temperature.*
- *That is independent of discontinuities connected to the use of comfort categories.*

Family of indices	Long-term discomfort indices	Index based on a comfort model	Index dependent on comfort categories	Symmetric index	Index applicable only to summer	Index provided with a comfort threshold
Percentage indices	Percentage outside the (PMV) range	F	✓	✓		✓
	Percentage outside the $(\theta_{op, PMV})$ range	F	✓	✓		✓
	Percentage outside the $(\theta_{op, Adaptive})$ range	A _{EU}	✓	✓		✓
	CIBSE guide J criterion				✓	✓
	CIBSE guide A criterion				✓	✓
Cumulative indices	PPD weighted criterion	F	✓			
	Accumulated PPD	F		✓		
	Degree-hour criterion	F	✓			
	Degree-hour criterion	A _{EU}	✓			
Risk indices	Exceedance _{PPD}	F	✓		✓	
	Exceedance _{Adaptive}	A _{USA}	✓		✓	
	Nicol et al.’s Overheating risk	A _{EU}			✓	
	Robinson-Haldi’s Overheating risk				✓	✓
	Average PPD	F		✓		

F Fanger model, A_{EU} EN adaptive model, A_{USA} ASHRAE adaptive model

Figure 20. *Long-term thermal comfort indices and their performance (Carlucci, 2013)*

Talghani et al. (2013) researched the difference between the previously mentioned ISO EN-7730 standard and two other standards; ASHRAE 55-2010 and the Dutch ATG guideline. In order to distinguish the three standards, yet another category of thermal comfort indices is to be introduced. All previously discussed thermal comfort indices and formulas can be divided into two groups; the ones based on studies in climate chambers and those in field studies. (Talghani et al., 2013). The studies in climate chambers led to the definition of the PMV and PPD, whereas the field studies eventually led to the adaptive comfort index. The adaptive comfort index is based on the following hypothesis:

“The adaptive hypothesis predicts that contextual factors and past thermal history modify building occupants’ thermal expectations and preferences. One of the predictions of the adaptive hypothesis is that people in warm climate zones prefer warmer indoor temperatures than people living in cold climate zones.” (de Dear, 1998, p.1)

In other words, the conditions of the outside environment are related to the level of thermal comfort experienced indoors. This parameter is not taken into account in all the climate chamber based comfort indices. ASHRAE did tests in actual buildings to achieve a database of thermal comfort experiments containing over 21,000 observations from 160 buildings across the world. (de Dear, 1998). ASHRAE compared calculated PMV ratings to actual levels of thermal comfort experienced by people at different times of the year to include the parameter of the outdoor thermal environment. ASHRAE concluded the following:

“The static predicted means vote (PMV) model was shown to be partially adaptive by accounting for behavioral adjustments, and fully explained adaptation occurring in HVAC buildings. Occupants in naturally ventilated buildings were tolerant of a significantly wider range of temperatures, explained by a combination of both behavioral adjustment and psychological adaptation. These results formed the basis of a proposal for a variable indoor temperature standard.” (de Dear, 1998, p.1).

In other words, the adaptive comfort models take two more parameters into account; the prevailing mean outdoor temperature and the type of ventilation in a building. The studies also suggested the PMV and PPD are more appropriate for HVAC controlled buildings, and the adaptive comfort index for naturally ventilated buildings.

Elaboration on components

The NEN-EN-ISO-7730 standard describes six components needed to calculate the PMV; clothing, activity, air- and mean radiant temperature, air velocity and humidity. The adaptive thermal comfort models adds two more parameters; prevailing mean outdoor temperature and type of ventilation. This makes a total of eight separate components contributing to thermal comfort which will be elaborated in the next few paragraphs.

Clothing

The influence of an individual's clothing on the PMV thermal comfort index is based on the insulation effect of the clothing. The insulation effect of clothes is measured in the unit Clo, 1 Clo equals 0.155 m²K/W. (Engineering ToolBox, 2004). For common, non-special thermal insulation, clothing, the Clo value can range from 0 to 1 where:

Clo = 0

Corresponds to a naked person

Clo = 1

Corresponds to the insulating value of clothing needed to maintain a person in comfort sitting at rest in a room at 21 °C (70 °F) with air movement of 0.1 m/s and humidity less than 50% - typically a person wearing a business suit.

The table shown in the figure below shows Clo values for common types of clothing, which can be used in PMV calculations. This table conforms to the more extensive table of the standard NEN-EN-ISO-9920 (ISO, 2007)

Clothing		Insulation	
		Clo	m ² K/W
Nude		0	0
Underwear - pants	Pantyhose	0.02	0.003
	Panties	0.03	0.005
	Briefs	0.04	0.006
	Pants 1/2 long legs made of wool	0.06	0.009
	Pants long legs	0.1	0.016
Underwear - shirts	Bra	0.01	0.002
	Shirt sleeveless	0.06	0.009
	T-shirt	0.09	0.014
	Shirt with long sleeves	0.12	0.019
	Half-slip in nylon	0.14	0.022
Shirts	Tube top	0.06	0.009
	Short sleeve	0.09	0.014
	Light blouse with long sleeves	0.15	0.023
	Light shirt with long sleeves	0.20	0.031
	Normal with long sleeves	0.25	0.039
	Flannel shirt with long sleeves	0.30	0.047
	Long sleeves with turtleneck blouse	0.34	0.053
Trousers	Shorts	0.06	0.009
	Walking shorts	0.11	0.017
	Light trousers	0.20	0.031
	Normal trousers	0.25	0.039
	Flannel trousers	0.28	0.043
Coveralls	Overalls	0.28	0.043
	Daily wear, belted	0.49	0.076
Highly-insulating coveralls	Work	0.50	0.078
	Multi-component with filling	1.03	0.160
Sweaters	Fiber-pelt	1.13	0.175
	Sleeveless vest	0.12	0.019
	Thin sweater	0.20	0.031
	Long thin sleeves with turtleneck	0.26	0.040
	Thick sweater	0.35	0.054
Jacket	Long thick sleeves with turtleneck	0.37	0.057
	Vest	0.13	0.020
	Light summer jacket	0.25	0.039
	Smock	0.30	0.047
Coats and over-jackets and over-trousers	Jacket	0.35	0.054
	Overalls multi-component	0.52	0.081
	Down jacket	0.55	0.085
	Coat	0.80	0.123
Sundries	Parka	0.70	0.109
	Socks	0.02	0.003
	Thin soled shoes	0.02	0.003
	Quilted fleece slippers	0.03	0.005
	Thick soled shoes	0.04	0.006
	Thick ankle socks	0.05	0.008
	Boots	0.05	0.008
	Thick long socks	0.10	0.016
Skirts, dresses	Light skirt 15 cm. above knee	0.01	0.002
	Light skirt 15 cm. below knee	0.18	0.028
	Heavy skirt knee-length	0.25	0.039
	Light dress sleeveless	0.25	0.039
	Winter dress long sleeves	0.40	0.062
Sleepwear	Under shorts	0.10	0.016
	Short gown thin strap	0.15	0.023
	Long gown long sleeve	0.30	0.047
	Hospital gown	0.31	0.048
	long pajamas with long sleeve	0.50	0.078
Robes	Body sleep with feet	0.72	0.112
	Long sleeve, wrap, short	0.41	0.064
	Long sleeve, wrap, long	0.53	0.082

Figure 21. Clothing values for various outfits (Engineering ToolBox, 2004)

Activity

The influence of an individual's activity on the PMV thermal comfort index is based on the amount of energy burned by the body to execute the certain activity. The metabolic rate, or human body heat production, is usually measured in Met. The metabolic rate of a relaxed seated person is one Met, where 1 Met = 58 W/m² (356 Btu/hr). (Engineering ToolBox, 2004). Generally speaking, the Met value for doing nothing is around 1 and while heavy exercising the Met value is around 10.

The table shown in the figure below shows Met values for common types of activities, which can be used in PMV calculations. This table is conform the more extensive table of the standard NEN-EN-ISO-8996 (ISO, 2004)

Activity	Met - Metabolic Rate			
	W/m ²	W ⁽¹⁾	Btu/hr ⁽¹⁾	Met
Reclining, Sleeping	46	83	282	0.8
Seated relaxed	58	104	356	1.0
Standing at rest	70	126	430	1.2
Sedentary activity (office, dwelling, school, laboratory)	70	126	430	1.2
Car driving	80	144	491	1.4
Graphic profession - Book Binder	85	153	522	1.5
Standing, light activity (shopping, laboratory, light industry)	93	167	571	1.6
Teacher	95	171	583	1.6
Domestic work -shaving, washing and dressing	100	180	614	1.7
Walking on the level, 2 km/h	110	198	675	1.9
Standing, medium activity (shop assistant, domestic work)	116	209	712	2.0
Building industry - Brick laying (Block of 15.3 kg)	125	225	768	2.2
Washing dishes standing	145	261	890	2.5
Domestic work - raking leaves on the lawn	170	306	1043	2.9
Domestic work - washing by hand and ironing (120-220 W)	170	306	1043	2.9
Iron and steel - ramming the mold with a pneumatic hammer	175	315	1075	3.0
Building industry - forming the mold	180	324	1105	3.1
Walking on the level, 5 km/h	200	360	1228	3.4
Forestry - cutting across the grain with a one-man power saw	205	369	1259	3.5
Volleyball, Bicycling (15 km/h)	232	418	1424	4.0
Calisthenics	261	470	1602	4.5
Building industry - loading a wheelbarrow with stones and mortar	275	495	1688	4.7
Golf, Softball	290	522	1780	5.0
Gymnastics	319	574	1959	5.5
Aerobic Dancing, Swimming	348	624	2137	6.0
Sports - Ice skating, 18 km/h, Bicycling (20 km/h)	360	648	2210	6.2
Agriculture - digging with a spade (24 lifts/min.)	380	674	2333	6.5
Skiing on level (good snow, 9 km/h), Backpacking, Skating ice or roller, Basketball, Tennis	405	729	2487	7.0
Handball, Hockey, Racquetball, Cross County Skiing, Soccer	464	835	2848	8.0
Running 12 min/mile, Forestry - working with an axe (weight 2 kg. 33 blows/min.)	500	900	3070	8.5
Sports - Running in 15 km/h	550	990	3377	9.5

Figure 22. Clothing values for various outfits (Engineering ToolBox, 2004)

Air temperature

The air temperature is the temperature measured inside the room. This is also referred to as the Dry-bulb temperature. The dry-bulb temperature is the most commonly used air temperature. It is called the dry-bulb temperature, as the thermometer temperature is not effected by moisture in the air. (Engineering ToolBox, 2004). So the air temperature is the temperature measured with a common thermometer which is surrounded by air. The figure below shows how the dry-bulb- is measured compared to the wet-bulb- and dew-bulb temperature, two other commonly used air temperatures.

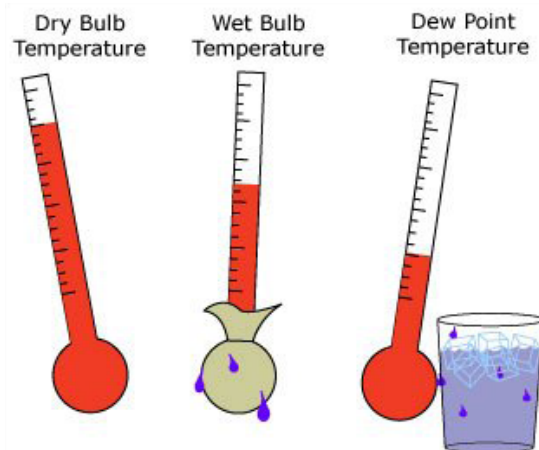


Figure 23. *Dry bulb temperature compared to wet- and dew point temperature (http://evapopedia.com)*

Mean radiant temperature (MRT)

The mean radiant temperature is defined as following:

“The mean radiant temperature (MRT) is defined as the uniform temperature of an imaginary enclosure in which the radiant heat transfer from the human body is equal to the radiant heat transfer in the actual non-uniform enclosure.”
(ISO, 2005).

In other words, the MRT is the temperature on the human skin caused by radiant heat reflecting of the surrounding surfaces. ISO (2005) gives the following formula to calculate the MRT. This is however, a simplification, because all walls are assumed to be black with a high radiation emittance value. In essence the MRT is an addition of all the surrounding surfaces temperatures factored by their angle factor in relation to the building occupant.

$$MRT^4 = T_1^4 F_{p-1} + T_2^4 F_{p-2} + \dots + T_n^4 F_{p-n}$$

MRT = Mean Radiant Temperature;
 T_n = Temperature of surface “n”, in Kelvins;
 F_{p-n} = Angle factor between a person and surface “n”.

Figure 24. *MRT formula (ISO, 2005)*

Air velocity

Air velocity, often also referred to as air speed, is defined as following in comfort standards:

“The average speed of the air to which the body is exposed, with respect to location and time.” ASHRAE (2013)

Air flows in a room at a certain speed as a result of ventilation. Therefore, the air velocity is highly depending on the used HVAC systems. ISO (2005) states that for a standard situation, and air velocity of between 0,1 and 0,25 m/s are reasonable values.

Humidity

Humidity defined the amount of water vapor in the air. It can be expressed as an absolute or relative value. (Engineering ToolBox, 2004). The air’s ability to hold water increases when the air temperature increases. This relation can be shown in a psychrometric chart which is shown in the figure below. In the context of the PMV thermal comfort index two quantities of humidity are of interest; the relative humidity and the humidity ratio.

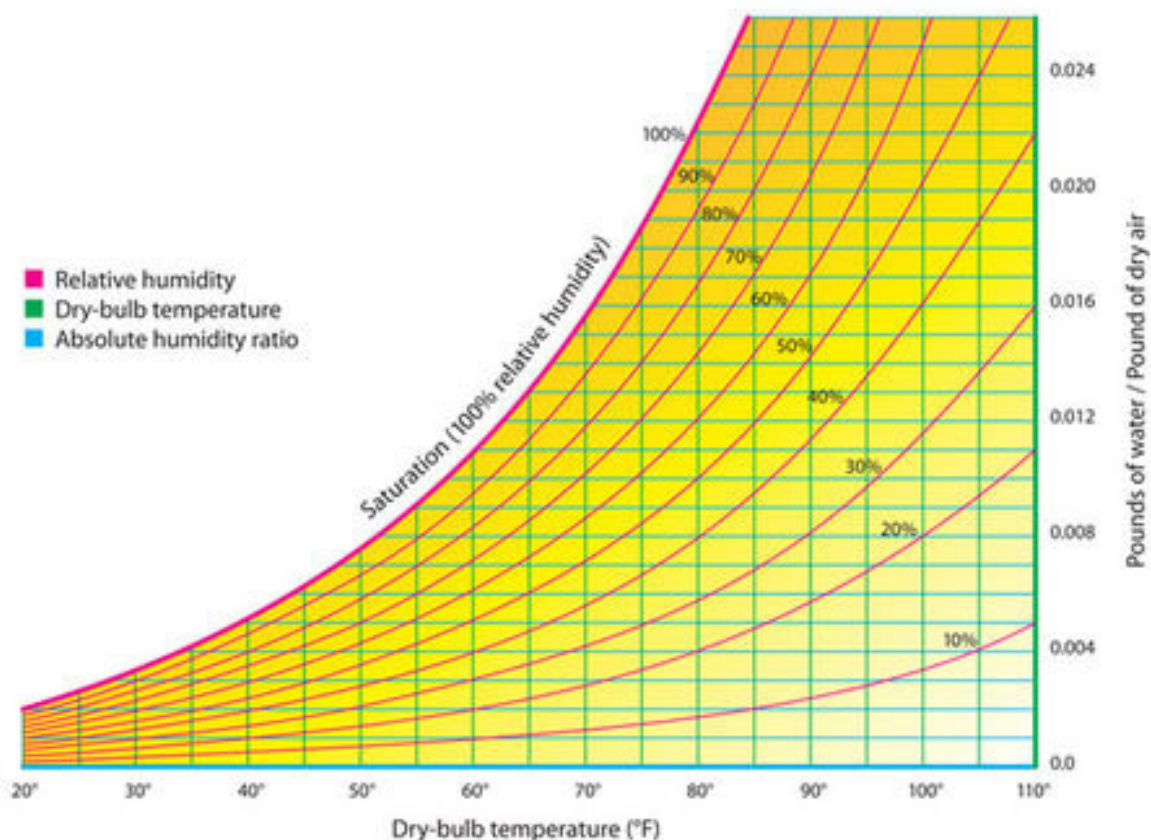


Figure 25. *Psychrometric chart for humidity in relation to the dry bulb temperature* (www.buildinggreen.com/primer/basics-psychrometric-chart)

Relative humidity:

The relative humidity describes the ratio of the actual vapor pressure in relation the maximum possible pressure at the specific dry-bulb air temperature. (Engineering ToolBox, 2004). The formula for the relative humidity is given in the following formula:

$$\Phi = p_w / p_{ws} \cdot 100\%$$

Where:

Φ = relative humidity [%]

p_w = vapor partial pressure [Pa]

p_{ws} = saturation vapor partial pressure at the actual dry bulb temperature [Pa]. This is the vapor pressure at maximum content of water gas in air, before it starts to condense out as liquid water.

Humidity ratio:

The humidity ratio describes the amount of vapor as a ratio of the mass of the vapor in relation to the mass of the dry air. (Engineering ToolBox, 2004).

$$x = m_w / m_a$$

Where:

x = humidity ratio ($\text{kg}_{\text{water}}/\text{kg}_{\text{dry_air}}$, $\text{lb}_{\text{water}}/\text{lb}_{\text{dry_air}}$)

m_w = mass of water vapor (kg, lb)

m_a = mass of dry air (kg, lb)

Prevailing mean outdoor temperature

ASHRAE (2017) introduced the prevailing mean outdoor temperature as an average outdoor dry-bulb temperature. It is defines as the arithmetic average of mean outdoor temperatures for a period of at least 7 and at most 30 sequential days.

Type of ventilation

The adaptive thermal comfort models addresses a difference between mechanically and naturally ventilated buildings. Occupants of buildings with HVAC systems are used to the static, automatically controlled thermal environment. Occupants of naturally ventilated buildings are used to be more interactive with the thermal environment by means of opening windows for instance. Generally speaking HVAC buildings have a more narrow range for thermal comfort compared to naturally ventilated buildings. (de Dear, 2002).

2.2.3 - Calculation methods

This paragraph about the calculation methods of thermal comfort will combine all the previously elaborated to actually quantify the level of thermal comfort. Three methods will be discussed; The Predicted Mean Vote (PMV), the Predicted Percentage Dissatisfied (PPD) and the adaptive thermal comfort method, each in their dedicated paragraph. All three methods will be discussed as described in the International Organization for Standardization standards NEN-EN-ISO-7730 (ISO, 2005) and NEN-EN-15251 (CEN, 2007).

Predicted mean vote (PMV)

Prior to stating how the PMV has to be calculated, ISO (2005) gives the following definition of the Predicted mean vote;

“The PMV is an index that predicts the mean value of the votes of a large group of persons on the 7-point thermal sensation scale (see fig. 27), based on that heat balance of the human body. Thermal balance is obtained when the internal heat production in the body is equal to the loss of heat to the environment.” (ISO, 2005, p.12).

The best level of thermal comfort is reached with a PMV value of 0, higher means to warm and lower means to cool. ISO (2005) specifies to calculate the PMV using equations (1) to (4), which are shown below. All quantities used in the formulas have been explained previously, or can be derived from the previously explained quantities.

$$PMV = [0,303 \cdot \exp(-0,036 \cdot M) + 0,028] \cdot \left\{ \begin{aligned} &(M - W) - 3,05 \cdot 10^{-3} \cdot [5\,733 - 6,99 \cdot (M - W) - p_a] - 0,42 \cdot [(M - W) - 58,15] \\ &- 1,7 \cdot 10^{-5} \cdot M \cdot (5\,867 - p_a) - 0,0014 \cdot M \cdot (34 - t_a) \\ &- 3,96 \cdot 10^{-8} \cdot f_{cl} \cdot [(t_{cl} + 273)^4 - (\bar{t}_r + 273)^4] - f_{cl} \cdot h_c \cdot (t_{cl} - t_a) \end{aligned} \right\} \quad (1)$$

$$t_{cl} = 35,7 - 0,028 \cdot (M - W) - I_{cl} \cdot \left\{ 3,96 \cdot 10^{-8} \cdot f_{cl} \cdot [(t_{cl} + 273)^4 - (\bar{t}_r + 273)^4] + f_{cl} \cdot h_c \cdot (t_{cl} - t_a) \right\} \quad (2)$$

$$h_c = \begin{cases} 2,38 \cdot |t_{cl} - t_a|^{0,25} & \text{for } 2,38 \cdot |t_{cl} - t_a|^{0,25} > 12,1 \cdot \sqrt{v_{ar}} \\ 12,1 \cdot \sqrt{v_{ar}} & \text{for } 2,38 \cdot |t_{cl} - t_a|^{0,25} < 12,1 \cdot \sqrt{v_{ar}} \end{cases} \quad (3)$$

$$f_{cl} = \begin{cases} 1,00 + 1,290 I_{cl} & \text{for } I_{cl} \leq 0,078 \text{ m}^2 \cdot \text{K/W} \\ 1,05 + 0,645 I_{cl} & \text{for } I_{cl} > 0,078 \text{ m}^2 \cdot \text{K/W} \end{cases} \quad (4)$$

where

- M is the metabolic rate, in watts per square metre (W/m²);
- W is the effective mechanical power, in watts per square metre (W/m²);
- I_{cl} is the clothing insulation, in square metres kelvin per watt (m² · K/W);
- f_{cl} is the clothing surface area factor;
- t_a is the air temperature, in degrees Celsius (°C);
- \bar{t}_r is the mean radiant temperature, in degrees Celsius (°C);
- v_{ar} is the relative air velocity, in metres per second (m/s);
- p_a is the water vapour partial pressure, in pascals (Pa);
- h_c is the convective heat transfer coefficient, in watts per square metre kelvin [W/(m² · K)];
- t_{cl} is the clothing surface temperature, in degrees Celsius (°C).

Figure 26. *PMV equations (ISO, 2005)*

+ 3	Hot
+ 2	Warm
+ 1	Slightly warm
0	Neutral
- 1	Slightly cool
- 2	Cool
- 3	Cold

Figure 27. *7-point thermal sensation scale (ISO, 2005)*

In the EN-ISO-15251 standard by the International Organization for Standardization (CEN, 2007) sets requirements for the PMV based on four different categories, like shown in the figure below. The required category is based on the program of the room, like shown in the figure below as well. The figure also includes minimum and maximum operative temperature requirements stated by CEN (2007). This means the indoor air temperature may not exceed these values, regardless of the PMV score.

Category	Thermal state of the body as a whole	
	PPD %	Predicted Mean Vote
I	< 6	-0,2 < PMV < + 0,2
II	< 10	-0,5 < PMV < + 0,5
III	< 15	-0,7 < PMV < + 0,7
IV	> 15	PMV < -0,7; or +0,7 < PMV

Figure 28. PMV categories (ISO, 2007)

Type of building/ space	Category	Operative temperature °C	
		Minimum for heating (winter season), ~ 1,0 clo	Maximum for cooling (summer season), ~ 0,5 clo
Residential buildings: living spaces (bed rooms, drawing room, kitchen etc) Sedentary ~ 1,2 met	I	21,0	25,5
	II	20,0	26,0
	III	18,0	27,0
Residential buildings: other spaces: storages, halls, etc) Standing-walking ~ 1,6 met	I	18,0	
	II	16,0	
	III	14,0	
Single office (cellular office) Sedentary ~ 1,2 met	I	21,0	25,5
	II	20,0	26,0
	III	19,0	27,0
Landscape office (open plan office) Sedentary ~ 1,2 met	I	21,0	25,5
	II	20,0	26,0
	III	19,0	27,0
Conference room Sedentary ~ 1,2 met	I	21,0	25,5
	II	20,0	26,0
	III	19,0	27,0
Auditorium Sedentary ~ 1,2 met	I	21,0	25,5
	II	20,0	26,0
	III	19,0	27,0
Cafeteria/Restaurant Sedentary ~ 1,2 met	I	21,0	25,5
	II	20,0	26,0
	III	19,0	27,0
Classroom Sedentary ~ 1,2 met	I	21,0	25,0
	II	20,0	26,0
	III	19,0	27,0
Kindergarten Standing/walking ~ 1,4 met	I	19,0	24,5
	II	17,5	25,5
	III	16,5	26,0
Department store Standing-walking ~ 1,6 met	I	17,5	24,0
	II	16,0	25,0
	III	15,0	26,0

Figure 29. PMV categories requirements per program (ISO, 2007)

Predicted percentage dissatisfied (PPD)

ISO (2005), in the standard NEN-EN-ISO-7730, defines the predicted percentage dissatisfied as following:

“The PPD is an index that establishes a quantitative prediction of the percentage of thermally dissatisfied people who feel too cool or too warm. For the purposes of this International Standard, thermally dissatisfied people are those who will vote hot, warm, cool or cold on the 7-point thermal sensation scale” (ISO, 2005, p.14)

Thermally dissatisfied means a PMV vote which is not zero. The PPD is derived from the PMV using formula (5). (ISO, 2005). The relationship can also be expressed in a graph or a table containing key values, like shown in the figures below.

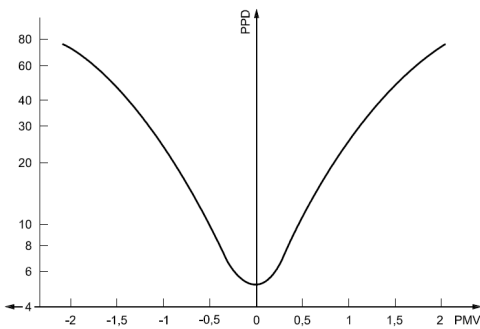


Figure 30. PPD graph (ISO, 2005)

PMV	PPD	Persons predicted to vote ^a		
		%		
		0	-1, 0 or +1	-2, -1, 0, +1 or +2
+2	75	5	25	70
+1	25	30	75	95
+0,5	10	55	90	98
0	5	60	95	100
-0,5	10	55	90	98
-1	25	30	75	95
-2	75	5	25	70

^a Based on experiments involving 1 300 subjects.

Figure 31. PPD key values table (ISO, 2005)

Adaptive thermal comfort

CEN standard NEN-EN-15251 (CEN, 2007), describes only requirements for the adaptive thermal comfort index for building without mechanical cooling systems. As stated previously, occupants of buildings without mechanical HVAC systems are more easily satisfied with the thermal environment. Therefore, only this buildings with this type of ventilation are included in the standard. The adaptive thermal comfort index is only valid for offices and dwellings, where windows can easily be opened and occupants have the availability to change their clothing, as stated in CEN standard NEN-EN-15251. The adaptive thermal comfort index uses the same four categories as the PMV and PPD for stating requirements for the ratio between the prevailing mean outdoor temperature, which is explained previously, and the operative temperature. The operative temperature is very similar to the mean radiant temperature (MRT). The operative temperature is invented by Dufton in 1929 as is calculated using the formula in the figure below.

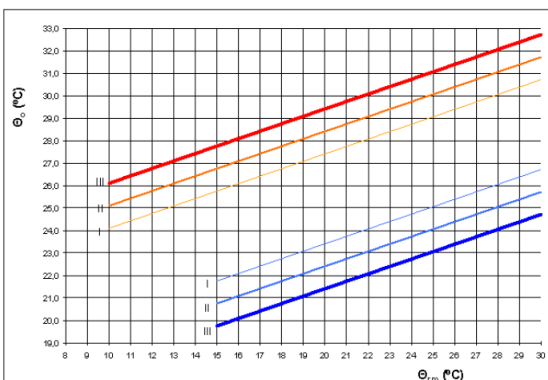


Figure 33. Adaptive thermal index graph (ISO, 2007)

$$t_o = \frac{(h_r t_{mr} + h_c t_a)}{h_r + h_c}$$

where,

h_c = convective heat transfer coefficient

h_r = linear radiative heat transfer coefficient

t_a = air temperature

t_{mr} = mean radiant temperature

Figure 32. Operative temperature formula (Dufton, 1929)

CBE Thermal Comfort Tool

In order to make the three main methods for quantifying thermal comfort more accessible to architectural designers, Tyler et al. (2017), representing the Center for the Built environment, developed the CBE Thermal Comfort Tool, which is freely accessible. By supplying the parameters, which are all explained previously, the tool calculates the PMV, PPD or adaptive thermal comfort index. These values are all calculated using the formulas shown previously. The tool can also be switched to the ASHRAE standard. Since this is an American standard, the ISO standard is more relevant for this research and thus the ASHRAE standard are disregarded in this research. The tool supplies resulting images like shown in the figures below.

For the PMV and PPD indexes, the tool gives resulting category and various psychrometric charts. The green area's on the chart show the first three categories and give extra insight in the effect of the various contributing components of the PMV and PPD results.

For the adaptive method, the tool gives a resulting graph of the adaptive chart. This gains more insight in the effect of the various contributing components of the adaptive thermal comfort index results.

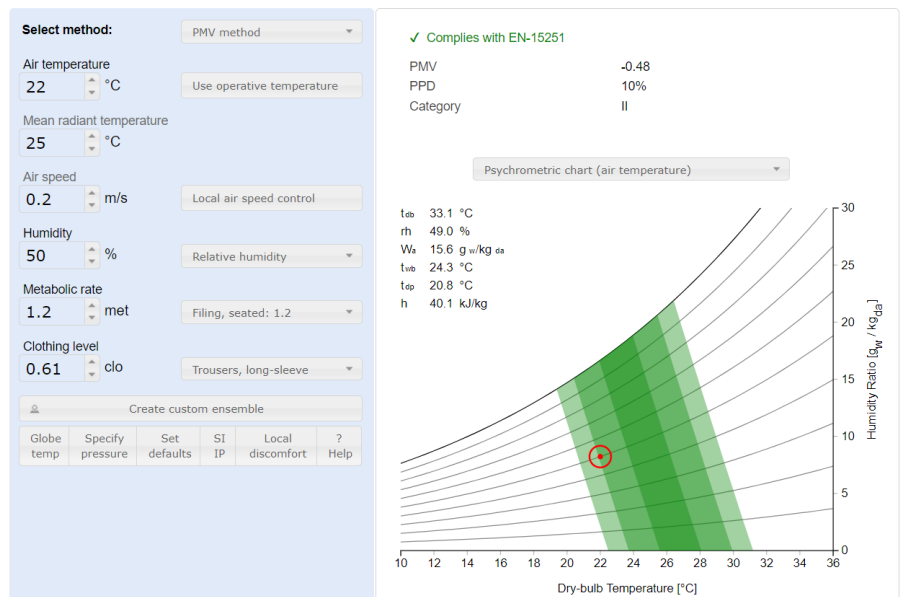


Figure 34. *CBE Thermal Comfort Tool PMV and PPD (Tyler et al., 2017)*

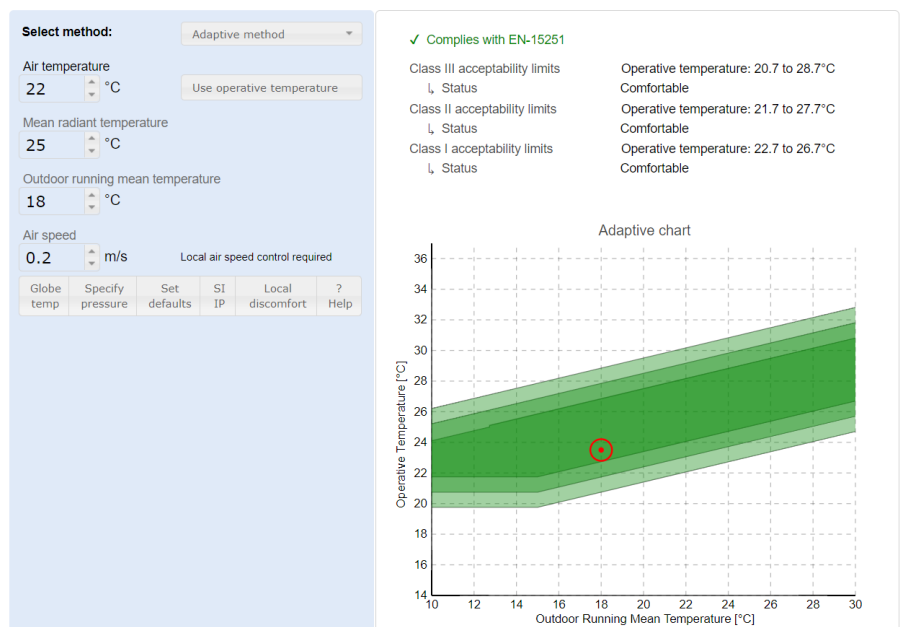


Figure 35. *CBE Thermal Comfort Tool Adaptive method (Tyler et al., 2017)*

2.2.4 - Relation to sun shading

The previous paragraphs have spoken about thermal comfort. One of the important contributing factors is the MRT, which is based on the temperature in the room. The sun has influence on the temperature inside the room, this process is called solar gain.

Solar gain is the energy from the sun which enters the room through the windows. More glass means more energy can enter the room. The energy entering the room will make the temperature rise. The amount of energy which enters the room per m^2 of glazing depends on four different parameters; the direction of the sun in relation to the building, the direct normal radiation of the sun-rays, the g-value of the glazing and the sun shading.

Direction of the sun:

The direction of the sun is depending on the time of the day, the day of the year, and the location on the globe. Towards the poles, the inclination of the sun is much lower compared to the equatorial regions. The figure below shows the annual sun paths at three different latitudes. Generally speaking, buildings on the northern hemisphere will have more solar gain at the south façade, as shown in the figure below. For the southern hemisphere this is vice versa.

Direct normal radiation:

The direct normal radiation is the amount of energy received from the sun parallel to its direction. The amount of normal radiation, like the direction of the sun, differs throughout the days, seasons and location on the globe. The image below shows an overview of how the annual and daily average normal radiation around the globe.

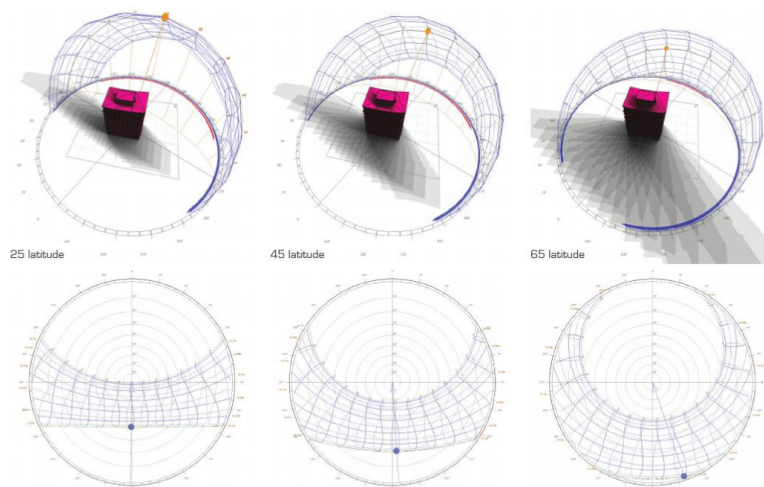


Figure 36. Annual sun-path's for different latitudes (Watt, 2016)

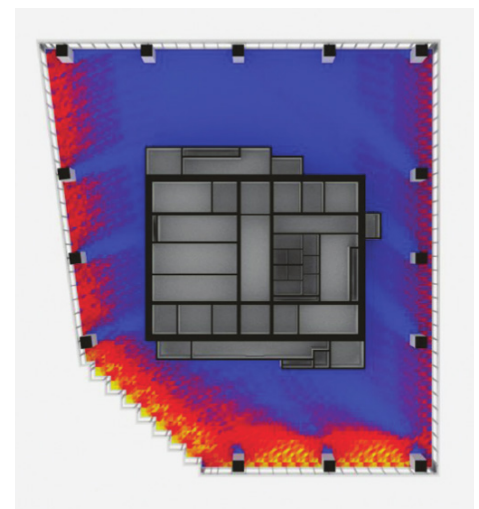


Figure 37. Solar gain in floorplan (Watt, 2016)

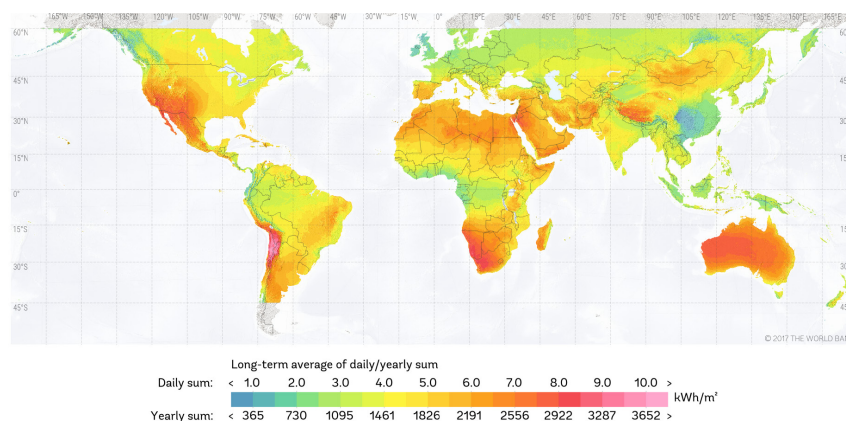


Figure 38. Global average normal direct radiation values (google.com)

Glazing g-value:

The g-value, also referred to as ZTA-value in Dutch literature, is a material property of the glazing. It describes how much of the solar radiation energy gets inside the building, expressed in a percentage of the total incoming solar radiation, as shown in the image below. The first two factors; direction and direct normal radiation determine how much infra-red radiation falls onto the window. The g-value determines how much of this energy enters the room behind the glazing.

Sun shading:

The sun shading can be designed to counteract solar gain. This can be done in various ways. A simple example of a sun shading system is the solar screen, which can be lowered in front of the window. In essence the screen has a g-value, just like the glazing and thus reduces the amount of energy falling onto the window and therefore the amount of energy entering the room. Another method is to apply a reflective coating to the glazing which will reflect a portion of the radiation back into the atmosphere. Yet another method is to place geometry in front of the window, blocking the solar radiation. This way the sun shading can influence the amount of solar gain. By doing so, the sun shading will also influence the level of thermal comfort experienced by occupants in the room. (Kuhn, Bühler and Platzer, 2001). Different strategies for controlling the amount of solar gain will be given in sections 4.2 and 6.1

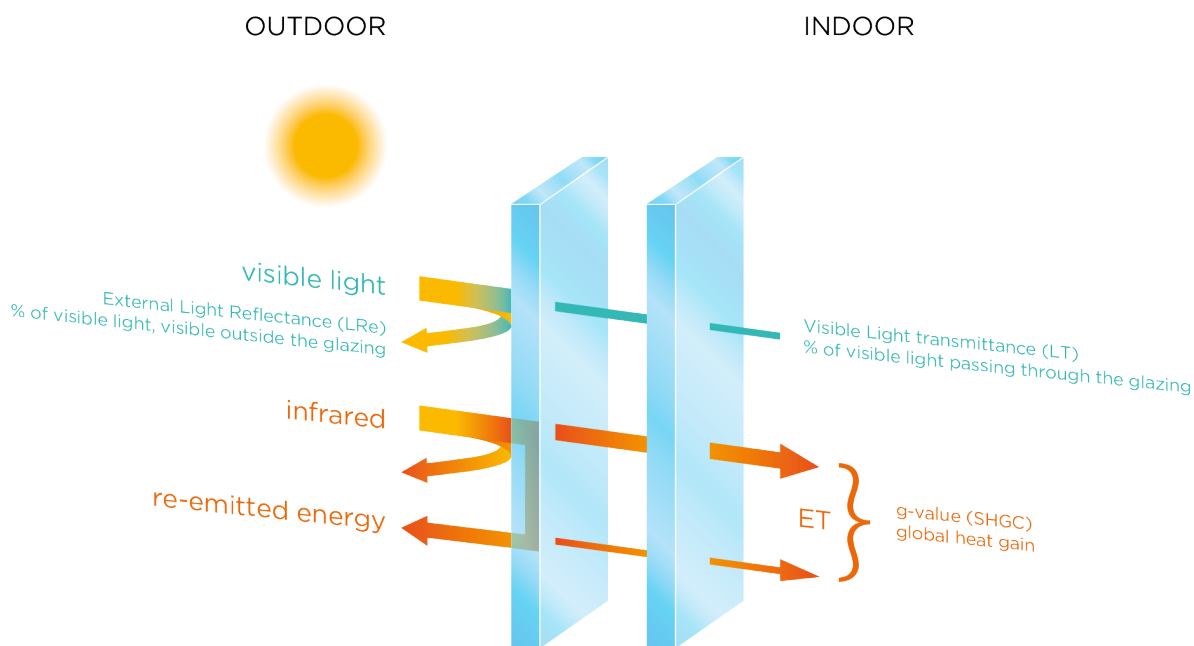


Figure 39. *G-value of a window* (www.greenbuilding.saint-gobain.com)

2.2.5 - References

1. ASHRAE Standard 55-2017 (2017), Thermal Environmental Conditions for Human Occupancy. Atlanta, GA
2. Bell, S. (2011). A beginner's guide to humidity measurement. Queen's Printer and Controller of HMSO.
3. Carlucci, S. (2013). Thermal comfort assessment of buildings. [Milano]: Milano.
4. de Dear, R. (2002). Thermal comfort in naturally ventilated buildings: revisions to ASHRAE Standard 55. *Energy and Buildings*, 34(6), pp.549-561.
5. de Dear, R. (1998). Developing an Adaptive Model of Thermal Comfort and Preference. *ASHRAE Transactions*, 104.
6. Engineering ToolBox, (2004). Clo - Clothing and Thermal Insulation. [online] Available at: https://www.engineeringtoolbox.com/clo-clothing-thermal-insulation-d_732.html
7. Engineering ToolBox, (2004). Dry Bulb, Wet Bulb and Dew Point Temperatures. [online] Available at: https://www.engineeringtoolbox.com/dry-wet-bulb-dew-point-air-d_682.htm
8. Engineering ToolBox, (2004). Met - Metabolic Rate. [online] Available at: https://www.engineeringtoolbox.com/met-metabolic-rate-d_733.html
9. Engineering ToolBox, (2004). Relative Humidity in Air. [online] Available at: https://www.engineeringtoolbox.com/relative-humidity-air-d_687.html
10. European Committee for Standardization (CEN). (2007). NEN-EN-15251: Indoor environmental input parameters for design and assessment of energy performance of buildings addressing indoor air quality, thermal environment, lighting and acoustics.
11. International Committee for Standardization (ISO). (2005). NEN-EN-ISO-7730: Ergonomics of the thermal environment – Analytical determination and interpretation of thermal comfort using calculations of the PMV and PPD indices and local thermal comfort criteria.
12. International Committee for Standardization (ISO). (2007). NEN-EN-ISO-9920: Ergonomics of the thermal environment -Estimation of thermal insulation and water vapour resistance of a clothing ensemble
13. International Committee for Standardization (ISO). (2004). NEN-EN-ISO-8996: Ergonomics of the thermal environment -Determination of metabolic rate
14. Hoyt Tyler, Schiavon Stefano, Piccioli Alberto, Cheung Toby, Moon Dustin, and Steinfeld Kyle, 2017, CBE Thermal Comfort Tool. Center for the Built Environment, University of California Berkeley, <http://comfort.cbe.berkeley.edu/>
15. MacPherson, R. (1962). The Assessment of the Thermal Environment. A Review. *Occupational and Environmental Medicine*, 19(3), pp.151-164.
16. Fanger, P.O. (1970). *Thermal Comfort*. Danish Technical Press, Copenhagen
17. Talghani et al. (2013). A review into thermal comfort in buildings. *Renewable and Sustainable Energy Reviews*, 26.

18. Kuhn, T., Bühler, C. and Platzler, W. (2001). Evaluation of overheating protection with sun-shading systems. *Solar Energy*, 69, pp.59-74.
19. Watts, A. (2016). *Modern construction handbook*. Retrieved from <https://ebookcentral-proquest-com.tudelft.idm.oclc.org>

2.3 - Fundamentals of performative computational architecture

As stated in the introduction of this report, the performative computational Architecture (PCA) method is an emerging design tool with lots of applications across the field of architectural design. (Ekici, Cubukcuoglu, Turrin, and Sariyildiz, 2019) (Shi and Yang, 2013). This section will first explain the principles of the PCA method and high-light some of its promising applications. After wards, the section will describe the PCA more in-depth according to its three-stepped framework, in relation to sun shading design.

2.3.1 - Principles of PCA

Performative computational architecture is based on a three-phase cycle which is iteratively looped until the best solution is found. The first step is generating geometry, based on input parameters. The second step is about evaluating the performance of the geometry using digital simulations. The third step uses a search method to find the most desirable performance by altering the input parameters. This is often done by using an evolutionary algorithm. (Ekici et al., 2019). The PCA method is shown below in figure below.

Another interpretation of the PCA method is an automatized upgrade of the performance driven architectural design process, which has gained in popularity among architects over the past few decades. (Shi and Yang, 2013). In principle the philosophy of performance driven design is to make design choices based on performance analysis instead of the conventional architectural qualities of space and form. A graphic presentation of the performance driven architectural design process is given in figure 41. This workflow does also contain an iterative loop, similar to the PCA process. The main advantage of the PCA process over the performance driven design process, is the automatization of the adjusting of the conceptual design by properly implementing the form-finding phase and the use of search algorithms in the optimisation phase.

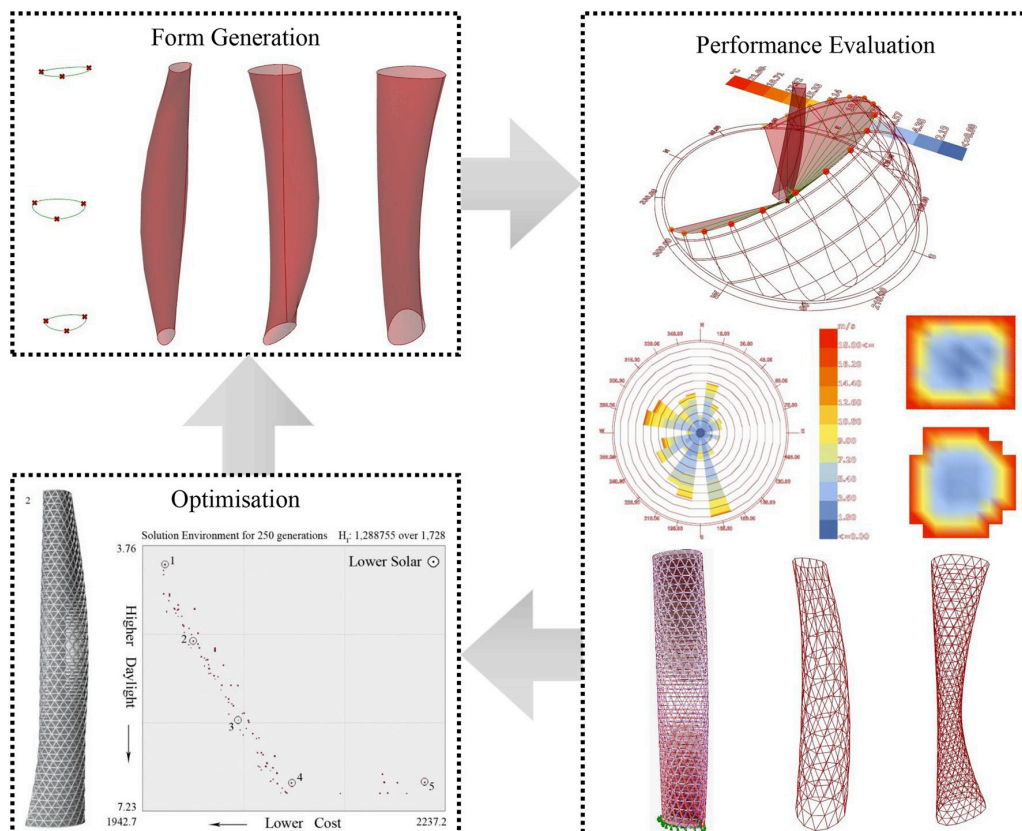


Figure 40. *The performative computational architecture framework (Ekici et al., 2019)*

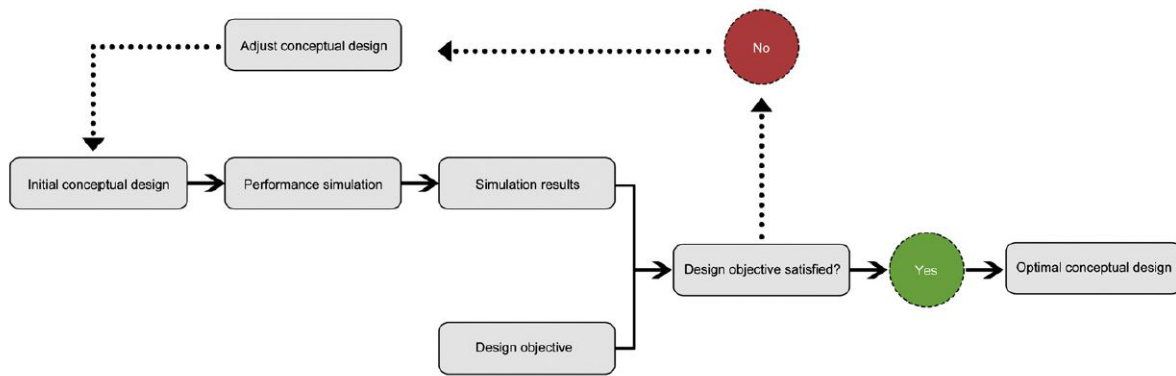


Figure 43. *The performance driven design workflow (Shi and Yang, 2013)*

The paper of Ekici et al. (2019) tries to summarize the evolution of the method over the period from 1998 to 2018 by reviewing 100 researches involving the PCA method. In order to systematically investigate the researches, they needed to be categorized. Therefore, the PCA taxonomy can be used (Ekici et al., 2019). The taxonomy consists of four main categories, subdivided in sub-categories. The taxonomy and pie chart showing the distribution of categories in the 100 researches reviewed by Ekici et al. (2019). are shown in the figures below. It is interesting to see that the sustainability category is domination the field of PCA applications.

As the taxonomy categorizes the precedes studies on PCA according to the nature of their optimization process goal, it does not give insight which aspects of the building are optimized. Ekici et al. (2019) describes these aspects as 'form-finding parameters'. Figure 43 shows the number of papers available within the 100 researches of the review per form-finding parameter. It is interesting to see that window-to-wall ratio and shading are the two most dominant parameters. This concludes that PCA has a lot of potential for optimizing the shape of the façade openings and sun shading systems based on the performance on various sub-categories of the sustainability category within the PCA taxonomy.

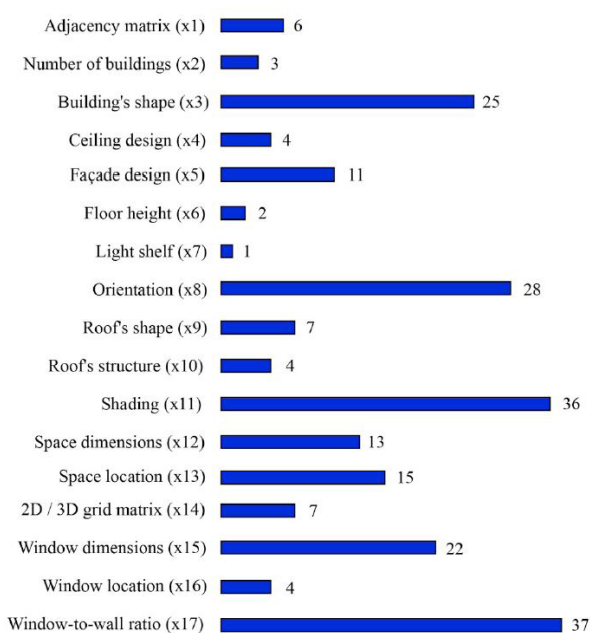


Figure 42. *Number of available research papers per form-finding parameter (Ekici et al., 2019)*

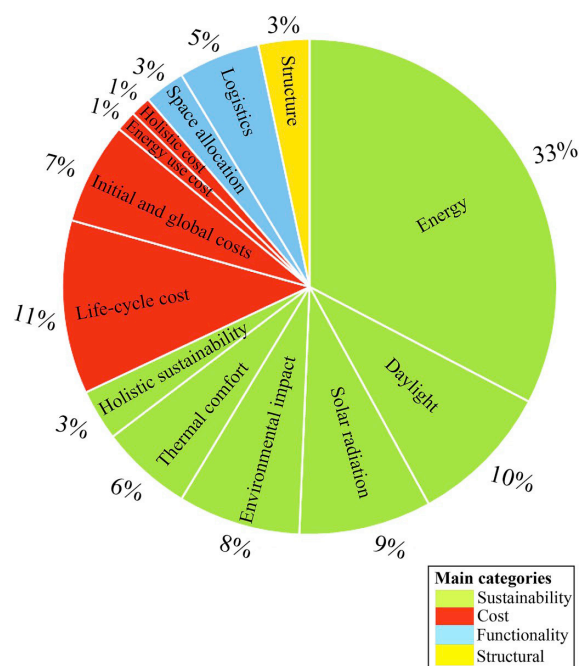


Figure 41. *Distributions of sub-categories (Ekici et al., 2019)*

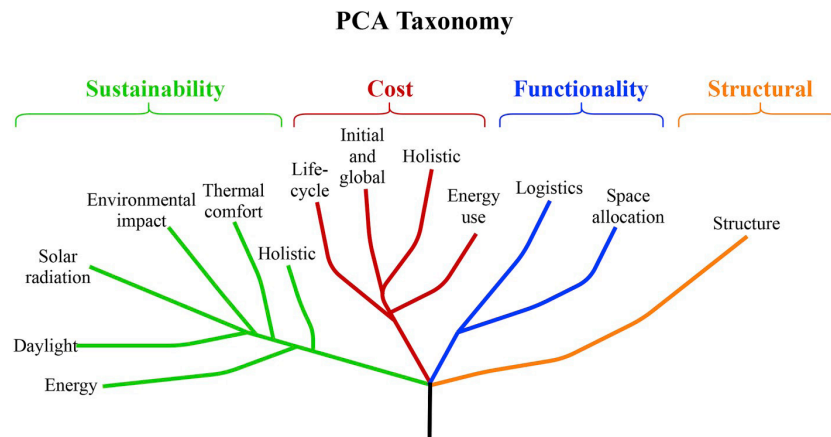


Figure 44. PCA taxonomy (Ekici et al., 2019)

The indication of the potential for sun shading design is confirmed by Eltaweel & Yuehong (2017) in their literature review on applications for parametric design for improving daylight availability and energy saving. The review contains nine in-depth researches about optimizing sun shading devices for visual comfort using the PCA method. An example is given to illustrate a simple implementation of the PCA method. The goal in this example is to find the optimal angle for the louvers to bring as much indirect light room, which often contributes to an increased level of visual comfort for the building occupants. The example is illustrated in the figure below. If this example is put into the PCA framework it can be broken down in three steps:

1. Form-finding: Geometry for the louvers was made using a parametric script. The main parameters for the PCA process is the angle of the louvers. In this example the software Grasshopper was used. The advantages of this software will be elaborated in the next paragraph.
2. Performance evaluation: In this example the performance was the amount of light on the ceiling of a fictional room behind the louvers. How this performance is evaluated exactly is not of importance for the example, but this paper will elaborate further on this phase in paragraph 2.3.3
3. Optimization: In this case only a single optimizing objective is used; maximize the amount of indirect light on the ceiling. In the example is stated 'generative algorithms' are used for this phase, but no further elaboration is given. This paper will address the optimization phase in paragraph 2.3.4

The review concludes the following, stating that PCA methods will be a promising direction for the design of sun shading systems for the future:

"The use of parametric design within daylight can improve the performance of buildings' design, daylighting and energy saving in the early stages of design. Link with buildings' thermal performance simulation and visual comfort will be an attractive direction for parametric design in daylighting for future research." "The use of parametric design within daylight can improve the performance of buildings' design, daylighting and energy saving in the early stages of design. Link with buildings' thermal performance simulation and visual comfort will be an attractive direction for parametric design in daylighting for future research." (Eltaweel & , 2017, p. 1102).

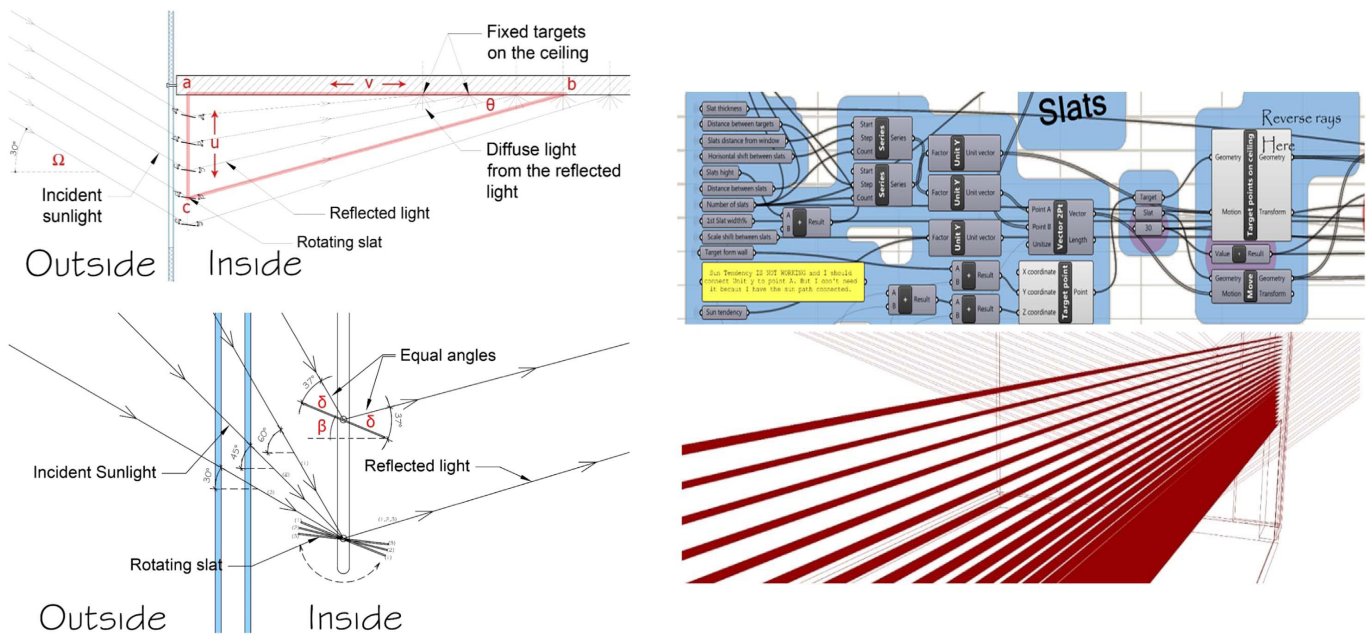


Figure 45. PCA shading application diagram (Eltaweel & Yuehong, 2017)

2.3.2 - The form-finding phase of PCA for sun shading design

The first step of the PCA method is the form-finding phase. Within the framework form-finding is defined as:

“The architectural design exploration aiming to satisfy predetermined building performance aspects via computational optimisation in order to provide sufficient information to the decision makers.” (Ekici et al., 2019, p.358)

This main goal in this phase is to design geometry based on using parametric modelling. When used for form finding, like this phase of the PCA method, parametric modelling is the process of making a geometrical representation with parameterized components or attributes, meaning they are derived from input parameters. (Barrios, 2005). In order to explain parametric modelling, the first important concept is the input parameters. A parameter can be defined as following:

“A quantity whose value is selected for the particular circumstances and in relation to which other variable quantities may be expressed” (Oxford Dictionary, 2019)

In the context of parametric modelling this quantity is a parameter of a geometrical shape, such as a length, width, height, angle or diameter. In other cases the parameters might also be a number defining an amount of repetitions or number of iterations. All geometry generated by the parametric script is derived from these input parameters using mathematical alterations, often made using some kind of scripting or coding. This way the resulting geometry will change according to changes made to the values of the input parameters, being the essence of parametric modelling in the form-finding phase of the PCA method.

There are many solutions available for parametric geometry modelling. However, solutions offering integration with performance evaluation and optimisation capabilities are limited. In addition, a proper 3D user-friendly interface is also important for applying parametric modelling in architectural design, even further limiting the scope of appropriate tools (Wortmann, 2018). Wortmann (2018) also identifies a selection of three tools for parametric modelling fitting the scope.

The first one is Grasshopper, developed by Rutten (2010). This software package is integrated in Rhinoceros 3D, a software package for 3D modelling of geometry gaining in popularity due to its relatively prominent ability to work with complex geometry. Grasshopper offers options to integrate other plug-ins for the performance evaluation and optimisation phase (Wortmann, 2018). The second tool is Dynamo. This tool has similar capabilities as Grasshopper, the main difference being the host software. Grasshopper is integrated in Rhinoceros, whereas Dynamo is integrated within Autodesk Revit. Revit is one of the leading software packages for Building Information Modelling (BIM) and is used commonly in commercial architectural practice. Dynamo offers the option to use other plug-ins for the other two phases as well, although the number of available plug-ins is more limited compared to Grasshopper (Wortmann, 2018). The third tool is Design builder. The main benefit of this tool is it offers options for conducting all three phases of the PCA process within the same interface and does not rely on external plug-ins. At the same time this feature also limits the modelling freedom in regard to the form-finding phase (Wortmann, 2018).

A review about the use of parametric modelling tools, including 23 researches is made by Touloupaki and Theodosiou (2017). The review identified Grasshopper in combination with Rhinoceros as the dominating software for the application of architectural design. However, Dynamo is gaining in popularity due to its direct integration with BIM software (Touloupaki and Theodosiou, 2017). Based on this conclusion, the assumption is made that Grasshopper will be used for the practical part of this research as well.

The software of Grasshopper relies on blocks of coding called components. The coding is hidden inside the component, only revealing the in- and outputs of the script. Components can be drawn onto a canvas to connect the in- and outputs. The main advantages of Grasshopper are its graphic interface, making it reasonably easy to use for architect and building technology engineers and the fact it's open source. This means other people can make new components, which can be downloaded for free or a small fee. The developers of Grasshopper state the following about the software:

“For designers who are exploring new shapes using generative algorithms, Grasshopper® is a graphical algorithm editor tightly integrated with Rhino’s 3-D modelling tools. Unlike RhinoScript, Grasshopper requires no knowledge of programming or scripting, but still allows designers to build form generators from the simple to the awe-inspiring.”
(Grasshopper3d.com, 2019)

The figure below shown an example of a Grasshopper script being used to generate a piece of geometry. In this case a series of circles which make up the base shape of a vase. The components called 'Length' 'V count' and 'Width' represent the input parameters. These values can be altered, with altering of the vase shape as a result. The same principle applies to design geometry for sun shading, like the example given by Eltaweel and Yuehong (2017) where the input parameter is the angle of the louvers .

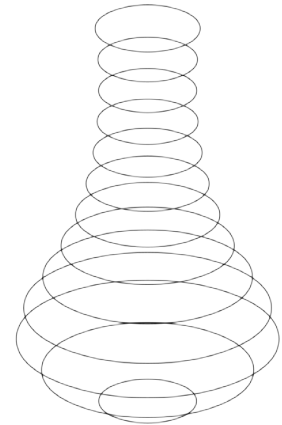
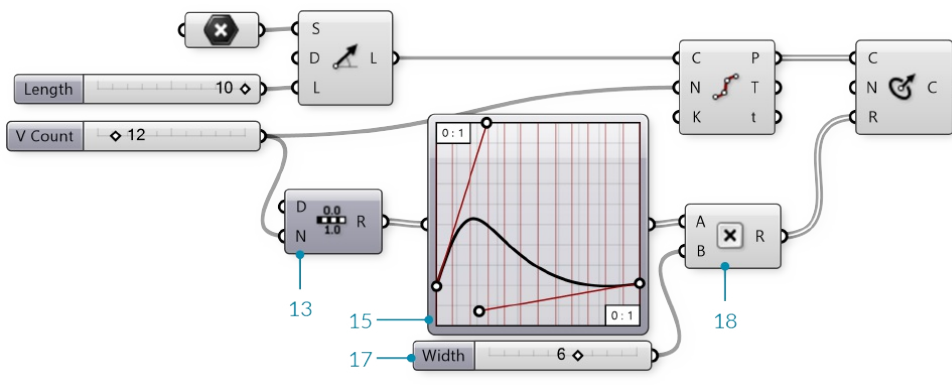


Figure 46. An example of a Grasshopper script (Mode lab, 2019)

When parametric modelling is used in the form-finding phase of the PCA method for designing sun shading it means the concept of the shading needs to be parameterised. The process of parametrization can be defined as rationalization and translation of requirements into a parametric structure. (Gane and Haymaker, 2010). Important in the process is to identify the input parameters and define a logical, hierarchical associations in the sun shading conceptual shape. These associations can be translated to mathematical relations defining the shape. These relations can be recreated using coding, which is available in components in software packages as Grasshopper. By following the process of parameterization a shading concept is transformed into a parametric model.

Setting up a parametric model of the sun shading geometry of chosen concepts will a design task, as explained in the introduction of this report. The definition of the inputs of this parametric model is dependent on the typology of the chosen sun shading systems. A more in depth analysis of different parametric models for sun shading systems is given in section 5 of the review.

2.3.3 - The performance evaluation phase of PCA for sun shading design

The second step of the PCA method is the performance evaluation phase. It is simply defined as measuring the performance of geometry on certain objectives. Within the framework performance evaluation is important because:

“The predictions and numeric assessments of performance aspects can be integrated into the architectural design process in order to investigate how well the design eventually meets the requirements.” (Ekici et al., 2019, p.358)

The performance evaluation gives the designer feedback on design choices in the form of measurable performance values. This allow the designers to systematically assess the capability of a certain design choice to satisfy various requirements. The performance evaluation is a more reliable source of feedback compared to the traditional way of evaluating design alternatives using intuition, know-how and judgment. (Hubka and Eder, 1987). In the relation to sun shading design, common performance indicators are visual and thermal comfort metrics.

There are many available tools for evaluating the performance of visual and thermal comfort. An overview of some of the common available tools is given by Kirimat et al. (2016) in a review of simulation techniques for sun shading performance. The review included 109 researches on sun shading simulations conducted in the period between 1996 and 2015. The review concluded Energyplus and Radiance to be the two leading tools for the performance analysis phase (see fig. 48). Other available tools include; DOE-2, IES-VE, TAS, TRNSYS, ESP-r, Lightscape, Designbuilding, Fluent, DIVA, Ecotect and IENUS.

These two performance evaluation tools can be integrated in Grasshopper, the software of choice for the form-find phase, as explained in the previous paragraph. The connection between Grasshopper and Energyplus / Radiance can be made using the plug-ins of Ladybug (LB) and Honeybee (HB). Therefore, these tools are assumed to be used in the continuation of this research.

LB & HB allow the designer to analyze and visualize the effects of environmental data packages on geometry. This environmental data comes in the form of EPW files, which are freely accessible online. The developers state the following about Ladybug and Honeybee:

“Ladybug allows you to import and analyze standard weather data in Grasshopper; draw diagrams like Sun-path, wind-rose, radiation-rose, etc; customize the diagrams in several ways; run radiation analysis, shadow studies, and view analysis. Honeybee connects Grasshopper3D to validated simulation engines such as Energyplus, Radiance, Daysim and OpenStudio for building energy, comfort, daylighting and lighting simulation.” (Food4rhino, 2019)

There are various possibilities for evaluating the performance of geometry based on this weather data, like shown in the figure below. Because of the scope of this research, only possibilities for evaluating visual and thermal comfort will be discussed in this paragraph. The performance evaluation phase in relation to sun shading design can be subdivided in three sub-phases:

1. The preparation of the evaluation setup
2. The Radiance/energy plus simulation
3. The interpretation of the results

The next few paragraphs will discuss each sub-phase in depth in relation to the available tools in Ladybug & Honeybee

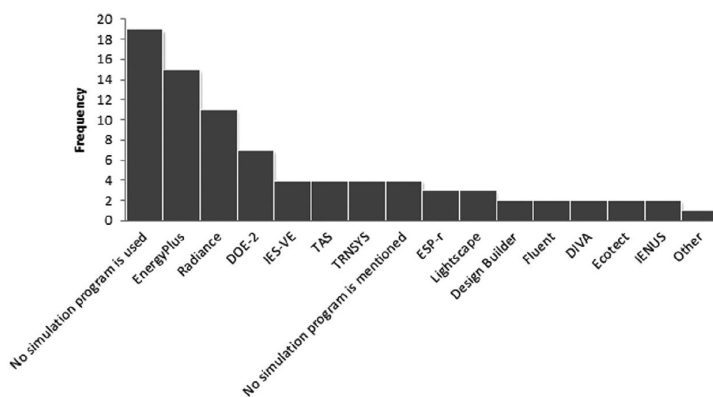


Figure 48. *Distribution of the tools for performance evaluation (Kirimat et al., 2016)*

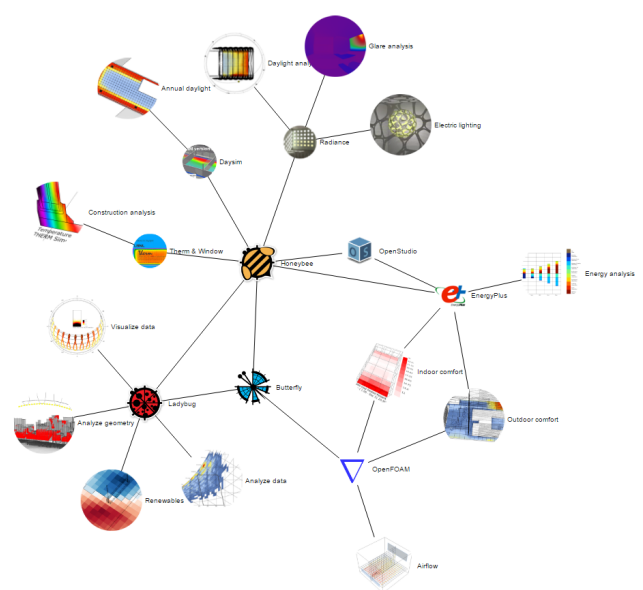


Figure 47. *Possibilities for performance evaluation in LB & HB (Food4rhino, 2019)*

The preparation of the evaluation setup

The evaluation set-up to measure the performance of visual comfort is comparable to a physical set-up. An example for this is the lighting study conducted by Dubois (2001). He created a test room filled with sensors to measure the indoor illuminance. The sensors are placed in a grid like shown in the figure below. To measure glare a camera was placed in the room to mimic the human eye. All of this was done in a room dressed like a common office and an empty room for reference.

Thermal comfort is defined by contributing factors which are equal across the room. Therefore, these digital sensors don't have to be placed in the model, but will be generated by the software itself.

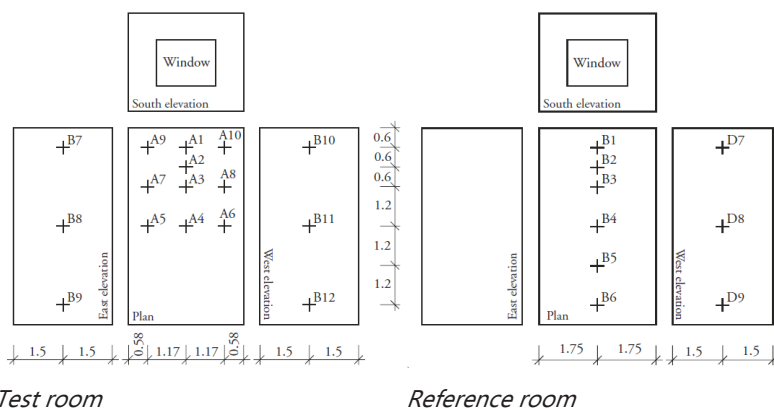
The test room can be created using either Grasshopper or Rhino geometry. Afterwards LB & HB components are used to apply information to the surfaces making up the digital evaluation setup. This is done in the form of materials. These materials include parameters like conductivity, reflectivity, g-values for glazing, etc. The software also includes components for setting up an analysis grid, similar to the grid of sensors in the research of Dubois (2001).



Figure 49. Test setup exterior (Dubois, 2001)



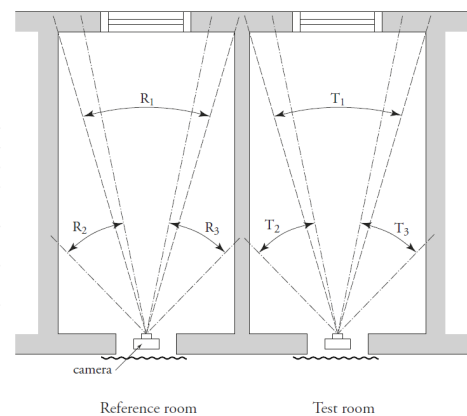
Figure 50. Test setup interior (Dubois, 2001)



Test room

Reference room

Figure 51. Placement of illuminance sensors (Dubois, 2001)



Reference room

Test room

Figure 52. Placement of luminance camera (Dubois, 2001)

Preparation components in LB & HB

Honeybee works with two kind of materials; Radiance (RAD) materials and Energyplus (EP) materials. The first one is used for the calculations for visual comfort and the second for thermal comfort calculations. Figure 52 shows the material components and their inputs for the RAD materials and EP materials. All geometry in the model needs to have a material assigned. For the thermal comfort analysis, the test room geometry needs to have some more data assigned. For this the components in the image 53 can be used. The test point component of LB & HB is used to create an analysis grid of digital measurement instruments with the test room to mimic the situation as created by Dubois (2001) in his physical performance evaluation. This component is shown in fig. 54

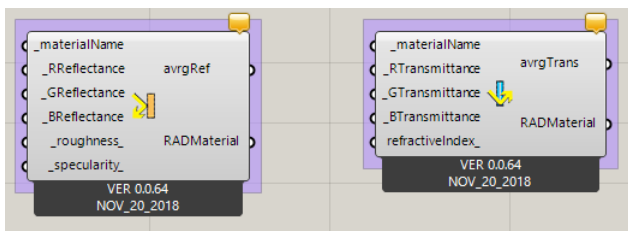


Figure 53. Radiance (RAD) material components in HB & LB (by author)

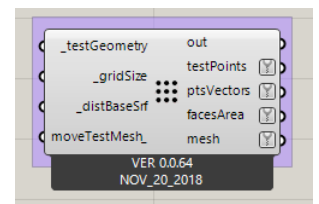


Figure 56. Analysis grid component in HB & LB (by author)

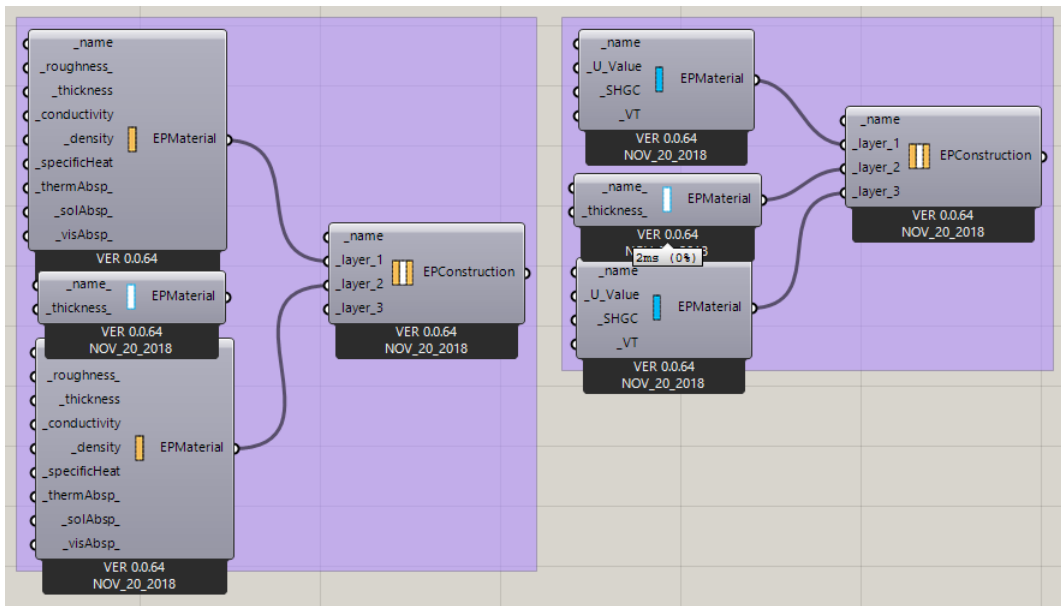


Figure 54. Energy Plus (EP) material components in HB & LB (by author)

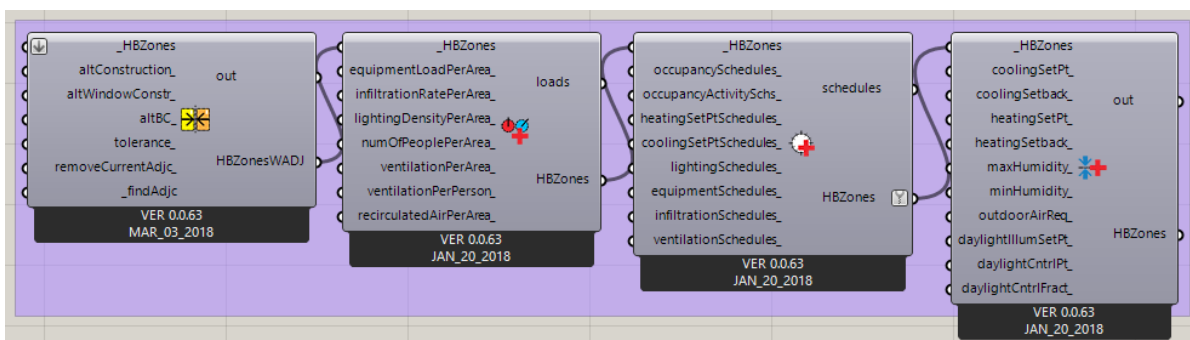


Figure 55. Additional geometry information for thermal simulation components in HB & LB (by author)

The Radiance/energy plus simulation

The data of the evaluation setup is fed to the core-components that run the simulations. These simulations are based on the formula's explained in section 1 and 2 of this literature review, various other formula's and ray-tracing algorithms. The relation of LB & HB to the simulation engines is shown in figure 55. Simulations for visual comfort are done by Dayism and Radiance, simulations for thermal comfort by Openstudio and Energyplus. This figure also indicates the need for an EPW file, containing the weather data. These core-components also need some general information about the analysis; the analysis period and the analysis type. The analysis period determined the period within the year taken into account and the type determined the what quantities need to be simulated.

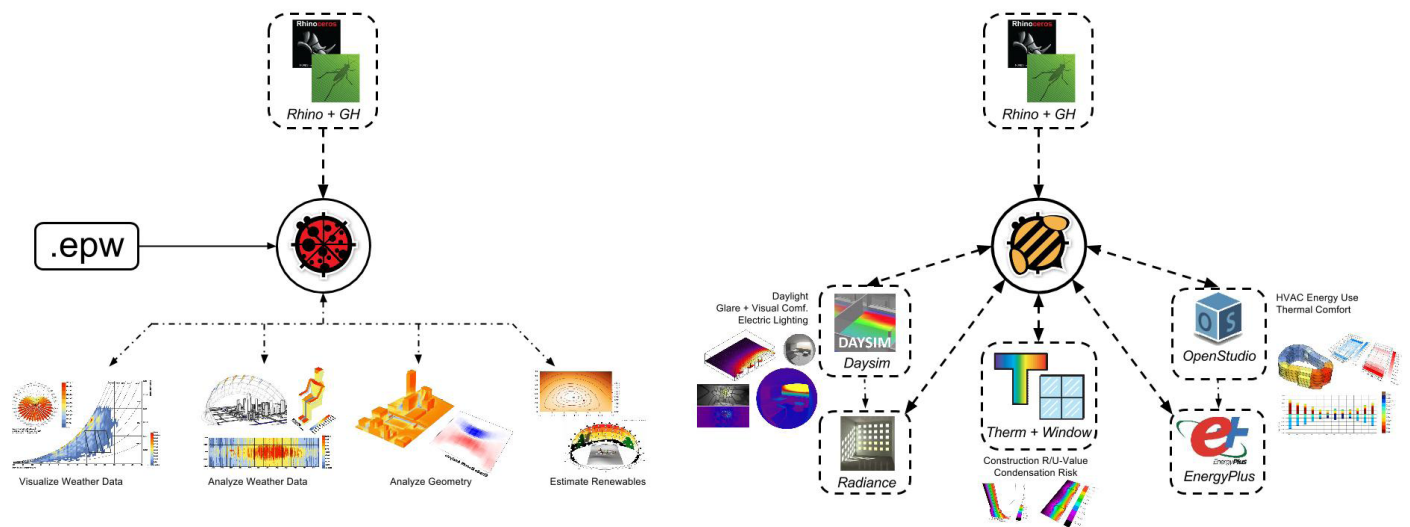


Figure 57. Relation between HB & LB and the simulation software (Food4rhino, 2019)

Radiance/Energy Plus components in LB & HB

The Radiance engine, for daylight calculations requires the analysis type settings in the form of recipes. The first one is for daylight factor simulations, the second one for absolute illuminance simulations. The last type component is a stand-alone engine and is used for the glare simulations, as shown in figure 56. The thermal comfort simulations are done by Energyplus. The options for the analysis type are set by using the components in the image 56.

The components in figure 57 are used to set the analysis period for the various analyses. For visual comfort simulations this means picking some specific key moments and for the thermal comfort calculations this regards an entire year.

EPW files contains climate data of various location around the world. All available data within the file can be extracted using the component shown in figure 58. These files can be freely accessed at: [https:// Energyplus.net/weather](https://Energyplus.net/weather).

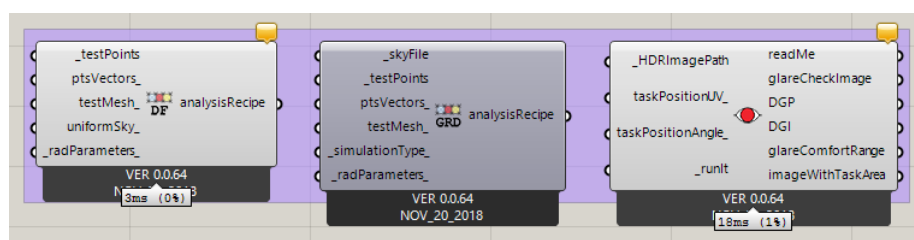


Figure 58. LB & HB components for DF, absolute illuminance and glare simulations (by author)

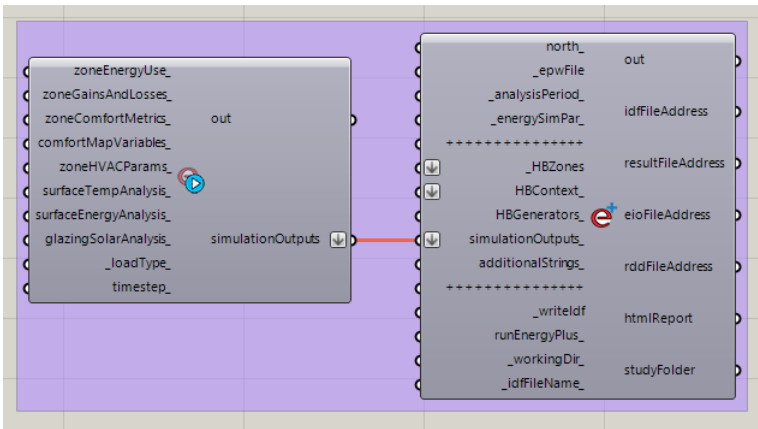


Figure 59. LB & HB components thermal comfort simulations (by author)

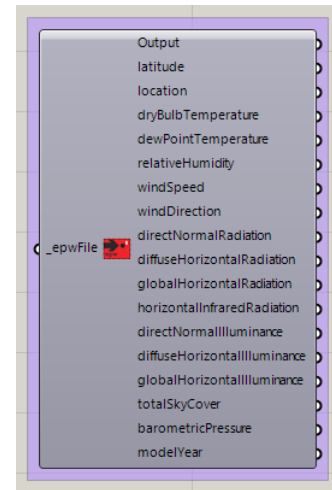


Figure 60. LB & HB EPW file (by author)

The interpretation of the results

The last step is the interpretation of the results. Where the core-components only measure direct quantities by a digital simulation, other components are needed to transform these direct quantities to indices addressing visual and thermal comfort, such as the Daylight factor, PMV or adaptive comfort method. The components doing this translation rely on various formulas shown in section 1 and 2 combined with data directly from the EPW file such as the outside dry bulb temperature or the global outdoor illumination.

Interpretation components in LB & HB

The results for the daylight factor and the absolute illuminance values can be read directly from the Radiance engine component. The results from the glare analysis can be read from the independent glare simulation component. Both components are shown in the figure 59

The results for the thermal comfort simulation can be read from the Energyplus engine component. In order to translate the results to PMV or PPD values, the left component in the image 60 can be used. The right component is for translating to an adaptive comfort value.

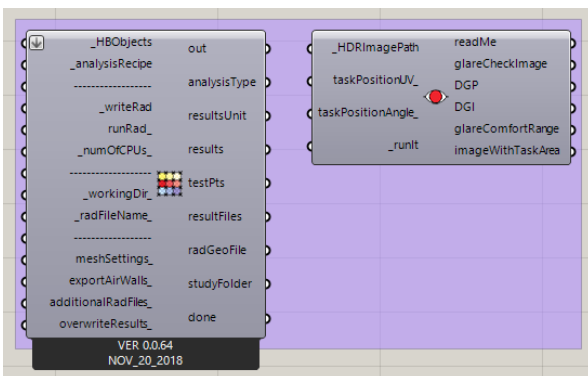


Figure 61. LB & HB components for interpreting visual comfort (by author)

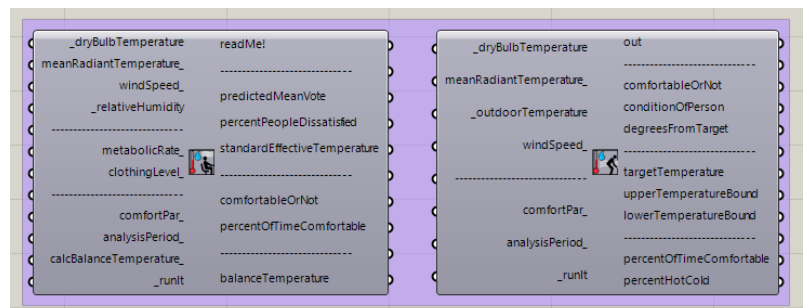


Figure 62. LB & HB components for interpreting thermal comfort (by author)

2.3.4 - The optimization phase of PCA sun shading design

The final phase of the PCA method is the optimization phase. Hubka and Eder (1987) 30 years ago already stated that performance evaluation is a very useful form of feedback for designers to make design choices. The main goal in the optimization phase is to let the computer make this design choices instead. These choices come in the form of altering the input parameters of the form-finding phase, based on the results of the performance evaluation. Therefore, the optimization process requires a conditional statement. In this case the conditional statement would involve the level of visual and thermal comfort. This way they search for a better design options within the boundaries of the form-finding input parameters. The exact way of searching can be conducted in many ways and is always expressed in al algorithm. Multiple researches have shown optimization methods based on metaheuristics are the best suited for the PCA method. (Machairas, Tsangrassoulis and Axarli, 2014; Evins, 2013; Ciftcioglu, Sariyildiz and Bitterman, 2007). This is because they often find near-perfect results in a reasonable time, can handle larger numbers of input parameters and avoid local minimums and maximums compared to other searching algorithms. (Huang and Niu, 2016; Machairas, Tsangrassoulis and Axarli, 2014; Michalewicz and Fogel, 2004). The metaheuristic methods are based on phenomena observed in nature and can be divided in evolutionary computation (EC) and swarm intelligence (SI), which are schematically shown in image 61 and defined as following:

“Swarm intelligence (SI) and evolutionary computation (EC) are two powerful optimisation methods in metaheuristics. SI uses intelligent multi-agent systems inspired by the behaviour of social swarms. Conversely, EC uses procedures inspired by the biological evolution of the Darwinian theory” (Ekici et al., 2019, p.356)

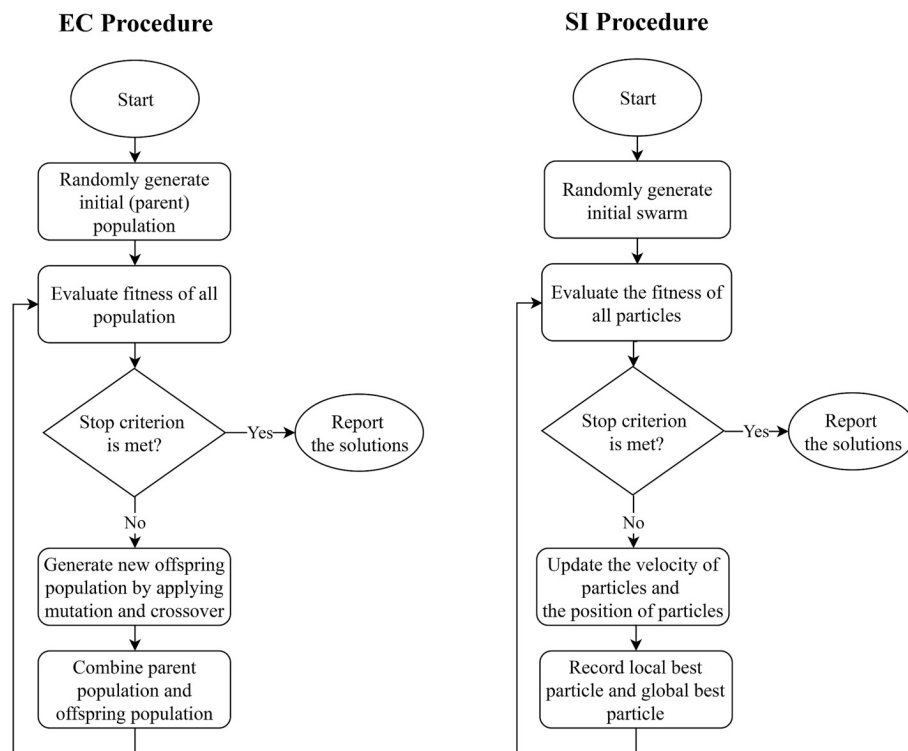


Figure 63. *The schematic procedures of the evolutionary computation and swarm intelligence categories (Ekici et al., 2019)*

Evolutionary computation

In evolutionary computation, the algorithm starts with a random combination of input parameters values which are encoded in virtual genes. This group forms the initial population and are crossed over to form a new generation of input values. Input values with bad results are removed from the gene pool, this way each generation will have better performance results. In order to prevent local minimums and maximums, a small portion of the population is mutated. This way the process results in a final set of values for the input parameters with the optimal performance. Two common algorithms within this category are the genetic algorithm (GA) proposed by Holland and Goldberg (1989) and the differential evolution (DE), invented by Storn and Price (2019).

Swarm intelligence

This category focuses on finding relation between the input parameters themselves and in relation to the performance evaluation. The methods are based on the behaviour of swarms of animals, such as bees, ants, birds, are land mammals living in groups. The swarm knows more than the individual members, because information about interaction with the environment is being shared. This allows for finding better performance within the range of values for the input parameters. Two common algorithms within the category are the Particle swarm optimisation (PSO), discovered by Eberhart and Kennedy (1995) and the ant colony optimisation (ACO) proposed by Dorigo, Birattari, and Stutzle (2006).

The algorithm of choice

Ekici et al. (2019) conclude the Generic algorithm was most commonly used for single objective optimization and the NSGA-II method for multi-objective optimizations. The distribution of used algorithms and amounts of objectives among the 100 researches reviewed by Ekici et al. (2019) is shown in the image below:

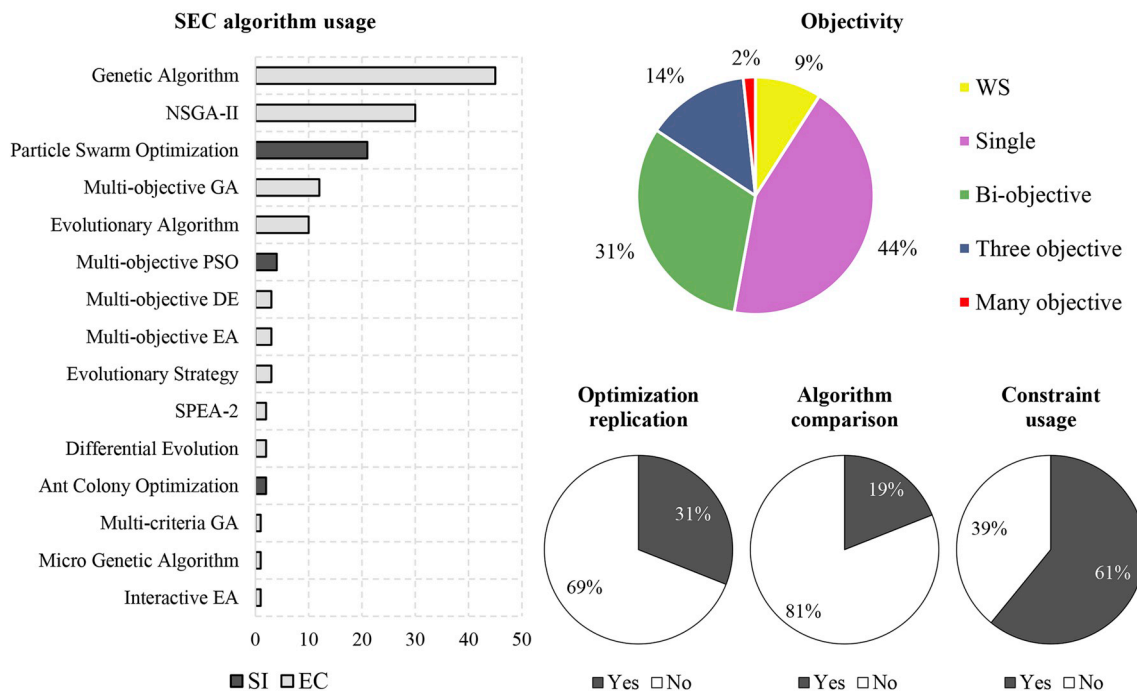


Figure 64. Usage of algorithms and objectivity among 100 researches (Ekici et al., 2019)

Since this research aims to optimize performance on both visual and thermal comfort it is categorized as a multi-objective optimization. The exact number and formulation of the objectives is yet to be determined. NSGA-II is a fast multi-objective evolutionary algorithm which is based on the non-dominated sorting approach. This specific algorithm has been proven to have a better spread of solutions and offers a faster convergence towards a near-perfect performance. (Deb et al., 2002)

Since the form-finding and performance evaluation phase are assumed to be conducted within the interface of Grasshopper, it can be argued to conduct the optimisation phase within the same interface as well, in order to keep the workflow as simple and thus efficient as possible. Because of the open-source nature of the plug-in system for Grasshopper, various optimisation plug-ins have been developed. However, the methodology behind these plug-ins is often concealed, limiting customisation. Based on this concealing of the inner workings, these optimisation plug-ins can be topologized as block-box plug-ins (Wortmann, 2018). Some of the available options for Grasshopper integrated optimisation plug-ins include: GUI: Goat, Octopus, Silvereye, Opossum, Nelder-Mead Optimization, and Design Space Exploration. The most promising of these, based on its interactive GUI, is Octopuss (Wortmann, 2018).

The standard Octopus interface is shown below. The graph, in figure 63 shows the performance of all solutions on the various performance objectives. The objectives are represented by the axes of the 3D graph. The other graph in figure 64 shows the convergence towards an optimal solution. Octopus uses the SPEA-2 and HypE algorithms from ETH Zurich by default, but other algorithms can be used as well. The developers state the following about Octopus:

“Octopus was originally made for Multi-Objective Evolutionary Optimization. It allows the search for many goals at once, producing a range of optimized trade-off solutions between the extremes of each goal.” (Food4rhino, 2019)

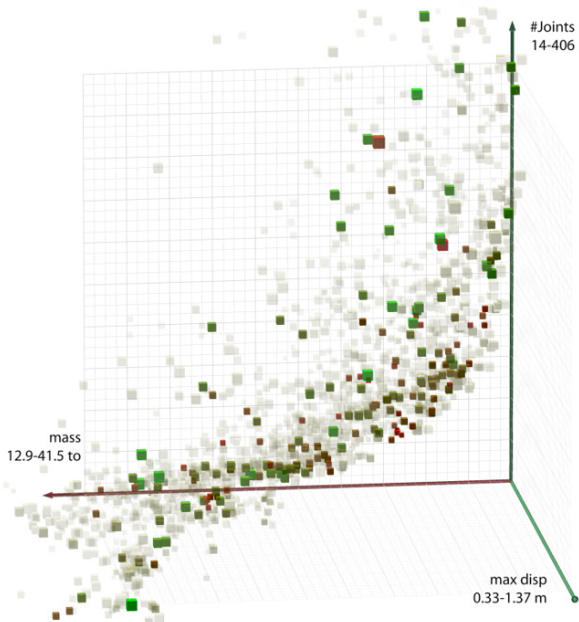


Figure 65. Standard Octopus interface - 3D graph (Food4rhino, 2019)

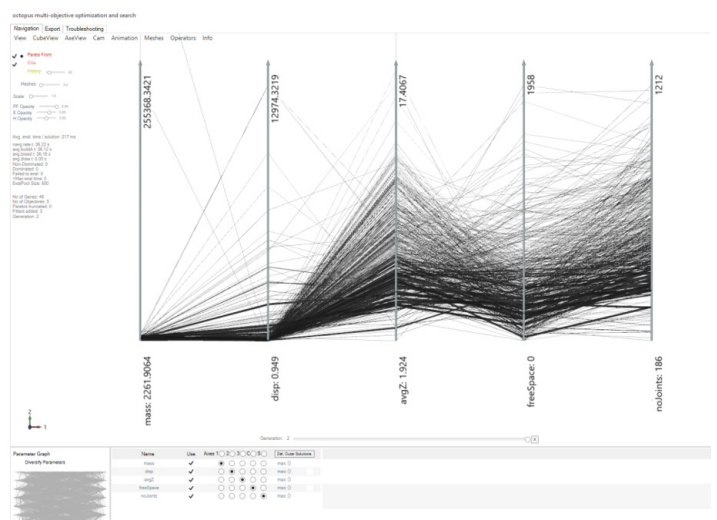


Figure 66. Standard Octopus interface - convergence graph (Food4rhino, 2019)

Another tool with potential for optimisation is ModeFRONTIER. This software package is solely aimed at the optimisation phase and relies on integration with other software for the other two phases. The software does offer option for an integration with a Grasshopper script performing the form-finding and performance evaluation phases. As overview of the standard interface is given in figure 67. In addition to some of the classical search algorithms elaborated above, ModeFRONTIER offers the use a novelty algorithm, developed by the company themselves. This searching algorithm is called PiOpt, is Pareto-based and uses surrogate models (Montrone et al. 2014).

The main advantage of ModeFRONTIER compared to other tools such as Octopus is the wide variety of result analysis tools, including scatter plots (Pareto frontier), parallel/radial coordinates, self-organizing maps and k-clustering. These tools help the designer interpreting the optimisation results. The following few paragraphs will briefly discuss all of the incorporated analysis tools mentioned before.

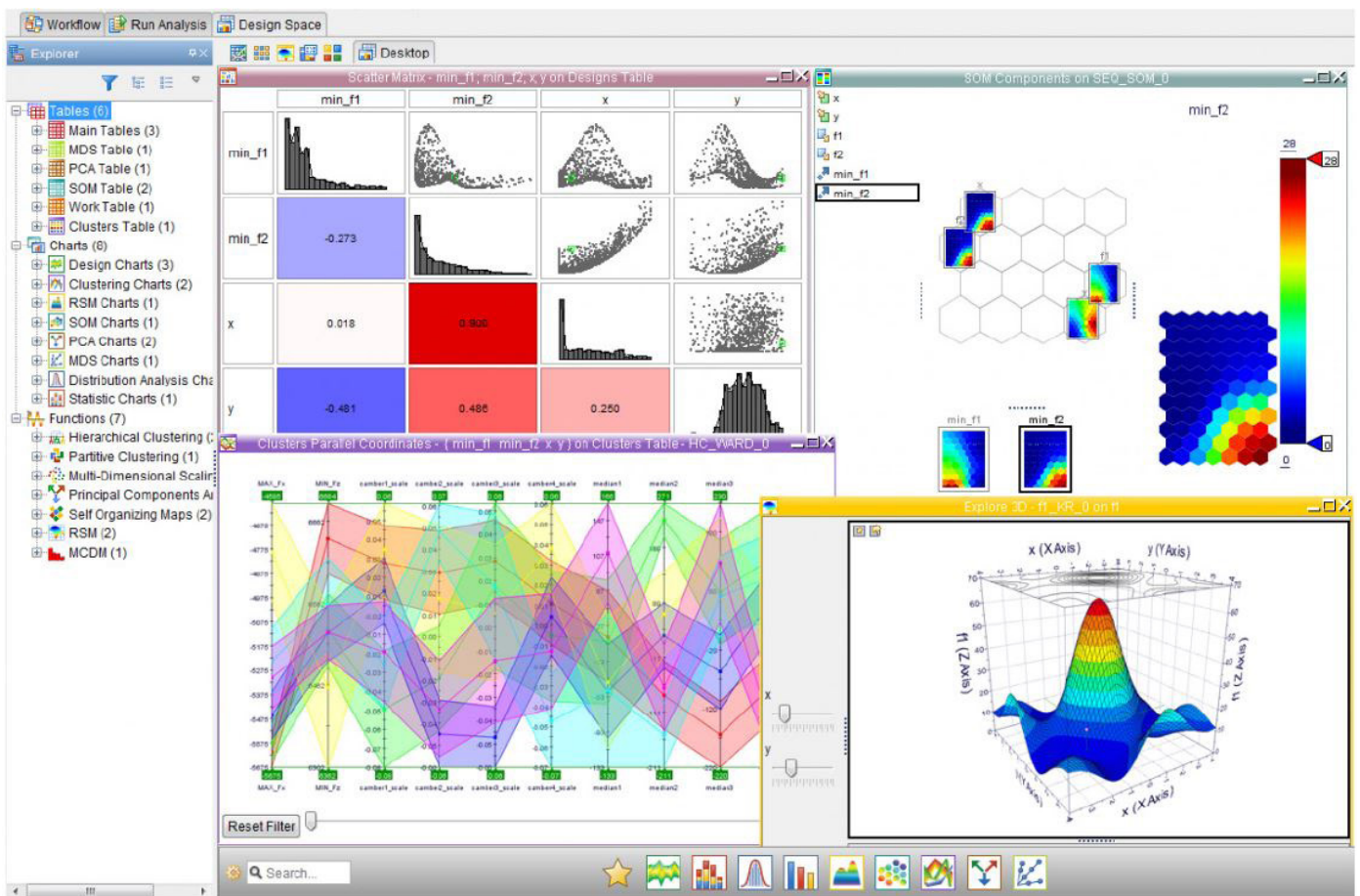


Figure 67. Standard ModeFRONTIER interface - post optimisation analysis (Wortmann, 2018)

Scatter plots (Pareto frontier)

Scatter plots are the most common analysis tool for interpreting optimisation results (Wortmann, 2018). The tool plots all evaluated designs on a 2D or 3D fitness landscape, showing the performance of the designs on respectively two or three objectives. Figure 68 shows an example of a 2D scatter plot. The yellow solutions are the outer-most solutions on the scatterplot and make up the Pareto front. By definition, the performance on one objective cannot be increased without decreasing performance on other objectives, for these solutions. The Pareto front helps designers to understand the relation between performance on different objectives and provides a set of optimal solutions (Radford and Gero 1980).

Parallel/radial coordinates

The visual presentation of the scatterplot, including the Pareto front, works fine for 2D and 3D fitness landscapes, but for higher dimensional optimisations, other visualization methods are required. The most common of these is the method of parallel coordinates (Wortmann, 2018). This technique is first proposed for the PCA method by Wegman (1990) and is based on plotting the performance on various objectives on multiple axes, which can be placed either parallel or in a radial system (see fig. 69). Another option of this visualization technique is to include input parameters in the same system as the objectives.

Self-organizing maps

Self-organizing maps are a tool to visualize high-dimensional fitness landscapes as well, proposed to use for the PCA process by Harding (2016). The tool is based on neural networks that organize higher dimensional data in 2D grids, based on the levels of similarity. A big disadvantage of this tool is the distortion of the design space because this mapping is nondeterministic and varying for each parameter (Wortmann, 2018). The parallel projection method is often used to visualize the groups of the self-organizing maps.

K-means clustering

The analysis tool of k-means clustering is a method for grouping solutions into groups based on unsupervised machine learning, first proposed by MacQueen (1967). This tool serves the same purpose as the self-organizing maps, but is more commonly used. Grouping the solutions into clusters will help to gain insight in the relation between input parameters and the performance on various objectives (Wortmann, 2018).

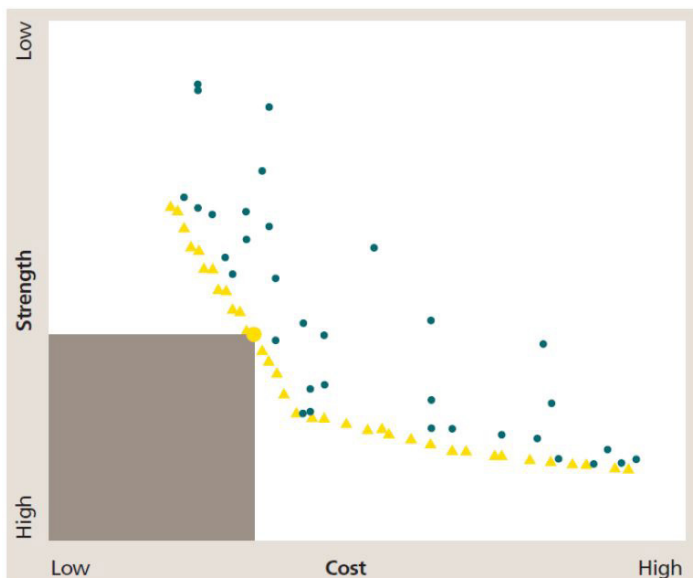


Figure 68. Example of scatter plot (Pareto front) analysis (Wortmann, 2018)

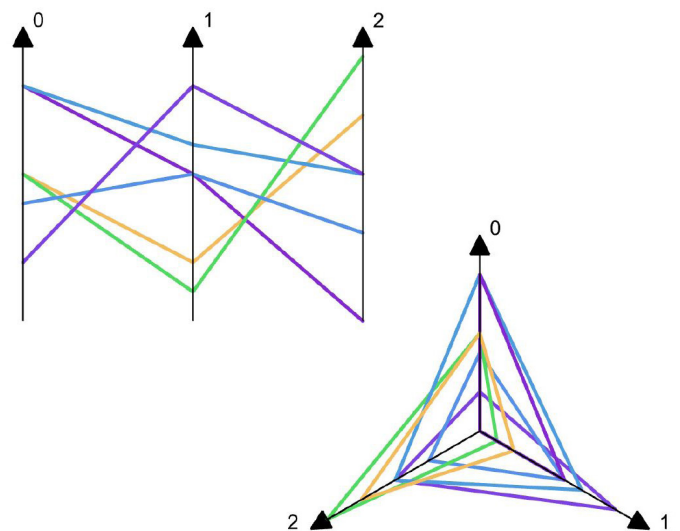


Figure 69. Example of parallel/radial coordinates analyses (Wortmann, 2018)

2.3.5 - References

1. Ekici, B., Cubukcuoglu, C., Turrin, M. and Sariyildiz, I. (2019). Performative computational architecture using swarm and evolutionary optimisation: A review. *Building and Environment*, 147, pp.356-371.
2. Shi, X. and Yang, W. (2013). Performance-driven architectural design and optimization technique from a perspective of architects. *Automation in Construction*, 32, pp.125-135.
3. Eltaweel, A. and Yuehong. (2017). Parametric design and daylighting: A literature review. *Renewable and Sustainable Energy Reviews*, 73, pp.1086-1103.
4. Sariyildiz, Performative computational design, Keynote speech, Proceedings of ICONARCH-I: International Congress of Architecture-I, Konya, Turkey, 15-17 November 2012, Selcuk University, 2012.
5. Mode Lab. (2019). *The Grasshopper Primer* (3rd ed.). Web-based.
6. Barrios, C., 2005, Transformations on Parametric Design Models. In: *Computer Aided Architectural Design Futures*, Springer, Netherlands, pp. 393-400.
7. Wortmann, T. (2018). Efficient, Visual, and Interactive Design Optimisation with Model-based Methods.. Ph.D. Xi'an Jiaotong-Liverpool University.
8. Touloupaki, E. and Theodosiou, T. (2017). Performance Simulation Integrated in Parametric 3D Modeling as a Method for Early Stage Design Optimization—A Review. *Energies*, 10(5), p.637.
9. Gane, V., Haymaker, J., Fischer, M., & Bazjanac, V. (2013). Application of design scenarios methodology to evaluate the effectiveness of transparent parametric design spaces. *Journal of Architectural Engineering*, 20(2)
10. Hubka, V. and Ernst Eder, W. (1987). A scientific approach to engineering design. *Design Studies*, 8(3), pp.123-137.
11. Machairas, V., Tsangrassoulis, A. and Axarli, K. (2014). Algorithms for optimization of building design: A review. *Journal of Renewable and Sustainable Energy*, 31, pp.101-112.
12. Ciftcioglu, O., Sariyildiz, I. and Bitterman, M. (2007). Building performance analysis supported by GA. In: *IEEE Congress on Evolutionary Computation*.
13. Evins, R. (2013). A review of computational optimisation methods applied to sustainable building design. *Renewable and Sustainable Energy Reviews*, 22, pp.230-245.
14. Huang, Y. and Niu, J. (2016). Optimal building envelope design based on simulated performance: History, current status and new potentials. *Energy and Buildings*, 117, pp.387-398.
15. Michalewicz, Z. and Fogel, D. (2004). *How to solve it: modern heuristics*. Berlin: Springer.
16. Holland, J. and Goldberg, D. (1989). *Genetic algorithms in search, optimization and machine learning*. Massachusetts: Addison-Wesley.
17. Storn, R. and Price, K. (2019). Differential Evolution – A Simple and Efficient Heuristic for global Optimization over Continuous Spaces. *Journal of Global Optimization*, 11(4), pp.341–359.

18. Eberhart, R. and Kennedy, J. (1995). A new optimizer using particle swarm theory. In: International Symposium on Micro Machine and Human Science. MHS'95.
19. Dorigo, M., Birattari, M. and Stutzle, T. (2006). Ant colony optimization. IEEE Computational intelligence magazine, 1(4), pp.28-39.
20. Deb, K., Pratap, A., Agarwal, S. and Meyarivan, T. (2002). A fast and elitist multiobjective genetic algorithm: NSGA-II. IEEE Transactions on Evolutionary Computation, 6(2), pp.182 - 197.
21. Oxford Dictionary. (2019). "parameter"
22. Grasshopper3d.com. (2019). Grasshopper. [online] Available at: <https://www.Grasshopper3d.com>
23. Food4Rhino. (2019). Food4Rhino. [online] Available at: <http://www.food4rhino.com>
24. Dubois, M.C. (2001), Impact of Solar Shading Devices on Daylight Quality: Measurements in Experimental Office Rooms, Department of Construction and Architecture, Lund University, Lund.
25. Harding, J. (2016). Dimensionality Reduction for Parametric Design Exploration. In: Adriaenssens S, Gramazio F, Kohler M, et al. (eds) Advances in Architectural Geometry 2016. vdf, Zurich, CH pp 274–287
26. Montrone T, Turco A, Rigoni E (2014) FAST Optimizers: General Description. ESTECO, Trieste, IT
27. MacQueen, J. (1967). Some methods for classification and analysis of multivariate observations. In: Proceedings of the Fifth Berkeley Symposium on Mathematical Statistics and Probability, Volume 1: Statistics. University of California Press, Berkley, CA pp 281–297
28. Radford, A.D and Gero, J.S. (1980). On Optimization in Computer Aided Architectural Design. Building and Environment 15, pp 73–80
29. Wegman, E.J. (1990) Hyperdimensional Data Analysis Using Parallel Coordinates. Journal of the American Statistical Association 85:411, pp 664–675

2.4 - Fundamentals of sun shading in contemporary high-rise

2.4.1 - The relevance

Trends in contemporary high-rise

Before diving into the relevance of sun shading in contemporary high-rise building, it is of importance to define contemporary high-rise. This can be done by watching trends within this field of architecture. Some common trends and their consequences for the relevance of sun shading will be given in this paragraph.

The first observed trend to be discussed is about material use for the façade. MacErlean (2018) states the following in her article about why sky scrapers remain the top choice for contemporary high-rise buildings:

“Glass towers are one of the great symbols of the modern age — and their glazed facades, not to mention the technology behind them, are evolving in response to climate change and modern tastes”. (MacErlean, 2018)

The main reasons for this trend are the appeal of power is has to major corporations and the maximizing of natural daylight inside the building, which enhances the work environment. (MacErlean, 2018). The trend is also observed by Nickelson-Cole (2016) in the article about the impact of high-rise buildings with all-glass exteriors on the evolution of modern cities by stating:

“Glass still predominates as we approach 2020” (Nickelson-Cole, 2016)

Chow et al. (2009) noticed this phenomenon happening to the architecture industry in general already 10 year ago by stating:

“Highly glazed buildings have become a worldwide design trend in modern architecture for whatever climate.” (Chow et al., 2009, p.212)

Chow et al. (2009) defines the reason for this trend to be the important role of glazing in buildings, as it can enhance the quality of life. Secondary, it also reflects an image of transparency, modernity, interaction, freshness and natural brightness, which is in demand by large companies

MacErlean (2018) also states eight out of 10 of the world’s top high-rise buildings are design with glass as the dominant exterior material. If the top ten is interpreted as the ten tallest buildings, the list would be as shown in figure 65. A photographic overview of the listed buildings is given in figure 66, supporting the statement about the dominance of glass among the world’s top skyscraper exteriors.

#	Building Name	City	Height (m)	Height (ft)	Floors	Completion	Material	Use
1	Burj Khalifa	Dubai (AE)	828	2,717	163	2010	steel/concrete	office / residential / hotel
2	Shanghai Tower	Shanghai (CN)	632	2,073	128	2015	composite	hotel / office
3	Makkah Royal Clock Tower	Mecca (SA)	601	1,972	120	2012	steel/concrete	other / hotel
4	Ping An Finance Center	Shenzhen (CN)	599.1	1,965	115	2017	composite	office
5	Lotte World Tower	Seoul (KR)	554.5	1,819	123	2017	composite	hotel / residential / office / retail
6	One World Trade Center	New York City (US)	541.3	1,776	94	2014	composite	office
7	Guangzhou CTF Finance Centre	Guangzhou (CN)	530	1,739	111	2016	composite	hotel / residential / office
8	China Zun	Beijing (CN)	527.7	1,731	108	2018	composite	office
9	TAIPEI 101	Taipei (TW)	508	1,667	101	2004	composite	office
10	Shanghai World Financial Center	Shanghai (CN)	492	1,614	101	2008	composite	hotel / office

Figure 70. *The world’s ten tallest building in order of height (CTBUH, 2019)*



Figure 71. *Photographic overview of the world's ten tallest buildings exteriors (www.google.com)*

The second trend in contemporary high-rise is related to the usage of the building. In figure 5 can also be noted that nine out of ten of the world’s tallest buildings have a (partial) office function. In fact, when the scope is decreased, CTBUH (2019) shows high-rises with an office function are clearly the domination among buildings taller than 200 meters, as shown in figure 7. In total, this dataset contains 2542 buildings worldwide, of which 1022 have an office function.

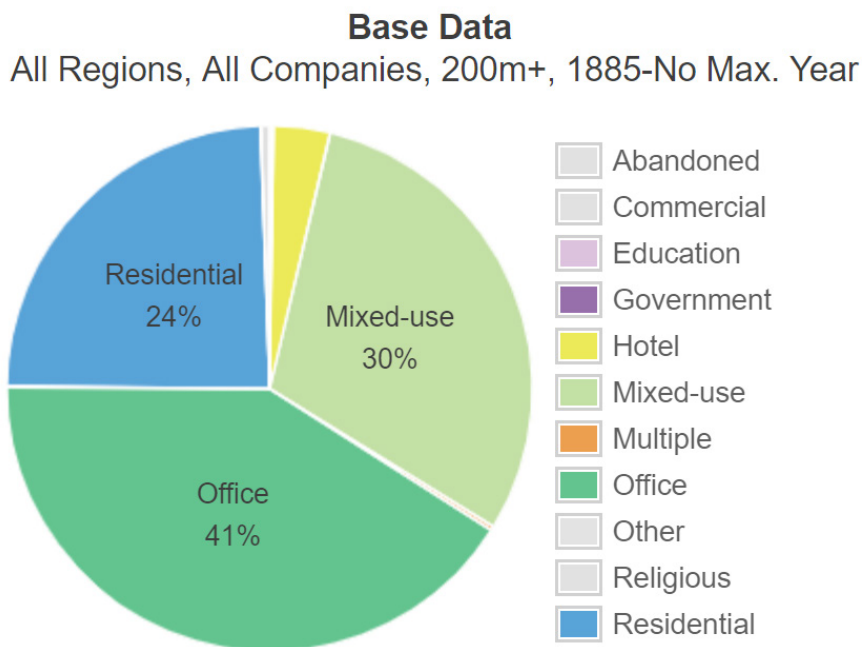


Figure 72. Building functions of 2542 global 200m+ buildings (CTBUH, 2019)

The consequences of all-glass exteriors for high-rise office buildings

These all-glass exteriors have their architectural value, but this facade typology also has consequences for the level of visual and thermal comfort, due to the large amount of incoming solar radiation. In order to make sure the building does not overheat and occupants do not experience glare, is it necessary to apply suitable solutions to limit the incoming solar radiation. (Evola et al., 2017). In order to gain insight to what solutions provide visual and thermal comfort to an all-glass exterior office building for a case study in Italy, Evola et al. (2017) compared multiple sun shading systems and found the following conclusions:

“Adoption of suitable shading devices in highly-glazed office buildings is of the uttermost importance, as it allows to significantly reduce the energy needs for space cooling and to improve thermal comfort while limiting indoor overheating. Moreover, the indoor daylight illuminance keeps suitable levels to allow visual tasks”.
(Evola et al., 2017, p.354)

“The present study suggests that the design of highly glazed office buildings must be tackled through dynamic simulations involving both visual and thermal comfort, and must be optimized case by case.”
(Evola et al., 2017, p.355)

2.4.2 - Technical requirements

Basic sun shading requirements

It has already been made clear two requirements for sun shading are providing visual and thermal comfort. However, there are more requirements to sun shading. Kuhn, Bühler and Platzer (2001) conducted a research to evaluate the effectiveness of different sun shading systems. The research gives five more additional requirements; low costs, high reliability, aesthetics, technical requirements and protection. It also subdivides the requirements of visual and thermal comfort. The entire list of requirements is shown in figure 68.

The next few following paragraphs will each describe additional requirements based on the scope of this research. They will be added to the requirements scheme of Kuhn, Bühler and Platzer (2001) in different colors in order to distinguish the nature of the various requirements. In addition, building standard will be consulted to quantify requirements when needed.

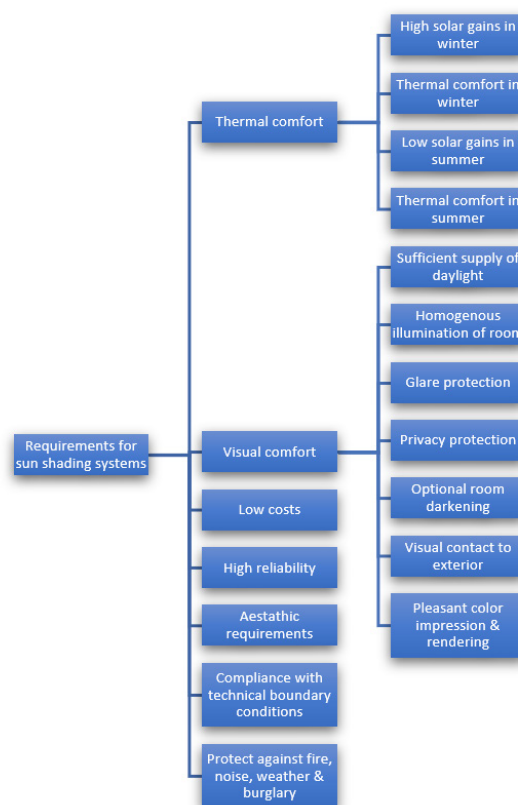


Figure 73. Sun shading requirements (Kuhn, Bühler and Platzer, 2001)

Additional requirements for high-rise buildings

Because high-rise buildings are usually substantially taller than their direct context, sun shading systems require some additional requirements. This absence of context makes high-rise buildings are more vulnerable to wind loads. Rofail and Kwok (1999) researched the effects of shading systems on the distribution of wind loads on the facades of high-rise buildings. The study compared the effect of three common shading systems with are integrated as exterior façade elements, concluding the following:

“Although the facade elements tend to reduce the side wall pressures, which are the most critical in terms of cladding design, they can also significantly increase windward wall pressures.” (Rofail and Kwok, 1999, p.6)

Figure 69 shows a typical wind analysis for a high-rise. As a results of wind hitting the windward side of the building, the air at the sides of the building is blown away. This creates an under pressure are the sides of the building. Because of this, the wind forces at the side walls of the building are pointing outwards. This makes the façade cladding, and thus exterior sun shading system, at risk to be pulled off the building. Because shading elements reduce the speed of air flow around the building, this outward force at the side walls is reduced when sun shading is applied. However, this also results in a build up of air at the windward side, increasing the direct inward force of the wind of this façade. (Rofail and Kwok, 1999)

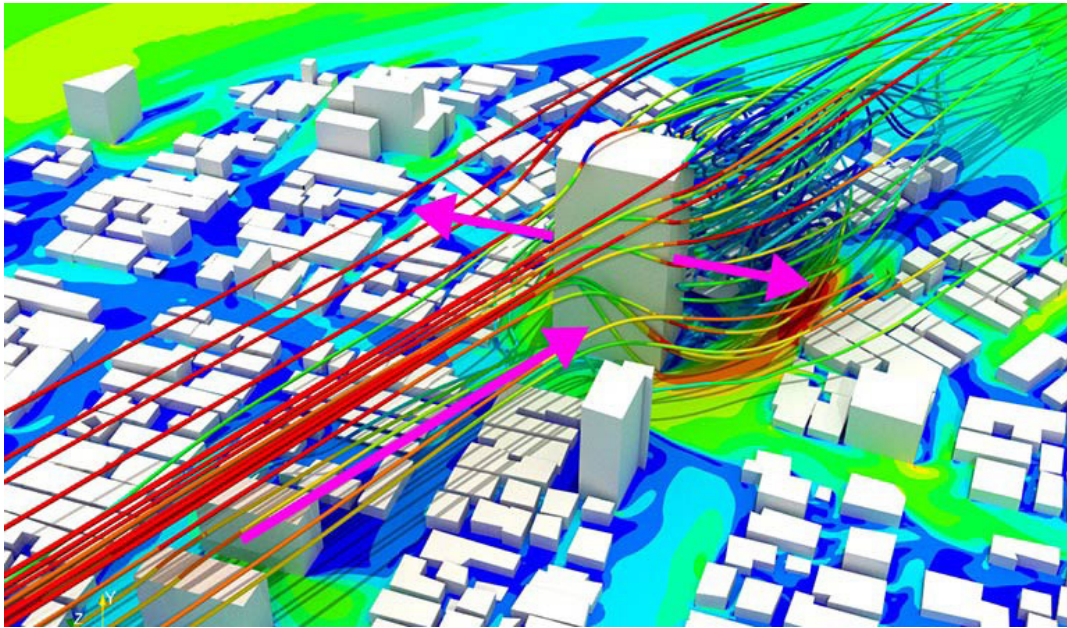


Figure 74. Typical wind force analysis on a high-rise building (Google.com, edited by author)

Another common issue for high-rise is cleaning and maintenance for the façade exterior. Because these surfaces are hard to reach, systems for accessing the exterior should be integrated in high-rise buildings from an early project phase (BCA, 2017). This integration means all parts of the façade are relatively easily accessible. Various systems have been proposed and the BCA of Singapore (2017) distinguishes six different façade access systems, in descending order of feasibility for high-rise. These are; the building maintenance unit (BMU), monorail, temporary suspended working platform (TSWP), rope access, ground-based access and ladders & gantries. A photographic overview of the different systems is given in figure 70. In essence, façade maintenance in high-rise buildings is usually done by lowering workers from the roof using any of the systems mentioned above. This means the sun shading systems should be design to allow for integration of one of the systems and allow workers using the systems to easily reach the façade, thus limiting the use of external sun shading

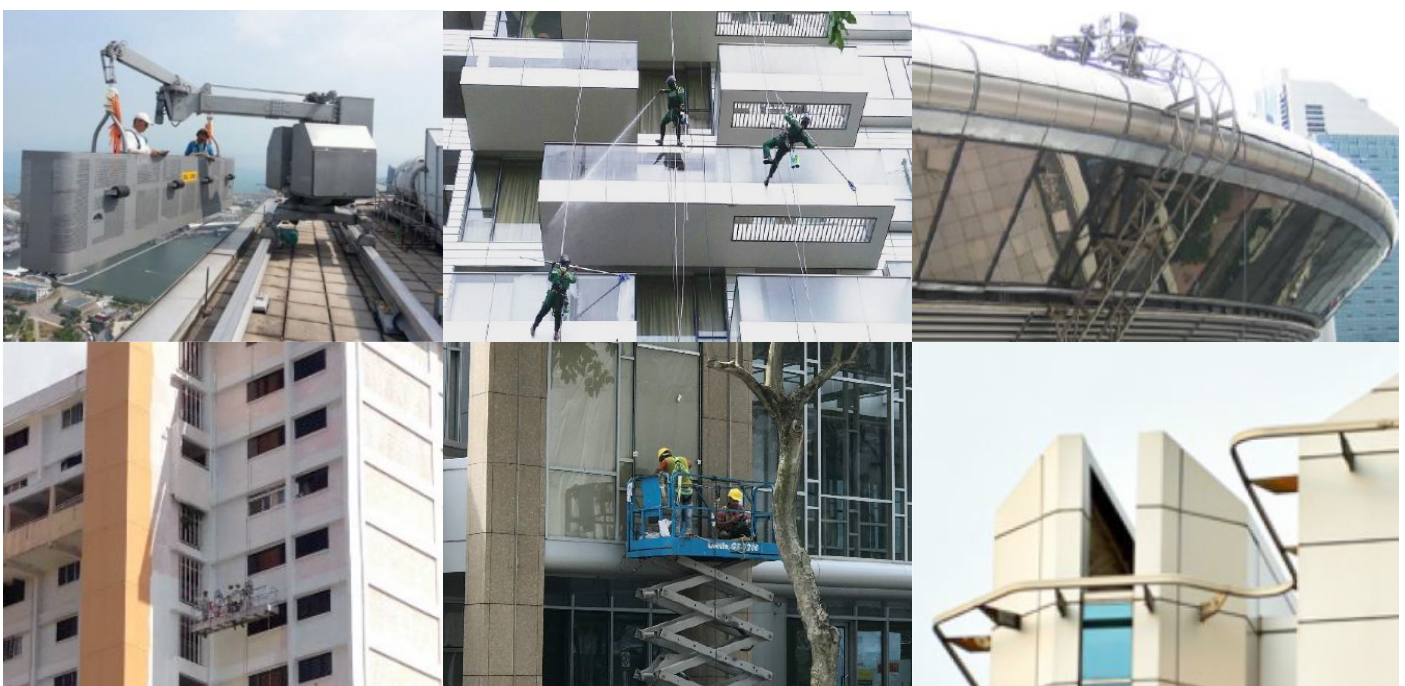


Figure 75. Photographic overview of facade access strategies (BCA, 2017)

Over the recent years, there has also been a development in using robots for basic maintenance such as window cleaning. Systems are still in development, but are proposed to be cheaper and safer than the traditional systems categorized by the BCA of Singapore (2017). Rajesh et al. (2019) conducted a study on how to optimize maintenance robots on high-rise buildings. A schematic drawing of the concept is given in figure 72. The sun shading of the future requires to adapted to these future developments in façade maintenance as well. The research concluded the following about the system, proving these systems have potential for the future:

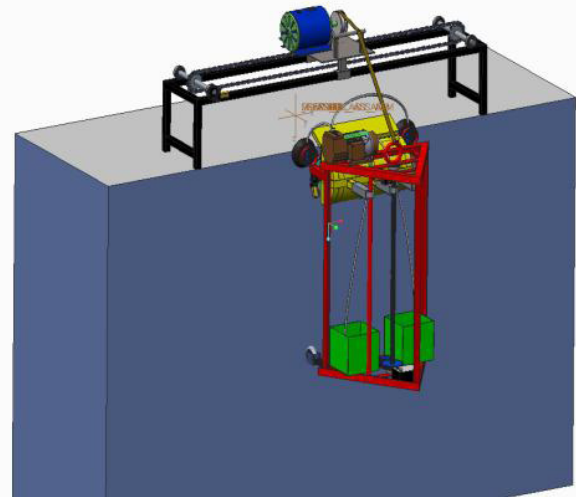


Figure 77. Schematic drawing of maintenance robot for high-rise (Rajesh et al. 2019)

“This contemporary design of these kinds of cleaners helps to overcome the limitations of the existing technologies in façade cleaning system. The rate of cleaning is moderate but the quality of the cleaning is much more superior.”
 (Rajesh et al., 2019, p.6884)

Additional requirements for an all-glass exteriors

The additional requirements for an all-glass exterior are largely based on aesthetic requirements. Even though the additional requirement for wind loads and maintenance restrict the application of exterior shading, this requirement restricts it even more. External sun shading should be limited as much as possible to maintain the all-glass exterior appearance.

Many office buildings with all-glass exteriors rely on the double skin façade principle, because this offers a solution to the overheating problem discussed earlier. (Gratia and De Herde, 2007). Double skin facades consist of two layers of glass, hence the name double skin. This way the cavity in between the panes can be used to ventilate heat to the outside in cooling periods or as a heat buffer in heating periods. (Watts, 2016). This principle is illustrated in figure 71.

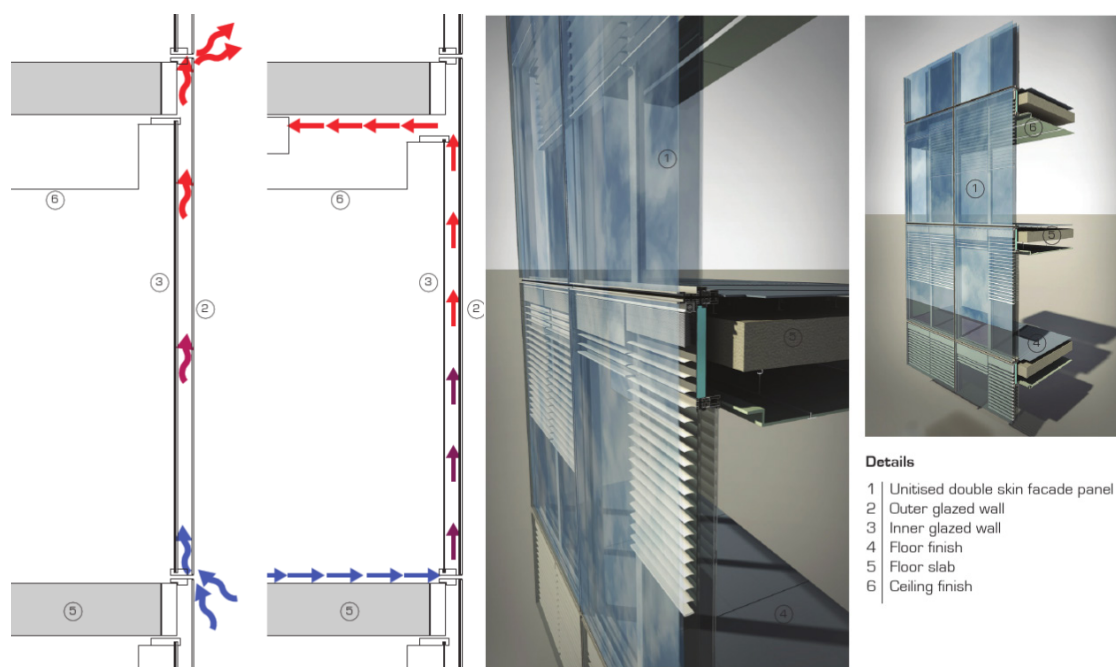


Figure 76. The ventilation principle of a double skin facade (Watts, 2016)

- Details**
- 1 Unitised double skin facade panel
 - 2 Outer glazed wall
 - 3 Inner glazed wall
 - 4 Floor finish
 - 5 Floor slab
 - 6 Ceiling finish

Since exterior sun shading is not feasible due to wind loads, accessibility for maintenance and architectural appeal, other positions must be considered. Placing the shading on the interior is not feasible because it does not reduce the amount of solar gain by blocking radiation coming in the room (Gratia and De Herde, 2007). The principle of solar gain in relation to exterior or interior shading is graphically explain in figure 73.

However, like the images of Watt (2016) already suggested, there is a third placement option when using a double skin façade. This option involves placing the sun shading in between the two layers of glass. Gratia and De Herde (2007) conducted a research on the optimal position for sun shading within the cavity of a double skin façade. Three systems where compared; the sun shading placed against the windows of the inside skin, placed against the outside skin or in the middle of the cavity. The study concluded the following:

“This study has showed the great influence that the position and the colour of the blinds have on the cooling consumption in an office building with a double-skin. It also highlights the importance of the opening of the double-skin.” (Gratia and De Herde, 2007, p.373)

In regard to determining the optimal position, which has proven to be of great influence, the results are shown in figure 75. The results show the optimal position of sun shading is in the middle of the cavity. This way the ventilation principle of the double skin façade is least obstructed. (Gratia and De Herde, 2007). The ventilation inside the double skin façade can be measured in terms of air speed. Figure 74 shows the difference in air speed.

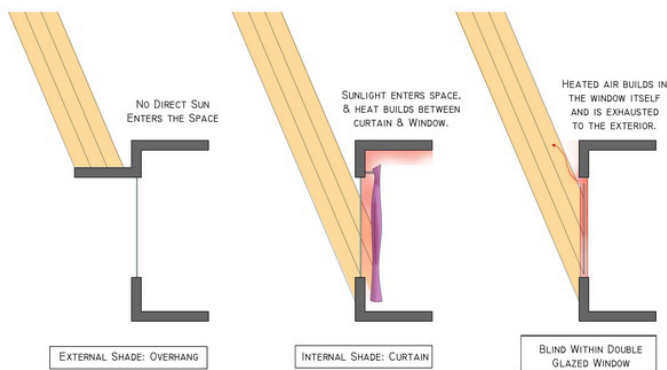


Figure 78. *Solar gain in relation to shading positioning (Google.com)*

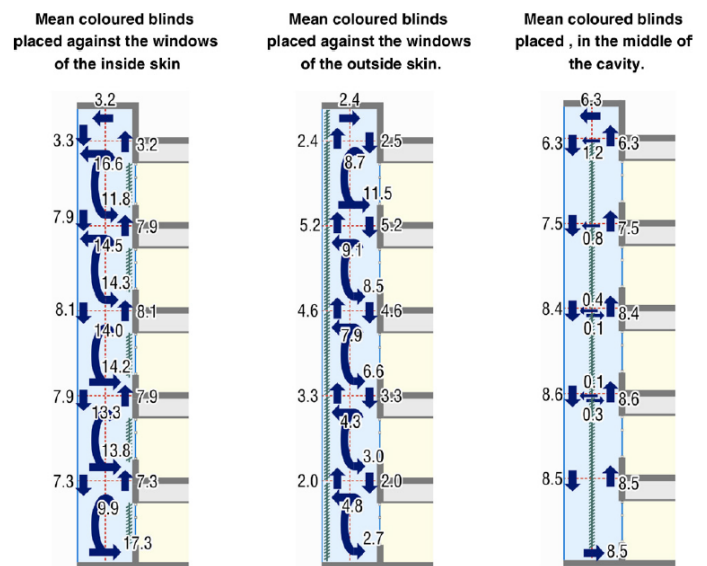


Figure 79. *Ventilation air speeds (Grata and De Herde, 2007)*

	Double-skin closed		Double-skin opened	
	Mean coloured blinds	Light coloured blinds	Mean coloured blinds	Light coloured blinds
Blinds placed against the windows of the inside skin	926 kWh/day	894 kWh/day	834 kWh/day	812 kWh/day
Blinds placed against the windows of the outside skin	-6.0%	-7.2%	-8.9%	-6.2%
Blinds placed in the middle of the cavity	-13.5%	-14.1%	-13.9%	-12.4%

Figure 80. *Optimal position of shading within cavity in relation to cooling loads Grata and De Herde, 2007)*

Additional requirements for office buildings

The official requirements on visual and thermal comfort for office buildings varies from country to country, but there are some international building codes describing requirements for office buildings. National codes are often based on these international versions.

Visual comfort:

A reliable source for office building visual comfort requirements is the European standard NEN-EN-12464, about indoor workspace illuminance. The standard gives many requirement tables, based on specific work environments. The requirement table for a standard office is shown in figure 76. The requirements address the following quantities; minimum maintained illuminance, maximum UGR limit, minimum illuminance uniformity and the minimum color rendering index. These quantities are explained in section 1 of this literature review. Specific requirements are added for activities involving Display Screen Equipment (DSE). These extra requirements state the lighting must be appropriate for all tasks performed at the work station, both tasks that do involve the display screen and tasks that do not.

Thermal comfort:

A reliable source for office building thermal comfort requirements is the international standard NEN-EN-ISO-7730, about the ergonomics of the thermal environment. This standard explains how the PMV, PPD and adapted comfort are calculated as described in section 2 of the literature review. The requirements for thermal comfort are based on this PMV, PPD and adapted comfort quantities and given in NEN-EN-ISO-15251. PMV and PPD are used for building with mechanical cooling systems and the adaptive method is used for natural ventilated buildings. The requirements for office buildings are divided in performance categories, in order to design a healthy building it should meet the requirements for category I. The requirements of the different categories in relation to the PMV, PPD are found in figures 77 and 78.

Ref. no.	Type of area, task or activity	E_m lx	UGR_{lim} -	U_0 -	R_a -	Specific requirements
5.26.1	Filing, copying, etc.	300	19	0,40	80	
5.26.2	Writing, typing, reading, data processing	500	19	0,60	80	DSE-work, see 4.9.
5.26.3	Technical drawing	750	16	0,70	80	
5.26.4	CAD work stations	500	19	0,60	80	DSE-work, see 4.9.
5.26.5	Conference and meeting rooms	500	19	0,60	80	Lighting should be controllable.
5.26.6	Reception desk	300	22	0,60	80	
5.26.7	Archives	200	25	0,40	80	

Figure 81. Visual comfort requirements for office buildings (CEN, 2005)

Category	Thermal state of the body as a whole	
	PPD %	Predicted Mean Vote
I	< 6	-0,2 < PMV < + 0,2
II	< 10	-0,5 < PMV < + 0,5
III	< 15	-0,7 < PMV < + 0,7
IV	> 15	PMV < -0,7; or +0,7 < PMV

Figure 82. Thermal comfort requirements for office buildings (CEN, 2005)

Type of building/ space	Category	Operative temperature °C	
		Minimum for heating (winter season), ~ 1,0 clo	Maximum for cooling (summer season), ~ 0,5 clo
Single office (cellular office) Sedentary ~ 1,2 met	I	21,0	25,5
	II	20,0	26,0
	III	19,0	27,0
Landscape office (open plan office) Sedentary ~ 1,2 met	I	21,0	25,5
	II	20,0	26,0
	III	19,0	27,0
Conference room Sedentary ~ 1,2 met	I	21,0	25,5
	II	20,0	26,0
	III	19,0	27,0

Figure 83. Thermal comfort requirements for office buildings (ISO, 2005)

2.4.3 - Local climate

The location, with the climate of that location in particular. In locations with a hot climate, solar radiation is undesirable the entire year, while in regions with more temperate climates, solar radiation is often desirable in winter time, but undesirable in summer time. (O'Brien et al., 2013; Al-Obaidi et al., 2016). Therefore, the requirements for sun shading to help increase the levels of visual and thermal comfort is very dependent on the location. (Tzempelikos et al., 2007; Khoroshiltseva et al., 2016).

In terms of risk for visual and thermal comfort, the tropic climate is very demanding. As a result of relatively high levels of solar radiation, overheating and glare can become serious risk in this region. (Al-Tamimi & Fadzil, 2011). This means improving the sun shading of high-rise office buildings with all-glass exteriors is the most challenging in the tropical climate. Therefore, this will be the scope of this research.

In order to gain understanding of the local climate, every research on sun shading design should include a climate analysis. Like elaborated in the previous section, Ladybug & Honeybee offer tools to conduct these climate analyses based on the climate data in the EPW files. These files can be downloaded for many cities/weather stations around the world. As an example, a brief climate study on the tropic climate by Al-Masrani et al. (2018) is shown in figure 79. This includes a geographic definition of the global tropic climate zone and weather data analyses of three cities close to the equator. The analyses include the direct radiation, diffuse radiation and the dry-bulb temperature.

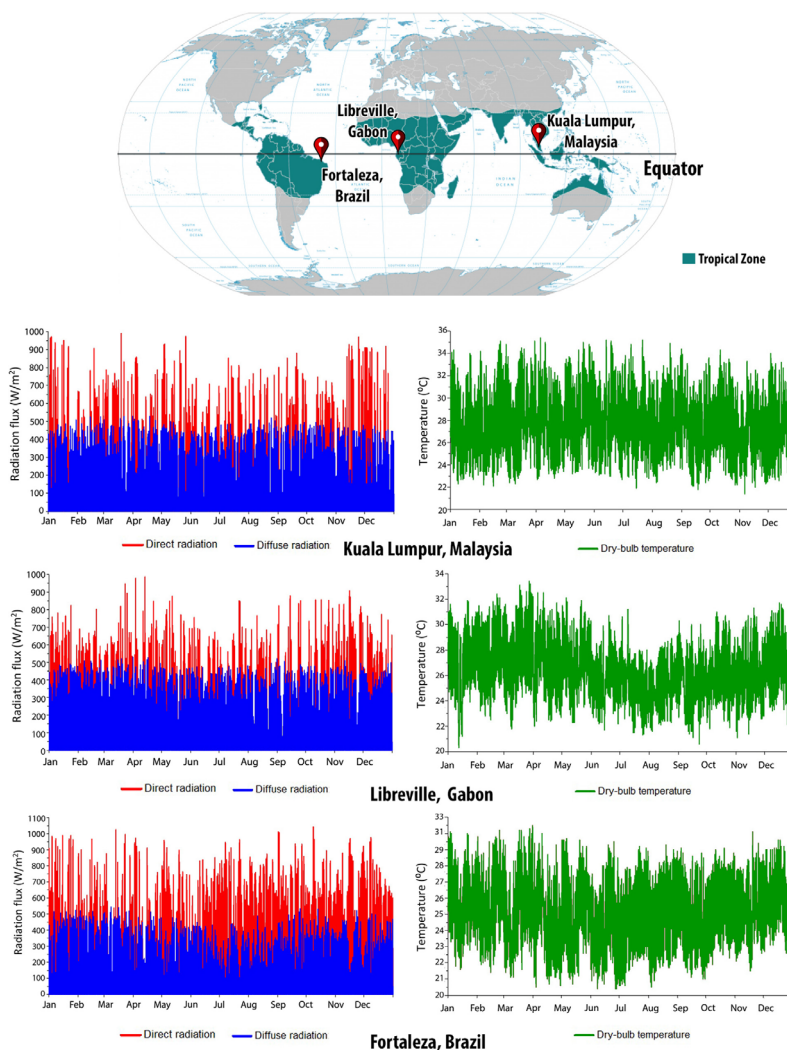


Figure 84. Analysis of the tropical climate (Al-Masrani et al., 2018)

2.4.4 - The potential for PCA implementation

The previous two paragraphs have described PCA's potential for sun shading and the challenge to ensure thermal and visual comfort in high-rise office buildings with all-glass exteriors in tropical climates. Ekici et al. (2019) reviewed one hundred different case studies on PCA. Figure 9 shows the biggest percentage of these studies revolve office buildings, but figure 10 shows the amount of studies involving high-rise buildings is relatively low.

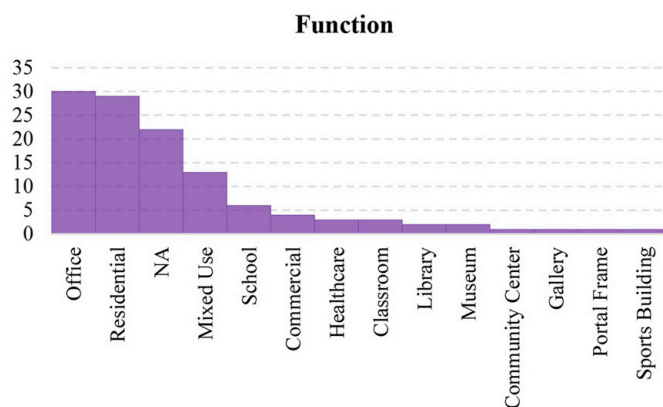


Figure 85. Case studies per function (Ekici et al., 2019)

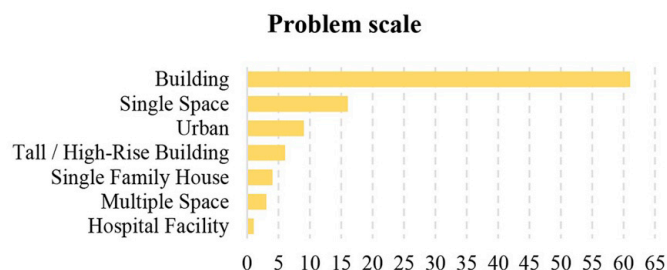


Figure 86. Case studies per problem scale (Ekici et al., 2019)

The six studies involving high-rise buildings with the review of Ekici et al. (2019) includes the studies listed below. All studies do in fact involve high-rise buildings, but when after examining the abstracts, none of the studies involved optimizing the sun shading in high-rise for improving the visual and thermal comfort.

"This research proposes a two-stage design optimization approach which is applied to a prototype passively designed high-rise residential building under different ventilation modes and thermal load requirements. Machine learning methods are employed to develop surrogate models for improving the computation efficiency of the multi-objective optimization process." (Chen, X. and Yang, H., 2017, p.541)

"The paper applies a computer-based method involving evolutionary search, Pareto optimization, and color filtering to investigate the tradeoff between the life-cycle profitability of high-rise commercial office buildings and their load-path safety against progressive collapse under abnormal loading." (Khajehpour and Grierson, 2003, p. 279)

"This study presents building corner aerodynamic optimization procedure (AOP) to reduce the wind load, by coupling an optimization algorithm, large eddy simulation (LES) and an artificial neural network (ANN) based surrogate model." (Elshaer, Bitsuamlak and El Damatty, 2017, p.133)

"This paper seeks to investigate methodology on the seamless integration for constructing a climate-conscious building envelope." (Yi, 2014, p.159)

"This work presents a study of solar potential maximization over a district and its relation with urban shape." (Vermeulen et al., 2015, p.1)

"As a result of following the code, most tall apartment buildings exhibit similar building layouts in which major facades face south, thereby sacrificing design diversity, creativity, and identity. To ease the problem, this paper proposes an alternative method for optimizing a building's access to direct sunlight." (Yi and Kim, 2015, p.236)

The study of Al-Masrani, S., Al-Obaidi, K., Zalin, N. and Aida Isma, M. (2018) reviewed the applications of the PCA process, but whereas the paper of Ekici et al. (2019) reviews the applications of PCA in general, focuses this paper on sun shading in particular. The goal of the study is to investigate the challenges and future trends of sun shading systems applied to office buildings in the tropics. This thesis will to build further on these challenges and future trends to design the sun shading of the future. Many of the research reviewed by Al-Masrani et al. (2018) include traces of the PCA method, but not the entire iterative loop. The projects all include a performance evaluation phase, but many leak the form-finding phase and/or optimization phase. This thesis hopes to find ways to implement the entire PCA method to improve the existing sun shading systems for high-rise office buildings with all-glass exteriors in tropic climates.

In order to systematize the review, Al-Masrani et al. (2018) introduced a classification system for the precedence studies, shown in image 82. The highlighted category in the image below contains precedes who also include a parametric form-finding phase, and the paper also mentions the software of Ladybug & Honeybee being used to evaluate the performance. According to the review paper, it is not clear if the optimization phase was included as well. However, since the form-finding phase and performance evaluation phase are used with the Grasshopper interface, implementing the optimization phase should be possible. Some of the case studies within the review will analyzed more in-depth in the next section, in order to reveal in what extend the PCA was correctly used in these case studies. However, based on the bigger picture of the review, Al-Masrani et al. (2018) concluded the following about the challenges and future trends for sun shading design in high-rise office building in the tropics:

Passive sun shading for high-rise office buildings in tropical climates:

“The majority of shading studies in the tropics adopted fixed shading devices, and most literature has identified egg-crate devices as the best device to improve daylight and thermal performance.” (Al-Masrani et al., 2018, p.869)

Active sun shading for fixed high-rise office buildings in tropical climates:

“Performance and the applicability of intelligent building systems, this design faces many criticisms due to its complexity, cost and high operational energy.” (Al-Masrani et al., 2018, p.869)

Hybrid sun shading for high-rise office buildings in tropical climates:

“The performances of dynamic complex geometries and shape morphing shading systems have not yet been explored in the tropics. Consequently, studies must urgently assess the performance of more adaptive geometries in addition to biomimetic approaches represented by hybrid shading systems in a tropical climate.” (Al-Masrani et al., 2018, p.869)

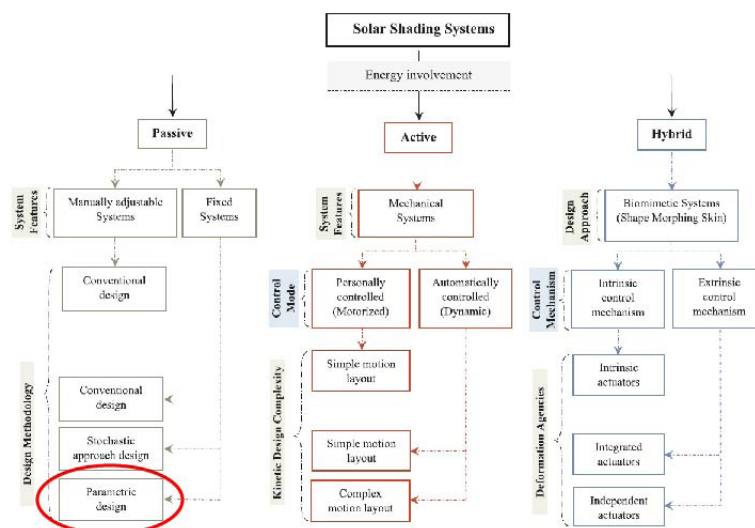


Figure 87. The three categories of sun shading systems (Al-Masrani et al., 2018)

2.4.5 - References

1. Evola, G., Gullo, F. and Marletta, L. (2017). The role of shading devices to improve thermal and visual comfort in existing glazed buildings. *Energy Procedia*, 134, pp.346-355.
2. MacErlean, N. (2019). Why glass remains the top choice for today's skyscrapers. [online] JLL Real Views. Available at: <https://www.jllrealviews.com/trends/design/glass-remains-top-choice-todays-skyscrapers/>
3. Nicholson-Cole, D. (2016). Rise of the glass giants: how modern cities are forcing skyscrapers to evolve. [online] The conversation. Available at: <http://theconversation.com/rise-of-the-glass-giants-how-modern-cities-are-forcing-skyscrapers-to-evolve-56843>
4. Chow, T., Li, C. and Lin, Z. (2010). Innovative solar windows for cooling-demand climate. *Solar Energy Materials and Solar Cells*, 94(2), pp.212-220.
5. Council on Tall Buildings and Urban Habitat (CTBUH). (2019). The Skyscraper Center. [online] Skyscrapercenter.com. Available at: <http://www.skyscrapercenter.com>
6. Kuhn, T., Bühler, C. and Platzer, W. (2001). Evaluation of overheating protection with sun-shading systems. *Solar Energy*, 69, pp.59-74.
7. Rofail, A. and Kwok, K. (1999). The effect of sunshading elements on cladding pressures. In: 10th International Conference on Wind Engineering.
8. Watts, A. (2016). Modern construction handbook. Retrieved from <https://ebookcentral-proquest-com.tudelft.idm.oclc.org>
9. Gratia, E. and De Herde, A. (2007). The most efficient position of shading devices in a double-skin facade. *Energy and Buildings*, 39(3), pp.364-373.
10. The Building and construction authority (BCA) (2017). The facade access design guide. Singapore.
11. Rajesh, S., Janarthanan, P., Pradeep Raj, G. and Jaichandran, A. (2019). Design and Optimization of High Rise Building Cleaner. *International Journal of Applied Engineering Research*, 13(9), pp.6881-6885.
12. O'Brien, W., Kapsis, K., Athienitis, A.K., 2013. Manually-operated window shade patterns in office buildings: a critical review. *Build. Environ.* 60, 319–338.
13. Al-Obaidi, K.M., Ismail, M.A., Abdul Rahman, A.M., 2016. Effective use of hybrid turbine ventilator to improve thermal performance in Malaysian tropical houses. *Build. Serv. Eng. Res. Technol.* 37 (6), 755–768.
14. Tzempelikos, A., Athienitis, A.K., Karava, P., 2007. Simulation of façade and envelope design options for a new institutional building. *Sol. Energy* 81 (9), 1088–1103.
15. Khoroshiltseva, M., Slanzi, D., Poli, I., 2016. A Pareto-based multi-objective optimization algorithm to design energy-efficient shading devices. *Appl. Energy* 184, 1400–1410.
16. Al-Tamimi, N. and Fadzil, S. (2011). The Potential of Shading Devices for Temperature Reduction in High-Rise Residential Buildings in the Tropics. *Procedia Engineering*, 21, pp.273-282.

17. Al-Masrani, S., Al-Obaidi, K., Zalin, N. and Aida Isma, M. (2018). Design optimisation of solar shading systems for tropical office buildings: Challenges and future trends. *Solar Energy*, 170, pp.849-872.
18. European Committee for Standardization (CEN). (2007). NEN-EN-15251: Indoor environmental input parameters for design and assessment of energy performance of buildings addressing indoor air quality, thermal environment, lighting and acoustics.
19. International Committee for Standardization (ISO). (2005). NEN-EN-ISO-7730: Ergonomics of the thermal environment – Analytical determination and interpretation of thermal comfort using calculations of the PMV and PPD indices and local thermal comfort criteria.
20. European Committee for Standardization (CEN). (2011). NEN-EN-12464: Light and lighting - Lighting of work places - Part1: Indoor work places
21. Vermeulen, T., Knopf-Lenoir, C., Villon, P. and Beckers, B. (2015). Urban layout optimization framework to maximize direct solar irradiation. *Computers, Environment and Urban Systems*, 51, pp.1-12.
22. Yi, H. (2014). Automated generation of optimised building envelope: simulation based multi-objective process using evolutionary algorithm. *International Journal of Sustainable Building Technology and Urban Development*, 5(3), pp.159-170.
23. Yi, Y. and Kim, H. (2015). Agent-based geometry optimization with Genetic Algorithm (GA) for tall apartment's solar right. *Solar Energy*, 113, pp.236-250.
24. Elshaer, A., Bitsuamlak, G. and El Damatty, A. (2017). Enhancing wind performance of tall buildings using corner aerodynamic optimization. *Engineering Structures*, 136, pp.133-148.
25. Khajehpour, S. and Grierson, D. (2003). Profitability versus safety of high-rise office buildings. *Structural and Multidisciplinary Optimization*, 25(4), pp.279-293.
26. Chen, X. and Yang, H. (2017). A multi-stage optimization of passively designed high-rise residential buildings in multiple building operation scenarios. *Applied Energy*, 206, pp.541-557.

Turin et al. (2011)

The case study discussed in this research is about a sun shading design for a large roof structure and is located in Milan, Italy. The structure has a square footprint spanning 50 meters in both directions and is supported by four tree-like column systems. The structure itself is double curved and based on a tessellation grid. The sun shading elements are triangular shaped roof peaks and can vary in inclination (see fig. 89). The inputs for the PCA process involve parameters for the following:

- The overall shape of the roof
- Density of the tessellation
- Local inclinations of the cladding panels
- Length of the shading extensions

Since Milan is located in a temperate climate, desirable performance varies through the seasons. In summertime it is feasible to reduce solar gain and promote cooling effects, such as the stack effect by opening up the roof peaks. While in wintertime it is feasible to increase solar gains and close the roof peaks to avoid heat loss. However, visual conditions need to be appropriate throughout the year. The goal of the study is to assess the summer in winter situation in parallel, in order to compare the final results. This is intended to substantiate the choice for either developing a fixed solution which is a compromise of both final results or developing a mechanical shading system which can adapt to the annual solar cycle. In total, three simulations were run; an annual simulation, one for just the month of June (summer) and one for just the month of December (winter). The objectives used for these simulations were as following:

Annual & Summer:

- Minimize the incident solar radiation
- Maximize the daylight factor

Winter:

- Maximize the incident solar radiation
- Maximize the daylight factor

The case could have used a bi-objective optimisation process, but instead it was chosen to combine both objectives into a single objective as following:

Annual & summer: Minimize ratio between incident solar radiation and daylight factor

Winter analysis: Maximize sum of incident solar radiation and daylight factor

The case study uses ParaGen, running on a network of computers, for the optimisation process. This software uses its own Generative Algorithm (GA). Since the case study involves a single-objective optimisation, there is only one optimal solution.

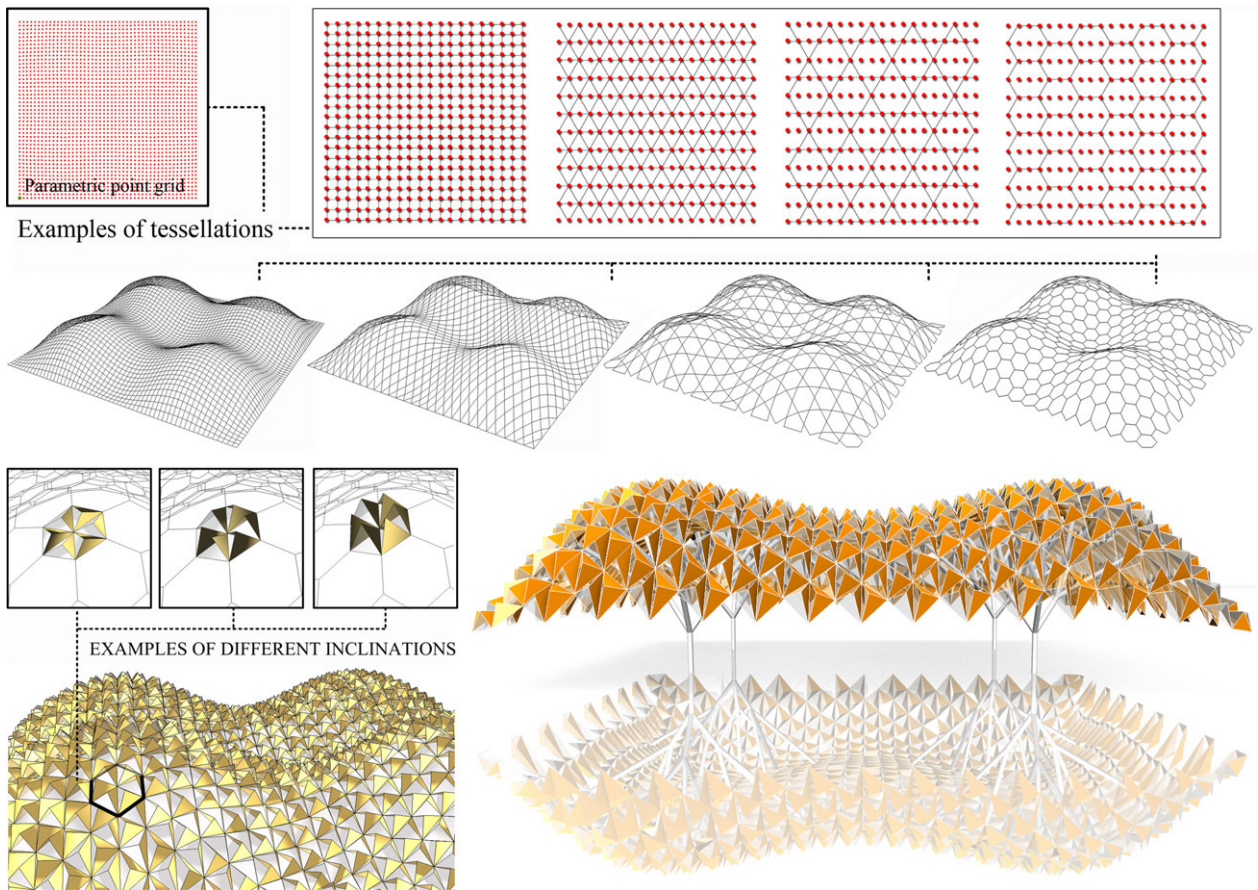


Figure 89. *The case study of Turrin et al. (2011)*

Yang et al. (2018)

The case study discussed in this research is about the design of a sports stadium, with the roof structure in particular. The roof features a number of steps in which openings for natural daylight are integrated. The perimeter of the roof serves as a natural daylight inlet as well. All daylight openings are suited with an exterior shading overhang (see fig. 90). All parameters used to generate this geometry are listed in figure 91. Other types of inputs include the occupancy schedule (see fig. 92), a weather file for the city of Wuhan which is derived from Chinese Standard Weather Data (CSWD) and a list of material parameters (see fig. 91).

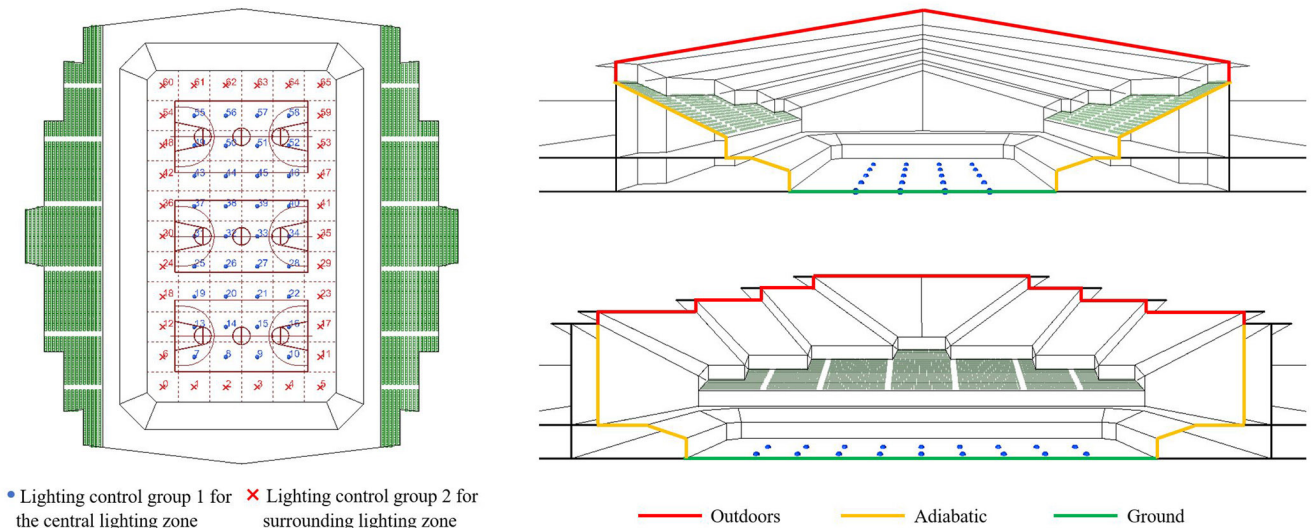
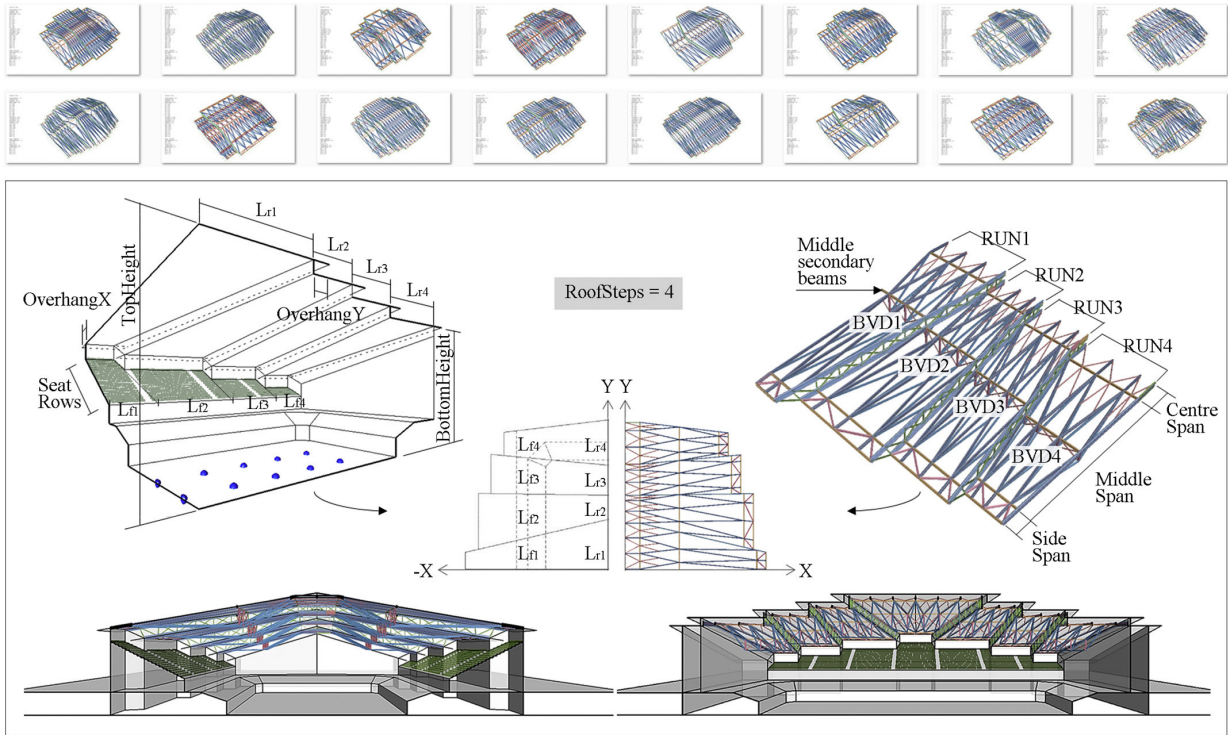


Figure 90. *The concept of the case study of Yang et al. (2018)*



Variable family	Variable full name	Variable short name	Data type	Lower bound	Upper bound	Intervals	Benchmark	Daylight and energy model parameter	Value		
Grandstand	Seat row number	Number of maximum seat rows (of the upper tier)	SeatRows	Int.	15 (19)	20 (24)	1	11	Wall reflectance	0.55	
	Roof step number	Number of roof steps	RoofSteps	Int.	2	5	1	2	Floor reflectance	0.30	
Building envelope	Roof height	Height of the highest ridge (m)	TopHeight	Float	25.00 (27.00)	30.00 (32.00)	0.01	26.00	Roof reflectance	0.75	
		Height of the lowest ridge (m)	BottomHeight	Float	15.00 (17.00)	20.00 (22.00)	0.01	24.00	Window Transmittance	0.40	
	Ridge division		Portion of the ridge of sub-roof 1	R1	Float	0.20	0.90	0.01	0.9	Lighting control type (lighting control group 1)	Always on during occupied hours, automatic dimming, 300-lx target
			Portion of the ridge of sub-roof 2	R2	Float	0.20	0.90	0.01	0.2	Lighting control type (lighting control group 2)	Always on during occupied hours, automatic dimming, 200-lx target
			Portion of the ridge of sub-roof 3	R3	Float	0.20	0.90	0.01	-	Lighting power density (lighting control group 1)	15.00 W/m ²
			Portion of the ridge of sub-roof 4	R4	Float	0.20	0.90	0.01	-	Lighting power density (lighting control group 2)	9.00 W/m ²
			Portion of the ridge of sub-roof 5	R5	Float	0.20	0.90	0.01	-	Wall U-value	0.72 W/m ² K
	Front row division		Portion of the front row under sub-roof 1	F1	Float	0.20	0.90	0.01	0.9	Ground floor U-value	3.70 W/m ² K
			Portion of the front row under sub-roof 2	F2	Float	0.20	0.90	0.01	0.2	Roof U-value	0.34 W/m ² K
			Portion of the front row under sub-roof 3	F3	Float	0.20	0.90	0.01	-	Window U-value	2.60 W/m ² K
			Portion of the front row under sub-roof 4	F4	Float	0.20	0.90	0.01	-	Window SHGC	0.37
			Portion of the front row under sub-roof 5	F5	Float	0.20	0.90	0.01	-	Window VT	0.62
	External shading	Shading dimension	Overhang depth in X axis (m)	OverhangX	Float	0.10	3.00	0.01	3.80	Cooling thermostat setpoint temperature	27 °C
			Overhang depth in Y axis (m)	OverhangY	Float	0.10	3.00	0.01	2.20	Cooling thermostat setback temperature	30 °C
	Roof structure	Span partition		Centre Span (m)	CentreSpan	Float	0.50	5.00	0.01	4.20	Heating thermostat setpoint temperature
			Middle Span Partition (fraction)	MiddleSpan	Float	0.10	0.90	0.01	0.50	Heating thermostat setback temperature	14 °C
			Side Span (m)	SideSpan	Float	0.50	5.00	0.01	4.20	Occupancy density	0.92 person/m ²
Beam vertical distance			Beam vertical distance for sub-roof 1 (m)	BVD1	Float	2.00	7.00 (6.00)	0.01	4.60	Equipment power density	2 W/m ²
			Beam vertical distance for sub-roof 2 (m)	BVD2	Float	2.00	7.00 (6.00)	0.01	2.00	Ventilation rate	15 m ³ /h person
			Beam vertical distance for sub-roof 3 (m)	BVD3	Float	2.00	7.00 (6.00)	0.01	-	Infiltration rate	4.5 m ³ /h m ²
			Beam vertical distance for sub-roof 4 (m)	BVD4	Float	2.00	7.00 (6.00)	0.01	-		
			Beam vertical distance for sub-roof 5 (m)	BVD5	Float	2.00	7.00 (6.00)	0.01	-		
Repeated unit number			Repeated unit number for sub-roof 1	RUN1	Int.	1	5	1	5		
			Repeated unit number for sub-roof 2	RUN2	Int.	1	5	1	1		
			Repeated unit number for sub-roof 3	RUN3	Int.	1	5	1	-		
			Repeated unit number for sub-roof 4	RUN4	Int.	1	5	1	-		
			Repeated unit number for sub-roof 5	RUN5	Int.	1	5	1	-		

Figure 91. The geometrical and material related input parameters of the case study of Yang et al. (2018)

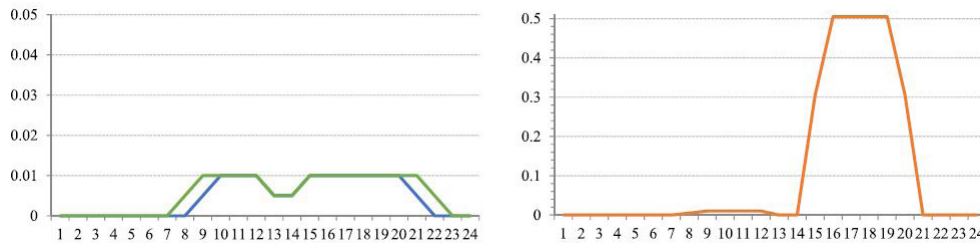


Figure 92. Occupancy of the case study of Yang et al. (2018) (mon-sat = left, sun = right)

The main goal of the case study is to reduce operational energy as much as possible while improving or maintaining daylight and thermal comfort. In order to do so, annual hourly daylight simulations were conducted using Daysim and annual energy simulations using Energyplus. Both simulations were done via Ladybug and Honeybee, the plug-ins within Grasshopper for connecting geometry and input parameters to the simulation software. The objectives of the case study are shown in figure 93 and include three comfort metric related objectives; the modified UDI (maximize), modified uniformity ratio (maximize) and the Energy use Intensity (minimize). The modified version refers to the original UDI metric, but instead of using a threshold of 50% of the annual occupation hours, this threshold can be set to any value. In the case of this research UDI-mod60 and UDI-mode65 are used, meaning a floor area receiving respectively 60% and 65% of annual occupation hours with illuminance levels in between 100 and 2000 lux is regarded as successful. The modified Uniformity ratio is used in this case because the uniformity of light is important for several sports played in the building. The modification refers to requirements specific to the building and are therefore beyond the scope of this research. The Energy Use Intensity is a common metric to measure the total annual energy consumption per square meter of floor area. It is the sum of energy loads for heating, cooling and lighting.

The energy load due to artificial lighting is calculated using a stepped workflow. The Daysim annual illuminance simulation is conducted first. Based on the illuminance values and the occupancy schedule, a schedule for the artificial lighting is generated. In combination with an energy usage for the armatures per square meters, this lighting schedule is then used by Energyplus to calculate the annual lighting load. This stepped workflow is used, because the illuminance simulations of Daysim tend to be significantly more accurate than those of Energyplus.

In addition to the three climate related objectives, there is one climate related constrain related to the operative temperature. This temperature may not fall below values described in standards. The case does involve one more objective; minimizing the total construction mass, but since this is of structural nature it is beyond the scope of this research. However, since this case study involves four objectives it can be regarded as a multi-objective optimisation.

Disciplines	Performance criteria	Objective functions	Constraints (to be calculated)	Constraints (set in models)
Architecture	C-value	-	-	60 mm
	Number of seats in the upper tier	-	> 3600	-
	Minimum space check (SC)	-	> 15 m	-
Climate	Modified Useful Daylight Illuminance (UDI _{mod})	Maximization	-	-
	Modified Uniformity Ratio (UR _{mod})	Maximization	-	-
Thermal	Operative temperature	-	-	See Table 3
Energy	Energy Use Intensity (EUI)	Minimization	-	-
Structure	Mass per square meter	Minimization	-	-
	Maximum utility check (UC)	-	< 0.9 (failed members < 2% of the total)	-
	Maximum displacement check (DC)	-	< 0.3 m	-

Figure 93. Objectives of Yang et al. (2018)

The case used the software of ModeFRONTIER for the optimisation phase (see fig. 94). The Grasshopper definition, also including the connections to Daysim and Energyplus via Ladybug and Honeybee, is loaded in the custom Mynode component forming the heart of the ModeFRONTIER workflow. The workflow starts with a DOE of 500 designs, generated by the Uniform Latin Hypercube (ULH) method. The process was not given a limitation to the total amount of evaluations, but instead was left running for approximately 51 hours on a 6-core/12-thread CPU computer. Right away, 87.6% of the original ULH generation was discarded due to violation of one or more constrains in the process. This called for a reassessment of input variables boundaries, which is proven to be an important step in the optimisation workflow. Afterwards a second set of DOE designs was generated using the same methodology. A useful tool for making this reassessment of input boundaries is the correlation diagram (see fig. 95). This enables the designer to gain insight in the effects of various input parameters in relation to the objectives. This showed objective variables from different disciplines are barely correlating. After completing the final ModeFRONTIER iteration, solutions are clustered using hierarchical clustering. This is helped to assess the relation between input parameters and the four objectives. In the case this is done for the input parameter of the amount of roof steps, because results showed this parameter was of great influence on the objectives (see fig. 96).

The full set of optimised solutions of the multi-objective optimisation can be visualized in the Pareto front. For visualisation purposes, the research used the objective for the modified uniformity ratio as a constrain instead. This results in a 3D Pareto front, showing the performance on the objectives of the modified UDI (maximize), Energy use Intensity (minimize) and mass (minimize). The result overview shows the total of 65 Pareto front solutions (see fig. 97). After completing this first iteration of the optimisation workflow, the research continues by repeating the optimisation several more times by zooming in on the promising clusters. This is done by reducing the boundaries for a portion of the input parameters, based on the Pareto front solutions and the cluster analyses. In this case the parameter for the amount of roof steps is reduced to a boundary between 2 and 3, before restarting the process. The research uses these multiple iterations to reduce the number of designs in the final Pareto front, and thus finding the desired solution by implementing the PCA process to its full extend.

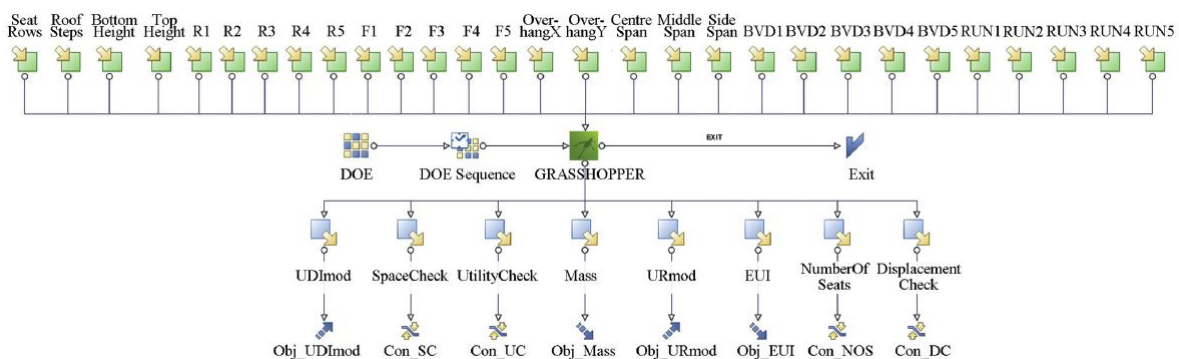


Figure 94. ModeFRONTIER workflow of the case study of Yang et al. (2018)

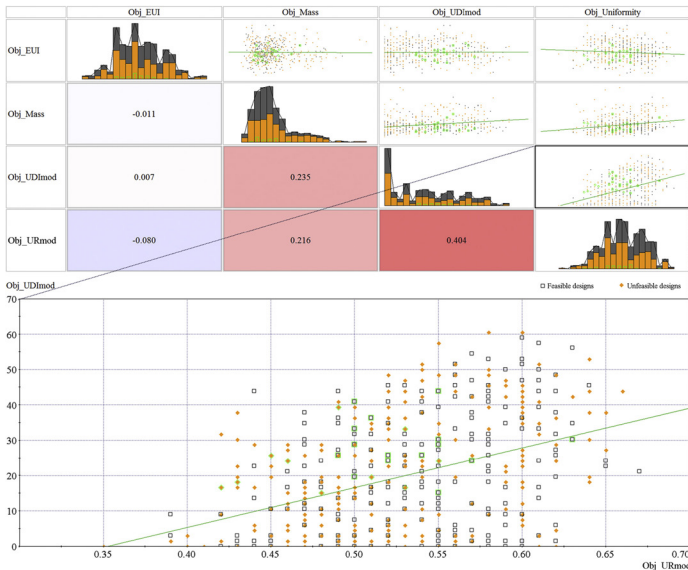


Figure 95. Correlation graph of Yang et al. (2018)

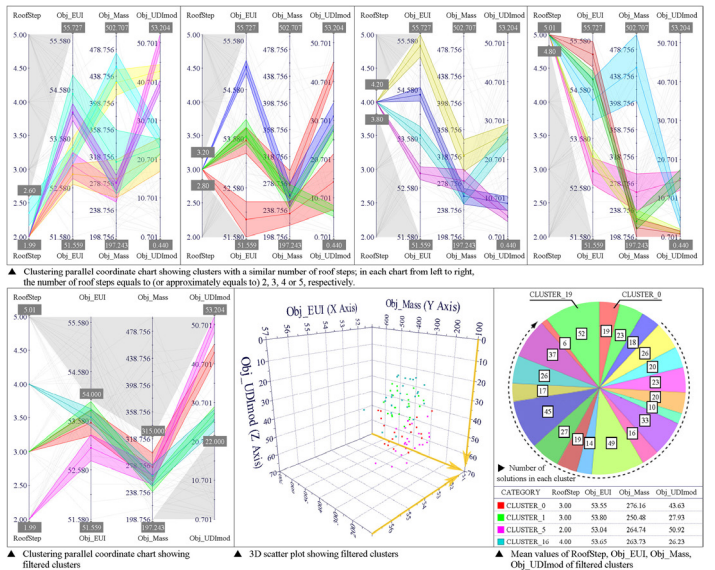
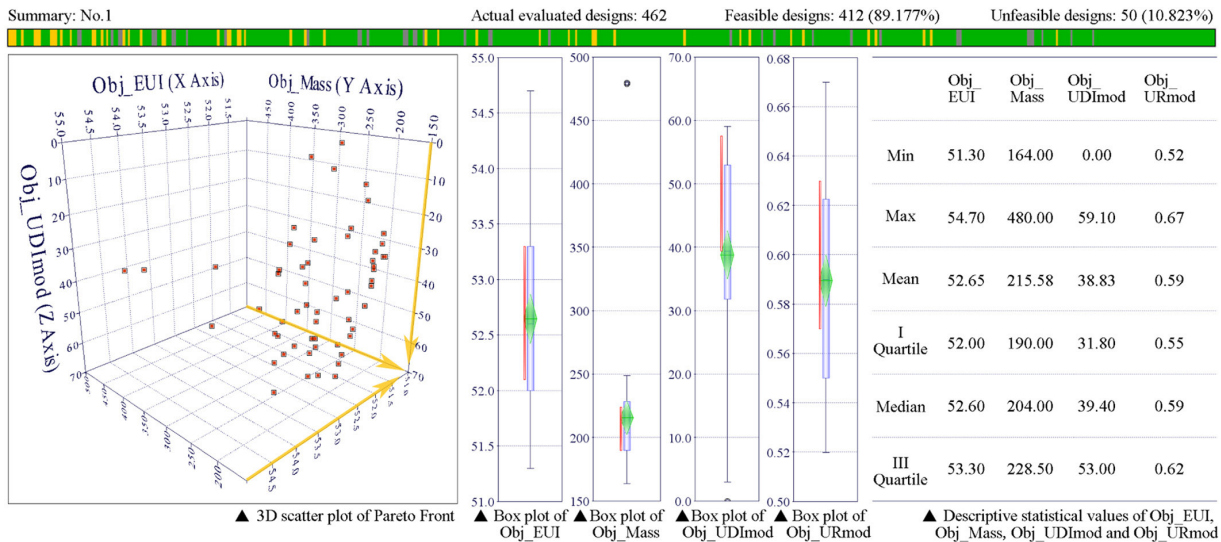
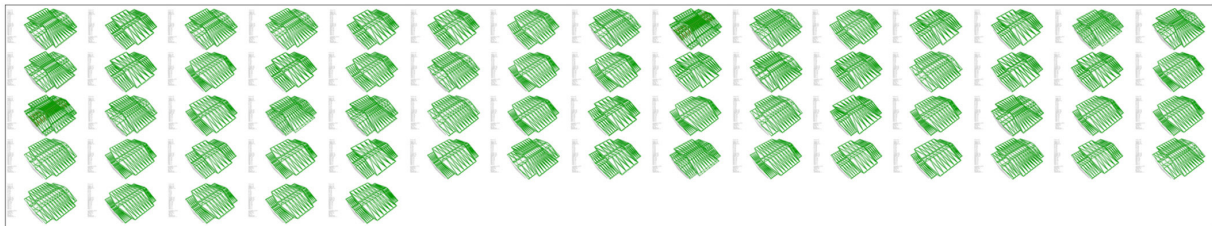


Figure 96. Cluster analysis of Yang et al. (2018)



▼ Geometries of Pareto solutions (65 Pareto solutions)



▼ Geometries of initial generation (25 initial solutions selected using UHL)

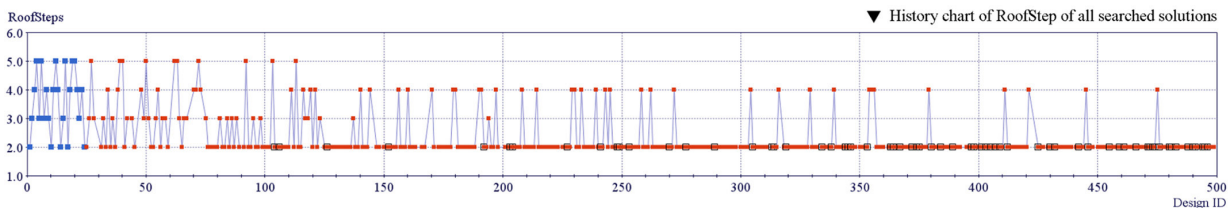


Figure 97. Pareto front solutions of the first optimisation iteration of the case study of Yang et al. (2018)

2.5.2 - Typology analysis

Based on the six selected researches of the previous paragraph, the implementation of the PCA process for sun shading design can be categorized according to typology (see fig. 98). This paragraph will continue by elaborating on each of the defined typologies.

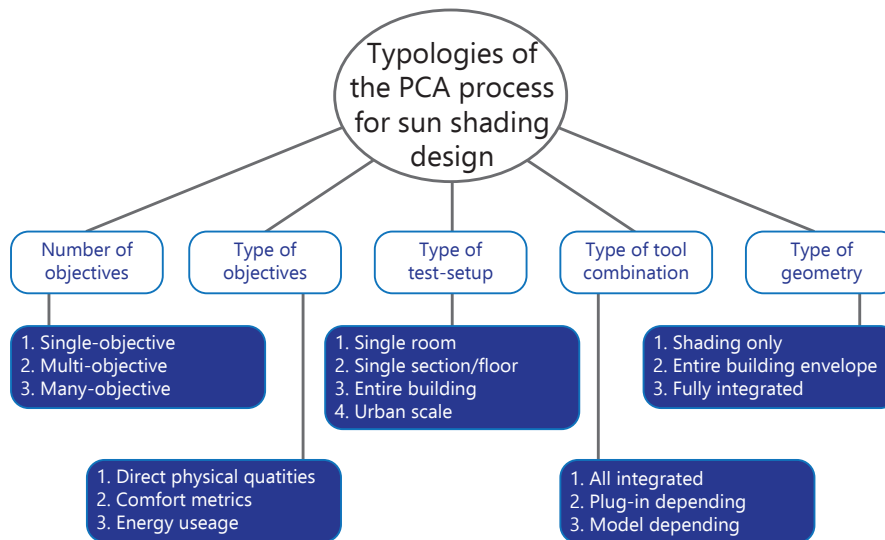


Figure 98. *PCA process for sun shading design typologies (by author)*

The number of objectives

First of all, the typology of the number of objectives. There are three categories; single-objective, multi-objective and many-objective. This typology refers to the number of objectives included in the optimisation phase of the PCA process. A single-objective optimisation is a process with just a single objective and will result in a single solution which can be considered best. The first case study fits this typology.

A multi-objective optimisation includes between two and four objectives. Optimal solutions for this category can be found in de Pareto frontier. An optimal solution can be defined by the property that no increase in performance on one objective can be achieved without decreasing the performance on other objectives. In the case of two objectives this is a 2D line spanning across the outer most solutions of the result splatter graph. For cases with three objectives the Pareto front can be visualized as a 3D surface spanning across the edge of a solution cloud. In the case of four objectives, additional techniques such as colors or animation are required to visual the Pareto frontier. The second case study fits this typology, as well as most of the PCA processes within the review of Ekici et al. (2019).

The last category, the many-objective optimisation, includes more than four objectives. Theoretically the optimal solution can also be found on the Pareto front, but visualizing and interpreting these results is complicated. This type of optimisation is far less often used in the PCA process and therefore beyond the scope of this research.

The type of objectives

When the PCA process is described in relation to sun shading design, the state-of-the-art overview concluded on three different types of objectives. It can be argued the order of these categories corresponds to an increasing level of simulation complexity.

The first category involves direct physical quantities, such as the amount of incident radiation and the daylight factor used in the first case study. The values representing this type of objective can be calculated using only the core ray-tracing and thermal dynamic simulations of the Radiance and Energyplus engines.

The second category are the objectives based on comfort metrics. Comfort metrics are intended to rate the level of visual or thermal comfort like explained in the first two chapters of this report. These comfort metrics are commonly based on multiple of the previously mentioned direct physical quantities, and therefore involve an increased level of complexity. The physical quantities calculated by the software engines serve as the input for comfort metric interpretation components.

The third category involves objectives based on energy usage. This is calculated by supplying setpoints for the heating and cooling installations to kick in. By combining this with some other HVAC system related parameters, the software is able to calculate the annual amount of energy use.

Test set-up

Another typology in which the PCA process for sun shading design can be categorised is the type of set-up. The test set-up refers to the arrangement of virtual test points and the geometry. The definition of the test set-up is of heavy influence on the total calculation time. Based on the researched case studies, four categories can be defined. In essence these four categories describe different levels of scale.

First of all, the single room. In this category the test set-up is kept as small as possible. This typology is often used buildings with a repetitive design of individual rooms, such as schools, close floor offices or hospitals.

One scale bigger is categorized as the building section or floor. This is often used for building without room repetition, but relatively separate sections. A section can refer to a wing of a building and a floor can refer to a floor in an open office interior design.

The third category is the entire building. This type of set-up is often used when a building has relatively low amount of room repetition. Other applications are the massing phase of the architectural design process in order to evaluate the performance of the envelope shape, or the performance check of a near definitive design at the final phase of the project.

Last of all, the urban scale. This is less relatable for sun shading in the traditional sense, but used to asses the shading effect of buildings on their surroundings, or vice versa.

The used tool set

Although the choice of software is not necessarily important, the capabilities should match the goal of the PCA process. This results in another typology for the PCA process in relation to shading design; the choice of software. However, since the software is merely a tool in the PCA process and software will always be evolving, the definition of these categories may change over time and even new categories might emerge. In general, there are now three main categories of software choices available.

The first category is the all integrated software package. This refers to software which is able to conduct all three phases of the PCA process within the same interface. One of the examples for this category in relation to sun shading design is Design builder.

Secondly, the category of plug-in dependent software packages. The two most commonly used for architectural design are Grasshopper (in combination with Rhino) and Dynamo (in combination with Revit). These software packages offer capabilities for the form-finding phase, but rely on other plug-ins to conduct the performance evaluation and optimisation phase. Most common plug-ins for the performance evaluation phase are Ladybug and Honeybee, they perform the simulations using the engines of Radiance, Daysim, Energyplus and Open studio. The most promising plug-in for the optimisation phase is Octopuss. (Wortmann, 2018)

The last category is the model dependent software packages. This category involves software aimed at the optimisation phase and integrating with other software to conduct the form-finding and performance evaluation phase. The big advantage of software in this category is the extended range of options for analysing the optimisation results. One of the software packages in this category is ModeFRONTIER, offering integration with many other packages.

Type of geometry

Lastly, the typology of the geometry that is affected by the input parameters in the PCA process. Within this typology, three categories can be defined. The first one refers to a workflow only parameterizing the shading itself. This is common for projects where many other design decisions are already taken. In projects where the sun shading is a more integrated part of the design process, the input parameters can control parts of the envelope itself as well. This is referred to as the second category; a form-finding set-up including the entire façade. In other cases, the PCA process is used for the complete design process and integrated with other performance simulations and objectives as well. While there are many others, common additional sets of simulations and objectives include the structural performance and architectural performance, such as the number of seats in stadium. This last category is referred to as fully integrated.

2.5.3 - References

1. Ekici, B., Cubukcuoglu, C., Turrin, M. and Sariyildiz, I. (2019). Performative computational architecture using swarm and evolutionary optimisation: A review. *Building and Environment*, 147, pp.356-371.
2. Turrin, M., von Buelow, P. and Stouffs, R. (2011). Design explorations of performance driven geometry in architectural design using parametric modeling and genetic algorithms. *Advanced Engineering Informatics*, 25(4), pp.656-675.
3. Futrell, B., Ozelkan, E. and Brentrup, D. (2015). Bi-objective optimization of building enclosure design for thermal and lighting performance. *Building and Environment*, 92, pp.591-602.
4. Chen, X., Yang, H. and Sun, K. (2016). A holistic passive design approach to optimize indoor environmental quality of a typical residential building in Hong Kong. *Energy*, 113, pp.267-281.
5. Chatzikonstantinou, I. and Sariyildiz, I. (2017). Addressing design preferences via auto-associative connectionist models: Application in sustainable architectural Façade design. *Automation in Construction*, 83, pp.108-120.
6. Zhang, A., Bokel, R., van den Dobbelsteen, A., Sun, Y., Huang, Q. and Zhang, Q. (2017). Optimization of thermal and daylight performance of school buildings based on a multi-objective genetic algorithm in the cold climate of China. *Energy and Buildings*, 139, pp.371-384.
7. Yang, D., Ren, S., Turrin, M., Sariyildiz, S. and Sun, Y. (2018). Multi-disciplinary and multi-objective optimization problem re-formulation in computational design exploration: A case of conceptual sports building design. *Automation in Construction*, 92, pp.242-269.
8. Kiritat, A., Koyunbaba, B., Chatzikonstantinou, I. and Sariyildiz, S. (2016). Review of simulation modeling for shading devices in buildings. *Renewable and Sustainable Energy Reviews*, 53, pp.23-49.
9. Wortmann, T. (2018). Efficient, Visual, and Interactive Design Optimisation with Model-based Methods.. Ph.D. Xi'an Jiaotong-Liverpool University.

2.6 - State of the art: Sun shading in high-rise

2.6.1 - Case studies

In order to get an overview of the state of the art of currently available sun shading systems for high-rise buildings, the review by Al-Masrani et al. (2018) will be used to generate a list of researches involving shading designs that fit the scope of this research. The goal of the review is to identify challenges and future trends for optimised solar shading designs for tropical office buildings. However, some of the researches involve non-tropic climates and/or other building usage types. In order to select the case studies relevant to this research, the following filters are used:

1. The location of the case study has to be close to one of the three proposed climate regions of this research, which are Singapore, Abu Dhabi and Brisbane.
2. The building usage type has to be 'office'
3. The factors must include either 'daylight', 'thermal' or 'energy'
4. The approach must include a simulation. This filter is set to make sure the sun shading design methodology can be integrated in the PCA process

Figure 99 to 102 show the complete selection meeting the criteria of the filters state above. The category of fixed shading design contains 8/29 researches meeting the filter criteria, the manually adjustable category 0/7, the kinetic dynamic category 4/17 and the hybrid category 5/20. This results in total list of 17/73 researches fitting the criteria. From each of the three categories containing researches that passed the filter, one case study will be selected for a more in depth analysis

No.	Study	System	Location	Building	Factors	Tools	Approach
1	Ossen et al. (2005)	Overhang	Kuala Lumpur/Malaysia	Office	Daylight Energy	- eQUEST-3 (DOE 2.2)	Theoretical & Simulation
2	Lee and Tavil (2007)	Overhang	Houston, Chicago /USA	Office	Daylight Energy	- DOE-2.1E	Theoretical & Simulation
3	Ho et al. (2008)	Overhang	Taiwan	Classroom	Daylight Energy	- Lightscape - Field study	Theoretical & Experimental
4	Kröger and Dorigo (2008)	Horizontal louvers	Brazil	Classrooms	Daylight	- Radiance	Theoretical & Simulation
5	Rao and Tzempelikos (2010)	Overhang	Lafayette/TN USA	Office	Daylight	- Ecotect - Multiple-bounce radiosity method	Theoretical & Simulation
6	Alzoubi and Al-Zoubi (2010)	Horizontal and Vertical louvers	Amman/Jordan	Office	Energy	- Lightscape	Theoretical & Simulation
7	Kim and Kim (2010)	Tilted louvers 45° Sloped External Shading	Seoul, Korea	Residential	Daylight Energy View	- Radiance - Virtual Environment (VE)/ scaled model	Theoretical & Simulation
8	Beaman and Bader (2010)	Interlocking hexagonal grid	Austin-Texas/USA.	Thermal Lab	Daylight	- Eco-tech- Field study	Theoretical & Experimental
9	Al-Tamimi and Fadil (2011)	Overhang, vertical fins and egg-crate	Penang/Malaysia	Residential	Thermal	- (IES < VE >) - Field study	Theoretical & Experimental
10	Mandalaki et al. (2012)	Thirteen shading models	Athens and Chania/Greece	Office	Energy	- Radiance - Energy Plus - Ecotect v5.60 - Daylight field study - Radiance	Theoretical & Experimental
11	Sherif et al. (2012a)	Solar screens	Al-Sadat /Egypt	Residential	Daylight	- Radiance	Theoretical & Simulation
12	Sherif et al. (2012b)	Solar screens	Jeddah/Saudi Arabia	Residential	Daylight	- Diva-for-Rhino	Theoretical & Simulation
13	Sherif et al. (2012c)	Solar screens	Kharga Oasis/ Egypt	Residential	Energy	- Energy Plus	Theoretical & Simulation
14	Sherif et al. (2013)	Solar screens	Kharga Oasis/Egypt	Residential	Energy	- Design Builder - Energy Plus	Theoretical & Simulation
15	Yassine (2013)	Overhangs, vertical fins, horizontal and vertical louvers	Dubai/UAE	Office	Energy	- IES (VE)	Theoretical & Simulation
16	Aldawoud (2013)	Overhangs and vertical fins	Phoenix, Arizona	Office	Thermal	- Design Builder	Theoretical & Simulation
17	Rahimzadeh et al. (2013)	Triangular panels claddings	Singapore	Multi Functions	Daylight	- DIVA For Rhino	Theoretical & Simulation
18	Emami et al. (2014)	Panometric ornamental solar screen	Iran	Office	Daylight Structure	- Rhino	Theoretical & Simulation
19	Freewan (2014)	Egg-crate, vertical fins and diagonal fins	Jordan	Office	Thermal Daylight	- IES/Sun Cast - Radiance - Field study	Theoretical & Experimental
20	Manzan (2014)	Flat panel device	Trieste and Rome/Italy	Office	Energy	- DAYSIM	Theoretical & Simulation
21	Anfin and Denan (2015)	Vertical overhang fins Egg-crate	Kuala Lumpur/Malaysia	Office	Thermal	- Field study	Experimental
22	Denan and Majid (2015)	Overhang, vertical fins and egg-crate	Kuala Lumpur/Malaysia	Office	Daylight	- Field study	Experimental
23	Sun et al. (2015)	Overhang	Hong Kong	Lab	Energy	- Mathematical equations - Simulation software	Theoretical & Simulation
24	Omidfar (2015)	Interdredes parametric solar screens	Boston/USA	Office	-Daylight- Energy	- Rhino	Theoretical & Simulation
25	Kim et al. (2015)	Panometric complex kinetic façades	Abu Dhabi, the United Arab Emirates	Office	Daylight	- Autodesk Revit and Dynamo	Theoretical & Simulation
26	Lau et al. (2016)	Overhang, vertical fins and egg-crate	Kuala Lumpur/Malaysia	Office	Energy	- IES (VE)	Theoretical & Simulation
27	Lim and Heng (2016)	Incline panels claddings	Kuala Lumpur/Malaysia	Office	Daylight	- Field study	Experimental
28	Khoroshilteva et al. (2016)	Overhangs and fins	Madrid/Spain	Residential	Thermal Energy	- Energy Plus	Theoretical & Simulation
29	Chi et al. (2018)	Solar screens	Seville,Spain	Office	Daylight Thermal Energy	- Diva-for-Grasshopper	Theoretical & Simulation

Figure 99. Selection of researches meeting the criteria of the fixed shading category

No.	Study	System	Location	Building	Factors	Tools	Approach
1	Kim et al. (2009)	Venetian Blinds	Seoul, Korea	Office	Energy	- Energy plus	Theoretical & Simulation
2	Ip et al. (2013)	Operable Roller Blinds	UK	Office	Thermal Life-cycle	- Field study - IES Virtual Environment	Theoretical & Experimental
3	Yao (2014a)	Moveable Roller Shade	Ningbo/China	Residential	Daylight/Thermal/Energy	- Field study	Theoretical & Experimental
4	Yao (2014b)	Moveable Sunshades	Ningbo/China	Office	Thermal	- Energy plus - Building Controls - Virtual Test Bed	Theoretical & Simulation
5	Dyke et al. (2015)	Moveable Blinds	Boise, ID, USA	Office	Energy	- Energy plus	Theoretical & Simulation
6	Yao et al. (2016a)	Moveable Sunshades	Ningbo/China	Office	Daylight	- Building Controls - Virtual Test Bed - Energy plus	Theoretical & Simulation

Figure 100. Selection of researches meeting the criteria of the manually adjustable category

No.	Study	System	Location	Building	Factors	Tools	Approach
1	Tzempelikos and Athienitis (2007)	Roller shade	Montréal/Canada	Office	Energy	- Energy plus	Theoretical & Simulation
2	Nielsen et al. (2011)	Fully retractable venetian blinds	Denmark	Office	Daylight Energy	- iDBuild - BuildingCalc - LightCalc	Theoretical & Simulation
3	Konstantoglou et al. (2013)	Non-Retractable Moveable Louver	Greece	Office	Daylight Energy	- Daysim	Theoretical & Simulation
4	Grobman and Yekutieli (2013)	Kinetic cladding	-	Office	Daylight/controlling	- Prototyping	Experimental
5	Yun et al. (2014)	Venetian blinds	South Korea	Office	Daylight Energy	- Energy Plus - DIVA-for-Rhino - Glare indices	Theoretical & Experimental
6	Yekutieli and Grobman (2014)	Kinetic cladding	-	Office	Daylight/controlling	- Field study - Prototyping	Experimental
7	Elghazi et al. (2014)	Origami	Cairo/Egypt	Residential	Daylight	- DIVA-for-Rhino	Theoretical & Simulation
8	Sjarifudin and Justina (2014)	Shading using parametric camshaft mechanism	Indonesia	Office	Daylight	- Ecotect - Analysis - Radiance	Theoretical & Simulation
9	Priatman et al. (2015)	Solar-powered vertical fins	Indonesia	Office	Daylight Thermal	- Field study	Experimental
10	Sabry et al. (2015)	Multi-layer kinetic skin	Cairo/Egypt	Office	Daylight	- DIVA-for-Rhino	Theoretical & Simulation
11	Bunning and Crawford (2016)	Venetian blind slats	Melbourne, Australia	Office	Life cycle Energy	- Design Builder - EnergyPlus	Experimental & Simulation
12	Ahmed et al. (2016)	Kinetic shading device	Cairo/Egypt	Residential	Thermal Energy	- Field Study	Experimental
13	Mahmoud and Elghazi (2016)	Parametric-based Kinetic Facade	Cairo/Egypt	Office	Daylight	- DIVA-for-Rhino	Theoretical & Simulation
14	Carletti et al. (2016)	Motorised venetian blinds	Italy	Residential	Daylight Thermal	- Field study	Experimental
15	Al-Obaidi et al. (2017a)	Dynamic Sliding	Malaysia	Low-rise buildings	Daylight	- Field Study	Theoretical & Experimental
16	Grobman et al. (2017)	Static louvers and dynamic louvers	Mediterranean climate	Office	Adapted Useful Daylight Illuminances	- DIVA-for-Rhino	Theoretical & Experimental
17	Elzeyadi (2017)	Dynamic façade shading typologies	Global	Office	Building energy performance and occupant smulti-comfort	- Review	Experimental Survey

Figure 101. Selection of researches meeting the criteria of the kinetic dynamic category

No.	Study	System	Material	Factors	Tools	Approach
1	LIFT Architects (2017)	Four-leafs Two-leafs Single-leaf	SMAs	Daylight Energy	- Empirical test on Physical model	Experimental
2	Doumpioti et al. (2010)	Elliptical apertures façade	SMAs	Daylight/ Ventilation	- Review	Theoretical
3	Khoo et al. (2011)	Curtain Blind	SMAs	Daylight thermal and visual communication	- Plug-in Grasshopper - Physical model	Experimental
4	Lienhard et al. (2011)	Flectofin Double Flectofin	GFRP	Structural behaviour	- (FEM)/ Newton-Raphson algorithms - Full scale Prototype	Theoretical & Experimental
5	Schleicher et al. (2011)	Curved-line folding	GFRP	Kinematical behaviour	- Finite element modelling (FEM)	Theoretical
6	Sung et al. (2011)	Glass panel shutter system	Biometal	Daylight View	- Simulation - Empirical test on Physical model	Experimental & Simulation
7	Dewidar et al. (2013)	Self-automated panels	SMAs	Daylight/Ventilation	- Review	Theoretical
8	Khoo and Salim (2013)	Blind and Blanket	SMAs	Daylight/Ventilation	- Fire Fly plug-in Grasshopper - Physical model	Experimental
9	Vergauwen et al. (2013)	Curved-line folding	-	Folding behaviour	- Grasshopper - Paper scaled-models	Theoretical & Experimental
10	Vergauwen et al. (2014a)	Curved-line folding	-	Folding behaviour	- Polypropylene scaled models	Experimental
11	Vergauwen et al. (2014b)	Curved-line folding	-	Folding behaviour	- Tachi Freeform Origami, - Kingkong - Grasshopper - FEM software	Theoretical & Simulation
12	Rossi et al. (2014)	Electronic/pneumatic façade system	Pne-net silicone elastomer	Daylight View	- Rhino - Physical model	Experimental & Simulation
13	Adriaenssens et al. (2014)	Shading Shells	Bimetal	Energy	- Ecotect /EFEN - Scaled-model	Theoretical & Experimental
14	Karamata and Andersen (2014)	Shape Variable Mashrabiya	-	Daylight	- DIVA-for-Rhino	Theoretical & Simulation
15	Pesenti et al. (2015a)	Origami patterns	SMAs	Actuation energy	- Grasshopper - Kangaroo Plug-in - Prototype	Theoretical & Experimental
16	Pesenti et al. (2015b)	Ron Resch Origami	SMAs	Daylight Energy	- Honeybee - Radiance - Daysim	Theoretical & Simulation
17	Schleicher et al. (2015)	Bending tepals	GFRP PMMA/ acrylic glass	Kinematical behaviour	- Energy plus - FEM software - FE-simulation	Theoretical & Simulation
18	Giovannini et al. (2015)	Shape Variable Mashrabiya	-	Daylight/ Energy	- DIVA-for-Rhino - Daysim	Theoretical & Simulation
19	Reichert et al. (2015)	Wooden veneer array	Wooden veneer	Folding behaviour	- Energy Plus - Simulation - Empirical test on Physical model	Experimental & Simulation
20	Florito et al. (2016)	Shape morphing solar shadings	Shape Memory Alloys (SMAs)	Daylight/Energy	- Review	Theoretical

Figure 102. Selection of researches meeting the criteria of the hybrid category

Lau et al. (2016)

The first case study selected for an in-depth analysis is the research by Lau et al. (2016), about the potential of shading devices and glazing configurations on cooling and energy savings for high-rise office buildings in the climate of Malaysia. This study is selected because it addresses the observed trend of the all-glass exterior for office buildings and the challenges involved in realizing this in the tropical climate. As an example, the climate of Malaysia is analysed, showing relative high levels of annual solar radiation and a minimal fluctuation in average outdoor temperatures over the seasons (see fig 103.).

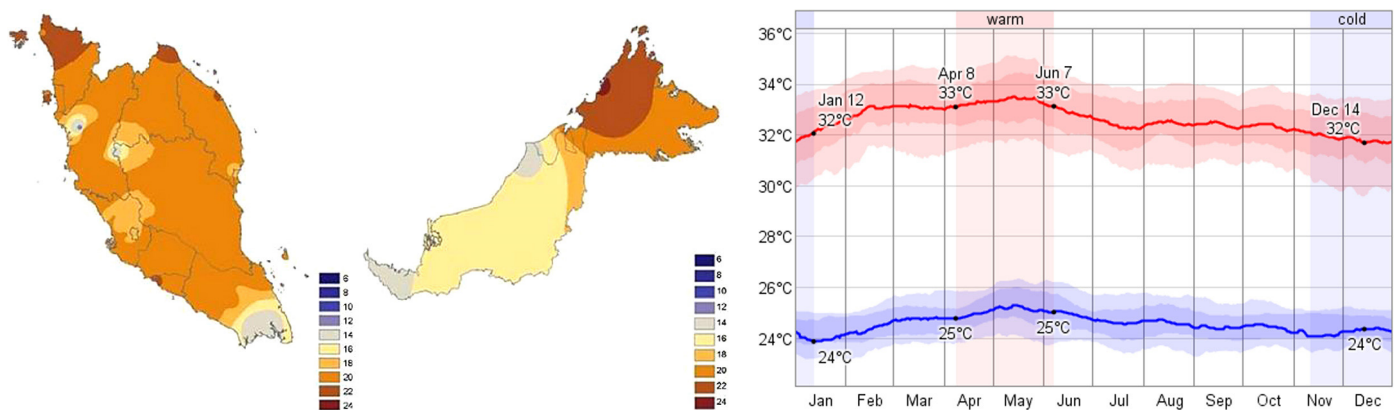


Figure 103. *Climate analysis of Malaysia in the study of Lau et al. (2016)*

Because of these minimal fluctuations and based on other studies (Offiong and Ukpoho, 2004) the research states external shading is the best choice for the tropic climate. Integration of this exterior shading with an all-glass façade remains an architectural challenge. In this study, the performance of three common types of sun shading are compared; horizontal overhangs, vertical fins and a combination of the two; the egg-crate sun shading system. The performance was compared for all four of the cardinal wind directions. To test this performance, a high-rise office building located at Jalan Munshi Abdullah, Kuala Lumpur was selected (see fig. 104). One of the main reasons for selecting this building is its window to wall ratio of 1. This means the façade is fully glazed, which is in line with the global trend of high-rise office buildings. The building contains a 4-story high lobby, with 41 floors of occupied office space above. The floor to floor height 4 meters and the square area of the rectangle footprint is 72,000 m². The design is based on an open floor office space on the perimeter of the building and a core with utilities in the center. The study concludes by defining the egg-crate system as the shading system with the best performance. This conclusion is found in many other studies within the fixed sun shading category of the review of Al-Masrani (2018), as it is also included in the final conclusion of the literature review itself.

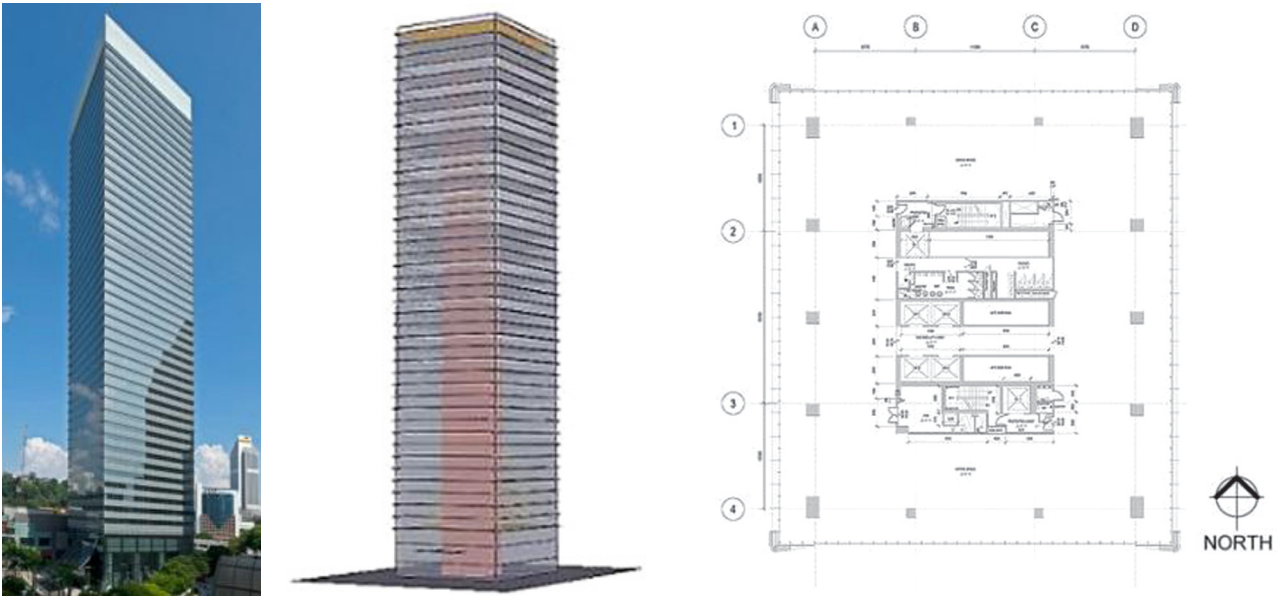


Figure 104. Case study building in the study of Lau et al. (2016)

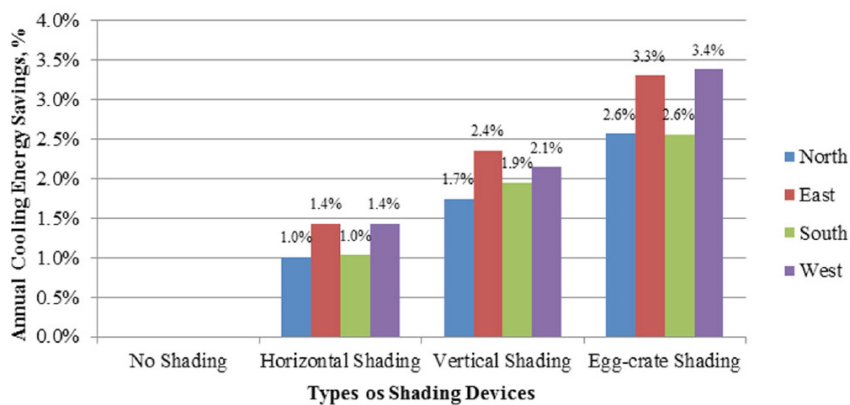


Figure 105. Results of the study of Lau et al. (2016)

Sabry et al. (2015)

The category of kinetic shading devices in the review of Al-Masrani (2018) refers to shading systems relying on complex mechanical systems to change the configuration of the shading elements. The research of Sabry et al. (2015) is about a building in Egypt with a kinetic solar shading consisting of two layers. The glazing behind the exterior shading system spans the entire façade. The inner layer consists of dynamic horizontal louvers, while the exterior layer is a dynamic skin based on folding triangles. The geometrical configuration of this skin is derived from three main variables; the depth of the horizontal louvers and the unit radius and rotation angle for the dynamic skin (see fig. 106). This dynamic skin is similar to the sun shading of the Al-Bahr towers (see fig. 107). In the case of this building, the dynamic skin is grouped in sections with are controlled by an automated computer system. (Attia, 2017).

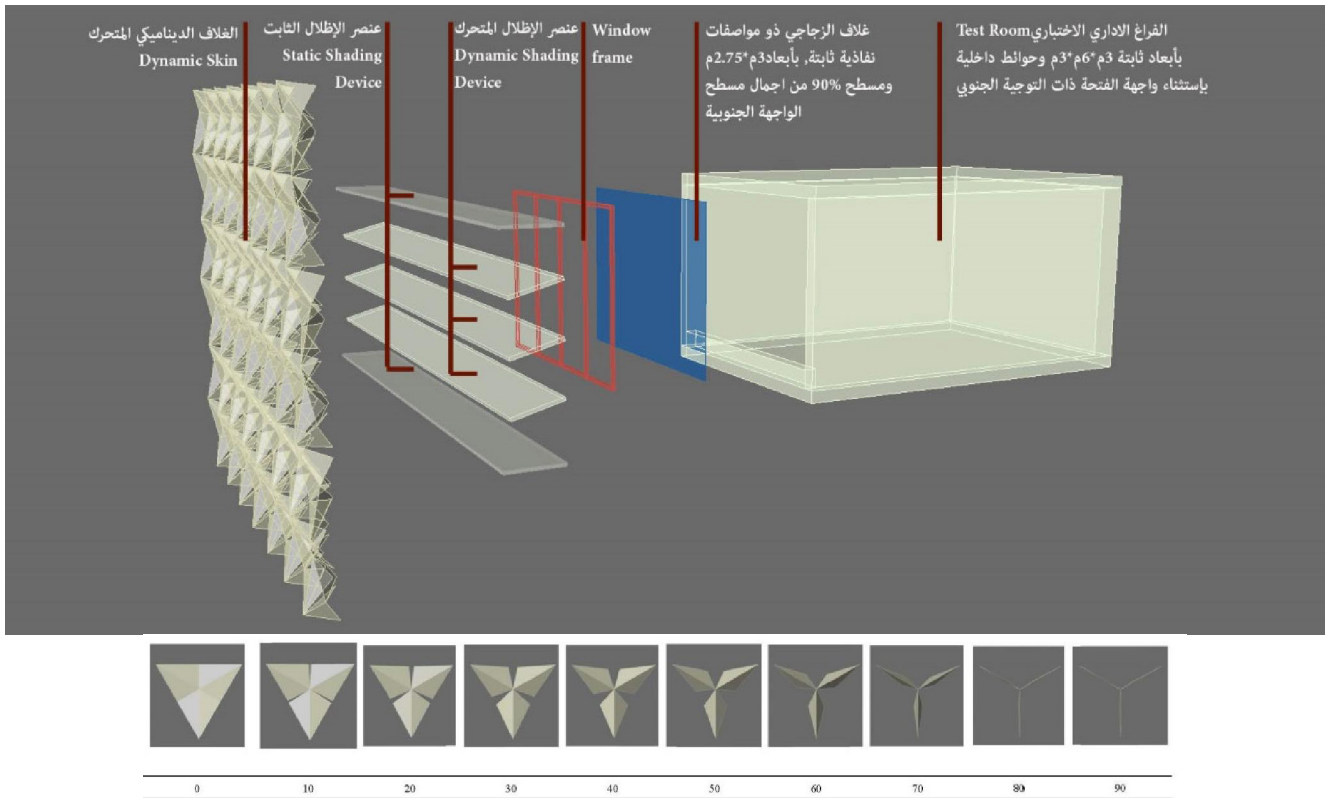


Figure 106. *Shading set-up in the study of Sabry et al. (2015)*



Figure 107. *Al Bahr Towers, United Arab Emirates (google.com)*

In the research of Sabry et al. (2015), the goal is to improve the natural daylight quality. This is done by evaluating the performance on two different visual comfort metrics; the spatial daylight autonomy (sDA 300/50%) and the annual sunlight exposure (ASE 1000/250). The sDA describes the sufficiency of daylight illuminance levels within a space, and is defined as the ratio of space area which achieves a daylight level above 300 lux for at least 50% of the annual occupation hours. The ASE describes the expected annual hours of visual comfort due to glare and is defined as a ratio of floor area where the direct illumination level is over 1000 lux for more than 250 hours of the total occupation hours.

In order to evaluate this performance, a Grasshopper model was set-up to generate the geometry. Diva was used to conduct the simulations of a single-room test set-up. Using this methodology, 320 different designs where tested. This methodology seems similar to the PCA process, however, there was no search algorithm involved in this case study. When projected on the PCA process this would be an optimisation phase with only one generation. The study concludes by giving the optimal configuration of input parameters for the shading concept in relation to the two objectives of the sDA (300/50%) and the ASE (1000/250) (see fig. 108):

“The research reached to the optimum of skin configurations which achieves the maximum levels of day light performance in office space and it is skin unit radius is (0.6m.), main shading devices depth (1.05m.), secondary shading devices depth (0.75m.) it is a constant value during simulation process, and (70°) to skin unit rotation angle, the skin reached to (100% SDA) and (3% ASE).” (Sabry et al. (2015)

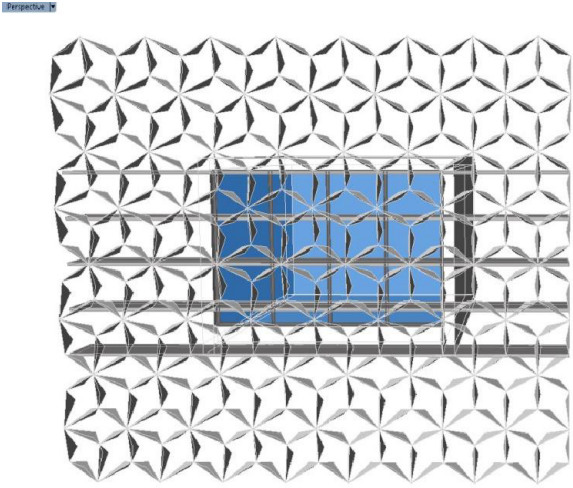
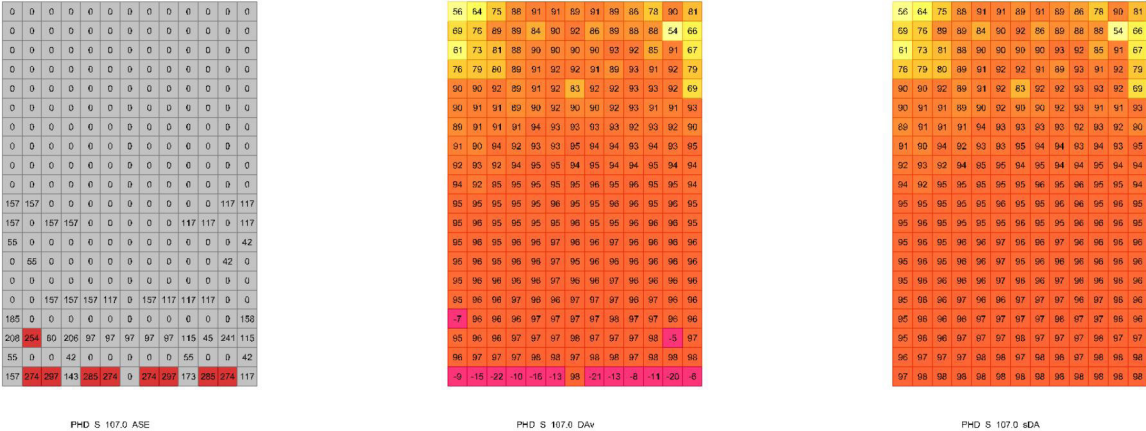


Figure 108. Results of the study of Sabry et al. (2015)

Pesenti et al. (2015)

The final case study involves a research of the hybrid category. Hybrid shading systems are based on the deformation capability of smart materials producing spatial movements. This process requires only a small amount of energy to be initiated and controlled. (Al-Obaidi et al., 2017). The main benefit of using the properties of the smart materials is eliminating the change of mechanical failure, which has proven to be a common issue for kinetic shading systems (Pesenti et al., 2015). According to Al-Masrani (2018), studies revolving hybrid shading systems are rarely conducted in the tropics, a need to be addressed in further studies.

The research selected from this category of shading systems is the one by Pesenti et al. (2015), because it aims to optimise the shading system by using visual and thermal comfort simulations, which is very similar to the goal of this thesis. The shape morphing of the geometry in the case study relies on Shape Memory Alloys (SMA), which are electrically activated. Previous research has set some boundaries for designing with SMA regarding deformation and materialization (Peraza-Hernandez et al., 2014). The same study also proposed origami based patterns to be promising design directions for hybrid sun shading systems, on which the research of Pesenti et al. (2015) continues.

For the case study, an origami pattern was designed, but because of the complex dynamic 3D geometry, preliminary simulations indicated some challenges. In order to overcome these challenges, the origami-based geometry was simplified to two sets of faces (see fig. 109). The effect of the origami structure opening up and closing down is mimicked by varying the opacity of these two sets of faces. Based on this methodology, a total of 27 design alternatives were generated (see fig. 110). These design alternatives resemble various contractive states of the actual 3D origami geometry

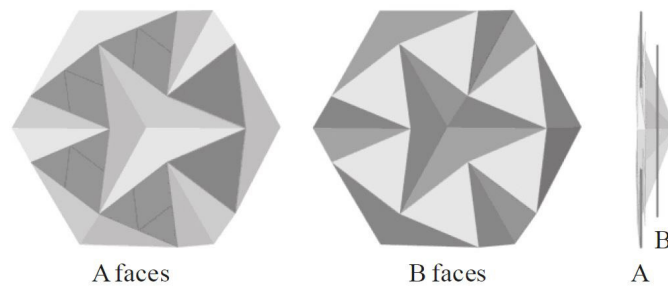


Figure 109. *Simplification diagram of the study of Pesenti et al. (2015)*

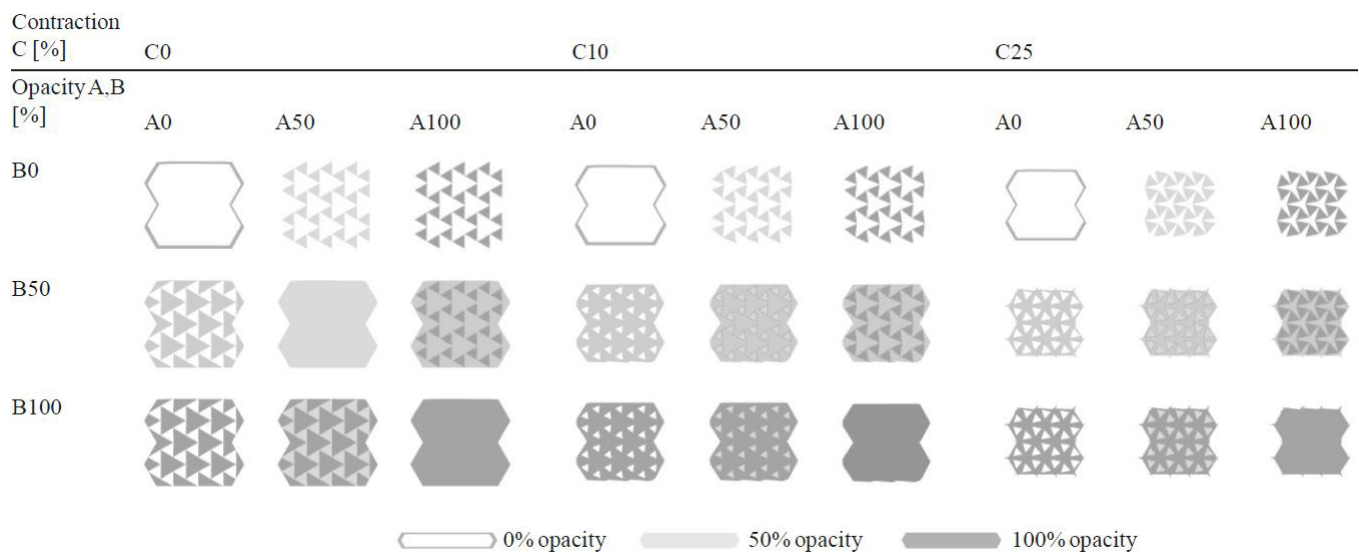


Figure 110. *Design alternatives of the study of Pesenti et al. (2015)*

The design alternatives were tested using a single room set-up of 3 by 5 meters, including a south faced window with a wall to wall ratio of 60%. This does not respond to the global trend of the all glass façade, but since this shading system is relatively modular, it can easily be continued along an all-glass façade. The location for the case study is Milan, Italy. This is not within a tropic climate region, but like already stated before, studies involving hybrid systems in the tropics have rarely been conducted (Al-Masrani, 2018).

The form-finding phase for this case study is conducted using Grasshopper, in combination with the plug-in of Ladybug and Honeybee. To assess the visual comfort, the integration of Radiance and Daysim were utilized, while for the thermal comfort, the integration with Energyplus was used. The performance indicators used for this case study are directly related to visual and thermal comfort metrics. To assess the daylight performance, the Useful Daylight Index (UDI), Daylight autonomy (DA) and Daylight Glare Probability Index (DGP) are used. For thermal comfort, the total amount of energy (TE) for heating, cooling and lighting is used. The results for each of the four metrics is given for all 27 design alternatives are shown in figure 111.

The case study concludes with selecting the best performance alternatives and translating them back to various contractions of the actual SMA and origami-based hybrid shading system. It also states the used methodology of assessing the performance was suited for these adaptive facades, but further research should include a more detailed model of the actual 3D origami geometry.

		Contraction C [%]			C0			C10			C25		
Opacity A, B [%]		A0	A50	A100	A0	A50	A100	A0	A50	A100	A0	A50	A100
B0	TE [kWh/m ² y]	109.7	96.2	91.6	109.7	93.5	88.6	109.7	91.5	79.1			
	UDI < 100 [%]	8.2	9.4	10.7	8.2	9.7	11.0	8.2	10.3	13.1			
	UDI 100-2000 [%]	67.2	70.1	74.2	67.2	70.0	73.4	67.2	70.5	74.0			
	UDI > 2000 [%]	24.6	20.5	15.1	24.6	20.3	15.6	24.6	19.2	13.0			
	DA > 500 [%]	78.3	74.5	67.3	78.3	73.6	65.2	78.3	69.6	45.2			
	DGP < 0.35 [%]	73.0	74.9	84.9	73.0	76.7	86.4	73.0	76.2	90.1			
B50	TE [kWh/m ² y]	91.2	86.7	89.1	97.0	83.0	88.9	64.0	69.8	84.5			
	UDI < 100 [%]	10.5	12.7	15.5	11.8	12.9	14.7	11.3	13.4	16.3			
	UDI 100-2000 [%]	70.2	76.5	84.5	74.1	81.6	85.3	70.6	82.2	79.1			
	UDI > 2000 [%]	19.3	11.3	0.0	14.1	5.6	0.0	18.1	4.4	4.5			
	DA > 500 [%]	68.9	62.3	49.9	64.3	59.6	51.8	65.9	57.4	42.9			
	DGP < 0.35 [%]	79.2	85.2	99.6	81.5	91.0	99.6	79.9	94.1	97.9			
B100	TE [kWh/m ² y]	95.2	100.3	144.1	133.3	148.2	144.1	85.1	112.7	144.1			
	UDI < 100 [%]	14.2	24.1	100.0*	46.0	59.6	100.0*	20.6	36.1	100.0*			
	UDI 100-2000 [%]	75.0	75.9	0.0*	53.5	40.3	0.0*	71.7	63.9	0.0*			
	UDI > 2000 [%]	10.8	0.0	0.0*	0.6	0.0	0.0*	7.7	0.0	0.0*			
	DA > 500 [%]	39.0	29.8	0.0*	6.7	0.0	0.0*	21.0	3.7	0.0*			
	DGP < 0.35 [%]	97.2	100.0	100.0*	99.2	100.0	100.0*	97.4	100.0	100*			

* shading completely opaque, therefore no natural light passes through the façade system

Figure 111. Results of the study of Pesenti et al. (2015)

2.6.2 - Typology analysis

The review of Al-Masrani (2018) used for selecting the case studies of the previous paragraph, includes a categorisation on typology of all researches included in the review (see fig. 112). The main categories are passive, active and hybrid. The passive category contains both the fixed system and the manually adjustable system categories discussed in the previous paragraph. The active category refers to the kinetic systems, whereas the hybrid category to the biomimetic systems based on smart material shape morphing. Each of the categories can be further subdivided individually. For the passive category this is based on the design methodology; conventional, stochastic or parametric. For the active category this based on the control type and the kinetic complexity. For the hybrid category this is done based on the control type and deformation agencies. This categorisation on typology can be used for many other shading designs for high-rise buildings as well.

It is remarkable that many of the researches include parts of the PCA process, although mostly the form-finding and performance evaluation phase. The optimisation phase is yet to be integrated to complete the entire PCA process. In addition, Al-Masrani (2018) drew the following conclusions for the three main categories:

Passive sun shading for high-rise office buildings in tropical climates:

“The majority of shading studies in the tropics adopted fixed shading devices, and most literature has identified egg-crate devices as the best device to improve daylight and thermal performance.” (Al-Masrani et al., 2018, p.869)

Active sun shading for high-rise office buildings in tropical climates:

“Performance and the applicability of intelligent building systems, this design faces many criticisms due to its complexity, cost and high operational energy.” (Al-Masrani et al., 2018, p.869)

Hybrid sun shading for high-rise office buildings in tropical climates:

“The performances of dynamic complex geometries and shape morphing shading systems have not yet been explored in the tropics. Consequently, studies must urgently assess the performance of more adaptive geometries in addition to biomimetic approaches represented by hybrid shading systems in a tropical climate.” (Al-Masrani et al., 2018, p.869)

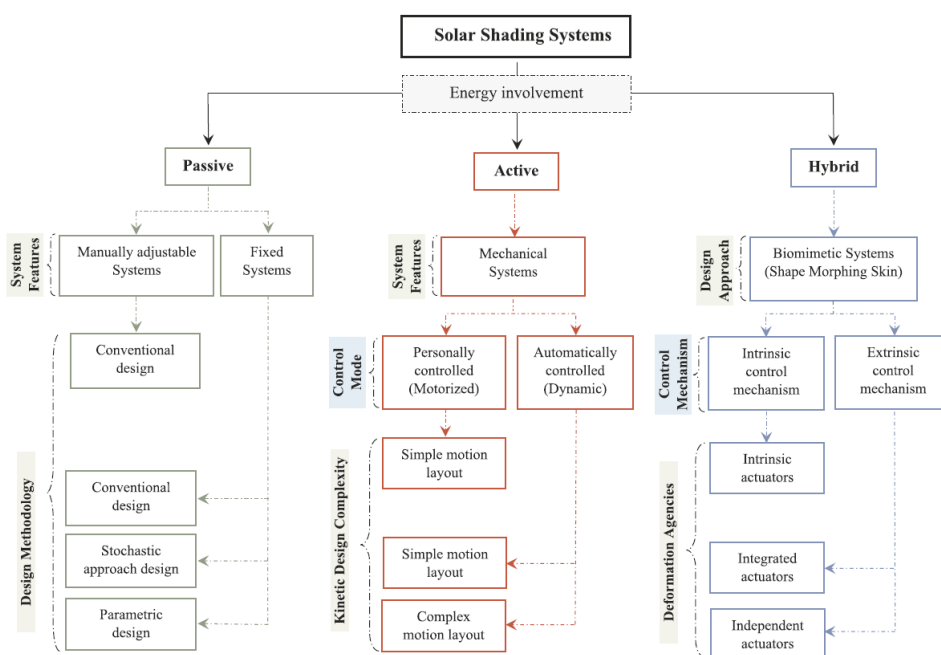


Figure 112. Sun shading typology categorization (Al-Masrani, 2018)

However, the system of Al-Masrani is not the only way to categorize sun shading systems based on typology. Another more traditional and simple method is to categorize the systems based on the placement. There are three categories; exterior, interior and integrated within a double-glazed window or double skin façade (see fig. 114). With the placement of the shading in mind, Raji (2018) has made a typology categorization for common systems applied in high-rise buildings (see fig. 115). The typology overview is completed with pro's and con's referring to the requirements for sun shading systems in high-rise buildings stated in paragraph 2.3.2.

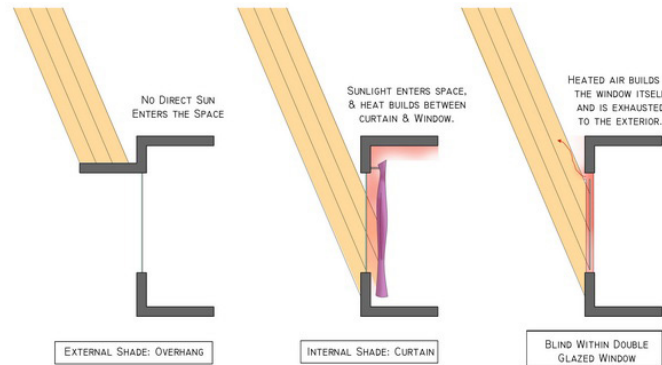


Figure 114. *Categorization of shading system typology based on placement (Google.com)*






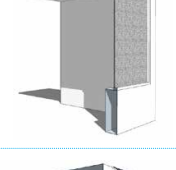
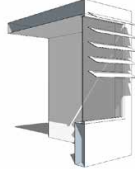
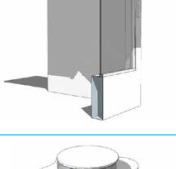


SHADING STRATEGY	Benefits and drawbacks	SHADING STRATEGY	Benefits and drawbacks
Manually operated or motorized venetian blinds inside the building	 <ul style="list-style-type: none"> Contribute effectively for glare control Lower installation and maintenance costs Ineffective at reducing the cooling loads Limit the access to outside views when they cover the entire window 	Overhang (fixed)	 <ul style="list-style-type: none"> Very effective at shading high sun angles in the summer, in particular for windows facing towards: <ul style="list-style-type: none"> South on the Northern Hemisphere South and north on the equator North on the Southern Hemisphere Ineffective at blocking low sun angles (not suitable for east- and west-facing windows) They are not an economical and aesthetically pleasing solution for high-rise buildings
Motorized blinds integrated in the intermediate space of a double-skin façade	 <ul style="list-style-type: none"> The outer skin of the double-skin façade provides an effective shield for blinds against rain, dust and wind; hence result in less maintenance More effective than indoor blinds at limiting the amount of heat radiated into the interior space The most viable option when the incorporation of exterior shading devices might cost a lot or is not safe It may cause overheating if there is no proper ventilation within the two layers of the building façade so they are less efficient than the external shadings for reducing the cooling load Limit the access to outside views when they cover the entire window 	Side fins (fixed)	 <ul style="list-style-type: none"> Effective for blocking sun from a south-easterly or south-westerly direction It can limit a panoramic view
Motorized venetian blinds on the external façade	 <ul style="list-style-type: none"> Blades can be set at different angles so that a very effective strategy for blocking low sun from entering east- or west-facing windows Can only be operated at wind speeds of lower than 10-15 m/s Prone to damage by rain, dust and wind Less viable solution for tall buildings due to impeded cleaning access and wind noise Limit the access to outside views when they cover the entire window 	Smart glass (electrochromic glazing)	 <ul style="list-style-type: none"> Allows for uninterrupted views In their darkened state, the increased heating (winter) and electric lighting loads might offset the cooling effect Not as effective as external shading devices to keep the solar radiation/heat from entering the building, especially in tropical climates with high amount of solar radiation
Fixed louvers	 <ul style="list-style-type: none"> Very effective at blocking low sun from entering east- or west-facing windows For heating-dominant climates in which passive heat gains are highly desired, louvers can increase the heating demand of the building in the winter; hence their application should be avoided on the south-facing windows (in the Northern Hemisphere) and on the north-facing windows (in the Southern Hemisphere) 	Façade-mounted solar PV	 <ul style="list-style-type: none"> Façades (and roof) of high-rise buildings offer a great opportunity for PV to provide shading and generate electricity Using PV on the facade has less output compared with using it on the roof
Recessed or projected balconies combined with greenery systems	 <ul style="list-style-type: none"> In tropical climates, recessed balconies are good strategies for providing deep permanent shading on the east and west sides when larger openings are needed to get access to daylight or natural ventilation Shading and evapotranspiration from implementing vegetation on balconies, sky gardens, roof or vertical greening can regulate the microclimate environment around and inside the building. However, in temperate climates attention should be paid to avoid shading the facade where passive solar gain is desired The effect of heat transfer through the increased surface by recessed terraces might offset the shading effect 	Self-shading façade	 <ul style="list-style-type: none"> Provide shading without blocking the views The effect of heat transfer through the increased surface might offset the shading effect

Figure 113. *An overview of sun shading strategies for high-rise office buildings (Raji, 2018)*

2.6.3 - References

1. Al-Masrani, S., Al-Obaidi, K., Zalin, N. and Aida Isma, M. (2018). Design optimisation of solar shading systems for tropical office buildings: Challenges and future trends. *Solar Energy*, 170, pp.849-872.
2. Lau, A., Salleh, E., Lim, C. and Sulaiman, M. (2016). Potential of shading devices and glazing configurations on cooling energy savings for high-rise office buildings in hot-humid climates: The case of Malaysia. *International Journal of Sustainable Built Environment*, 5(2), pp.387-399.
3. Sabry, S.M., El-Ela, M.M.A., Farag, M.A. (2015). Development of form proportions configurations in office building skins in order to improve daylight levels using "Parametric Design Methods". *J. Am. Sci.* 11 (11).
4. Pesenti, M., Masera, G. and Fiorito, F. (2015). Shaping an Origami Shading Device through Visual and Thermal Simulations. *Energy Procedia*, 78, pp.346-351.
5. Offiong, A. and Ukpoho, A. (2004). External window shading treatment effects on internal environmental temperature of buildings. *Renewable Energy*, 29(14), pp.2153-2165.
6. Attia, S. (2017). Evaluation of adaptive facades: The case study of Al Bahr Towers in the UAE. *QScience Connect*, 2017(2), p.6.
7. Al-Obaidi, K., Azzam Ismail, M., Hussein, H. and Abdul Rahman, A. (2017). Biomimetic building skins: An adaptive approach. *Renewable and Sustainable Energy Reviews*, 79, pp.1472-1491.
8. Raji, B. (2018). *Sustainable high-rises*. Delft: Delft University of Technology.

3. Practical research





3.1 - Conceptual sun shading design

3.1.1 - Eggcrate shading as start point

In order to select a sun shading concept with potential for high-rise buildings with all-glass exteriors, some conclusions can be made based on the fundamental theory and state of the art overviews.

First of all, the choice of sun shading typology based on the categorization of Al-Masrani (2018). The seasonal differences in radiation and outdoor temperatures are limited in the tropic climate (see fig. 103). This means the shading requirements are relatively constant throughout the year. The risk of overheating buildings in tropical climates is relatively big, meaning the solar radiation should be blocked throughout the entire year. In other words, there is only a limited heating period and an extensive cooling period. The choice for an all-glass façade results in a lot of this solar radiation entering the building, increasing the risk of overheating even more. In order to prevent this overheating, a combination of HVAC systems and sun shading strategy is needed.

Based on the conclusions that the requirements for sun shading for buildings with this façade typology, located in the tropical climate are constant throughout the year, it can be argued the fixed sun shading system category could contain a potential candidate for the selected shading system. The review of Al-Masrani (2018) showed there are multiple precedences based on a parametric design methodology, resulting in a dedicated sub-category in the typology scheme (see fig. 115). The review also concludes that for fixed shading systems, the egg-crate concept has the most potential in tropical climates, because multiple researches identify this concept to result in the most energy savings or highest comfort levels. One of these researches (Lau et al., 2016), which is analysed in paragraph 2.6.1 shows the egg-crate system performs better on all orientations compared to horizontal and vertical shading (see fig. 116). Based on these conclusions, it can be argued the egg-crate system could be a potential candidate for the selected shading system.

However, the standard version of the egg-crate systems discussed in the case study of Lau et al. (2016), does not comply with the all-glass exterior façade typology to the best possible extend. When this shading system is projected on the typology categorizing of the placement (see fig. 117), it would be placed in the exterior shading category. Based on this categorization and the included advantages and disadvantages regarding the performance the ability to prevent solar radiation from entering the building, it can be argued the façade integrated category could contain a potential candidate for the selected shading system.

The shading typology categorization of Raji (2018), showed there are advantages for placing the shading in the intermediate space of a double skin façade (see fig. 118). This solution would also fit the integrated placement category of the previous typology categorization. Although this category in the typologies of Raji (2018) contains a motorized blind shading system, this could be replaced by a fixed shading system as well. Especially in the tropic climate, where the requirements for sun shading are relatively constant through the year, this could be a potential category for containing a candidate for the selected shading system.

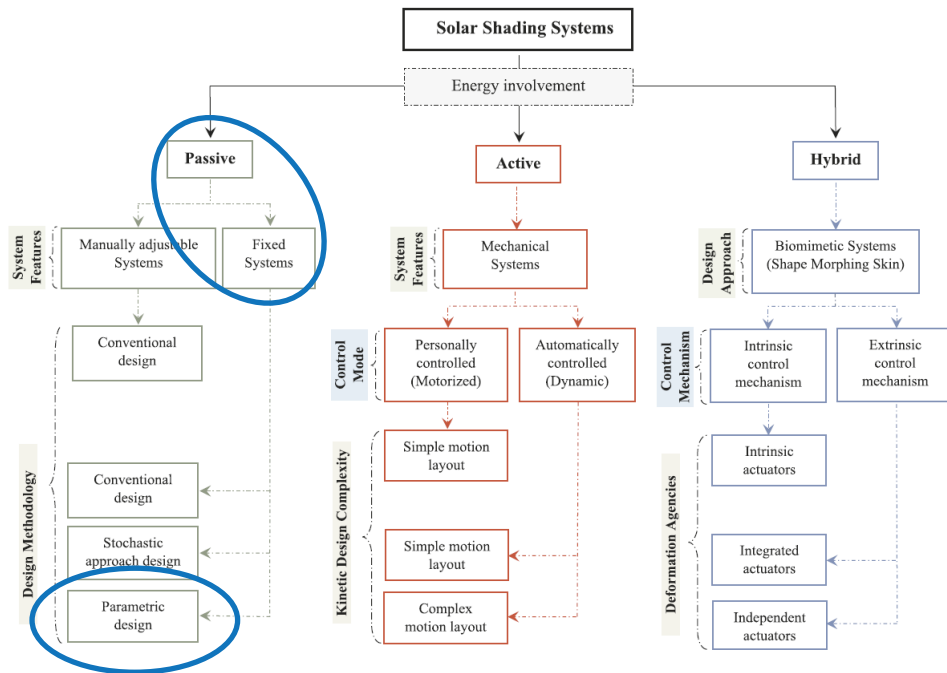


Figure 115. Selected sun shading system projected on typologies of Al-Masrani (2018)

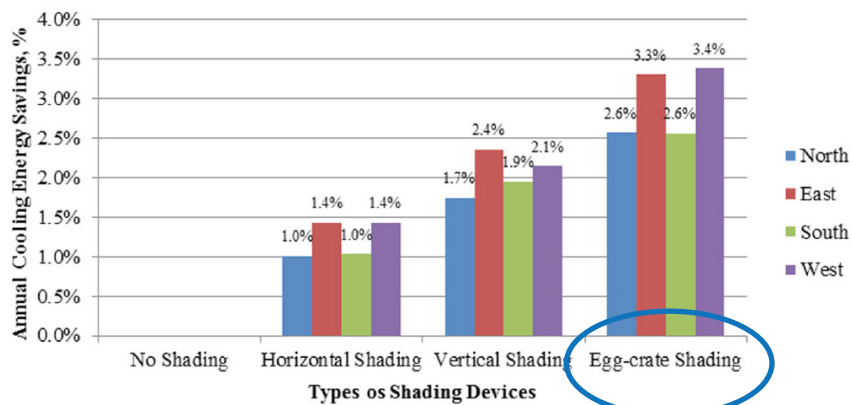
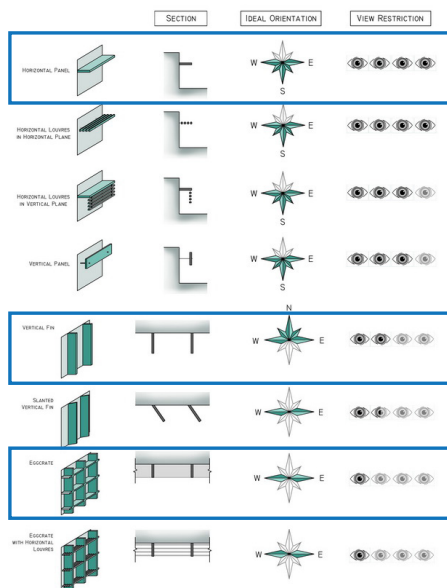


Figure 116. Research results (Lau et al., 2016)

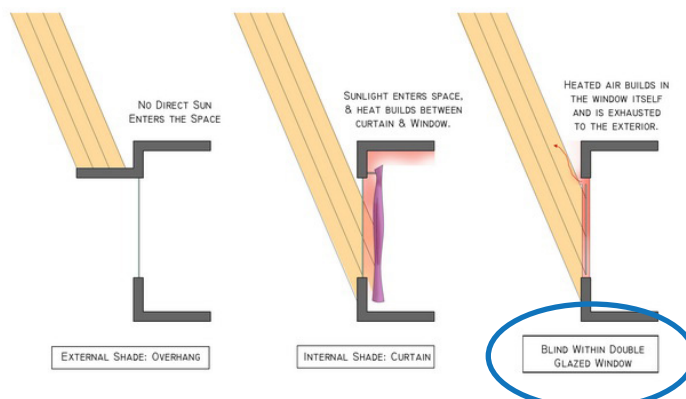


Figure 117. Selected sun shading system projected on placement typology (google.com)






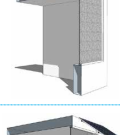

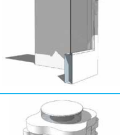


SHADING STRATEGY	Benefits and drawbacks	SHADING STRATEGY	Benefits and drawbacks
Manually operated or motorized venetian blinds inside the building	 <ul style="list-style-type: none"> Contribute effectively for glare control Lower installation and maintenance costs Ineffective at reducing the cooling loads Limit the access to outside views when they cover the entire window 	Overhang (fixed)	 <ul style="list-style-type: none"> Very effective at shading high sun angles in the summer, in particular for windows facing towards: <ul style="list-style-type: none"> South on the Northern Hemisphere South and north on the equator North on the Southern Hemisphere Ineffective at blocking low sun angles (not suitable for east- and west-facing windows) They are not an economical and aesthetically pleasing solution for high-rise buildings
Motorized blinds integrated in the intermediate space of a double-skin façade	 <ul style="list-style-type: none"> The outer skin of the double-skin façade provides an effective shield for blinds against rain, dust and wind, hence result in less maintenance More effective than indoor blinds at limiting the amount of heat radiated into the interior space The most viable option when the incorporation of exterior shading devices might cost a lot or is not safe It may cause overheating if there is no proper ventilation within the two layers of the building façade so they are less efficient than the external shadings for reducing the cooling load Limit the access to outside views when they cover the entire window 	Side fins (fixed)	 <ul style="list-style-type: none"> Effective for blocking sun from a south-easterly or south-westerly direction It can limit a panoramic view
Motorized venetian blinds on the external façade	 <ul style="list-style-type: none"> Blades can be set at different angles so that a very effective strategy for blocking low sun from entering east- or west-facing windows Can only be operated at wind speeds of lower than 10-15 m/s Prone to damage by rain, dust and wind Less viable solution for tall buildings due to impeded cleaning access and wind noise Limit the access to outside views when they cover the entire window 	Smart glass (electrochromic glazing)	 <ul style="list-style-type: none"> Allows for uninterrupted views In their darken state, the increased heating (winter) and electric lighting loads might offset the cooling effect Not as effective as external shading devices to keep the solar radiation/heat from entering the building, especially in tropical climates with high amount of solar radiation
Fixed louvers	 <ul style="list-style-type: none"> Very effective at blocking low sun from entering east- or west-facing windows For heating-dominant climates in which passive heat gains are highly desired, louvers can increase the heating demand of the building in the winter; hence their application should be avoided on the south-facing windows (in the Northern Hemisphere) and on the north-facing windows (in the Southern Hemisphere) 	Facade-mounted solar PV	 <ul style="list-style-type: none"> Facades (and roof) of high-rise buildings offer a great opportunity for PV to provide shading and generate electricity Using PV on the facade has less output compared with using it on the roof
Recessed or projected balconies combined with greenery systems	 <ul style="list-style-type: none"> In tropical climates, recessed balconies are good strategies for providing deep permanent shading on the east and west sides when larger openings are needed to get access to daylight or natural ventilation Shading and evapotranspiration from implementing vegetation on balconies, sky gardens, roof or vertical greening can regulate the microclimate environment around and inside the building. However, in temperate climates attention should be paid to avoid shading the facade where passive solar gain is desired The effect of heat transfer through the increased surface by recessed terraces might offset the shading effect 	Self-shading facade	 <ul style="list-style-type: none"> Provide shading without blocking the views The effect of heat transfer through the increased surface might offset the shading effect

Figure 118. Selected sun shading system projected on typologies of Raji (2018)

Based all conclusions stated before, a selection for the sun shading with potential was made. The selected sun shading system is the fixed egg-crate system, but since this is not beneficial to the all-glass exterior, the geometry will be placed inside a double skin cavity. This concept is based on the egg-crate geometry preventing a part of the solar radiation and direct daylight to enter the building, while the stack effect of the double skin façade will help to ventilate away the built-up of heat within the double skin cavity (see fig. 119). This sun shading system will be used as an example to show how the performance on thermal and visual comfort can be improved by applying the PCA method. The fixed geometry of the egg-crate system will be elaborated in the next paragraphs of this chapter. The double skin façade encasing the shading geometry will be elaborated in the next chapter.

Although this shading concept could be a possible sun shading system for a high-rise office building with an all-glass exterior in tropic climates, other systems with potential are promoted to be studied in further research as well. The choice for a different sun shading principle might result in a different implementation of the PCA method and different possibilities for improvement.

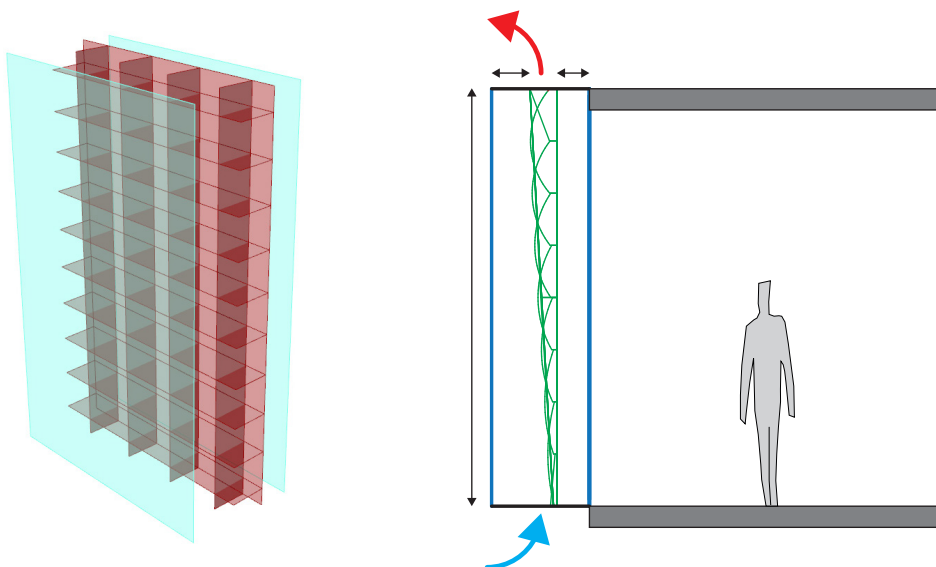


Figure 119. Selected sun shading system (by author)

3.1.2 - Parameterization

With the egg-crate concept as a selected start-point, the next step is to parameterize the concept. These parameters are essential for implementing the PCA method as stated in paragraph 2.3.2. The shading geometry will be generated for each façade panel individually. For the purpose of this research it is assumed all façade panels are of equal width. The only input needed to derive the shading and façade geometry is the outer perimeter of the building floorplan. This way the desired façade width and floor height can be set using the first two parameters of the shading geometry.

The first step in parameterizing the egg-crate is by dividing the system in horizontal and vertical elements, so both can be controlled individually (see fig. 120). This paragraph will continue to describe the parametrization process step by step.

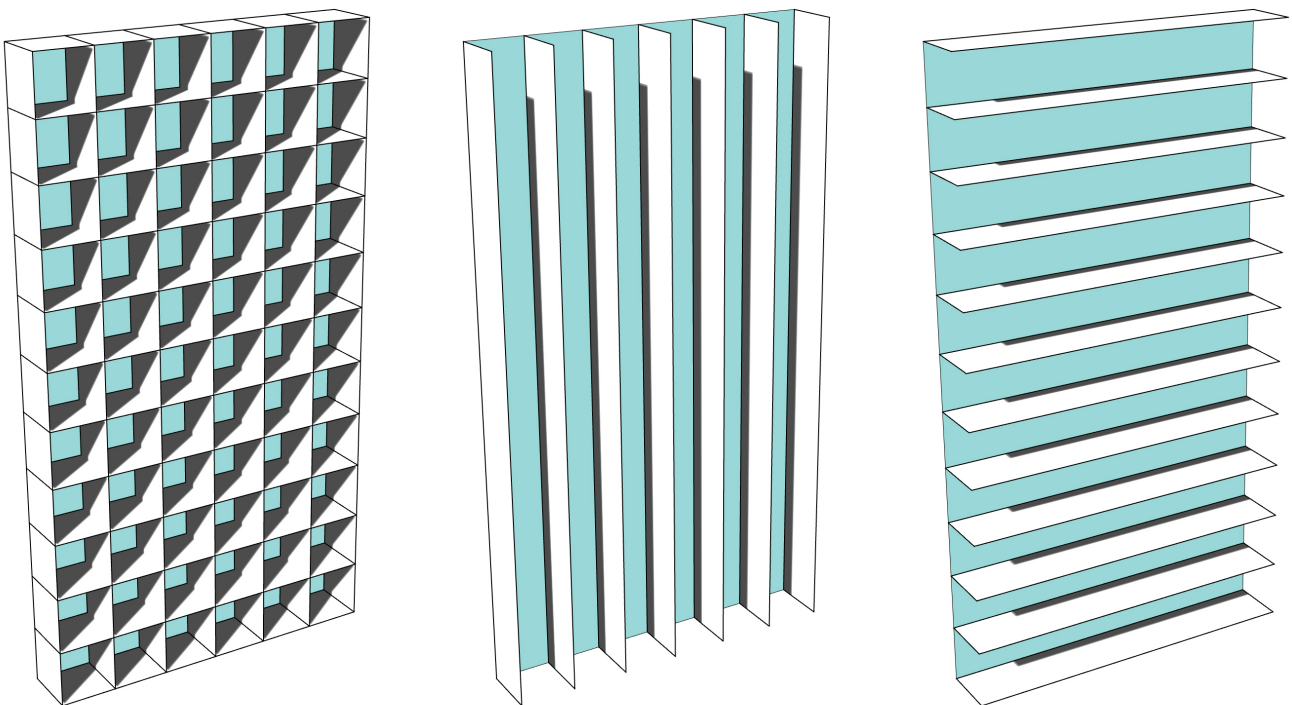
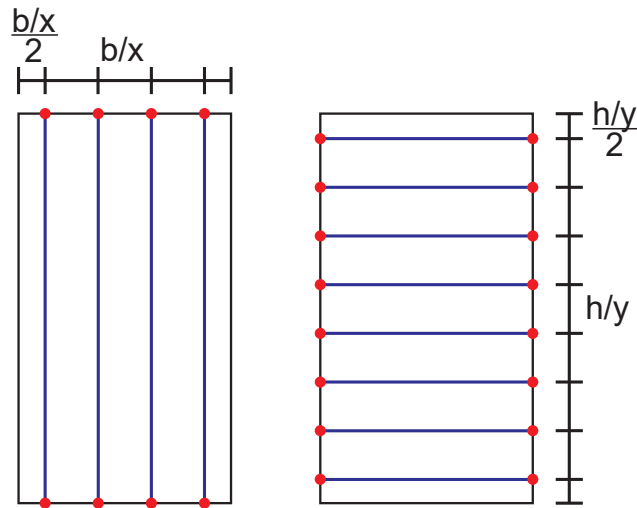


Figure 120. *Separation of vertical and horizontal elements (by author)*

Amount of divisions

The first parameter is the amount of divisions in the panel for the horizontal and vertical direction individually. Because making anchor points in the corner points had proven to result in more difficult connections and visual irregularities in the final geometry, all anchor points are displaced half a distance of elements. If the shifting angle is left on zero, as in a default version of the egg-crate, the amount of divisions input value is equal to the amount of shading elements in the corresponding direction (see fig. 121).



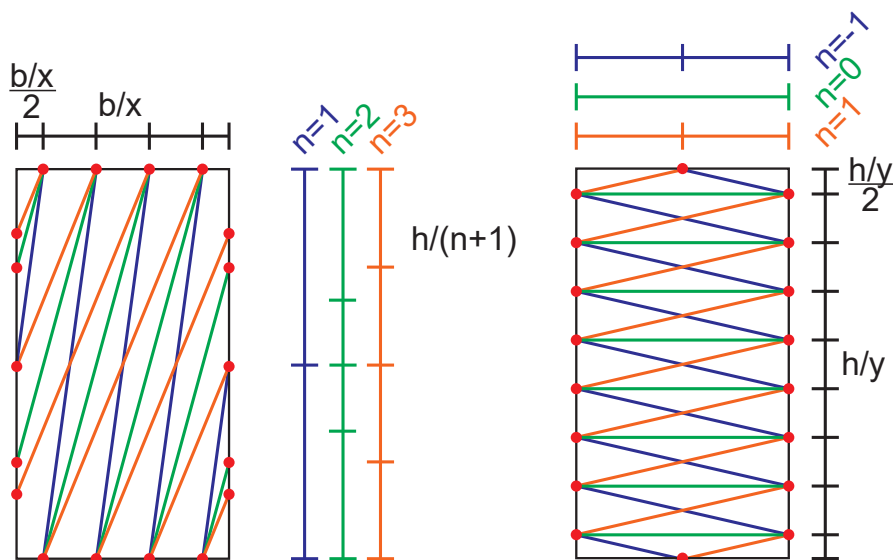
Legend

- w = Width of facade panel
- h = Height of panel
- x = Amount of divisions vertical (in example = 4)
- y = Amount of divisions horizontal (in example = 8)

Figure 121. *Amount of divisions diagram (by author)*

Shifting angle

The shifting angle determines the rotation of the horizontal and vertical elements of the panel. Instead of using a continuous parameter, the shifting angle is an integer determining the amount of anchor points and element shifts (see fig. 122). This method has two advantages. Firstly, it ensures the pattern of the shading geometry will be continuously along multiple façade panels and floor levels, resulting in more architectural quality (see fig. 123). Secondly, this means the connections are symmetrical, resulting in less unique parts when detailing the final design.



Legend

- w = Width of facade panel
- h = Height of panel
- x = Amount of divisions vertical (in example = 4)
- y = Amount of divisions horizontal (in example = 8)
- n = Shifting angle vertical (in example = 1,2,3)
- m = Shifting angle horizontal (in example = -1,0,1)

Figure 122. *Shifting angle diagram (by author)*

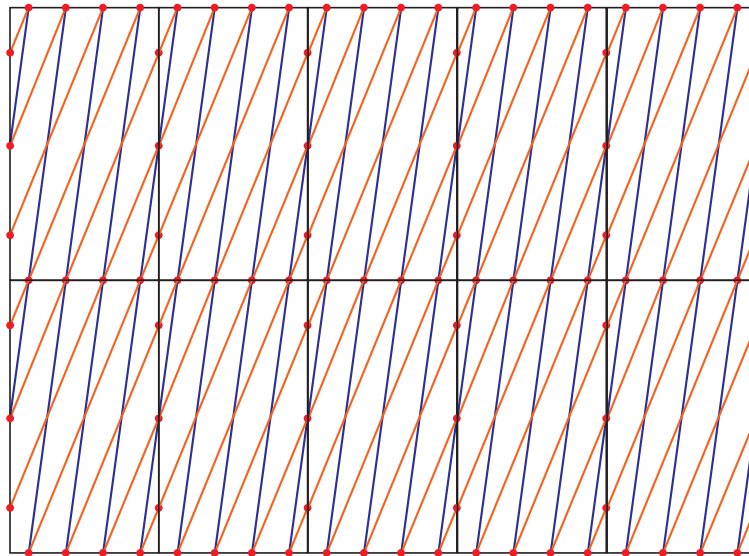


Figure 123. *Continuity across multiple facade panels (by author)*

Rotation angle

The rotation angle determines the rotation around the baseline for the horizontal and vertical panels individually. An angle of zero means the element is perpendicular to the façade-element. An angle of 90 results in elements in the same plane as the element, this also stands for a value of -90, but in this case the elements are rotated the other way around (see fig. 124).

Extrusion depth

The extrusion depth controls the total thickness of the shading geometry. The Grasshopper script relies on planes to define all geometrical properties based on the previously mentioned parameters. The actual geometry is attained by performing an intersection operation of the both the horizontal and vertical planes and a "cutting-box" (see fig. 125). The extrusion depth controls the depth of the cutting-box, which is a perpendicular extrusion of the façade panel. This method is feasible because it allows for customisation of the cutting-box. This can be used to account for façade curvature or to further control the final geometry of the shading. In addition, having control over the total width of the shading using this method is efficient for placing it inside a double skin cavity.

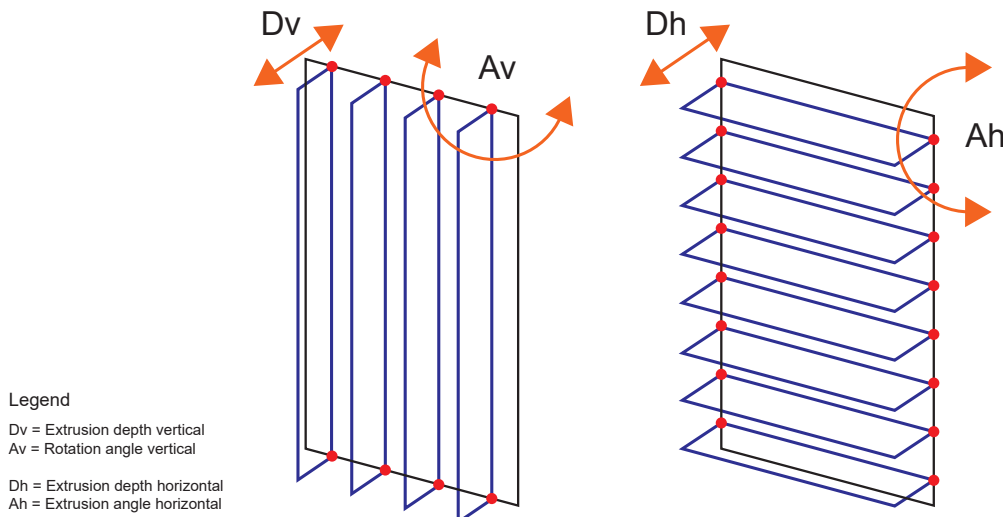


Figure 124. *Rotation angle and extrusion diagram (by author)*

Extrusion shape

Since geometry close to floor and ceiling level is less efficient for blocking solar radiation, the extrusion shape is modified within the boundaries of the original straight cutting-box. There are many methods for adjusting the extrusion shape. Since the exact shape is not necessarily important for the scope of this research, a methodology was chosen on aesthetic quality. However, one important feature in regard to implementing the PCA process, is the preference to define the extrusion shape with the least number of parameters possible.

In earlier stages of the design process, a methodology based on the Gaussian curve was adopted. This methodology uses only three parameters to control the shape. The first one controls the midpoint of the curve relative to the height of the façade panel. The width at this point is equal to the extrusion depth. The second parameter controls the extrusion depth at the top and bottom edges of the façade panel. This parameter can be set to the minimum width needed for structural and detailing requirements. The third parameter is the Q-value of the curve. In order to achieve a smooth shape with aesthetic properties, the Q-value for the bottom and top part of the curve are relative to the distance to the bottom and top edge of the panel. The shape of the gauss curve was then remapped to the interval between the total extrusion depth and the depth at the ends. (see fig. 126)

However, this methodology proved inefficient for the parametrization process, because the Q-value was not linearly changing the total volume of the cut-off shape. This made it difficult to properly set the boundaries for the input parameters in respect to the optimisation phase. Therefore, another methodology was adopted, based on the Bezier-curve. The methodology for defining the total extrusion depth and the depth at the end remained unchanged. The total amount of force used for the start and end vectors of the is equal to the height of the panel. The distribution for the bottom and top part is defined by the midpoint. The distribution of the force within the top and bottom parts itself is defined by the new Q-value (see fig 126). This value can vary from 0 to 1, eliminating the boundary definition problems caused by the gauss curve methodology. The change of this q-value is linearly related to the total area of the shape and thus the volume of the extrusion making up the cut-off shape (see fig. 125).

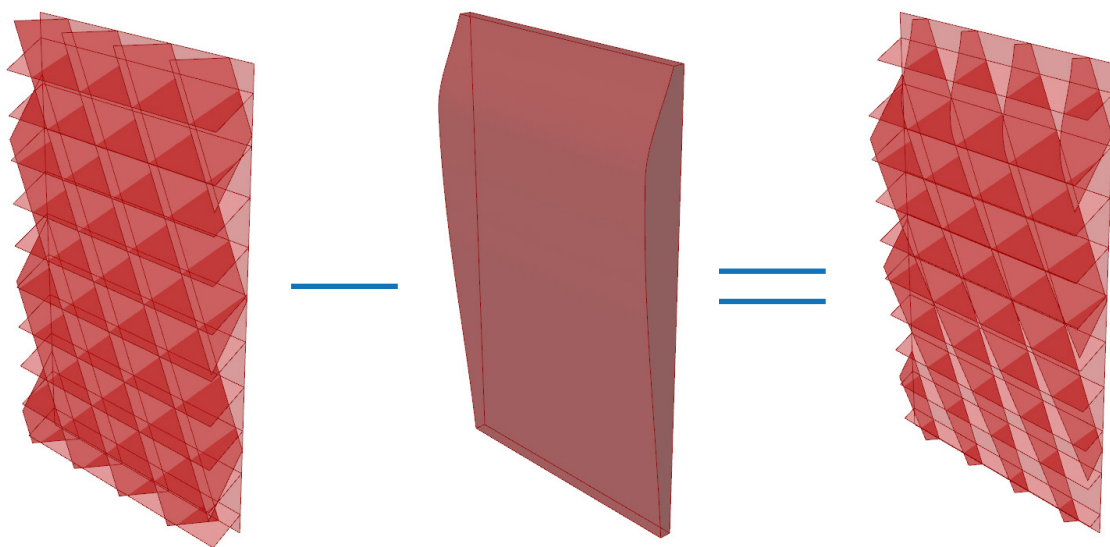
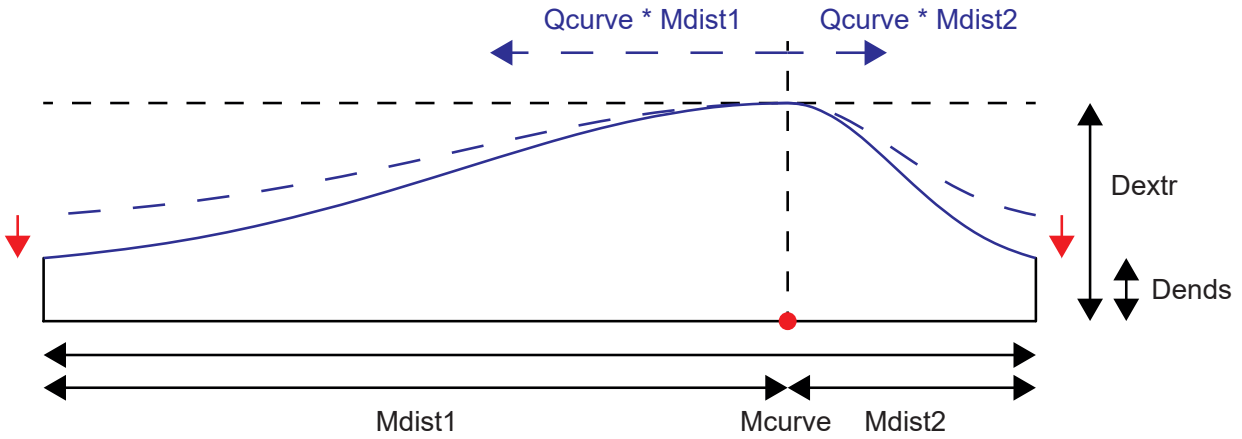


Figure 125. *Gaussian curve cutting-box (by author)*

Legend

- MCurve = Midpoint of gaussian curve
- QCurve = Q-value of gaussian curve
- Dends = Depth at connection points
- Dextr = Extrusion depth
- Mdist1 = Relative distance from end 1 to the midpoint
- Mdist2 = Relative distance from end 2 to the midpoint



Legend

- MCurve = Midpoint of gaussian curve
- QCurve = Q-value of gaussian curve
- Dends = Depth at connection points
- Dextr = Extrusion depth
- Mdist1 = Relative distance from end 1 to the midpoint
- Mdist2 = Relative distance from end 2 to the midpoint
- F1 = Force of start vector bottom bezier curve
- F2 = Force of end vector bottom bezier curve
- F3 = Force of start vector top bezier curve
- F4 = Force of end vector top bezier curve

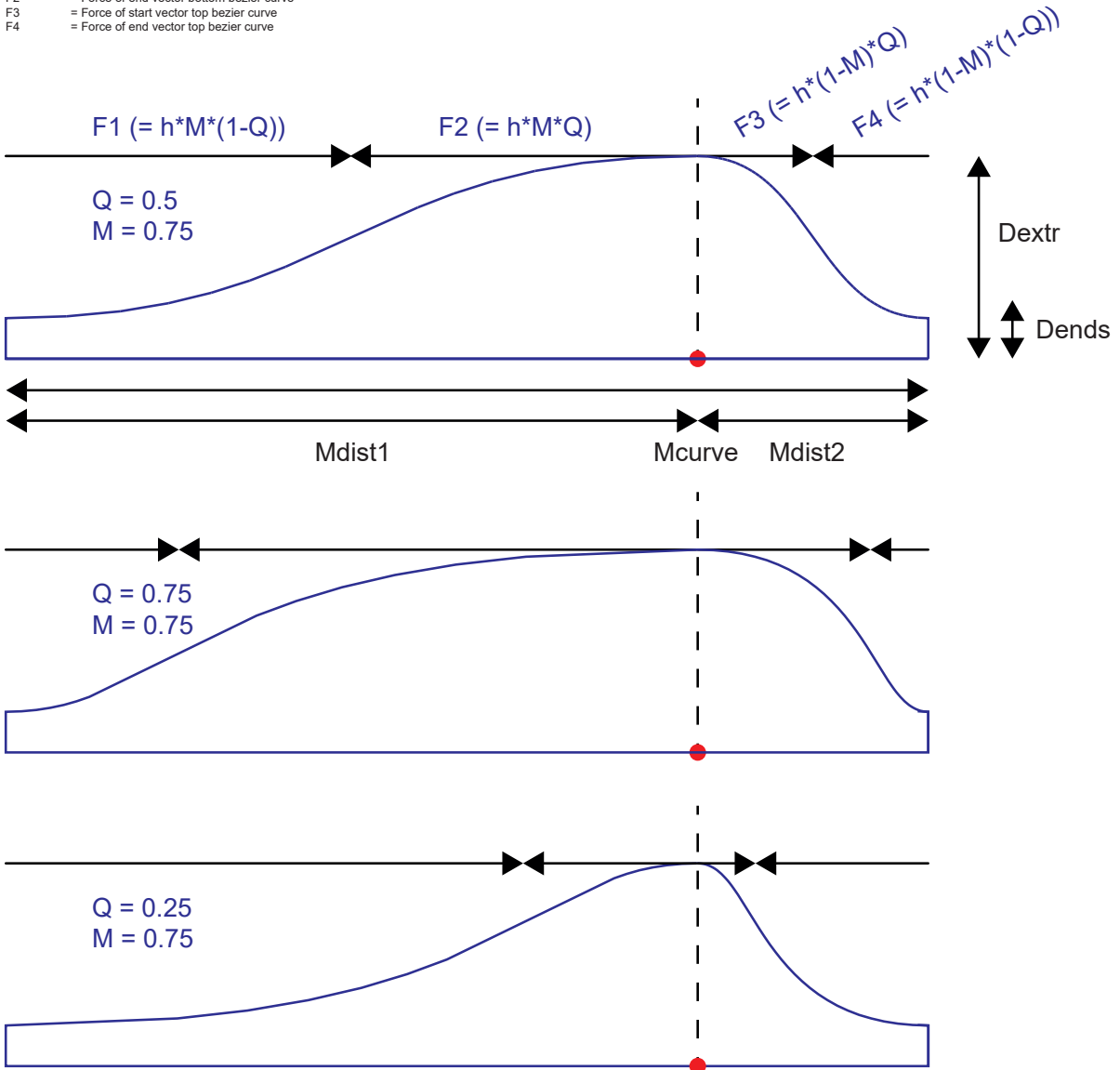


Figure 126. Gaussian curve and Bezier curve cut-off shapes diagram (by author)

3.1.3 - Free-form perimeter buildings

As stated in the previous paragraph, the script is able to derive the shading based on the outer perimeter of a building floorplan. Using this method, the shading could be generated for various floorplan designs. Since the scope of this research involves office high-rise buildings, it can be presumed the floorplan layout is free of interior walls, except from the core. This is in conjunction with the philosophy of the 'new way of working' and the freedom for companies to design their ideal office landscape. This paragraph will explain how the façade and shading geometry are derived from the outer perimeter line of the building. For the purpose of this research it is presumed all façade panels are equal in width, because this is most cost- and time efficient for the production process. Using this method, each façade panel can be identical, with only the shading geometry varying along the building perimeter.

For the purpose of this research, an example floorplan was developed, based on a default open plan office (see fig. 127). The shape of the oval is chosen because it contains a relatively large number of different curvatures.

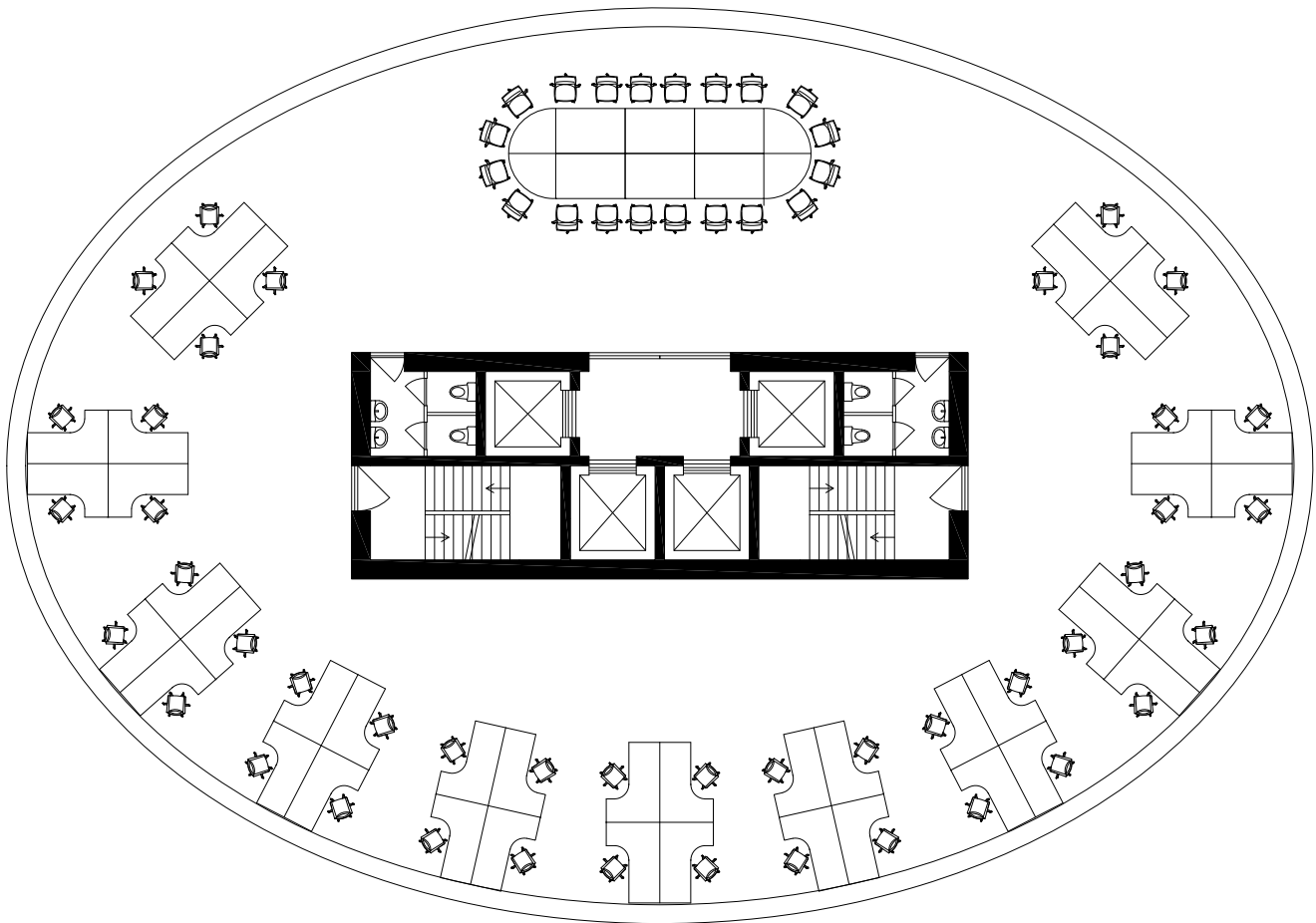


Figure 127. *Floorplan of example case (by author)*

Optimising the offset

In order to make sure façade panels of equal width will fit the building perimeter, the optimal offset from the original perimeter will be determined using a minor optimisation process. The input of this process is the building offset, which can be both positive or negative. The perimeter curve is divided into straight line segments with equal distance, based on the desired panel width. This will result in one line segment with a smaller length. The objective of the optimisation is a length as close to 0, or the desired panel width, as possible (see fig. 128). When running this optimisation, multiple offsets will be found, each corresponding to an increasing number of façade panels. Technically, these are all local optimum, but since the offset closest to the original perimeter is preferred, the desired solution can be determined. When this solution is reinstated in the script, the building outline will theoretically consist of all equal panels. However, in practice the outline will consist of almost all equal panels, with one panel which is slightly wider or narrower. The example floorplan is divided into 44 equal façade panels with a length of 2050, using an offset of -27 mm (see fig. 129).

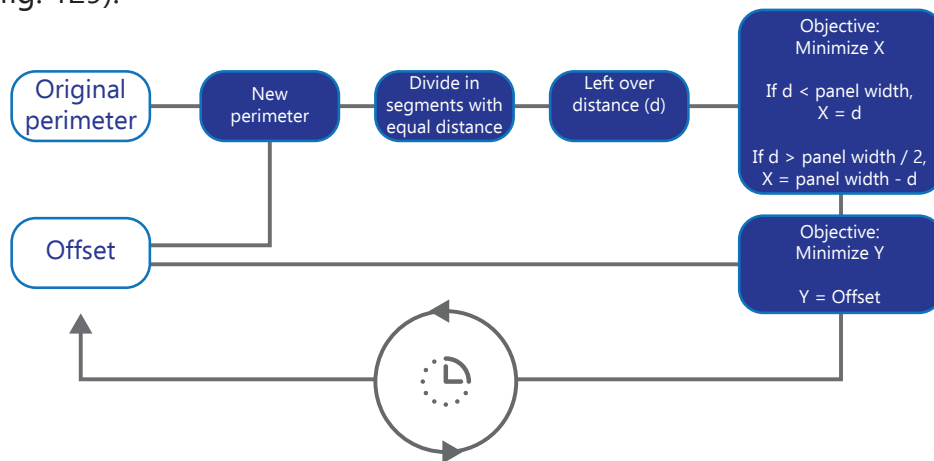


Figure 128. *Offset optimisation process (by author)*

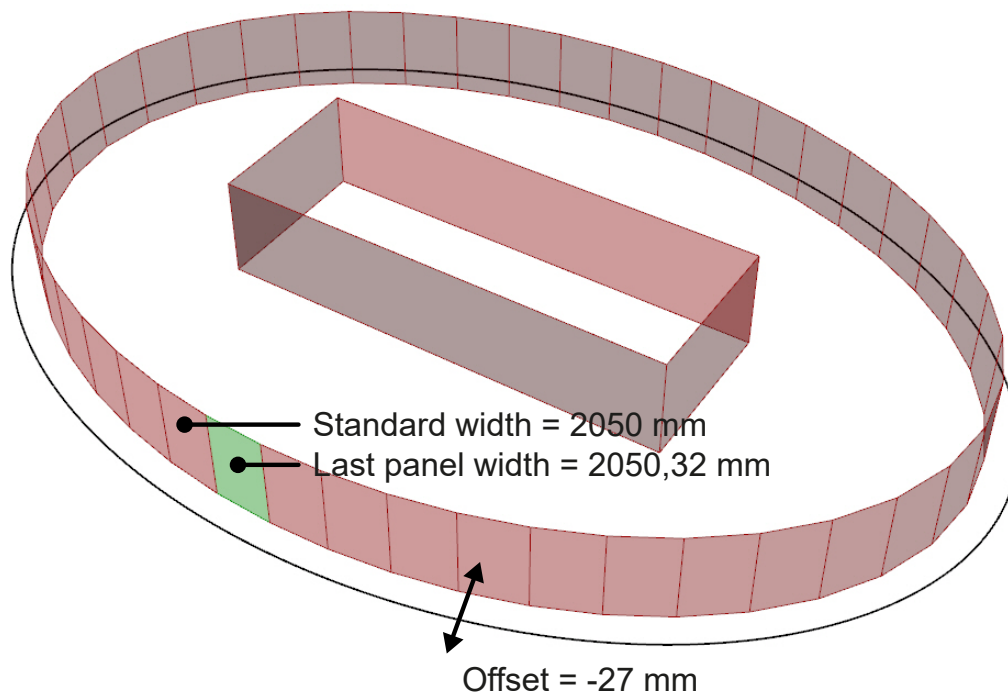


Figure 129. *Offset optimisation for the example floorplan (by author)*

The interpolation concept

Since shading design is highly related to the sunpath of the specific location, the ideal shape will be different for each orientation. When the building perimeter has a free form outline, like many contemporary office high-rise buildings, the building can have a unique orientation for each façade panel. This also accounts for the example floorplan (see fig. 127). Since this is the case, each façade panel would require an individual set of parameters to control the shape. This is highly unfeasible in relation to the PCA process, because less parameters can be optimised faster. One option would be to optimise the shading geometry one part at a time. This would work in buildings with a floorplan divided in rooms, each facing just a single façade. However, in the case of the free-form perimeter, especially in combination with an open plan office function, the room faces multiple orientations. To overcome this problem, the parameters for the shading parameters described in the previous paragraph can be set for the four cardinal orientations. Thereafter, the parameters for each of the individual façade panels are calculated using an interpolation of the four input parameter sets. Hence the name interpolation concept. The figures below illustrate this concept. The upper image shows a simplification, using only the scale of the panel as a parameter. The lower image shows the interpolation concept applied to the shading geometry and the example floor plan.

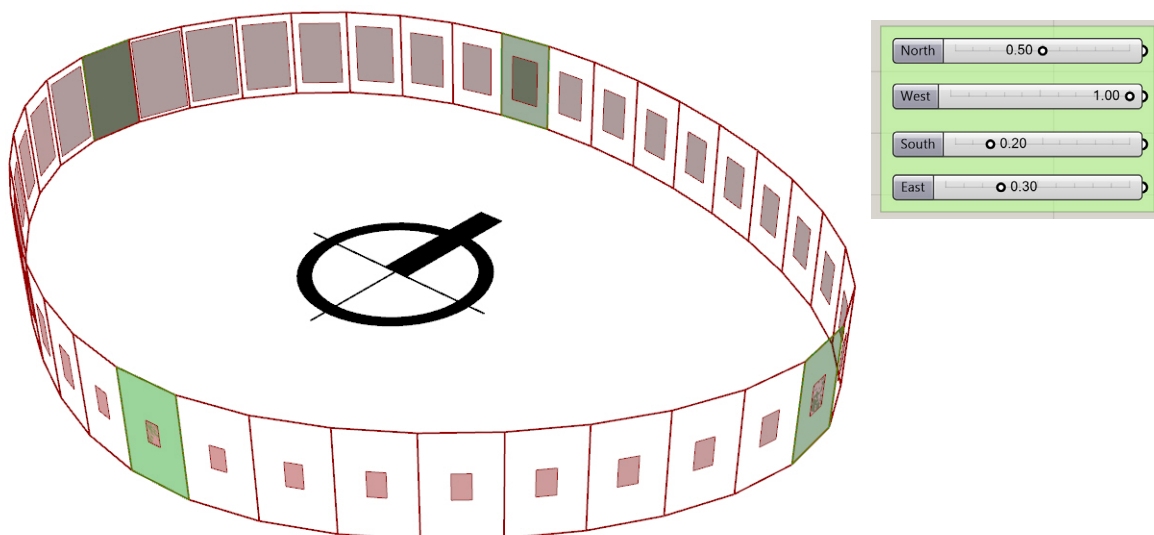


Figure 130. *Interpolation concept applied to example (by author)*

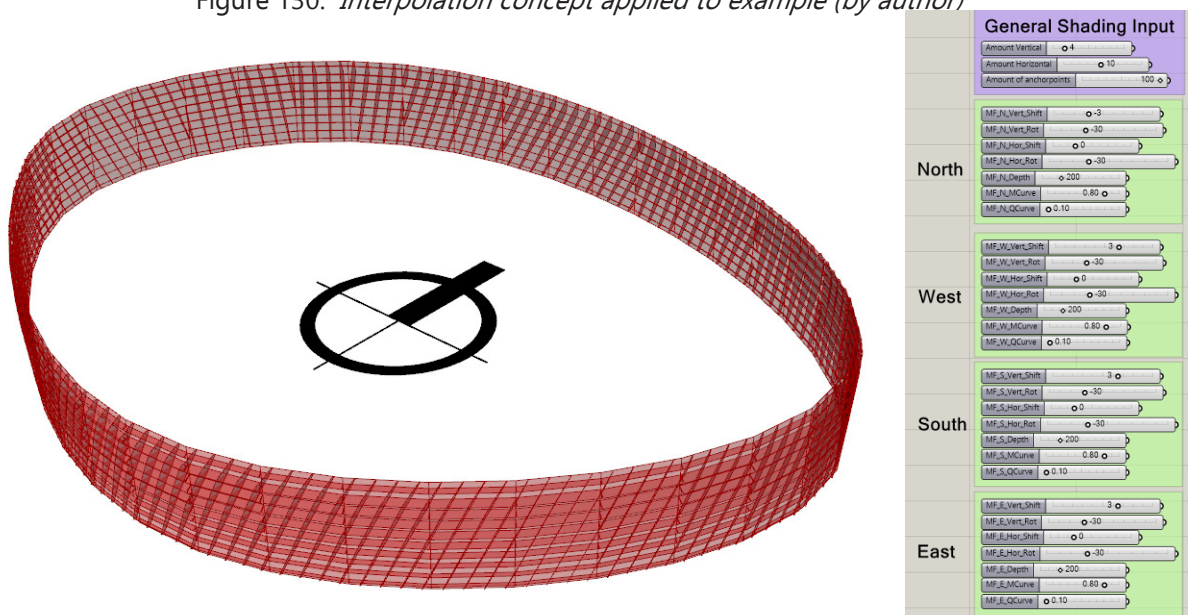


Figure 131. *Interpolation concept applied to sun shading (by author)*

3.1.4 - Shading & building parameters

Combining the parametrization process of the shading geometry, the optimisation of the offset and the interpolation concept results in the list of inputs as shown in figure 132.

The first group contains general building input parameters. The toggle switch enables the building perimeter optimisation process to run. Next are the perimeter and core curves, the only two geometrical inputs for the script. The desired panel width controls the width of all façade panels, except for the last one, which might slightly differ. The offset can either be negative or positive and controls an offset of the building perimeter in order to get the width of the last panel as close to the desired panel width as possible. The start perimeter controls the starting point on the perimeter curve where the panel division starts. For the example case the panel width is set to 2050 mm. The offset is determined by the perimeter optimisation process. For the example case this is set to -27 mm, resulting in a façade of 44 evenly distributed façade panels. The first 43 panels have a width of the desired 2050 mm, while the last panel has a width of 2050,3 mm. This difference of 0,3 mm is a neglectable difference within architectural design. The start parameter is left to 0 in the example case.

The following three general building input parameters include the floor height (3200 mm), which is de net floor height from floor to ceiling. The window trim width (50 mm) controls the width of the window trims of the interior façade. This width is not necessarily important for a simulation at this low level of complexity. However, Radiance does not allow windows to share and edge with the surface they are hosted into. Therefore, some distance between the window and the wall surface edges is required and 50 mm can be used as a default value for this. The last input of this group is the total cavity width (500 mm), controlling the distance between the interior and exterior glazing.

The second group of input parameters contains the general shading input. These parameters are equal for every façade panel. The first two parameters in this group are the vertical (4) and horizontal (8) amounts. Setting these the uniform for each façade panel will result in identical connection points for the elements in each façade panel, which is feasible in regard to the manufacturing process as stated in paragraph 3.1.1. The Gauss curve precision controls the amount of points defining the cutting-box curvature. A low value will result in simplified geometry, which is useful for simulation purposes, while a high value results in detailed geometry, useful for visualisation purposes. The cut-off shape selector allows for selecting between a default straight cutting-box and the Gauss curve cutting-box.

The third group contains the shading input parameters which are set using the interpolation concept. It is a group of seven parameters, identical for each of the four cardinal orientations. They include the vertical shift, vertical rotation, horizontal shift, horizontal rotation, the extrusion depth, the M-value of the Gauss curve and the Q-value of the Gauss curve, all of which have been elaborated in the previous paragraphs.

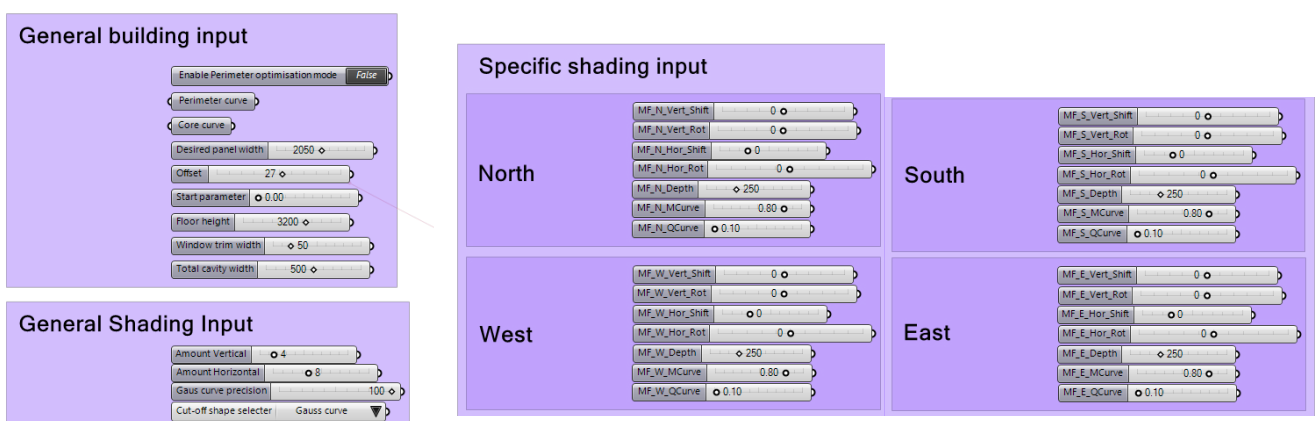


Figure 132. Overview of all shading and building parameters (by author)

3.2 - Test set-up design

3.2.1 - Office zone set-up

All geometry is generated in respect to the requirements of Ladybug and Honeybee, the software used to conduct the comfort simulations. In essence this software is merely an interface, connecting Grasshopper to energy simulation software Radiance, Dayism, Energyplus and Open studio. Since these underlying software packages require different inputs, corresponding parameters have to be assigned to the geometry.

Similar to the shading geometry discussed in the previous chapter, the test set-up geometry is also derived from the building perimeter. In addition to the outer perimeter, the perimeter curve of the core is also an input for this process. These two curves define the floor geometry of the office space test set-up, and the test-room mass when combined with the floor height. Exterior windows are generated with an offset from the façade panel outlines, representing a window trim. This entire mass, including the windows, is combined into a Honeybee zone. This zone is interpreted by the software as a room.

The first property assigned to the surfaces is the boundary condition. The software recognizes four kinds of boundary conditions; Interior, Exterior, Ground & Adiabatic. Interior means the adjacent zones will transfer energy to each other. Exterior means the zone will transfer energy with the outside environment. Ground means the zone will transfer energy with the earth. Adiabatic means the zone will not transfer heat at all. Since the example floorplan is part of an entire building, the floor and ceiling can be set to adiabatic, because other floors will heat up similar to the test floor. In order to simplify the calculation, the interior walls in the office zone representing the core, are also set to adiabatic, assuming no energy is transferred to the building core. Leaving only the façade to exchange heat with the outdoor environment (see fig. 134).

In terms of the geometrical set-up, the double skin zones are straight extrusions from the façade elements in the normal direction of the specific panel. The total width of the double skin cavity can be controlled with an input parameter. Based on the research of Grata and De Herde (2007), the total shading geometry will always be placed in the middle of the cavity. In order to make sure the geometry is generated correctly; the total double skin cavity must be wider than the shading geometry at all times (see fig. 133). The technical set-up of the double skin façade with integrated shading will be further addressed in the next paragraph.

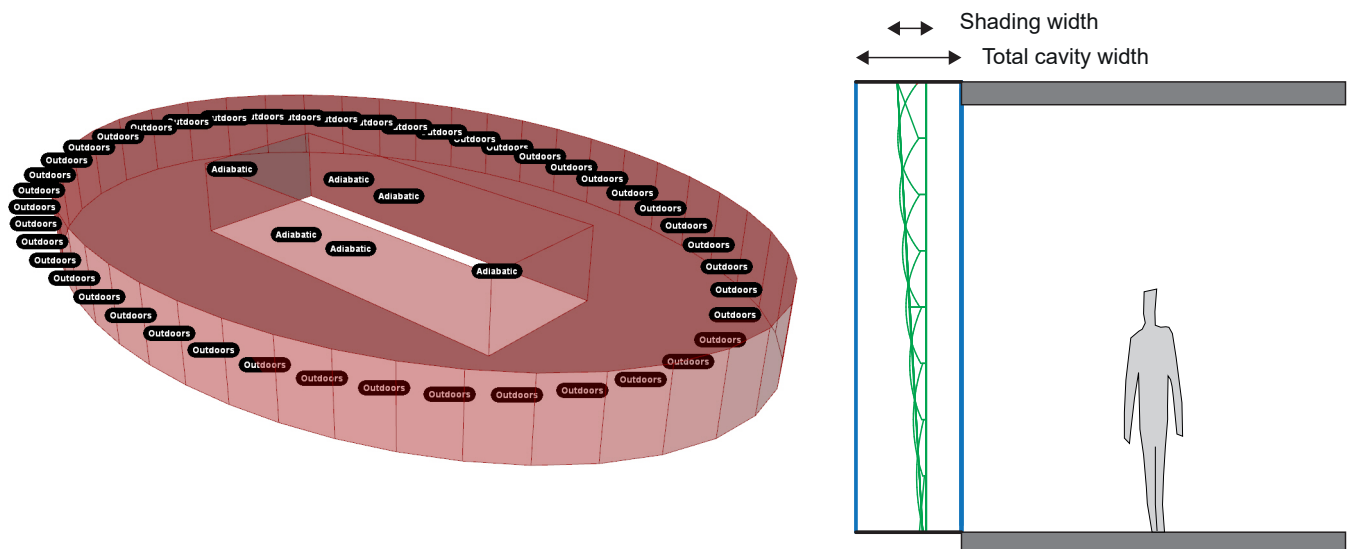


Figure 134. *Honeybee zone boundary conditions (by author)* Figure 133. *Shading geometry placement in double skin facade (by author)*

3.2.2 - Double skin facade set-up

Within the environment of Ladybug and Honeybee, there is no predefined methodology for modelling a double skin façade. However, an example found online is based upon modelling the double skin cavities as individual zones.

In earlier stages of this research, this methodology was adopted. For the example case this resulted in the office zone surrounded by 44 double skin façade zones (DSF zones). The shading geometry was included inside the DSF zones, which were naturally ventilated as a result of the stack effect. The stack effect is caused by air rising up when heated by solar radiation, causing a natural ventilation stream from the inlet at the bottom of the panel to the outlet at the top of set panel (see fig. 135).

However, preliminary simulation results showed the shading geometry did not have any influence on the annual thermal comfort. This is in contrast with the hypothesis, calling for a check of the simulation workflow. The software offers options for plotting the energy gains and losses for each zone. Among others, the numbers for energy transfers due to solar radiation and natural ventilation can be plotted. This showed the office was not gaining any energy due to solar radiation, in contrast to the hypothesis. This can be explained according to the energy scheme in relation to the mathematical concept behind Energyplus. The results did however show the working of the stack effect. It showed the energy losses due to natural ventilation almost counter the effect the energy gains due to solar irradiation.

In the simplified reality, the total solar radiation energy is split up in 3 components, like shown in the top part of figure 135. The first part is reflected back to the sky. The second part is absorbed by the air inside the double skin façade. The natural ventilation as a result of the stack effect will ventilate this energy out. The third part is absorbed by the office zone, causing temperatures to rise. However, the mathematical concept behind Energyplus only allows zones adjacent to the exterior to gain energy due to solar radiation. In other words, the solar radiation cannot travel through a zone into another zone. This limitation results in a false and unusable simulation, because the solar radiation energy entering the office zone is the normative energy transference in regard to the shading design.

To overcome this problem, the set-up for Energyplus is reduced to a single zone set-up, with only the office zone. The shading geometry and the side panels of the double skin façade are included in the simulation model as 'Energy plus shading geometry'. Since Energyplus does not allow for solar radiation traveling through materials, the exterior glazing surface is omitted, while the interior glazing is assigned the combined g-value of the two glazing panes (see fig. 135). This model assumes all energy gains within the DSF cavity due to solar irradiation are lost as a result of the natural stack effect ventilation. In reality some energy might still be trapped in the Double skin cavity, but the previously discussed analyses indicated that the stack effect is mathematically able to ventilate almost all energy out of the cavity.

The software for the daylight simulation, Radiance, is in contrast to Energyplus, capable of ray-tracing through multiple layers of Honeybee geometry. Therefore, the Radiance set-up is slightly different from the Energyplus set-up. Here the exterior glazing is left into place and both planes have an individually assigned visual transmittance coefficient value (see fig. 135).

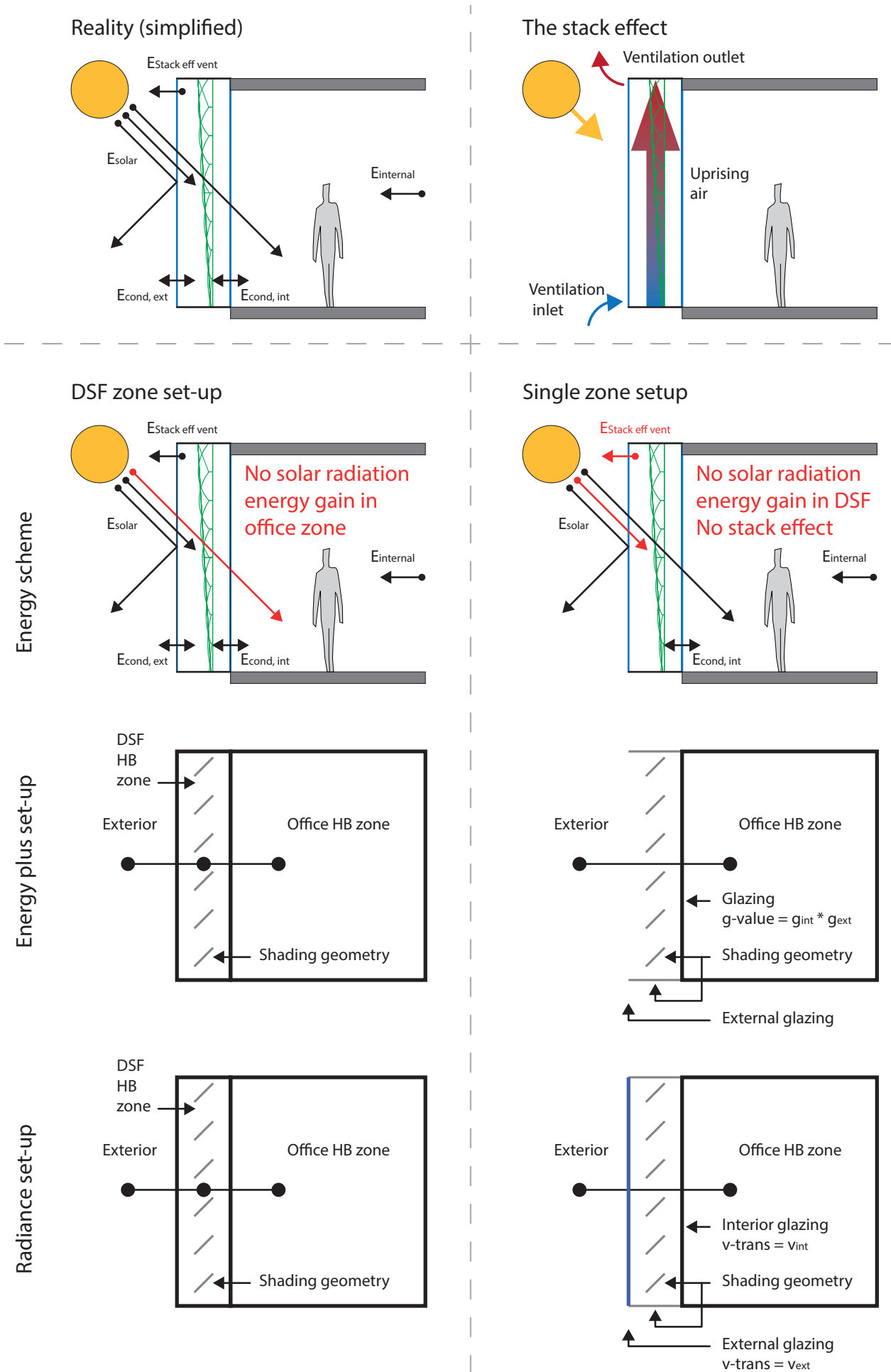


Figure 135. Energy transfer models: DSFzone vs single zone set-up in relation to Energyplus (by author)

3.2.3 - Material parameters

All generated geometry described previously needs to have a material assigned, in order for the simulation to correctly mimic the physical environment. Within Ladybug & Honeybee there are two kinds of material parameters.

The first one is for the ray-tracing simulations of Radiance and Daysim, used for the visual comfort simulations. Opaque materials require inputs for reflectance, roughness and specularity, transparent materials for transmittance, roughness and specularity. The input values used for the reflectance and transmittance are shown in figure 136. The values for roughness (0,05) and specularity (0) are left to default

The second type is for Energyplus and Openstudio to perform energy transfer simulations, used for assessing the thermal comfort performance. The software is based on 'Constructions' which are made-up of layered materials. The parameters for opaque materials include the roughness, R-value, thermal absorption coefficient, solar absorption coefficient and visual absorption coefficient. For transparent materials they include the U-value, g-value and visual transmittance coefficient. The input values for the R-value, U-value and g-value are given in figure 136. The values for roughness (Rough), thermal absorption coefficient (0.9), solar absorption coefficient (0.7) and visual absorption coefficient (0.7) are left to default.

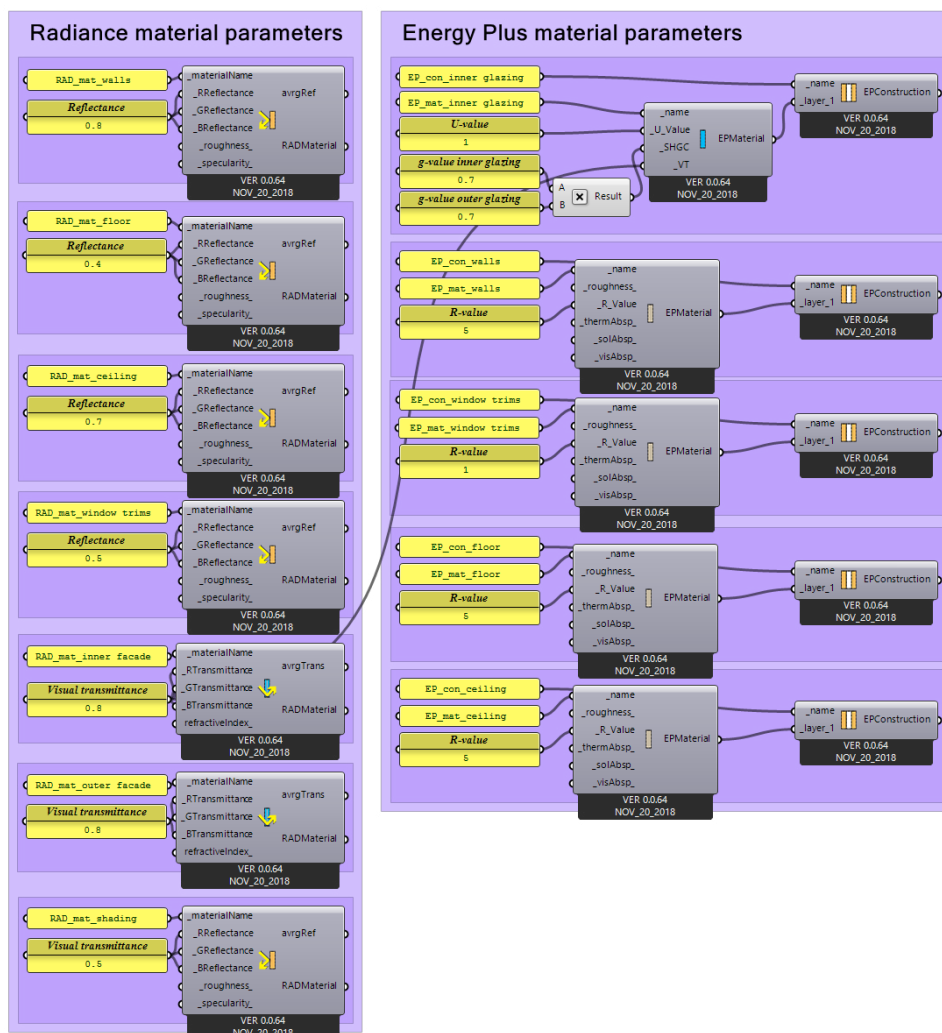


Figure 136. All materials parameters used in the simulations (by author)

3.2.4 - Occupancy, HVAC systems, Internal loads & Ventilation parameters

In order for the simulations to correctly mimic the physical environment, some more parameters are required, regarding occupancy, HVAC systems and lighting. To address annual dynamic values for these parameters, the software uses 'schedules'. These schedules are essentially a list of 8760 values, one for each hour of the year. They can be created using various tools for incorporating daily, weekly, monthly reoccurring patterns and even allow to incorporate the local national holidays in the annual schedule.

In the case of this research the occupancy is simplified to a binary situation, where the office is either entirely in use, or entirely out of use. If the system would be applied to a specific case, a more detailed schedule can be made, based on the business activities of the specific company. The occupancy is set by two input parameters; Workhours start (8) and Workhours end (18). The schedule for these parameters is set to count Saturdays, Sundays and holidays as days without occupation.

The HVAC system parameters controls the thermostat settings for the heating and cooling systems. For the example case they are defined shown in figure 137. The input values are based on achieving near optimal results for thermal comfort in preliminary simulations. The schedule for the heating and cooling setpoints is directly linked to the occupation schedule, meaning the HVAC systems are only engaged when the building is occupied. The software offers various options for detailing the specific heating and cooling systems, which can be useful for a specific case. For the example case however, the system is set to an 'ideal air system', which is the default setting.

The Internal load parameters control the amount of energy generated within the office zone. The equipment load (1.07639 W/m^2) and number of people per area (0.1 ppl/m^2) control the gains from equipment and building occupants. They are both linked to the occupancy schedule. The input values refer to the value when the building is fully in occupied and are left to default. The lighting load (10.7639 W/m^2) controls the internal gains from artificial lighting per floor area when switched on.

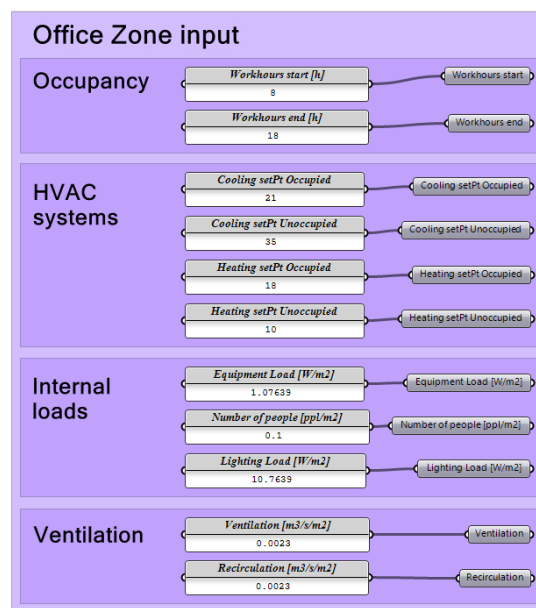


Figure 137. All Occupancy, HVAC, internal loads & ventilation parameters (by author)

3.3 - Performance evaluation

3.3.1 - Analysis input parameters

The methodology for the performance evaluation is based on the geometry and their corresponding parameters described earlier, as well as some other input parameters and local climate data. This data is recorded by weather station throughout the world and recorded in databases. The type of database compatible with Ladybug & Honeybee are provided by Energyplus is the form of Energyplus Weather files (EPW). These datasets can be downloaded for various locations around the world. For this research the data for Singapore, Abu Dhabi and Brisbane are used. The files are fed directly to the engine components of Radiance, Daysim, Open studio and Energyplus, which will be elaborated in the next paragraphs. The software packages use the various kinds of data stored in the EPW files. An overview of the available data within the files is given in figure 138.

Other input parameters for the analysis include general-, climate related-, analysis period- and resolution values. The general inputs are the analysis name, which is used for properly naming all files produced by the script, and the center point, which is used for visualization purposes only. The climate inputs include the directory of the EPW files mentioned earlier and a switch to select between the tree climates used in this research. It also includes the value for true north. A value ranging from 0 to 359 can define the true north for specific cases. When left to zero, which is done so for the example case, the software assumes the positive y-axis as the north direction. The analysis period controls the period for which the simulation is conducted. For the example case it is set from January 1st to December 31th, which are the default settings for an annual simulation. The resolution inputs control the simulations level of precision. The analysis grid, which will be further elaborated in the next paragraph, is based on the grid size input parameter and controls the average spacing of the grid. The analysis height refers to the height at which the daylight simulation is conducted. Many standards require daylight simulations to be conducted at desk height. Therefore, an input value of 700mm is used in the example case. The timestep refers to the timespan of the steps in the Energyplus simulations. The default value is hourly, which is also used in the example case. An overview of all analysis parameters is given in figure 139.

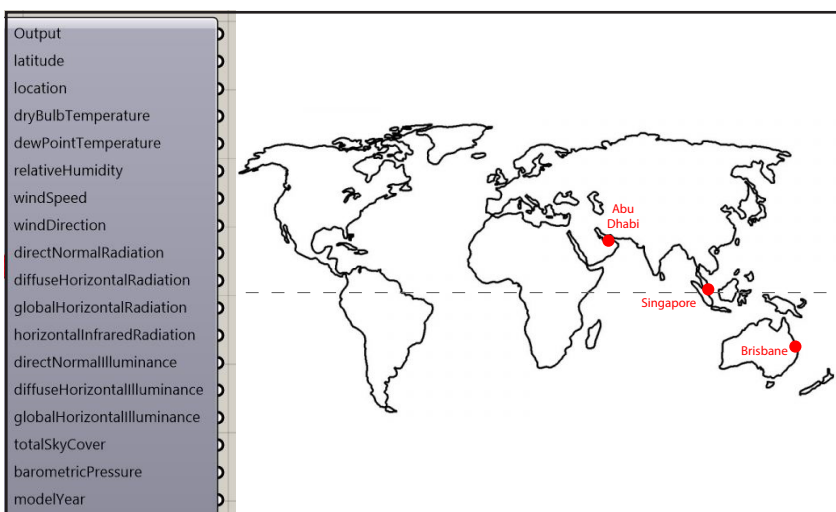


Figure 138. EPW weather data overview (by author)

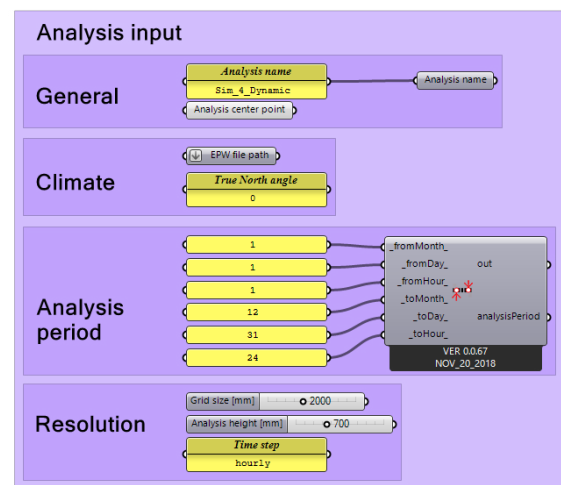


Figure 139. Analysis input parameters (by author)

3.3.2 - UDI evaluation

The UDI is calculated using a Daysim annual daylight simulation, following the workflow shown in figure 140. A set of virtual sensor points are distributed across the floor surface. Ladybug & Honeybee offer a component to set-up these points by automatically. However, this component can result in illogical distributions (see fig. 141). Therefore, it is feasible to create a custom component which distributes the virtual sensors more specifically. The methodology for the distribution way vary for different floorplans. In the case of the example floorplan, a methodology based on intertwining the core and outer perimeter in combination with a radial grid was used (see fig. 142).

Daysim calculates the absolute illumination levels in lux for each of the virtual sensors, for each hour of the year. The results will be saved in a results file, which can be read to calculate which sensors are within the threshold lux window at least 50% of the time. In the case of the example, the window is set between 300 and 2000 lux. However, this window may be altered for other business activity cases with other illuminance requirements. The area represented by the sensors exceeding the 50% of the annual office hours limit is summed to obtain the final UDI score. This score describes the percentage of floor area that is at least 50% of the annual office hours within the illuminance threshold window. In a later stage of this research, the threshold value was increased to 75% (see paragraph 3.4.3)

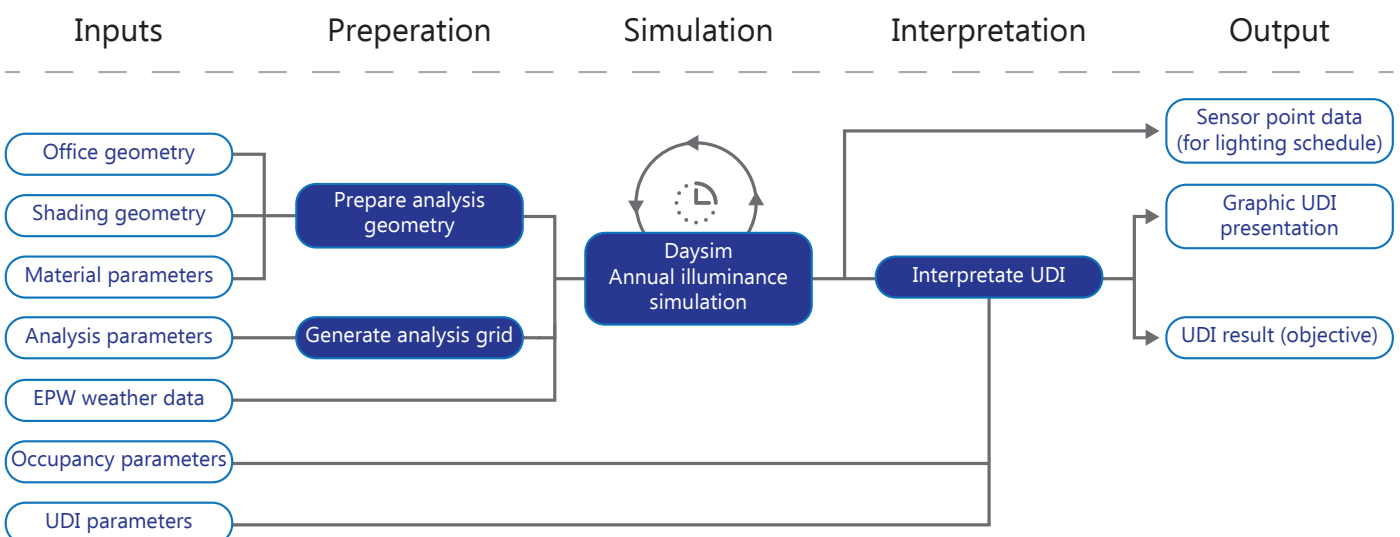


Figure 140. UDI workflow (by author)

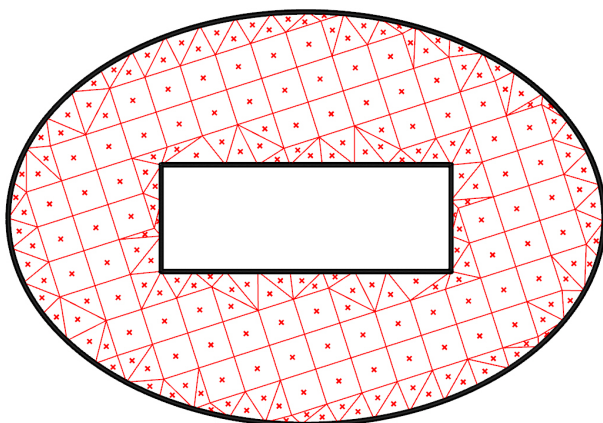


Figure 141. Analysis grid LB/HB (by author)

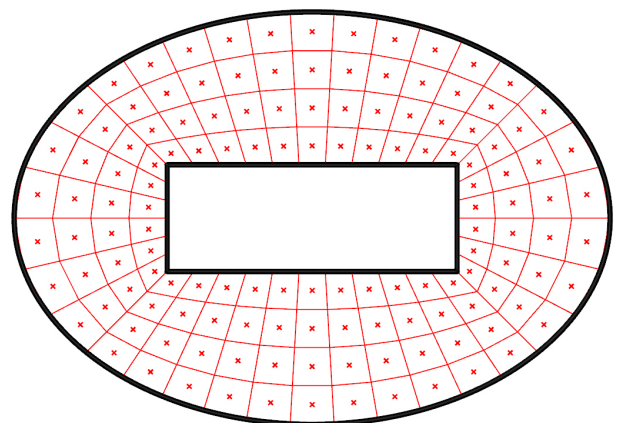


Figure 142. Analysis custom (by author)

3.3.3 - PMV evaluation

The PMV is calculated using an Open studio heat exchange simulation, following the workflow shown in figure 143. The simulations can be run in two parallel modes. The first one is with the HVAC system engaged. Running the simulation in this mode will help to set the heating and cooling setpoints correctly in respect to the PMV thermal comfort index. This will return the annual heating and cooling loads. Another option is to return the lighting loads. These are based on two inputs; the energy usage for lighting per square meter floor space and a lighting schedule.

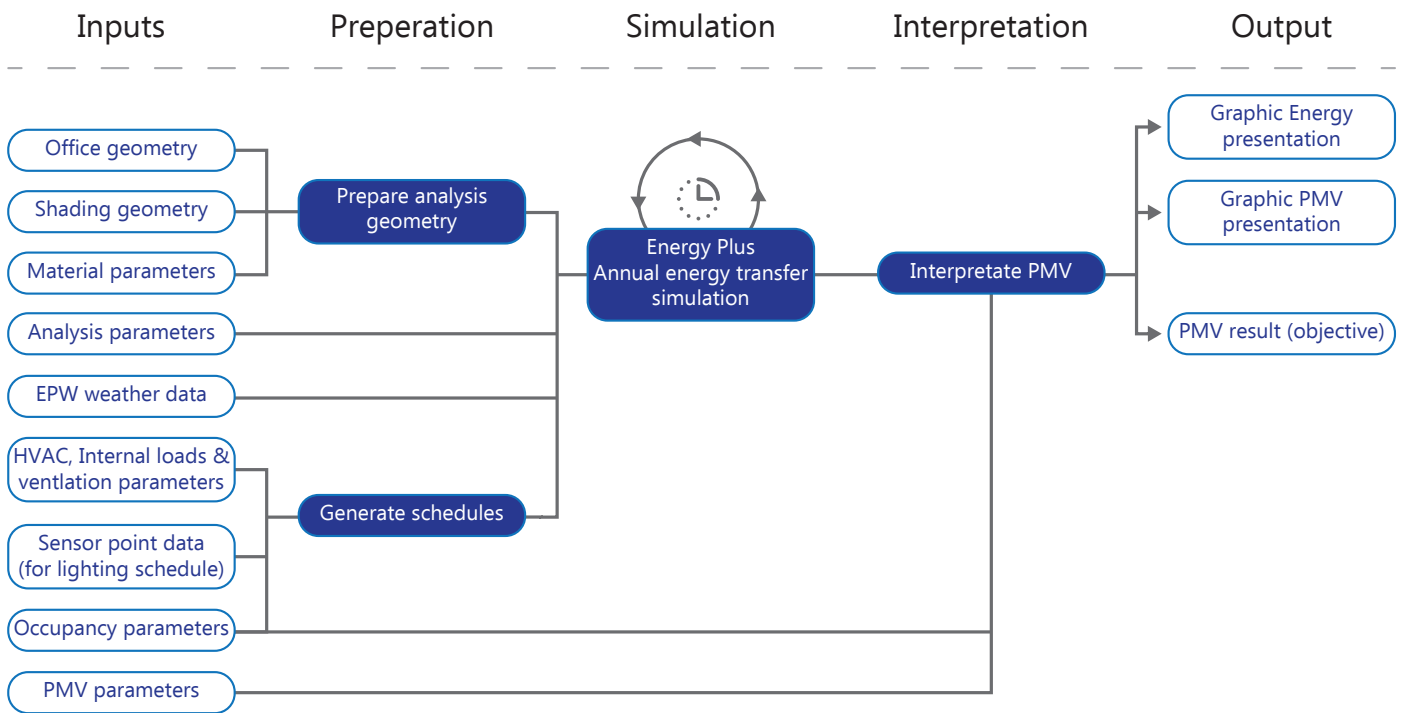


Figure 143. *PMV workflow (by author)*

This lighting schedule is derived from the UDI simulation by taking four points in the middle of the open space and registering the lux values and selecting the closest point in the analysis grid (see fig. 144 and 145). The schedule ensures all lights are off outside of working hours. When within working hours, each of the four points controls a quarter of the buildings artificial lighting, meaning at any given points in time either, 0%, 25%, 50%, 75% or 100% of the lights are switched on. The lights will be switched on when the bottom threshold of the UDI window is not met. In case of the example file this threshold is set to 300 lux.

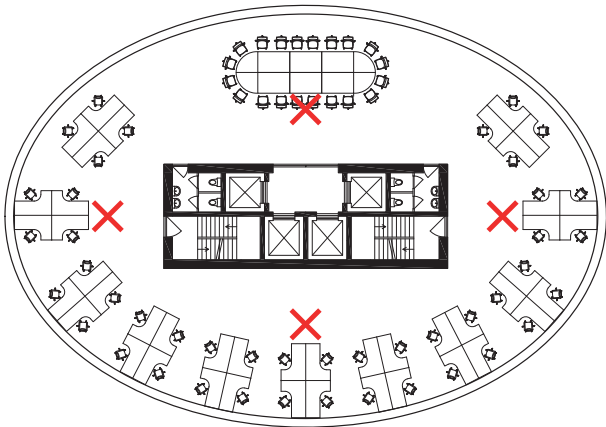


Figure 144. Location of lighting sensors (by author)

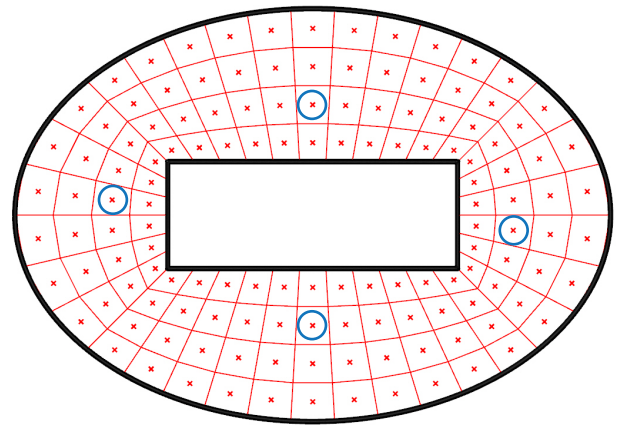


Figure 145. Closest analysis grid points (by author)

The second option is to run the simulation without any HVAC systems at all. This way the performance of the shading is measured by a change in PMV values. As a result, the demand for HVAC systems is decreased. However, the PMV simulation results in a value for each hour of the year, whereas the PCA process prefers a single value as an objective. One option could be to measure the percentage annual of working hours the PMV value is inside the comfort threshold window of $-0,5$ to $0,5$, similar to the UDI index. However, preliminary simulations show the PMV values are actually never within the acceptable boundaries in tropical climates. Therefore, the second method is more applicable for this climate zone. This method involves calculating the sum of annual exceedance of the threshold, meaning a PMV value between $-0,5$ and $0,5$ would count as 0. Any other PMV score will be altered by taking the absolute and subtracting with $0,5$. Using this method the annual PMV will be expressed as a theoretically infinite positive number, where 0 stands for always comfortable.

3.3.4 - DGP evaluation

The DGP is calculated using a Radiance image-based analysis, following the workflow shown in figure 146. The DGP index is depending on the positioning of the perceiver. Therefore, the seating arrangement serves as an input to place virtual mannequins. The exact methodology for placing the mannequins is open for interpretation. For the example case, seven mannequins are used and they are placed like shown in figure 147. The normal directions of the mannequins' faces are used for setting the camera positions for the glare simulation. This way, the cameras will mimic first-person views for the building occupants.

The glare analysis is run for 12 moments in the year. The months and times can be selected manually. For the example case they are set to March, June, September & December at 10:00, 13:00 and 16:00. This will result in 3 moments each in spring, summer and winter time evenly spread throughout a working day. For a specific case, these input parameters can be altered according to preferences. The day within the selected months are picked automatically, based on the highest daily total amount of normal direct radiation. This way, the normative days within each month will be selected.

In early stages of the research it was already determined the DGP would not be included as an objective. The use of the UDI already includes a limitation of glare, because of the upper boundary of 2000 lux of direct illuminance. However, the DGP evaluation can be used as a tool to check whether glare is an issue or not, because this metric is proven to be more precise at predicting glare than the UDI. When projected on the PCA method, it could be argued to include the DGP metric as a constrain. However, this has proven to be unfeasible, because of the relatively long calculation time needed for the DGP simulations.

The DGP check can be performed on a solution from the Pareto front to check if glare will be an issue or not. This can be done by selecting one of the mannequins and performing the analysis for this position. In order to make sure glare occurs for none of the occupants, it is advised to perform the glare analysis for multiple mannequins. The analysis will return a list of twelve DGP values, one for each moment of the year. Another option is to plot the first person fish-eye images, in order to see where in the visual field the glare is coming from.

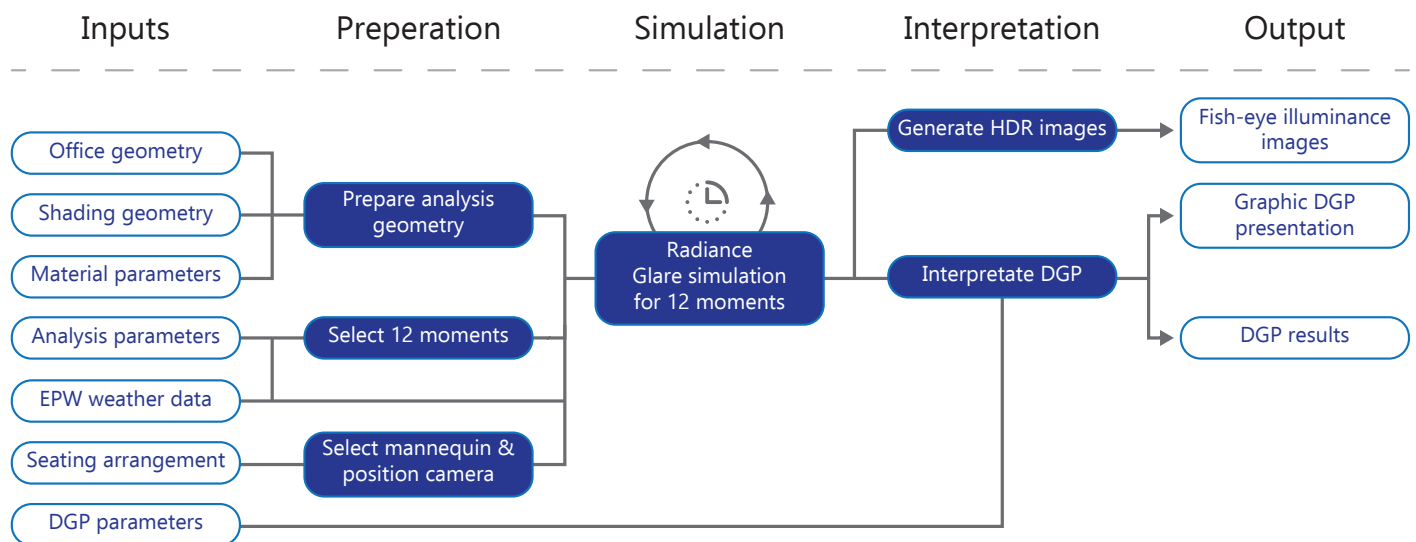


Figure 146. DGP workflow (by author)

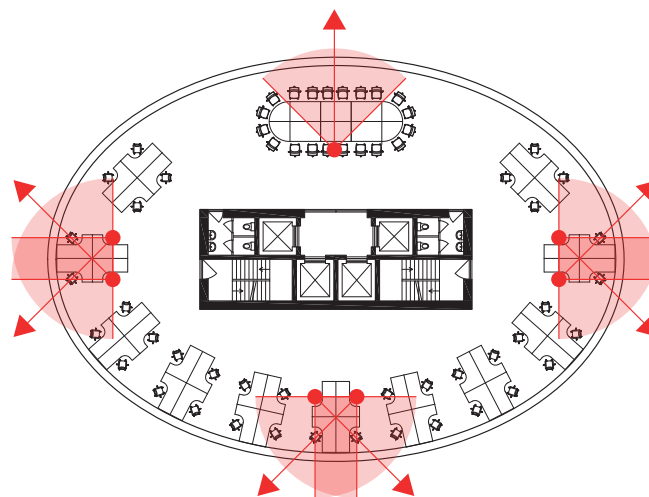


Figure 147. Closest analysis grid points (by author)

3.3.5 - Graphic presentation of results

An important part of the interpretation of preliminary results is the graphic presentation. Ladybug and Honeybee offer some built in option for composing graphs, coloured images, etc. However, when applying some computational scripting, custom components for displaying the results can be made as well. This paragraph will briefly explain some components developed for this research.

PMV

As stated previously, the PMV score will be returned by the simulation software as a list of numbers for each hour of the year. In order to gain insight in the annual distribution of PMV scores, a custom presentation component is developed. This will component takes the monthly averages of each hour of the day, resulting in a 2D table with the daily time on the y-axis and the months on the x-axis. The cells of the table are coloured according to the averaged PMV value, like explained by the legend. For instance, the bottom left corner cell will show the average PMV for all 01:00 moments in the month of January. An example of the custom PMV component is shown in the figure below. This method of taking an average is only used for interpretational purposes. The actual PMV score is derived from the entire set of annual hourly results, like explained in the previous paragraph.

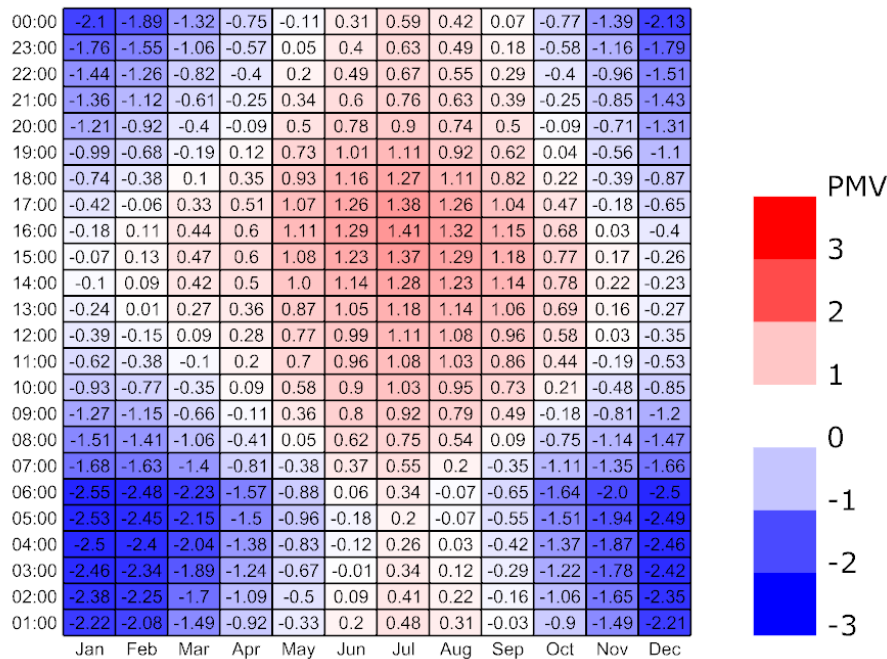


Figure 148. *Graphic presentation of PMV results (by author)*

UDI

The UDI is best interpreted as a floorplan overlay. The simulation returns three numbers per sensor point; the percentage of time the illuminance values are below, within and above the threshold window. Based on these three values, three floorplans can be generated, coloured according to the percentage of annual working hours (see fig. 149). The red floor plan represents the percentage of annual office hours the illuminance levels are above the threshold window and glare is likely to occur. The yellow one shows the percentage of annual office hours the floor are is within the threshold and visual comfort is ensured. The blue floorplan represents the percentage of annual office hour illuminance levels are too low and artificial lighting is switched on.

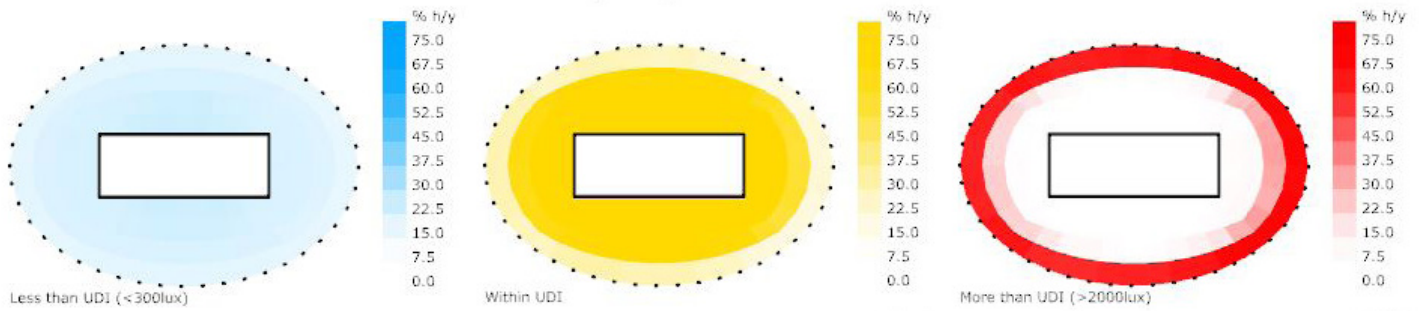


Figure 149. *Graphic presentation of UDI results (by author)*

Energy

The energy usages for heating, cooling and lighting are plotted in three separate graphs. The Y-axis represents monthly totals of energy use, while the x-axis represents an annual cycle of months. The number underneath each graph represents the total annual usage of energy for respectively heating, cooling and lighting. An example of the energy graphs is given in the figure below 150.

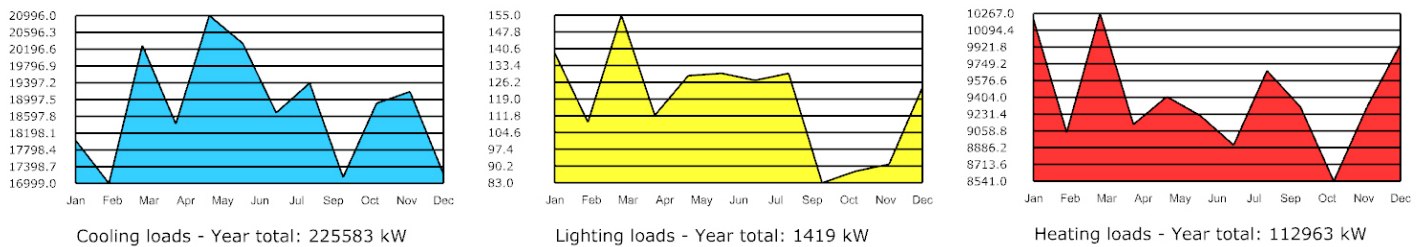


Figure 150. *Graphic presentation of Energy results (by author)*

DGP

The DGP scores can be plotted in a colored table, similar to the graphic results of the PMV (see fig. 151). The colors refer to the DGP result categorization. In addition, the fisheye-images of the individual glare analyses can be generated as-well (see fig. 151).

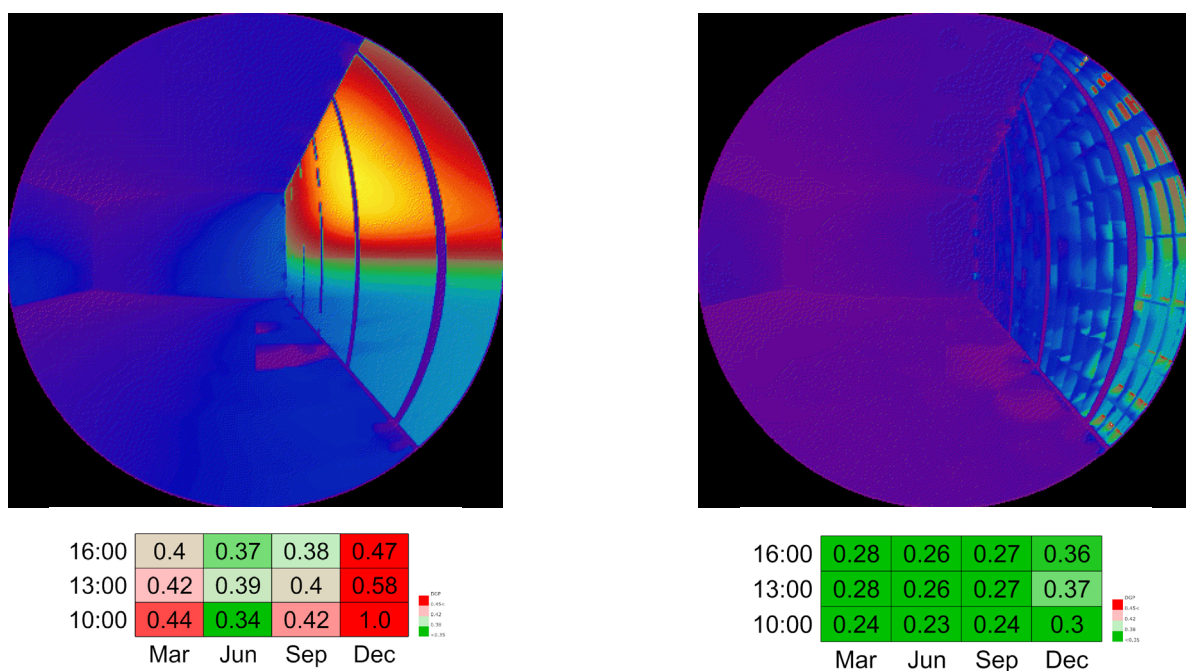


Figure 151. *Graphic presentation of DGP results (by author)*

3.4 - Optimisation

3.4.1 - Workflow definition

Until now, all methodology is modelled within the interface of Grasshopper, using Ladybug & Honeybee components for the performance evaluation. The next step within the process is the optimisation phase. The software used for this step is ModeFRONTIER, developed by ESTECO. ModeFRONTIER is able to adjust the input parameters, run the Grasshopper script and record the results (see fig. 152). When projected on the typology categorization scheme of paragraph 2.5.2 this would fit the model-depending category of the software choice.

An important part of the workflow definition in ModeFRONTIER is the distribution of evaluations. The software offers options to distribute the workload over multiple computers using a grid system. This also includes the options of using the powerful BK Renderfarm or the commercial Amazon EC2 cloud. Currently, running optimisations using ModeFRONTIER on the BK Renderfarm with officially supported integrations such as Matlab works perfectly well. However, the grid system on the BK Renderfarm does not work in combination with Ladybug and Honeybee inside the Grasshopper script. This problem is most likely caused, by the plug-ins of Ladybug and Honeybee not being intended to run in a render farm environment. Therefore, the only option is to run the optimisation on a single, powerful computer. Since the research involves a comparison between three different climates, the optimisation processes can be run separately on three different computers (see fig. 152). In order to make a valid comparison, the same settings were used for all three optimisations, only varying the EPW file in the Grasshopper script. The optimisations have been left running for 72 hours before collecting the results.

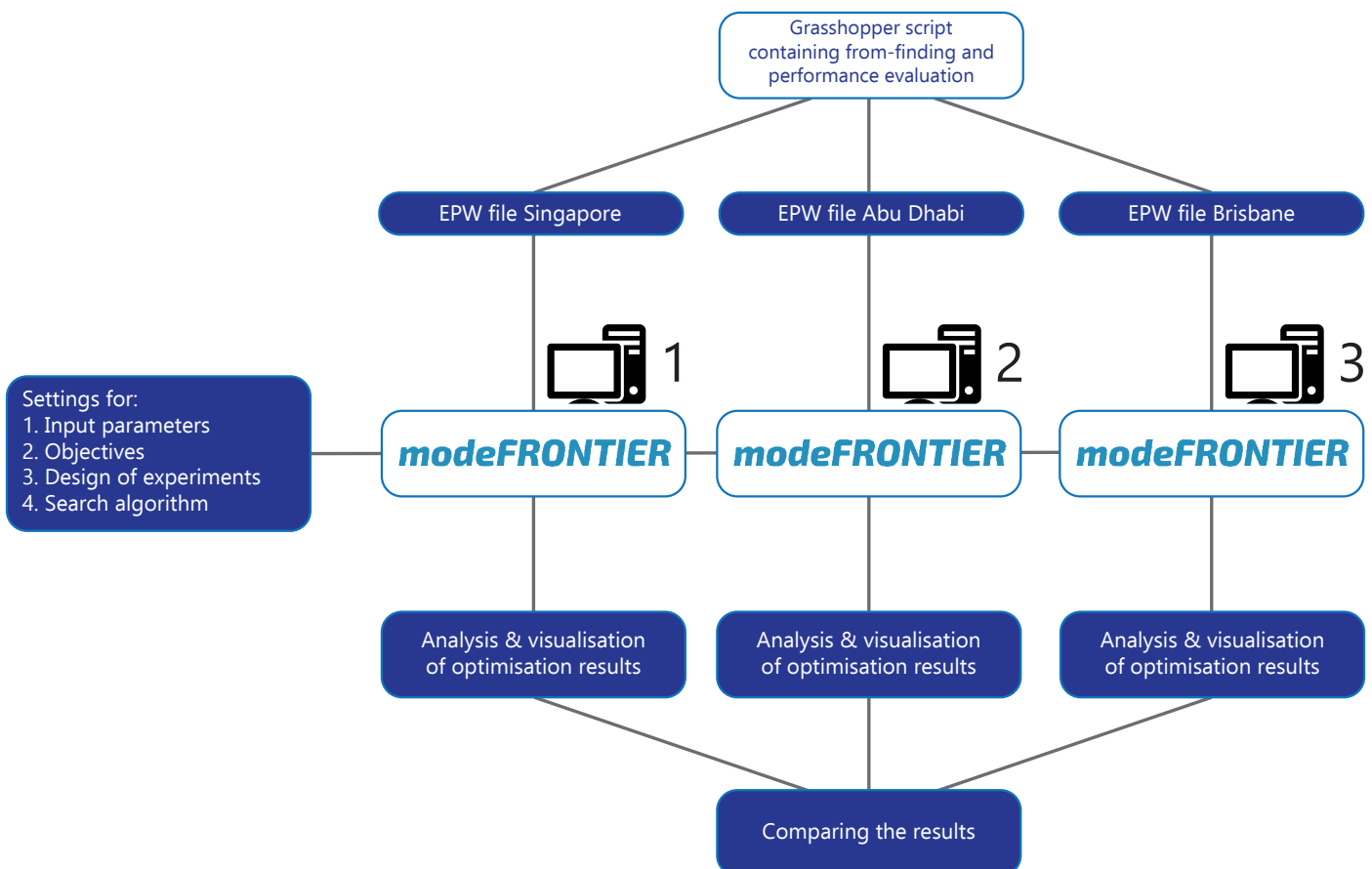


Figure 152. ModeFRONTIER workflow diagram (by author)

3.4.2 - Input parameters

As shown in fig. 153, the shading geometry definition is based on a total of 10 parameters. The first two control the dimensioning of the double skin cavity. The second two control the positioning of the anchor points of the shading geometry. Since the example file is based on identical façade panels units, these parameters are equal for all panels. In order to simplify the process in respect to the example case, this group of four parameters is set as following:

Total double skin cavity:	500mm	Amount vertical:	4
Shading width:	250mm	Amount horizontal:	8

This leaves a total of six parameters as inputs for the optimisation process. However, each parameter has to be multiplied by four in regard to the interpolation process, bringing the total input parameters to 24. Within the interface of ModeFRONTIER, the properties for the input parameters are defined as following:

Vertical shift

Type: Integer (Ordered, Steps of 1)
Bound: -3 to 3

Vertical rotation

Type: Integer (Ordered, Steps of 5)
Bound: -60 to 60

Horizontal shift

Type: Integer (Ordered, Steps of 1)
Bound: -3 to 3

Horizontal rotation

Type: Integer (Ordered, Steps of 5)
Bound: -60 to 60

Mid-point cut-off curve

Type: Number (Ordered, Steps of 0.05)
Bound: 0.5 to 0.9

Q-value cut-off curve

Type: Number (Ordered, Steps of 0.05)
Bound: 0.2 to 0.9

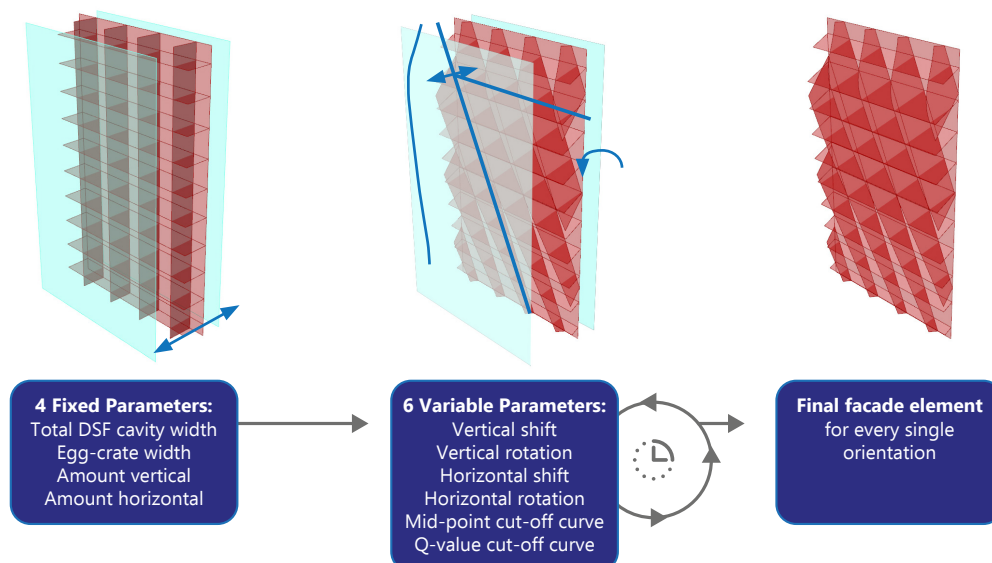


Figure 153. *Form-finding workflow (by author)*

3.4.3 - Objectives

The two-comfort metrics used as objectives for the optimisation process are the PMV and UDI score. The PMV score is the sum of all deviations from the comfort zone of -0,5 to 0,5, as explained in paragraph 3.3.2. The goal is to minimize the total annual deviation from the thermal comfort zone, so the PMV score needs to be minimized.

The UDI score is the percentage of floor area that receives sufficient absolute illuminance levels as least 50% of the working hours. Sufficient regards to the threshold window between 300 and 2000 lux. Lower levels lead to the need for artificial lighting and higher levels to an increased glare probability. Since preliminary simulations concluded an UDI score of 100% was easily reachable, this resulted in an undesired limitation on expressing the visual comfort. In order to overcome this challenge, the UDI mod-75 was adopted. This means the annual 50% of operative hours threshold is increased to 75%. The second case study in paragraph 2.5.1 used this solution to overcome the same problem as well. The goal is to maximize the amount of floor area meeting the requirements of the UDI mod-75, so the UDI score needs to be maximized.

Both comfort scores are calculated based on an hourly annual simulation. A complete overview of the ModeFRONTIER workflow is given in figure 154.

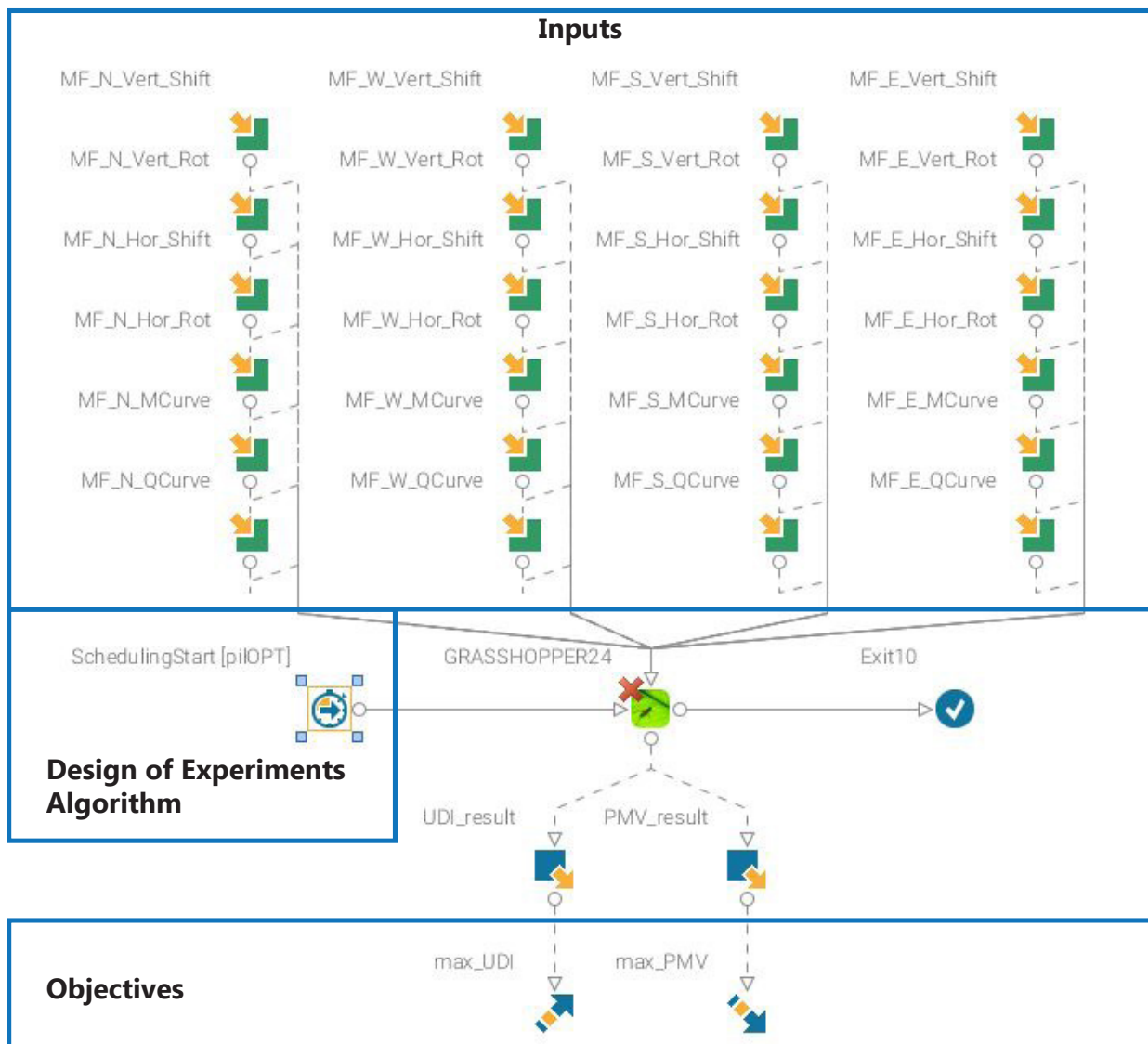


Figure 154. ModeFRONTIER workflow (by author)

3.4.4 - Design of experiments

Every optimisation process starts with a first generation of input values. This first generation is determined by the design of experiments (DOE). The preferred method for generating the DOE in the PCA process is the Uniform Latin Hypercube (UHL). The input values for the DOE are set like shown in figure 155. In order to make a valid comparison of the performance in different climates, the same Design of Experiments was used in all three optimisation runs.

3.4.5 - Algorithms

Like explained in paragraph 2.3.4, the most commonly used evolutionary algorithm for the PCA process is NGSA-II. However, preliminary iterations of the ModeFRONTIER job showed the PiOpt algorithm, developed by ESTECO themselves tended to converge faster to the Pareto front. Therefore, the PiOpt algorithm was used for the example case in this research and the input values are set like shown in figure 155. The total amount of evaluations is not really relevant, because the optimisation process will be terminated after a predetermined amount of time due to practical recourse limitations. The simulations will be left running for approximately 72 hours.

The image shows a software interface for configuring DOE and algorithm settings. It is organized into several sections:

- Parameters**:
 - Number of Designs [1,256000]: 50
- Advanced Parameters**:
 - Maximize Minimum Distance of Designs:
 - Minimize Correlation of Input Variables:
 - Minimize Unfeasible Design Number:
 - Reject Repeated Designs:
 - Random Generator Seed [0,999]: 1
- System Parameters**:
 - Multi-threading Policy: Use Maximum Number of Available Proc... (dropdown)
 - Number of Threads [1,8]: 8
- Algorithm Configuration**:
 - Algorithm Configuration: Self-Initializing (dropdown)
 - Number of Evaluations [1,20000]: 750

Figure 155. *ModeFRONTIER DOE and algorithm settings (by author)*

3.4.6 - Results overview

Raw results from ModeFRONTIER

This paragraph will discuss all results from the optimisations runs mentioned above. The ideal number of evaluations would be at least 500, based on a DOE of 50 and a total of 10 generations. However, with respect to the available computation facilities, the optimisations were left running over the weekend and had to be terminated after approximately 72 hours. Unfortunately, one of the three computers failed to stay activated over the weekend. The difference in number of evaluations on the other two computers is caused by a difference in computational power. This resulted in the following numbers of iterations:

Computer 1 (Singapore):	30 evaluations	(0 errors)
Computer 2 (Abu Dhabi):	261 evaluations	(4 errors)
Computer 3 (Brisbane):	188 evaluations	(27 errors)

Interpretation of designs resulting in errors

The results included an unexpected high number of errors, calling for an investigation of what is causing these errors. In order to do so, the input parameters of all 29 error results are checked for similarities in their input parameters (see fig. 156) The upper image shows the correlations for the optimisation of Abu Dhabi and the lower for Brisbane. It can be concluded that the errors are caused by a combination of input values near the thresholds of their corresponding parameters boundaries. In order to verify why this causes an error, the combination of input values can be reinstated directly in Grasshopper.

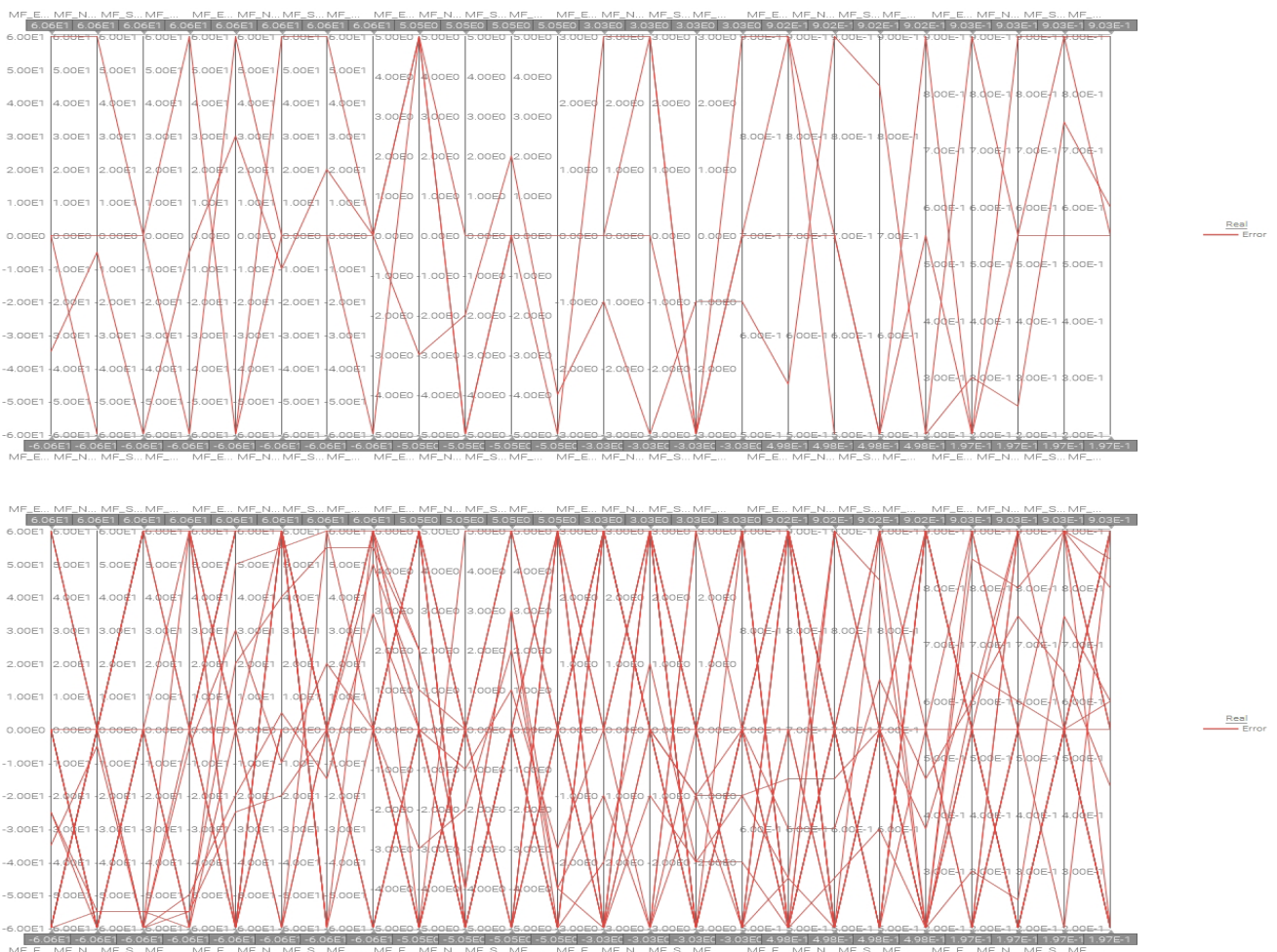


Figure 156. Error analysis (by author)

Pareto front analysis

This first method for analysing the results is plotting the Pareto fronts of all evaluations (see fig. 157 to 159). Since the UDI objective is to be maximized and the PMV objective to be minimized, the Pareto front is formed along the bottom right corner of the solution space. The colour of the dots indicates the evaluations ID number.

Singapore

Since the optimisation for Singapore only contains 30 evaluations, which are all part of the DOE, analysing these results is not really useful at this stage. Because of the lack of sufficient designs, an actual Pareto front cannot be defined. However, the selection tool of ModeFRONTIER does identify one Pareto front solution, situated in the bottom left corner of the solution space.

Abu Dhabi

Based on the colours of the dots, it can be concluded the Pareto front is indeed converging to the bottom left corner of the solution space. However, the Pareto front is not yet clearly formed due to an insufficient number of optimisation generations. The automatic selection tool of ModeFRONTIER identifies four Pareto front solutions.

Brisbane

Similar to the other two optimisations, the results for Brisbane do not include enough generations for the Pareto front to properly form. However, automatic selection identified 10 Pareto solutions.

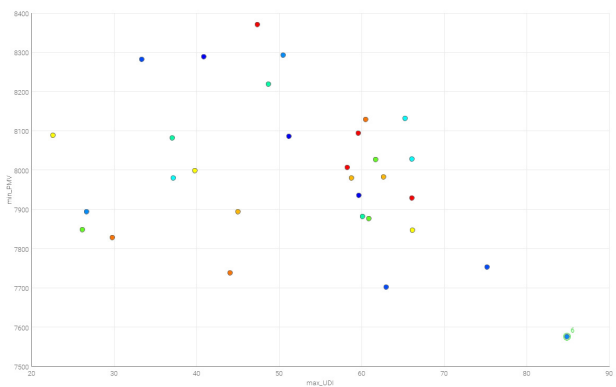


Figure 157. Pareto frontier Singapore (by author)

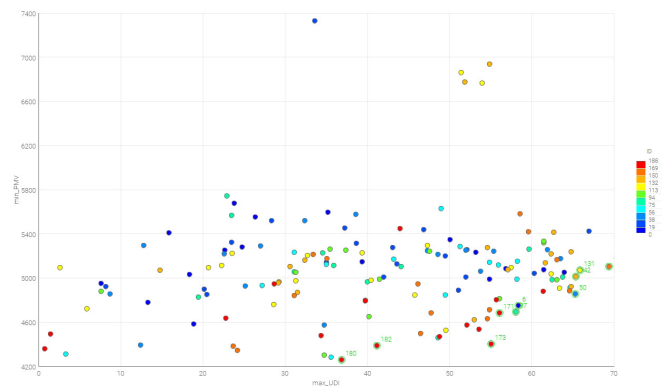


Figure 158. Pareto frontier Brisbane (by author)

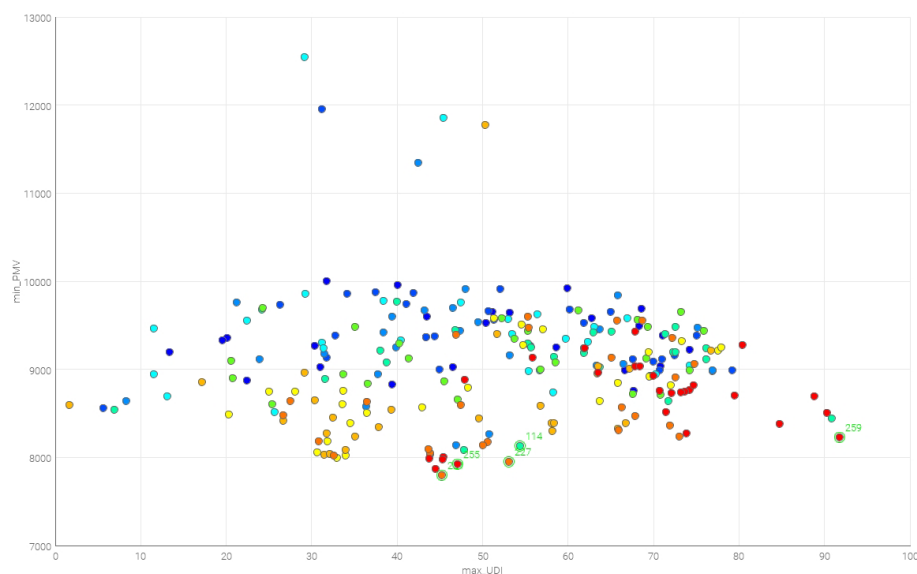


Figure 159. Pareto frontier Abu Dhabi (by author)

Input/output correlation analysis

The second analysing method used is the input/output correlation graph (see fig. 160 to 162). Due to the high number of input values, the correlation graph itself becomes hard to read, but the list of variable relations and their Pearson correlation shows come insight in relation between parameters.

For the same reasons as mentioned before, analysing the result set of the climate of Singapore for correlation is not useful at this stage. For the Abu Dhabi climate the correlation analysis identifies the horizontal rotation to be relatively heavily correlated to the PMV objective. For the climate of Brisbane, similar results can be found.

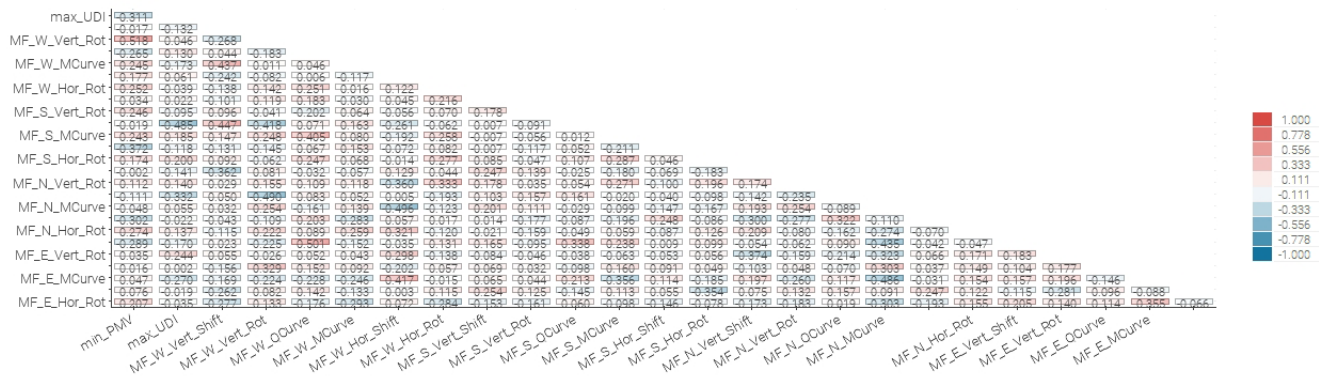


Figure 160. Correlation analysis Singapore (by author)

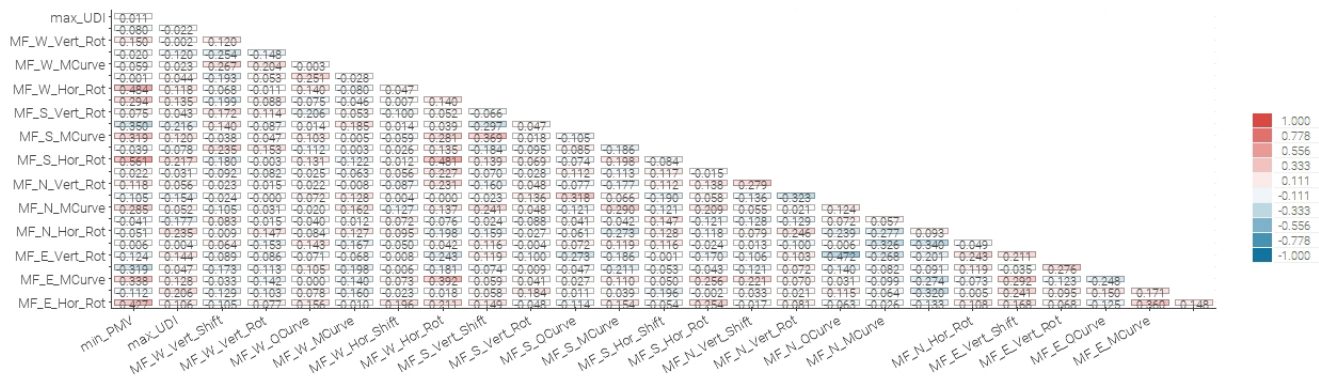


Figure 161. Correlation analysis Abu Dhabi (by author)

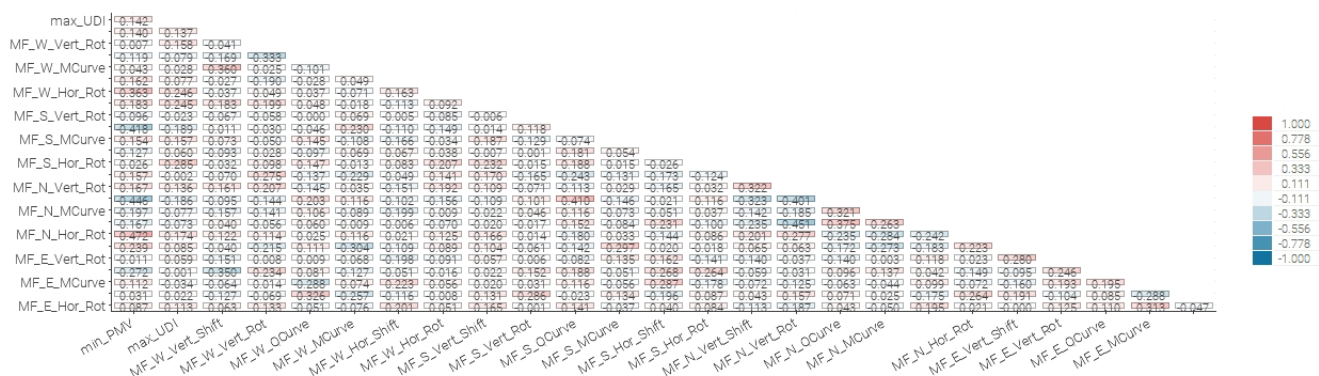


Figure 162. Correlation analysis Brisbane (by author)

Cluster analysis

The final used analysis method is the cluster analysis (standard hierarchical clustering), which was also used in the case study of Yang et al. (2018). This gave the following results for the different optimisation runs (See fig. 163 to 165). The blue cluster shows input values related to design with good performance on the PMV objective, whereas the yellow cluster shows designs performing well on the UDI objective.

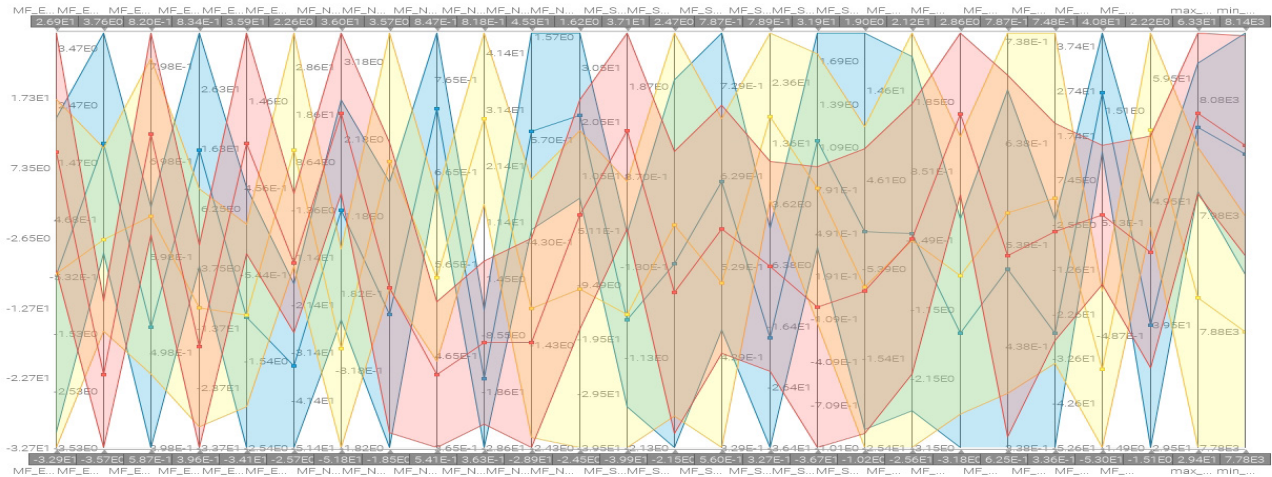


Figure 163. Cluster analysis Singapore (by author)

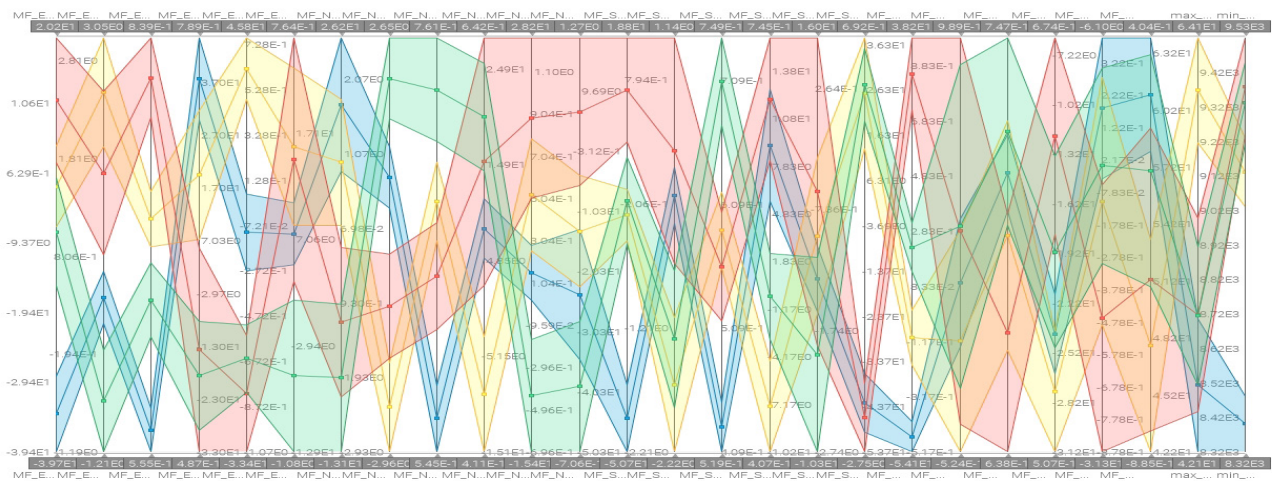


Figure 164. Cluster analysis Abu Dhabi (by author)

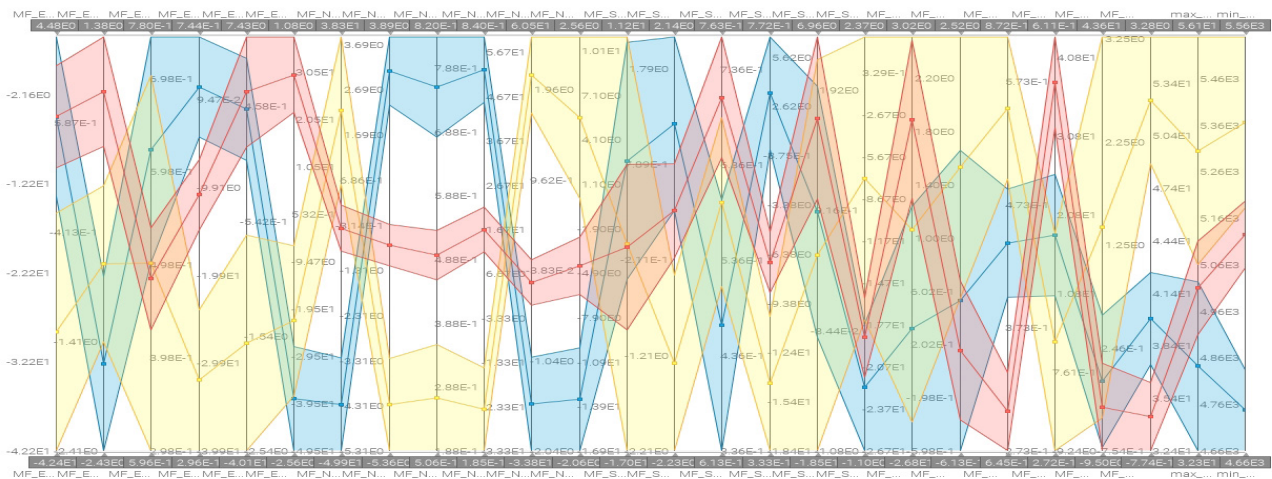


Figure 165. Cluster analysis Brisbane (by author)

3.4.7 - Conclusions on optimisation results

Based on the post-processing analysis techniques discussed in the previous paragraph, more conclusions about the example case can be made regarding the input parameters. Drawing these conclusions is an essential part of the PCA method, because it gives the designer insight in which parameters are important contributing factors to the performance on visual and thermal comfort and what value boundaries for these parameters represent good performance. This paragraph will continue by discussing some of the conclusions made based on the analysis of the results.

Reducing the input value boundaries of the rotation and Q-value parameters

This conclusion is based on the error analysis and reinstating some of the input value combinations in the Grasshopper script. Extreme values for the vertical rotation, horizontal rotation and q-value can result in invalid geometry, causing an error in the ModeFRONTIER design evaluation. In order to prevent future errors, the value boundaries are revised and set as following:

<i>Parameter</i>	<i>Original boundaries</i>	<i>Revised boundaries</i>
Horizontal rotation:	-60 to 60	-50 to 50
Vertical rotation:	-60 to 60	-50 to 50
Q-value:	0.2 to 0.9	0.3 to 0.9

Low correlation in the shifting parameters

Based on the Pearson correlation graphs, it can be concluded the values for shifting are actually not contributing that much to the visual and thermal performance of the sun shading, because of the correlation values are relatively close to zero. This means the input parameters for shifting can also be used to achieve a pleasing architectural appeal instead setting the values exactly to the optimisation result. This conclusion accounts for both the vertical and horizontal shifting parameters on all orientations in all three climates.

High correlation in the horizontal rotation

In contrast to the shifting parameters, the horizontal rotation parameters show a high Pearson correlation to the comfort objectives, especially to the PMV score. This means the horizontal rotation can be regarded as the most important input parameter. All correlations are positive, meaning a low input value for the horizontal rotation correlates to a low PMV score. This was expected, because a negative rotation means the horizontal shading elements are pointed at the ground, which is most efficient for blocking solar radiation. This conclusion accounts for both the vertical and horizontal shifting parameters on all orientations in all three climates.

High correlation in q-value

Similar to the horizontal shading, a high correlation can also be found for the q-value parameters, again especially related to the PMV score. In this case the correlation is negative, meaning a low q-value correlates with a high PMV score. This was also expected, because a low q-value corresponds with less sun shading material. This conclusion again accounts for both the vertical and horizontal shifting parameters on all orientations in all three climates.

Custom clustering

The hierarchical clustering helps to gain insight in what parameter values correspond to good performance. However, none of the clusters found by the hierarchical clustering algorithm regards a set of designs with a high UDI score and a low PMV score. Another method for gaining insight in this relationship is manually altering the filters of the objectives in a parallel coordinates graph. This will reveal a set of designs with good performance and the corresponding input values ensuring this performance. This analysis showed that for the Abu Dhabi climate the south façade is very closed compared to the north façade. In Brisbane this difference is vice versa. The analysis for Singapore does not give much insight in the relationship between input values and performance on the objectives, due to the lack of data in this analysis. (see fig. 166 to 168)

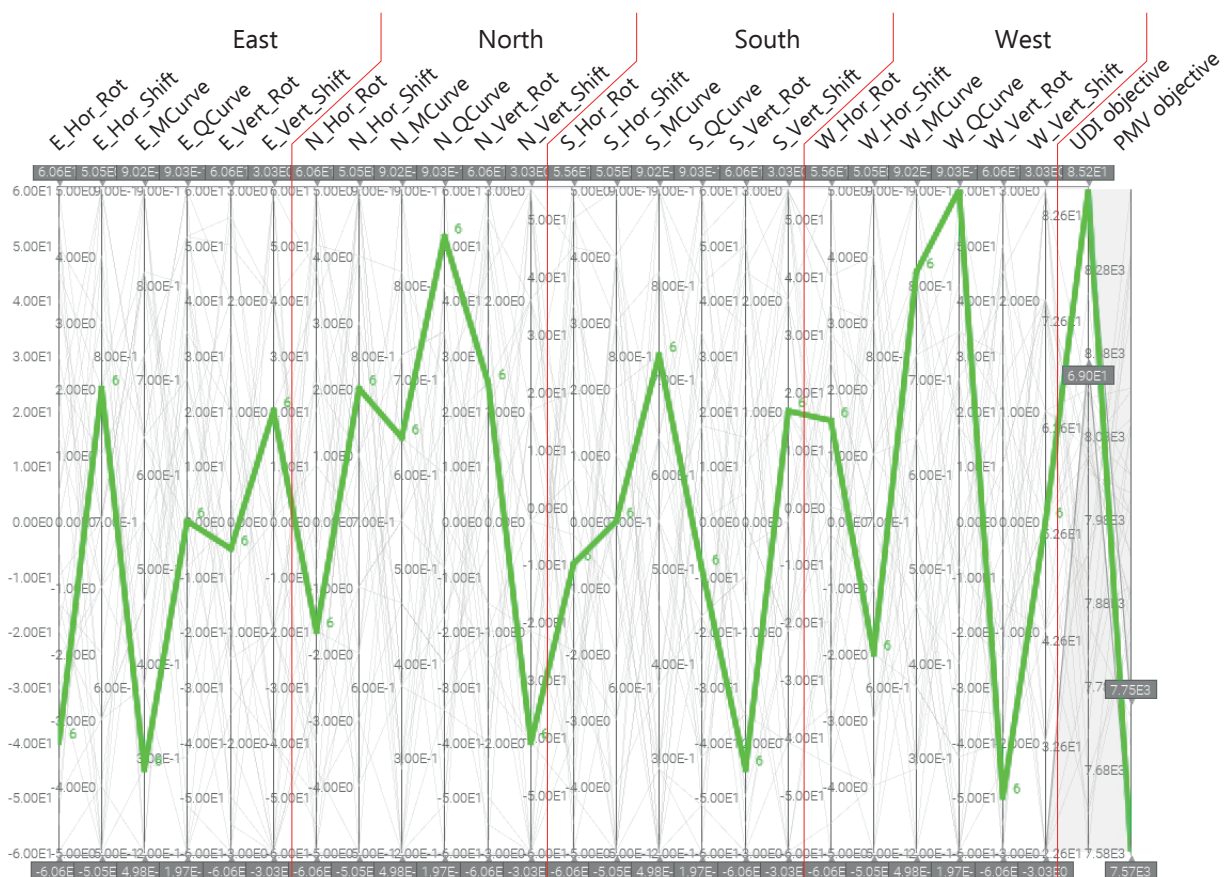


Figure 166. Custom clustering Singapore (by author)

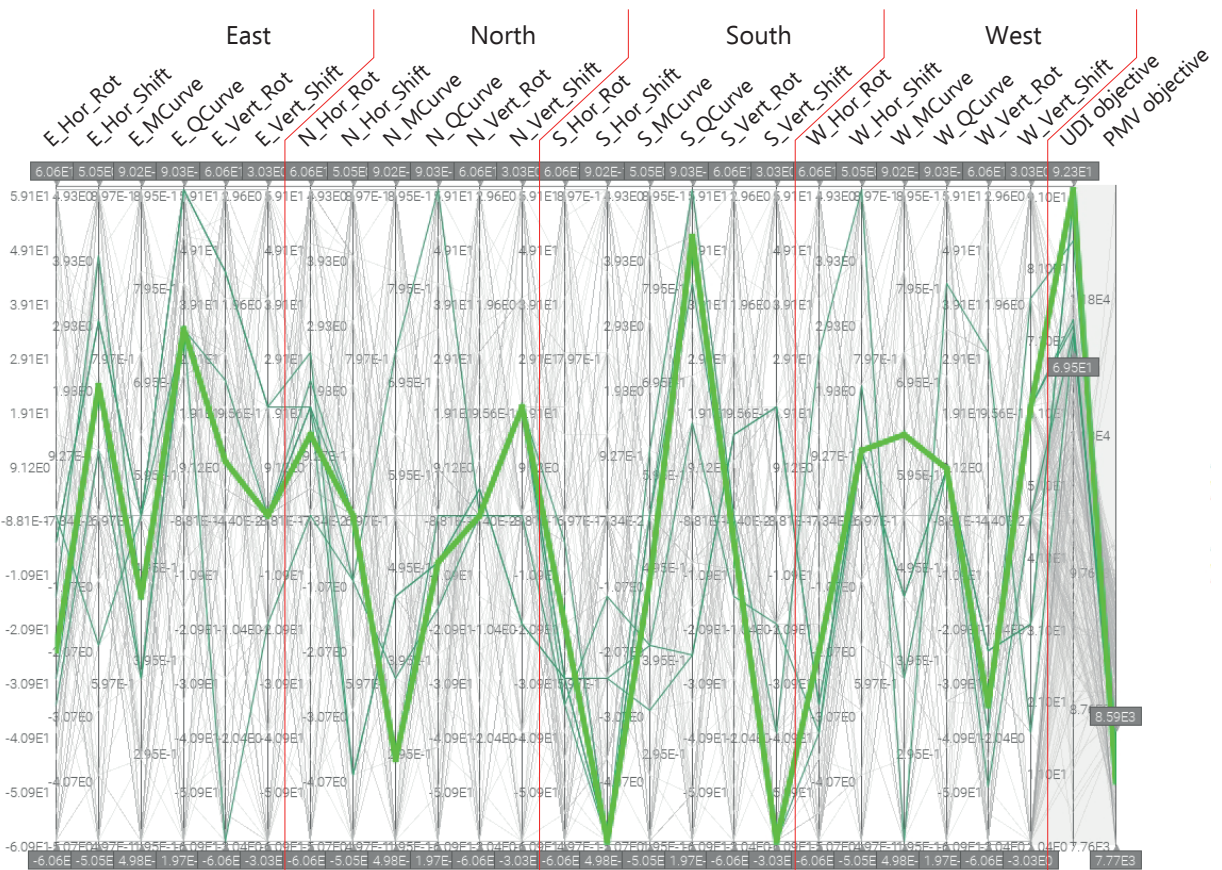


Figure 167. Custom clustering Abu Dhabi (by author)

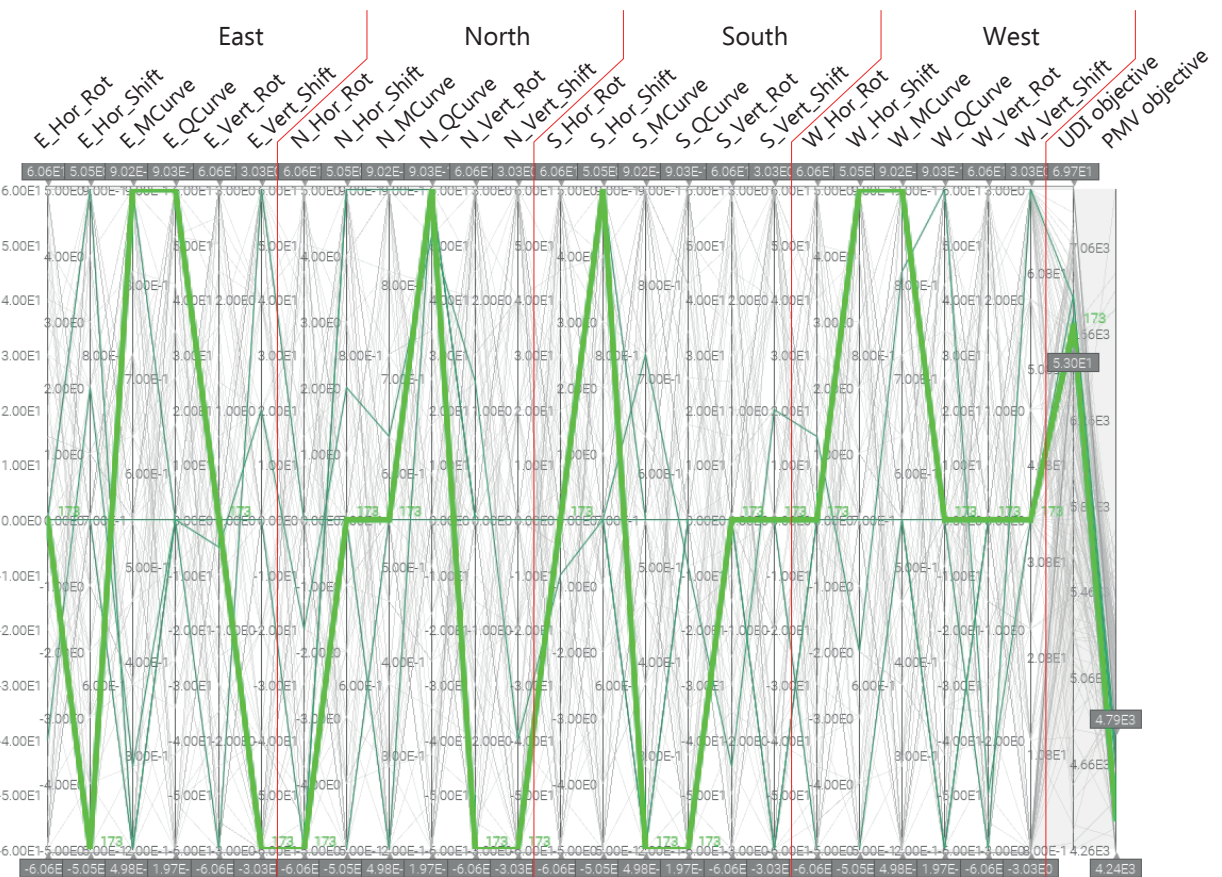


Figure 168. Custom clustering Abu Dhabi (by author)

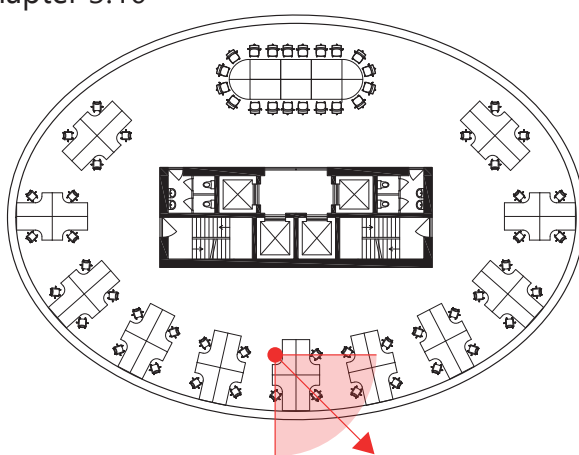
3.4.8 - The final assessment and design choice

Final assessment

The next step in the research is to select a design from the Pareto front in order to compare it to different design alternatives (see next chapter). The methodology for making a selection from the Pareto front is open for interpretation. In this case the decision making is based on various aspects. The first one is the performance on thermal and visual comfort, which are the two objectives in this optimisation in the form of the PMV and the UDI metrics. The Pareto front is defined as the set of solutions which cannot improve performance on one objective without decreasing performance on other objectives. So, the selection involves choosing a design based on the ratio between the performance on PMV and UDI. Since one of the goals of the study is to see if the sun shading system can be improved on both objectives, a balanced performance is preferred. This indicates the desired solution would be in the center of the Pareto front. In order to define the boundaries of this center, the performance of the "default egg-crate" (see next chapter) was used. Using this methodology, it is ensured the chosen design performs better than the default egg-crate alternative.

The second aspect used for the assessment is the DGP evaluation, which can be run to evaluate the designs performance on glare. This has been done for multiple designs and multiple mannequin locations. Figure 169 shows the results of an example DGP evaluation for a Pareto front solution in the climate of Abu Dhabi. It shows a high-glare probability for mid-day in wintertime. Indicating some form of interior dynamic light shading might be needed for this facade to address peak glare probability hours.

In addition to the performance on comfort metrics, architectural quality is also an aspect influencing the choice for a solution on the Pareto front. In order to rate the architectural quality, multiple methods can be used. The simplest method would be to plot the 3D images of all Pareto front solutions and compare them by eye. However, two more advanced methods are proposed in this research as well. The first one being the automatized production of physical models. This is based on an automatized workflow for translating the 3D geometry to vector files which can be read by a laser-cutting machine. This workflow is elaborated more in-depth in chapter 3.9. The second advanced method for assessing the architectural quality is the creation of VR-renderings. This can also be done using an automated workflow, which is elaborated more in-depth in chapter 3.10



16:00	0.34	0.29	0.3	0.38
13:00	0.37	0.33	0.35	0.5
10:00	0.35	0.32	0.34	0.43
	Mar	Jun	Sep	Dec

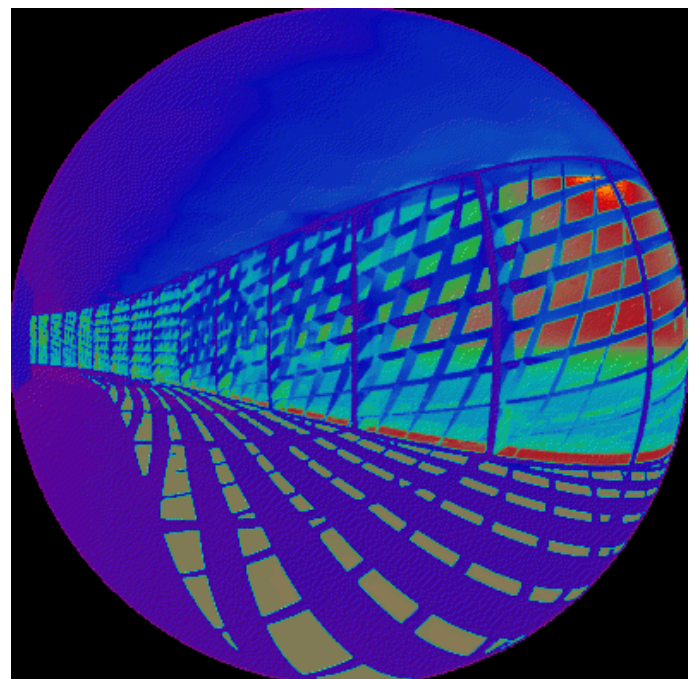


Figure 169. DGP analysis Pareto front solution of Abu Dhabi

Final choice

Based on the assessments of the aspects stated in the previous paragraph, a solution was selected from the Pareto front. This final choice is open to interpretation and in order to make sure the design actually is an optimal solution, more generations of the search algorithm are needed. However, choosing an option at this stage is required to be able to compare the performance with conventional shading systems. The choices for the different climates are made as following:

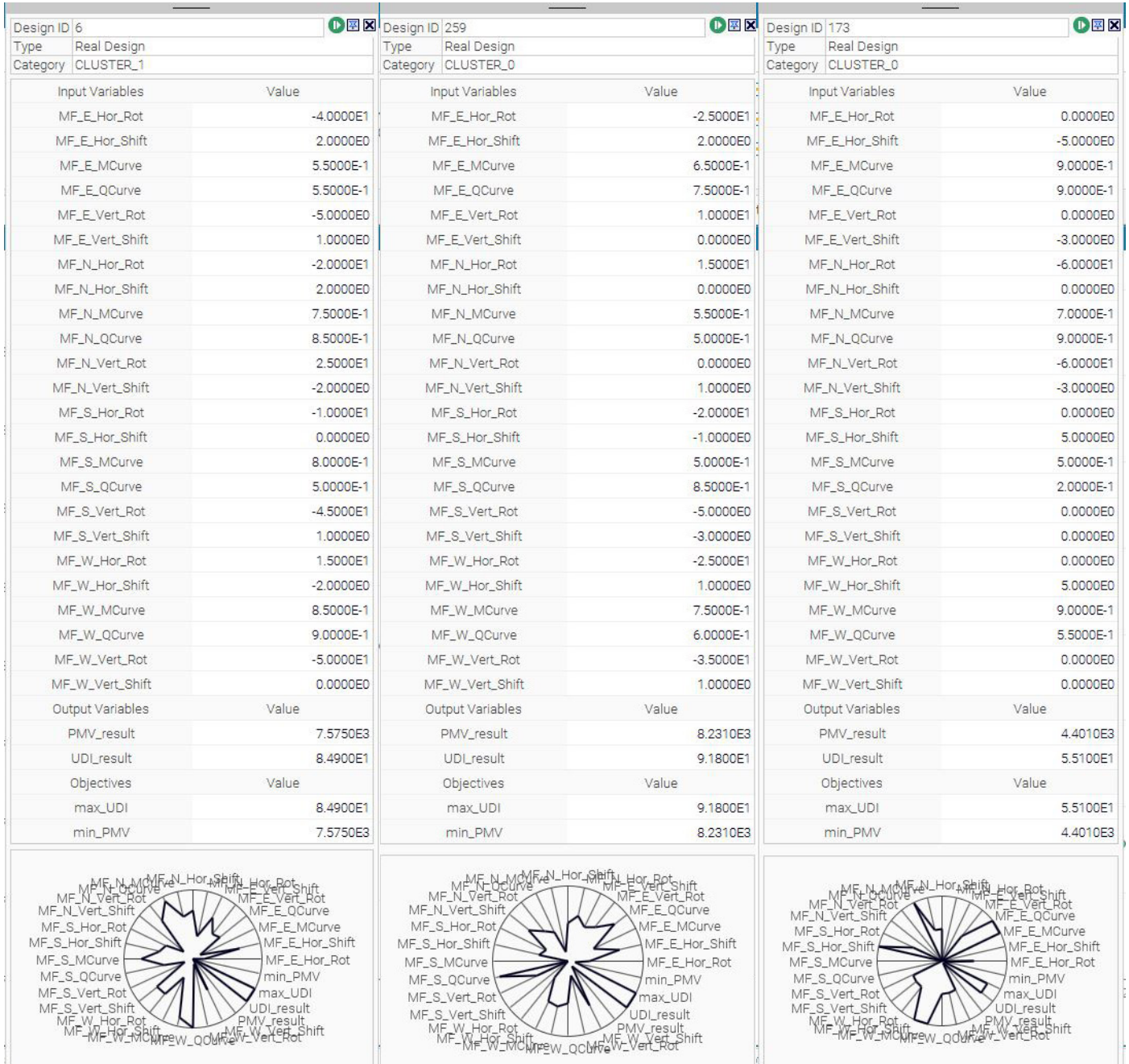


Figure 170. Choice Singapore (by author)

Figure 171. Choice Abu Dhabi (by author)

Figure 172. Choice Brisbane (by author)

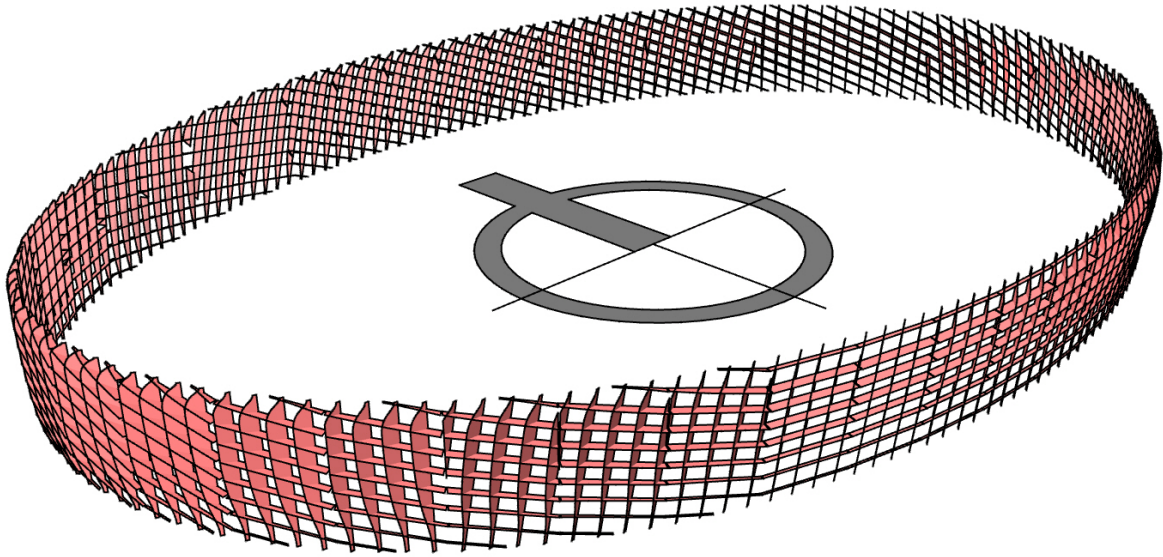


Figure 173. *Geometry choice Singapore*

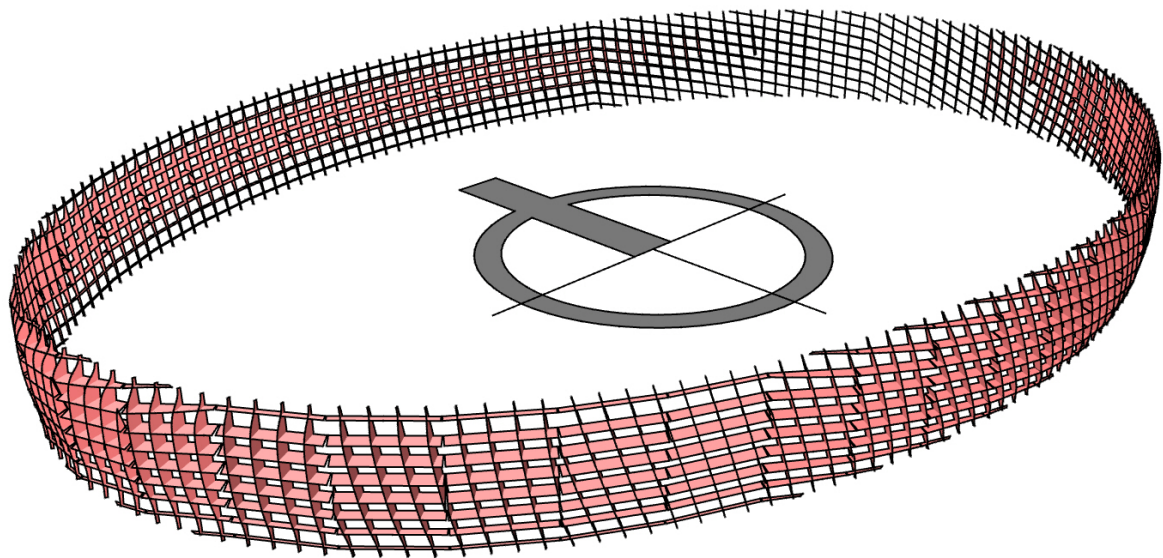


Figure 174. *Geometry choice Abu Dhabi*

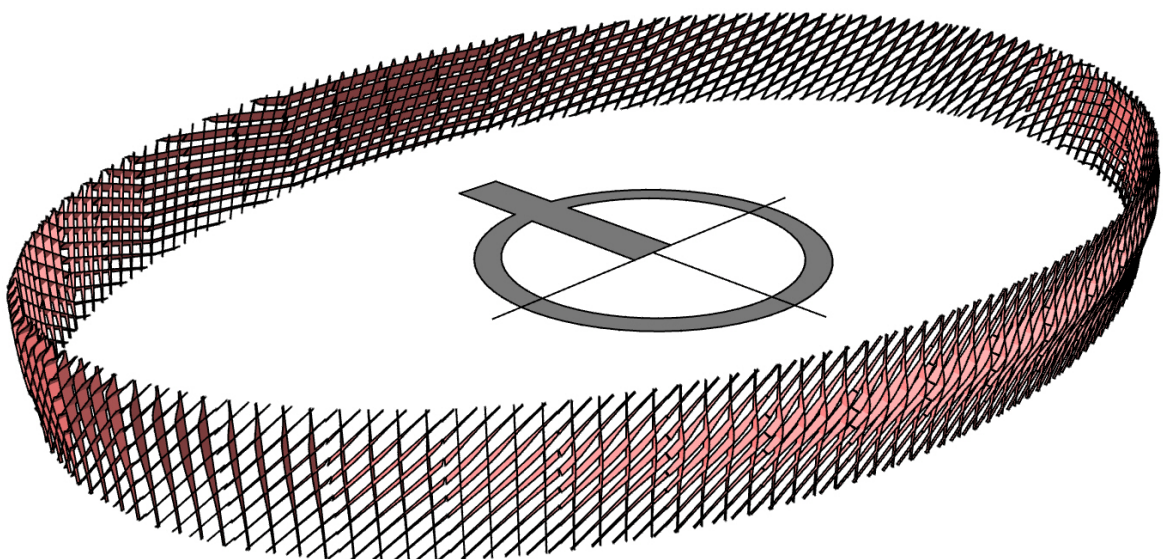


Figure 175. *Geometry choice Brisbane*

3.5 - Comparison

3.5.1 - Definition of alternative shading concepts

In order to assess to what extent the PCA process improved the shading, a comparison to conventional systems will be made in this chapter. The first two simulations involve reference measurements of a single skin façade and a regular 'empty' double skin façade with the dimensions as stated in paragraph 3.4.2. Three alternatives involve conventional systems; solar reflective shading, a default egg-crate system and default dynamic screen shading. All five alternatives will be compared to the solution chosen from the Pareto front in the previous paragraph.

The different design alternatives can be generated by including or excluding various parts of the Grasshopper script by using the toggles shown in figure 176. For simulation 1, the single façade, this means excluding both the DSF and the shading geometry. For simulation 2, the empty DSF, this means only excluding the shading geometry.

For the third simulation, involving the solar reflective glazing, the material parameters for the exterior shading are altered to a g-value and visual transmittance coefficient of both 0.4. The interior glazing remains unchanged with a g-value of 0.7 and a visual transmittance coefficient of 0.7.

The fourth simulation, involving the dynamic shading, a screen shading element was added in between the two glass planes with a g-value and visual transmittance coefficient of both 0.25 (see fig. 177). For this simulation, an additional performance evaluation was set-up. In order to assess the visual performance of this alternative, two daylight simulations were run in parallel; one with the dynamic shading up and one with the dynamic shading down. The hourly results for both simulations are collected and combined. Whether the shading is up or down is based on a logical statement; whenever the normal direct solar radiation gets above 300 W/m^2 , the dynamic shading goes down. The annual scheme for the dynamic shading is created for determining how to combine the two simulations together and as an input for the thermal comfort simulation. Energyplus allows for settings up shading geometry with an transparency schedule attached. The schedule contains a value of 1 (fully transparent) when the shading is up and 0.25 (the g-value) when the shading is down.

The last alternative, the "default sun shading" is generated using the default "cutting-box". All parameters for shifting and rotation are set to zero. Since this alternative is generated with the default cutting-box, it does not have parameters for the M and Q value of the cut-off box.

The alternatives will first be compared on the performance of the two optimisation objectives; the PMV and UDI score. Secondly, the two properties used to select the desirable solution from the Pareto front; the DGP score and the material usage. Thirdly the annual energy usage if the simulation is run with the ideal all-air system.

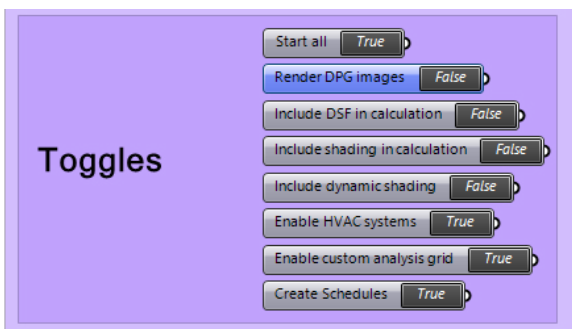


Figure 176. The toggles for generating the design alternatives (by author)

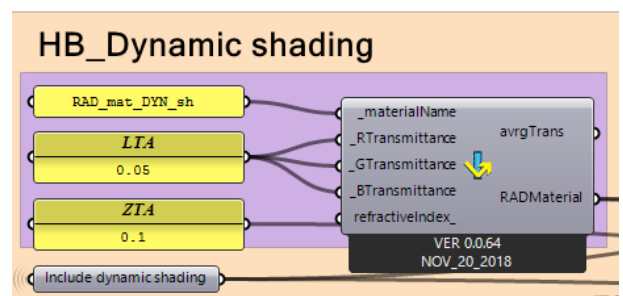
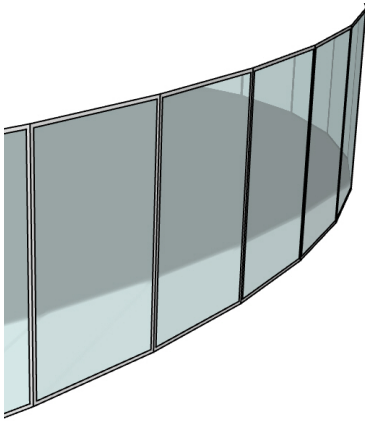
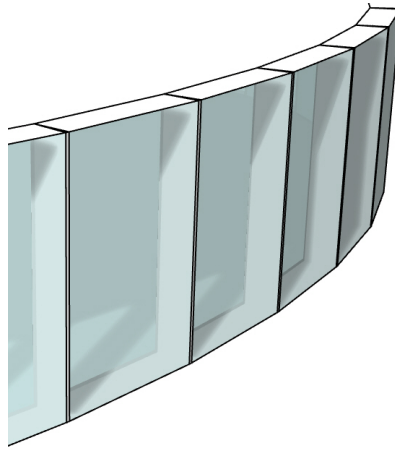


Figure 177. Material parameters for dynamic shading (by author)



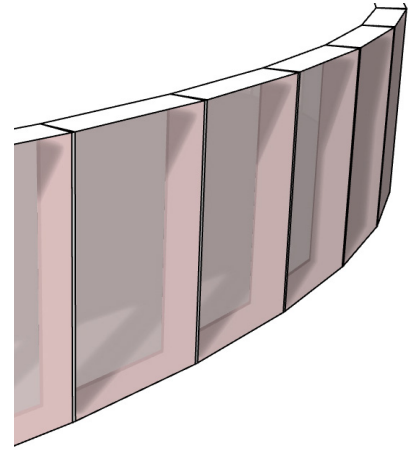
Simulation 1: Reference 1
Single skin facade

Total DSF width:	n/a
Egg-crate width:	n/a
Amount vertical:	n/a
Amount horizontal:	n/a
Vertical shift:	n/a
Vertical rotation:	n/a
Horizontal shift:	n/a
Horizontal rotation:	n/a
Mid-point curve:	n/a
Q-value curve:	n/a
g-value:	0.8
Visual trans.:	0.7



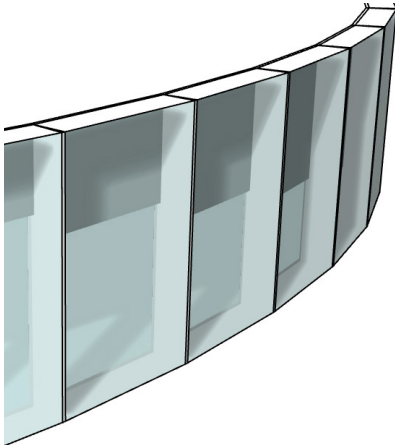
Simulation 2: Reference 2
"Empty" double skin facade

Total DSF width:	500mm
Egg-crate width:	n/a
Amount vertical:	n/a
Amount horizontal:	n/a
Vertical shift:	n/a
Vertical rotation:	n/a
Horizontal shift:	n/a
Horizontal rotation:	n/a
Mid-point curve:	n/a
Q-value curve:	n/a
g-value:	0.8
Visual trans.:	0.7



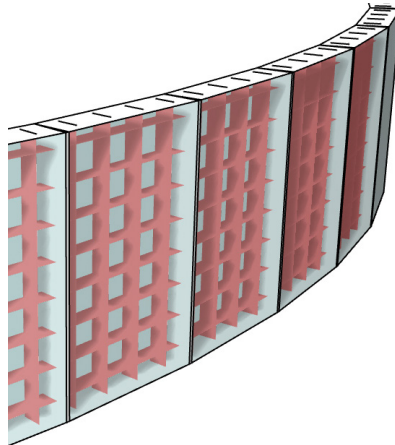
Simulation 3: Alternative A
Solar reflective glazing

Total DSF width:	500mm
Egg-crate width:	250mm
Amount vertical:	4
Amount horizontal:	8
Vertical shift:	0
Vertical rotation:	0
Horizontal shift:	0
Horizontal rotation:	0
Mid-point curve:	n/a
Q-value curve:	n/a
g-value:	In: 0.7 Ex: 0.4
Visual trans.:	In: 0.8 Ex: 0.4



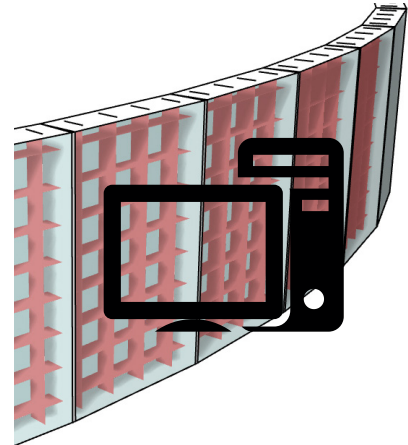
Simulation 4: Alternative B
Default dynamic screen shading

Total DSF width:	500mm
Egg-crate width:	n/a
Amount vertical:	n/a
Amount horizontal:	n/a
Vertical shift:	n/a
Vertical rotation:	n/a
Horizontal shift:	n/a
Horizontal rotation:	n/a
Mid-point curve:	n/a
Q-value curve:	n/a
g-value:	0.8
Visual trans.:	0.7



Simulation 5: Alternative C
"Default" egg-crate shading

Total DSF width:	500mm
Egg-crate width:	250mm
Amount vertical:	4
Amount horizontal:	8
Vertical shift:	0
Vertical rotation:	0
Horizontal shift:	0
Horizontal rotation:	0
Mid-point curve:	n/a
Q-value curve:	n/a
g-value:	0.8
Visual trans.:	0.7



Simulation 6: Optimised
by conventional approach

Total DSF width:	500mm
Egg-crate width:	250mm
Amount vertical:	4
Amount horizontal:	8
Vertical shift:	???
Vertical rotation:	???
Horizontal shift:	???
Horizontal rotation:	???
Mid-point curve:	???
Q-value curve:	???
g-value:	0.8
Visual trans.:	0.7

3.5.2 - Comparison of alternatives in three climates

When comparing the results, it has to be stated that the optimal solution can actually not be proven to be an optimal version due to insufficient data. However, comparison is still made to assess the performance in relation to the other alternatives (see fig. 179). A full overview of the graphic results is given in appendix I. The comfort metrics refer to a situation where all HVAC are disabled, the energy usage refers to a situation where an ideal all-air system with parameters as stated in paragraph 3.2.3 is conditioning the building.

The two references and the solar reflective glazing behave as expected, since their order represent a decreasing total g-value for the glazing. Dynamic shading within the double skin cavity does perform far worse on daylight in all climates. Even though the threshold value of 300 w/m² is common for automatic dynamic shading systems to close, it resulted in the following percentages of annual operative hours being closed:

Singapore: 16%
Abu Dhabi: 82%
Brisbane: 62%

For the climates of Abu Dhabi and Brisbane these percentages are relatively high. This can be explained by two contributing factors. Firstly, the fact that the fictive building in the example case uses operative hours from 08:00 to 18:00, resulting in an absence of evening hours. Secondly, the annual graphs for the cloud cover index can be plotted for all 3 climates as shown in the figure below. The total amount of sky cover is expressed in a domain ranging from 1 to 10. A score of 1 means no cloud cover, so completely sunny, whereas a score of 10 means totally clouded. The graphs indicates that the differences in annual closing percentages between the climates corresponds with the annual cloud cover index. Singapore is found to be clouded almost year-round, whereas Abu Dhabi is sunny almost year-round and Brisbane represents an intermediate annual cloud coverage.

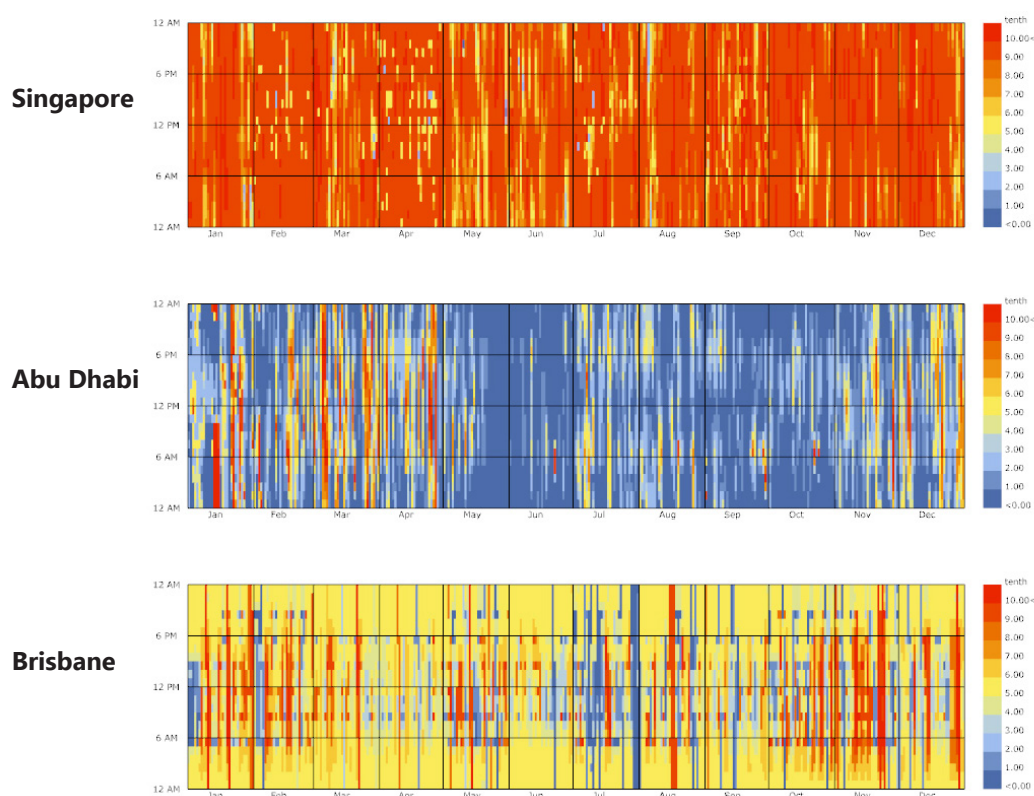


Figure 178. Annual cloud cover indices for the three climates (by author)

It can also be observed that the egg-crate system performs better than all alternatives before, in all three climates. The optimised version of the egg-crate does not perform better in all three climates yet. The main reason for this is the lack of data, like stated before. However, for the climate with the most evaluation, Abu Dhabi, the optimised version does in fact perform better on both objectives. Even though the comparison gives insight in the performance in regard to alternatives, the validity of the comparison between the default egg-crate and optimised egg-crate remain debatable, due to different amounts of shading material. This property of the design solution has not been taken into account as an objective, but in practice, the ratio between performance and material use does have an impact on the feasibility of a system. This is due to the fact that less material means less expenses, resulting in the system being a more favourable solution for future designers. Since the form-finding script does have inputs controlling the amount of material use, with the Q-value in particular, this observation raised debate whether including the material use as a to be minimized objective would result in a more feasible sun shading solution. The first proposal of improvement of methodology in the next chapter will touch upon this debate.

Singapore	Sim 1: Single skin facade	Sim 2: Empty double skin facade	Sim 3: Solar reflective glazing	Sim 4: Dynamic screen sun shading	Sim 5: Default egg-crate sun shading	Sim 6: Optimized egg-crate sun shading
Primair PMV score UDI score	11587 19.2%	9833 39.9%	8417 63.3%	9865 31.9%	7375 82.1%	7575 84.9%
Secundair Lighting Heating Cooling Total	1.426 kWh 0 kWh 227.471 kWh 228.897 kWh	1.680 kWh 0 kWh 215.556 kWh 217.236 kWh	3.447 kWh 0 kWh 206.193 kWh 209.640 kWh	10.381 kWh 0 kWh 217.731 kWh 228.112 kWh	2.437 kWh 0 kWh 198.032 kWh 200.469 kWh	

Abu Dhabi	Sim 1: Single skin facade	Sim 2: Empty double skin facade	Sim 3: Solar reflective glazing	Sim 4: Dynamic screen sun shading	Sim 5: Default egg-crate sun shading	Sim 6: Optimized egg-crate sun shading
Primair PMV score UDI score	14031 16.3%	11980 41.8%	10063 69.1%	9650 0.0%	8311 77.8%	8231 91.8%
Secundair Lighting Heating Cooling Total	479 kWh 280 kWh 177.938 kWh 178.695 kWh	676 kWh 268 kWh 161.805 kWh 162.749 kWh	4.109 kWh 267 kWh 148.341 kWh 152.717 kWh	14.214 kWh 248 kWh 147.623 kWh 162.085 kWh	1.407 kWh 266 kWh 134.865 kWh 136.538 kWh	

Brisbane	Sim 1: Single skin facade	Sim 2: Empty double skin facade	Sim 3: Solar reflective glazing	Sim 4: Dynamic screen sun shading	Sim 5: Default egg-crate sun shading	Sim 6: Optimized egg-crate sun shading
Primair PMV score UDI score	9072 14.2%	7251 40.0%	5761 54.4%	5696 0.0%	4460 70.1%	4401 55.1%
Secundair Lighting Heating Cooling Total	1.477 kWh 5.530 kWh 98.345 kWh 103.875 kWh	1.921 kWh 5.533 kWh 87.656 kWh 95.110 kWh	5.911 kWh 5.678 kWh 79.384 kWh 90.973 kWh	13.365 kWh 5.615 kWh 81.433 kWh 100.413 kWh	4.135 kWh 5584 kWh 70.335 kWh 80.054 kWh	

Figure 179. Results on performance on PMV, UDI and energy usage for the alternatives (by author)

3.6 - Challenge identification

As stated before in the previous paragraph, the main issue for properly analyzing the optimisation results is a lack of sufficient data. The most straightforward approach would be to let the optimisations run for a longer period of time. However, this would imply impracticalities, because the optimisations elaborated previously already took 72 hours to complete on high-end computers. Another approach would be to improve the workflow. The first step in doing so is to identify the challenges which limit the contemporary workflow. In essence the main challenge is to generate more data in a smaller amount of time. This can be done using two different approaches. The first one is to use the available computational power more efficiently whereas the second approach is to allow for more computational power to be used.

The first approach aims to use the computational power more efficiently by splitting the input parameters into two groups and optimise them using a stepped approach. This might help to generate more data in a lower amount of time, because the optimisation algorithm can use a smaller generation size and thereby theoretically converge faster to the Pareto front. A more elaborate description of the stepped approach is given in paragraph 3.6.1

The second approach aims to enable the use of the grid in the workflow. This will allow the optimisation process to split the computational tasks among multiple computers and thereby allow to generate more data in a lower amount of time. The concept of this grid-based optimisation approach is discussed in paragraph 3.6.2. In the final phase of this research this approach was explored more extensively, resulting in the development of the next generation workflow, which will be discussed further in chapters 3.7 and 3.8.

3.6.1 - The stepped approach

The stepped approach involves a reconsideration of the objectives and input variables of the ModeFRONTIER workflow. The comparison between the "default" egg-crate and the optimised version in the previous chapter is arguable not completely valid, because both options use a different amount of shading material. The "default" eggcrate is derived from the straight extruded cut-off shape and does not contain the values for defining the cut-off curve. The hypothesis is that these two parameters controlling the curve of the cut-off shape are independent from the other parameters. The input parameters of rotation and shifting control the performance of the panel in relation to the orientation, whereas the values for the mid-point and q-value of the curve merely controlling the efficiency of the material. However, this is an hypothesis and it remains debatable if the parameters for the case of the egg-crate sun shading can be indeed be divided in independent groups without cross-correlation.

In order to conclude on this matter, a new approach is proposed. If the hypothesis is found to be correct, this stepped approach might be able to help designers to converge to the desired solution faster. The conventional approach, used for the optimisations discussed in chapter 3.4, uses all the inputs for one single optimisation run based on two objectives; minimizing the annual PMV exceedance sum and maximizing the UDI (mod-75) score. The stepped approach is based on first running an optimisation which only includes the input parameters of rotation and shifting. In the second run, these objectives remain unchanged, and in addition a third objective is added. The new objective is minimizing the material use. Using this method, the results can be used to assess the relation between the effectiveness of the geometry and the relative performance on visual and thermal comfort. A workflow comparison regarding the conventional and stepped approach is given in figures 180 and 181.

Based on the results on this first optimisation, two sub-approaches with regard to the second optimisation are possible. The first one involves selecting an option from the Pareto front, based on the same criteria as before. This will result in fixing the four parameters of rotation and shifting, leaving only two variable inputs for the second optimisation run. The final desirable solution can be found in the 3D Pareto front of the second optimisation iteration. The second sub-approach is to perform hierarchical clustering analysis on the solutions of the Pareto front. This will result in gaining insight which input values correspond with high performance. Thereafter, this information can be used to decrease the domain of (some of) the input variables. As a result, the second optimisation run will still include some variable inputs. However, since the domain of these input parameters is decreased the optimisation will converge to the Pareto front faster. This second sub-approach of decreasing input variable domains, was also applied in the second case study discussed in paragraph 2.5.1.

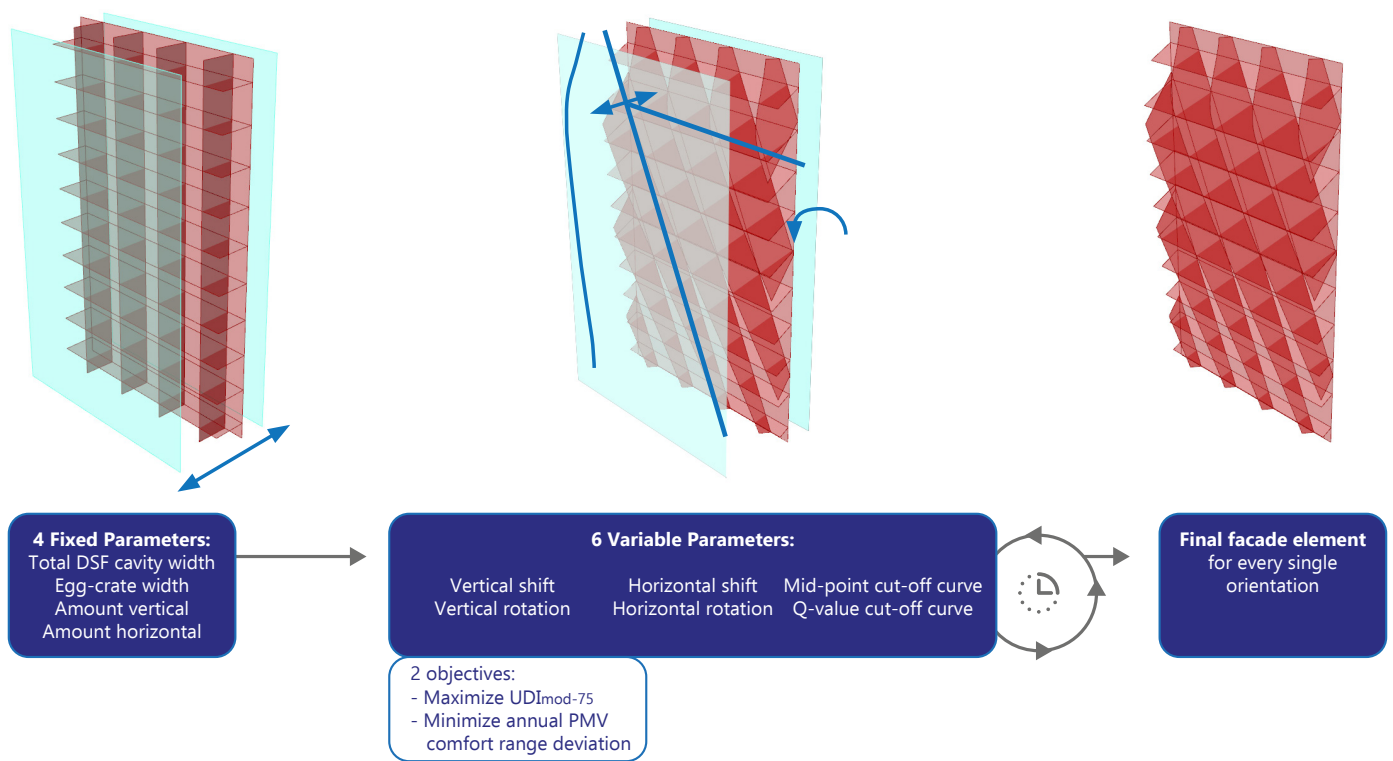


Figure 180. *Conventional approach (by author)*

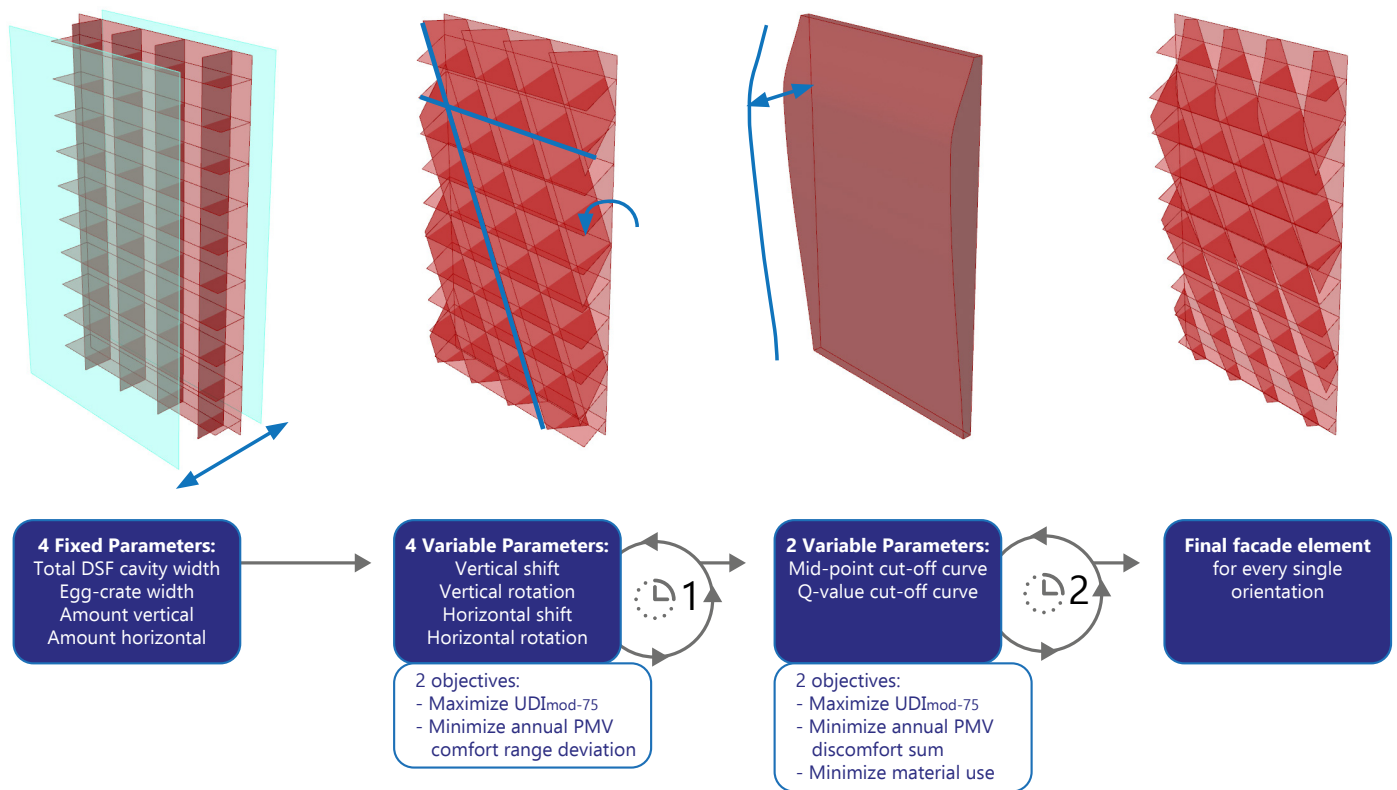


Figure 181. *Stepped approach (by author)*

3.6.2 - Grid based optimisation approach

The second improvement of methodology is regarding the workflow in ModeFRONTIER itself. The software is well suited for the application of improving the performance of sun shading using the PCA method. However, since integration with Grasshopper is currently only available through a custom myNode, some challenges regarding this integration are still present. Although researching the following newly proposed method is on the borderline of the software engineering realm, realizing it would have a large positive impact on the speed of the workflow.

This thesis is built on the current state of the art of integrating ModeFRONTIER and Grasshopper, where the ModeFRONTIER workflow is based around one single Grasshopper script. Within this script the form-finding and performance evolution are set-up using Ladybug and Honeybee. These performance evaluation plug-ins are the current standard for evaluation visual and thermal performance within Grasshopper. However, using Ladybug and Honeybee in the workflow causes challenges for harvesting the full potential of the Volta player grid. This grid can be used for distributing the workload across multiple computers. When combined with heavy computational power, this can drastically reduce the time required for the optimisation.

The first problem in the workflow is the need for a Rhinoceros license on every node within the grid. Since the amount of licenses are limited in commercial practice, this also limits the potential of the grid. The second problem is related to Ladybug and Honeybee not being intended for use in the grid. This prevents ModeFRONTIER from the ability to run parallel processes, which can be done with other simulation engines. As a result of these limitations, ModeFRONTIER is only able to evaluate a single design at a time for each of the limited number of computers.

In order to overcome this problem, a new ModeFRONTIER workflow is suggested. The concept of this new proposed workflow is based on only harvesting the power of the Volta player grid for the time-consuming processes; the actual simulations of Radiance, Daysim and Energyplus. Honeybee offers the capability of just preparing batch files for the simulations, instead of executing them within the Grasshopper interface. Thereafter these batch files can be send to the grid for execution. Radiance, Daysim and Energyplus themselves are freely accessible, therefore eliminating the challenge revolving the Rhinoceros licenses. When this concept is to be applied to an actual ModeFRONTIER workflow, the first two Grasshopper scripts should each give the directory of the prepared batchfile as an output. The execution nodes can be realized as a DOS script node, taking the batchfile directories as an input an give the result file address as an output. The final Grasshopper script should then give the final comfort metrics as an output. The application of this concept in ModeFRONTIER will be further discussed in the next chapter. In the case of this specific workflow for sun shading design, the process of preparing the batch files needs to be repeated twice, since the Energyplus simulation requires input from the result of the UDI evaluation in the form of a lighting schedule. A conceptual overview of the proposed workflow for further research is given in figure 182.

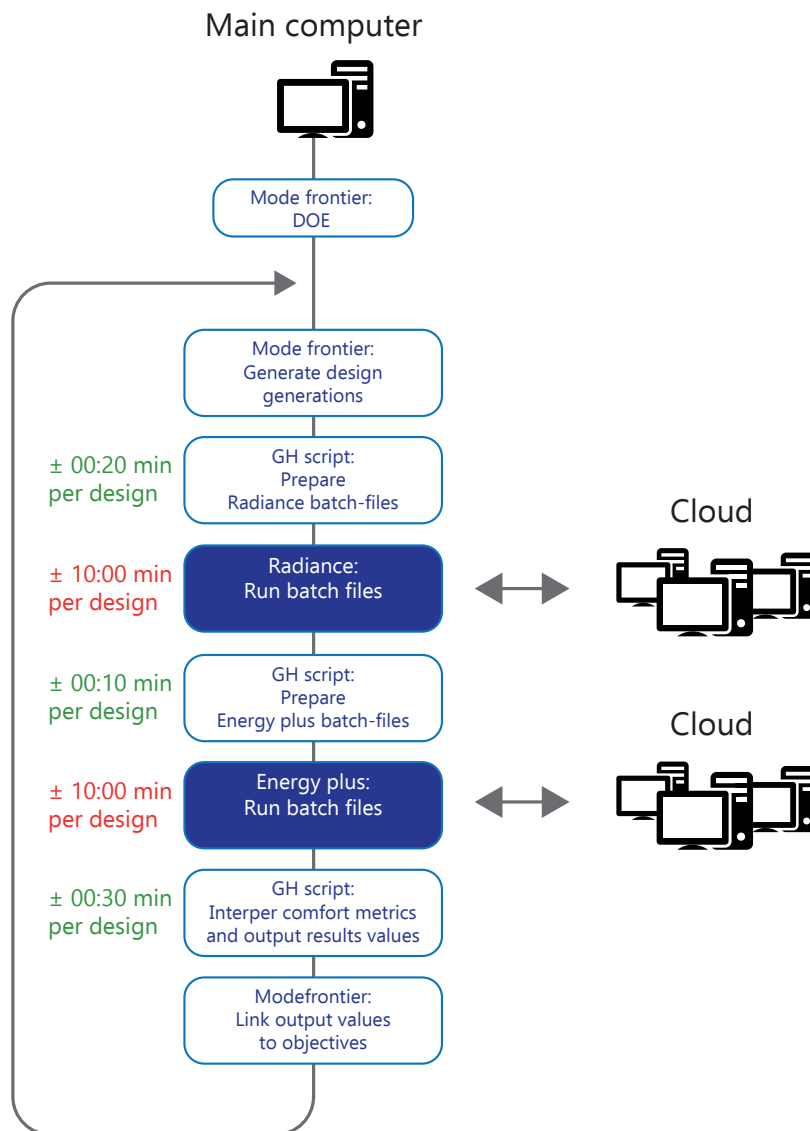


Figure 182. *Diagram for utilizing the power of the grid efficiently (by author)*

3.7 - Developing the next generation workflow

3.7.1 - The first conceptual setup: Separating the Grasshopper script

The main bottle neck with regard to cloud compatibility is related to the use of Grasshopper. Like explained in the previous chapter, the main concept of the next generation workflow is to use Grasshopper only to prepare the analyses and to interpret the results, but the actual execution of the visual and thermal simulations is done outside the Grasshopper environment. This means the ModeFRONTIER workflow is essentially split in three different sections, the preparation, execution and interpretation (see figure 183). Using this separation, the preparation and interpretation can be executed on one main computer, while the execution part can be split among multiple computers using the Volta grid. This means Rhinoceros, which is relatively expensive software, is only required on the main computer. All other computers in the grid only need installations of Radiance, Daysim, Open studio and Energyplus, which are all free of charge to use. The execution phase is conducted using a DOS script consisting of only a few lines of code. The script will execute the total of three batchfiles generated by the preparation phase and will return a true value when they all simulations are completed.

The first step in realizing this conceptual set-up is to split the Grasshopper script in two parts; preparation and interpretation, and define the required inputs and outputs. The separated version of the Grasshopper definitions can be found in Appendix III. The inputs for the first Grasshopper script remain the same as in the contemporary PCA workflow, same as the outputs for the second script. The outputs of the first script are the file directories for the analysis batch files, the directories of the result files which will be generated when the simulations are completed and the point matrix.

The matrix contains the three coordinates of the test points within the grid for the visual comfort simulation, as well as the floor area these points represent. This results in a matrix with 4 columns and a number of rows equal to the number of test points. This matrix is used to transfer the test point data between the First and second Grasshopper script, because this information is needed for the interpretation of the UDI comfort index. The complete overview of inputs and outputs is given below.

First GH script inputs:

- Horizontal rotation (x4 façade orientations)
- Horizontal shift (x4 façade orientations)
- Vertical rotation (x4 façade orientations)
- Vertical shift (x4 façade orientations)
- Midpoint of the curve (x4 façade orientations)
- Q-value of the curve (x4 façade orientations)

First GH script outputs:

- File directory of the Radiance batch files
(x2 because Radiance requires and initializing batch file, and a main batch file)
- File directory of the Energyplus simulation
- File directory of the Radiance result files
- File directory of the Energyplus result files
- The point matrix
- The total amount of sun shading material

Dos script inputs:

- File directory of the Radiance batch files
(x2 because Radiance requires and initializing batch file, and a main batch file)
- File directory of the Energyplus simulation

Dos script outputs:

- Boolean value

Second GH script inputs:

- Boolean value
- File directory of the Radiance result files
- File directory of the Energyplus result files
- The point matrix

Second GH script outputs:

- UDI comfort index
- PMV comfort index

The second step is to control the amount of concurrent processes, in other words, the amount of calculations which ModeFRONTIER is allowed to execute simultaneously in parallel. In the contemporary workflow the number of concurrent processes was limited to just one. This limitation is caused by the use of Ladybug and Honeybee, as they are not intended to operate in multiple simultaneous Grasshopper instances, which caused a challenge in preliminary test runs. In addition, multiple instances of Grasshopper are unfeasible, because this will result in relatively high CPU loads on the computers processor. When the processor is operating at full capacity and even more Grasshopper instances are started, some instances might stop responding.

In the next generation workflow however, the maximum number of concurrent processes is different per node. These differences amongst nodes can be controlled using the ModeFRONTIER queue nodes. This results in a workflow where the Grasshopper nodes are limited to one concurrent process, while the other nodes in the workflow can do a higher number of concurrent processes (see fig. 183). In the first conceptual setup this was tested on a common laptop with four concurrent processes. However, this number can be increased based on the specifications of the computer. This means that special farm computers could in theory process a relatively large number of concurrent processes. The TU Delft Architecture faculty does own such a farm computer, called the BK Renderfarm. Testing the next generation workflow on the BK Renderfarm will be discussed further in paragraph 3.7.8.

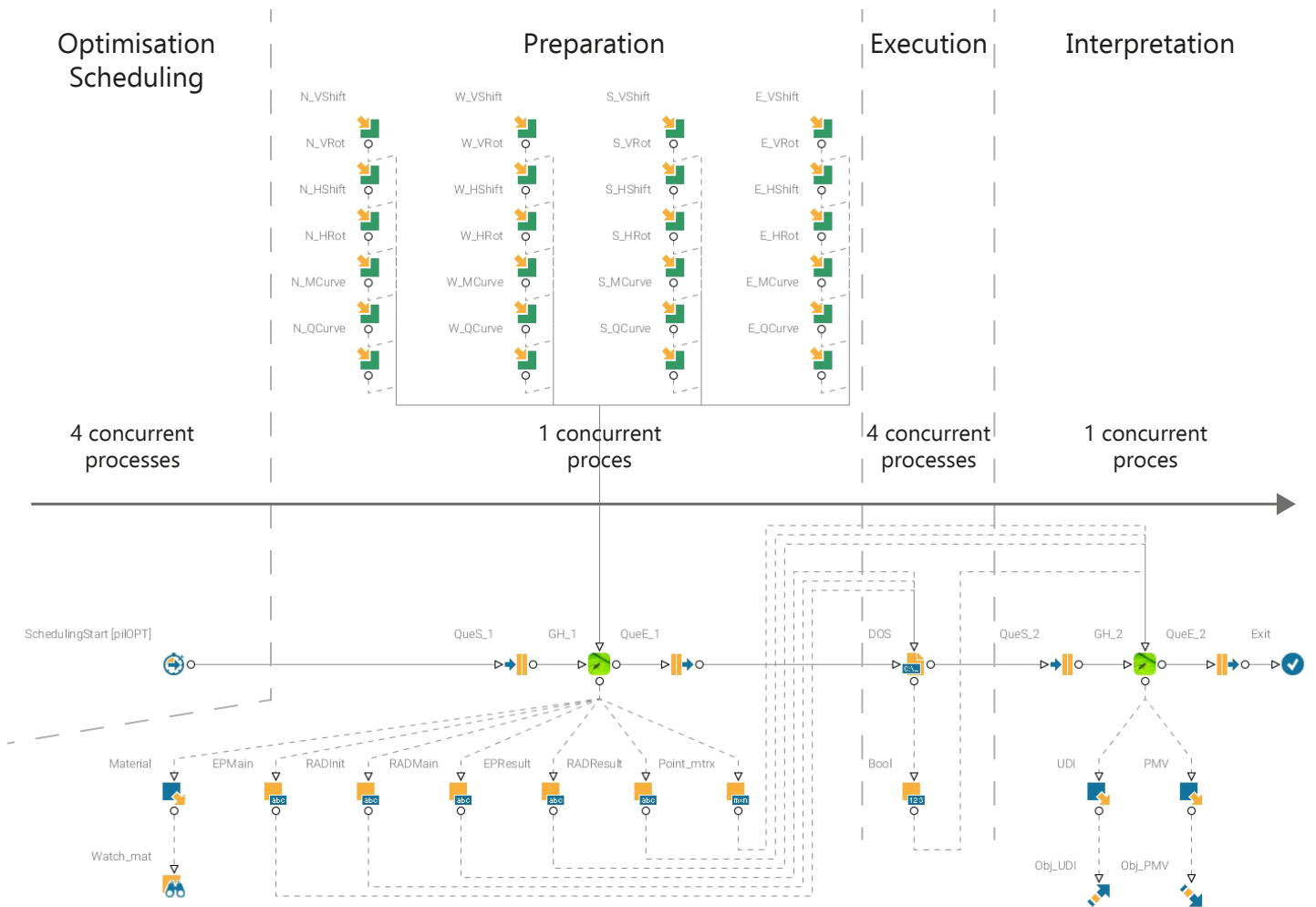


Figure 183. *First conceptual set-up of the next generation workflow (by author)*

3.7.2 - The lighting schedule issue

The first issue in implementing the next generation workflow is the lighting schedule. This schedule controls whether artificial lighting is turned on or not. In the contemporary workflow, this schedule is derived from the results of the visual comfort analysis and used as an input for the thermal comfort calculations. Meaning the visual comfort analysis will run first and the thermal comfort simulation will start afterwards. However, based on the nature of the next generation workflow discussed in the two previous paragraphs, this stepped analysis is not feasible anymore. This paragraph will continue discussing some approaches that have been tested to overcome this issue.

Option 1: Use 3 scripts in the ModeFRONTIER workflow

The first option would be use three Grasshopper scripts in the ModeFRONTIER workflow, like proposed in paragraph 3.6.2. In this case the middle script would prepare the Energyplus analysis based on the results of the Radiance simulation. This would be the preferred option with regard to achieving the same level of detail in the simulation as when using the contemporary workflow. However, other options which would enable the Energyplus simulation to be prepared without the results of the Radiance analysis would be preferred with respect to the development of the next generation workflow.

Option 2: Run a minor simulation for the lighting schedule

This option proposes to run a minor simulation, with just a few analysis points inside the first Grass-hopper script to generate the lighting schedule. For the example case this minor simulation would include 4 test grid points, since it includes 4 sensor points, like explained in paragraph 3.3.3. The main disadvantage of this option however, is the increased amount of time to prepare the simulation. In addition, running the minor simulation within the Grasshopper environment would imply it is required to be executed on the main computer. This would undermine the philosophy behind the next generation workflow.

Option 3: Use options within Energyplus to generate the lighting schedule

Energyplus also offers native options to generate a lighting schedule based on a sensor. In the contemporary workflow this option is not used, because Radiance daylight simulations are proven to be significantly more accurate compared to daylight simulations conducted by Energyplus. In addition, Honeybee only allows to prepare a single lighting sensor per room. Since the example case used four lighting sensors, this option is not really feasible.

Option 4: Utilize the additional strings input

When Energyplus is used as a stand-alone software package, multiple lighting sensors can be assigned per room in more recent versions. This option is unfortunately not yet assessable via Honeybee natively. However, the core Grasshopper component for preparing the Energyplus simulations has an input named 'additional strings'. This input enables more experienced users to add instructions to the Energyplus simulation batch file which are not assessable via Honeybee. So the fourth option would be to make a custom component which feeds the information of multiple lighting sensors to the main Energyplus component. However, developing this custom component would take too much time in respect to the focus of this thesis.

Option 5: Wait for the Honeybee update

Since more recent versions of Energyplus support the use of multiple lighting sensors per room, it is very likely this option will be added in future releases of Honeybee. Waiting for this update would be an alternative to the previous option, but this will not solve the lighting schedule issue for this thesis. This can however be an interesting direction for future research.

Option 6: Do not include artificial lighting

Since the results generated using the contemporary workflow indicate the energy usage for lighting is very small compared to the need for cooling, it can be argued that for the example case artificial lighting can be removed from the calculation entirely. One notable implication is the disability to directly compare the results of the contemporary and next generation workflow, since the used model will be different. However, this difference is not relevant to the development of the next generation workflow and will therefore be the direction chosen for the continuation of this research.

3.7.3 - Analysis numbering (custom node)

Since one of the core features of the next generation workflow is to prepare multiple analyses and executing them in parallel, each evaluation needs to be saved as a unique file to prevent overwriting. The most straight forward approach is to append a number to each analysis and save them all in a main working directory. In order to do so, a custom python component was written. The purpose of this component is to identify the number of folders already present in the main working directory. This number will be increased by one and will serve as the input for generating the analysis files of the new design. The code of this custom component, as well as the integration in the Grasshopper script can be found in appendix III.

3.7.4 - Delocalizing the EPW-file

Another challenge in making the workflow cloud compatible is the dependence on the EPW weather files. Previously these files were saved locally, but this caused problems for enabling the cloud functions. In order to overcome this challenge, Honeybee offers an option to download the weather files when running the Grasshopper files. The downloaded files will be saved in the main working directory that was mentioned earlier as well. The Grasshopper definition for this automatic downloading of EPW files can be found in appendix III.

3.7.5 - Preparing the Energyplus simulation (custom node)

Like mentioned earlier, the concept of the next generation workflow is to prepare the batch files for the analysis and to execute them outside of the Grasshopper interface. For the visual comfort simulation, which is conducted by a combination of Radiance and Daysim this was fairly easy, because Honeybee natively offers an option to only write the files and not running them. For the thermal calculations based on Energyplus however, this introduced another challenge. Natively, Honeybee only offers options to prepare the Energyplus IDF file, which cannot be directly executed by windows itself. In order to convert this IDF file to a batch-file, a modification of a the "re-run IDF" Honeybee component was necessary. The altered part of the code and Grasshopper integration can be found in Appendix III.

3.7.6 - Suppressing the Grasshopper multi-save pop-up (custom node)

There is one more challenge to overcome using a custom node; the suppression of the Grasshopper multi-save pop-up. This is a built-in feature of Grasshopper, which serves as safety feature to prevent the loss of work when closing Grasshopper. Previously, in the contemporary workflow this was not an issue, because the 'keep alive option' was enabled. This option makes sure each design evaluation is conducted in the same instance of Grasshopper. However, in the next generation workflow, utilizing the keep alive option was not possible, because there are two Grasshopper nodes within the ModeFRONTIER workflow. As a result of disabling this option, Rhino and Grasshopper are restarted for each design evaluation, introducing the multi-save pop-up. This pop-up requires to be closed by clicking OK before being able to proceed, which is very unfeasible for the next generation workflow, as it prevents automatization. In order to overcome this challenge, a custom VB script was used in order to suppress the multi-save pop-up by manually switching the 'is-changed flag' using Rhinoceros API coding. The code and Grasshopper integration can be found in Appendix III.

3.7.7 - Updating the Grasshopper custom MyNode

As stated in the problem statement of this thesis, the integration of Grasshopper is not an integration node provided with standard modeFRONTIER installations, but only supported through a custom myNode. This custom node is developed by ESTECO, the company behind modeFRONTIER, especially for academic use at the TU Delft. Due to this reason, the custom Grasshopper myNode was not implemented to cover all the possible use cases. Prior to this research, the output of strings and matrices was not yet possible. Other options for transferring the string and matrix data between the nodes were possible, but not the most elegant solution. Fortunately, the developers of ESTECO were so kind to add these features to the custom Grasshopper myNode especially for this research.

3.7.8 - Finalizing the next generation workflow

In order to increase convenience in making the next generation workflow cloud compatible, the input for the analysis numbering method were taken to the ModeFRONTIER workflow instead of being defined within the first Grasshopper script. This will make it easier to change the main working directory, because the Grasshopper script does not have to be opened. In addition, the two Grasshopper scripts are loaded in two project file nodes. This will make sure the two scripts are embedded in the ModeFRONTIER projects. This increases convenience, because there is no more need to copy the Grasshopper scripts along with the ModeFRONTIER project when placed onto a cloud environment. Lastly, the DOS script within the workflow is simplified. Preliminary results indicated the output boolean value is not necessarily needed, because ModeFRONTIER natively waits for each node to be completed before advancing to the next node in line. Therefore, this part of the DOS script was removed, leaving only three lines of code which will execute each of the three batch files. These final steps complete ModeFRONTIER set-up of the next generation workflow (see figure 184).

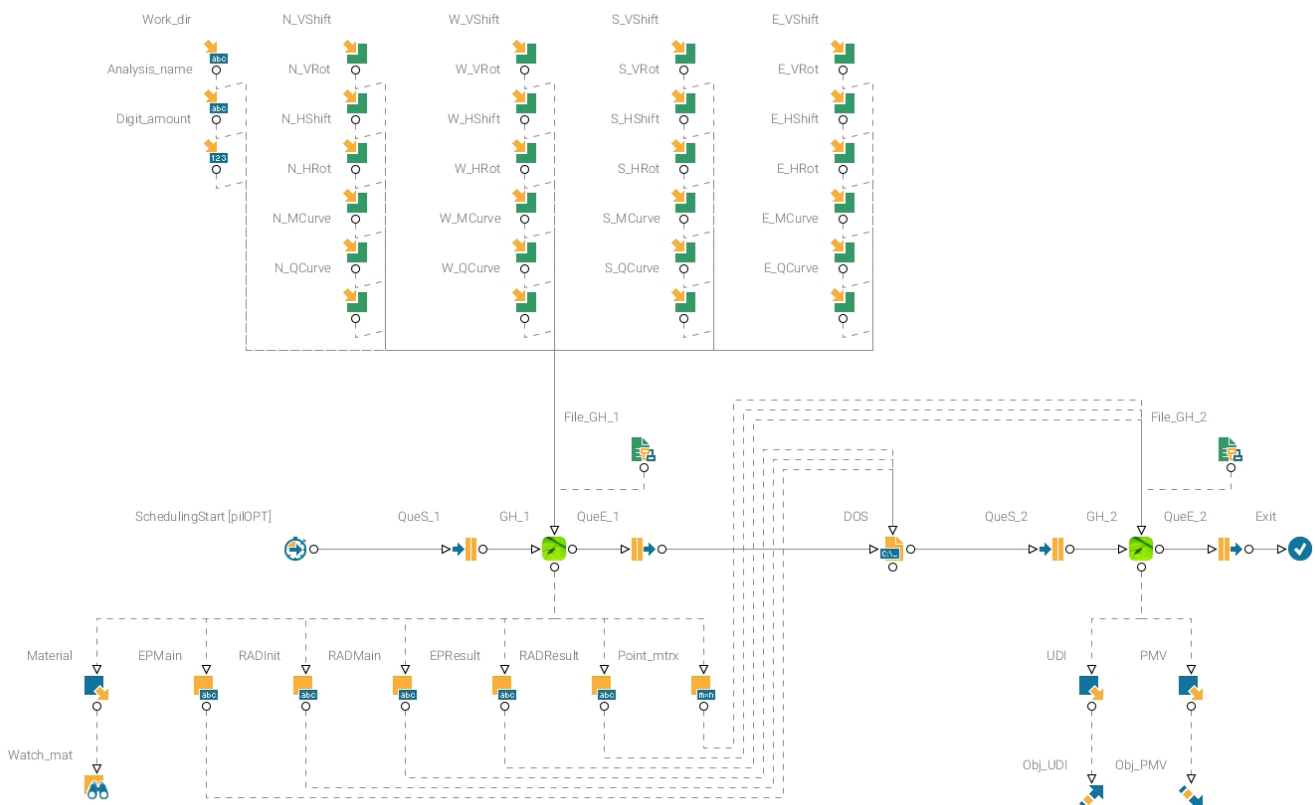


Figure 184. Finalized set-up of the next generation workflow (by author)

3.7.9 - Testing on the BK Renderfarm

The architecture faculty at the TU Delft is the proud owner of the BK Renderfarm. The farm was first set up in 2005 and is primarily used to serve as a solution for executing computational resource demanding rendering jobs externally. An internal article for the university about the BK Renderfarm written by Arno Freeke and Aytaç Balci (2018) describes the setup of the BK Renderfarm as cited below and the current hardware specifications are given in figure 185.

“The render farm consists of one master node and four render nodes. The master node distributes the render jobs over the four render nodes. With the current hardware there is a lot of computing/rendering power at our disposal. For optimal use of the available computing power, each render node is divided into several ‘instances’.” (Freeke & Balci, 2018)

In the final phase of this research, multiple tests with the next generation workflow were conducted on the BK Renderfarm under supervision of Aytaç Balci, one of the responsible staff members within the university for the BK Renderfarm. The first tests showed promising results, as the BK Renderfarm was able to execute the visual and thermal comfort simulations in parallel on different instances while executing the Grasshopper nodes in series on a single instance. For conducting the tests, the number of concurrent processes was set to four, sending one simulation each to four of the six available instances in the BK Renderfarm. In further research, this number can be increased to test the computational limits of the BK Renderfarm. The number of concurrent processes for the Grasshopper MyNodes and the Queue nodes is set to one, like explained earlier. The amount of concurrent processes for the overall run and DOS script can be set in the dedicated preference options (see fig. 186 and 187). Control over the amount of concurrent processes distributed over the grid is found in the Volta player (see fig. 188). In the context of the next generation workflow, it is advised to keep these numbers of concurrent processes equal in each of the preference option menus.

Node	Cores	Instances	CPU	Speed	Memory	Year of purchase
1	20	5	dual 10-core Xeon E5-2680v2	2.8 GHz	64 GB	2013
2	24	6	dual 12-core Xeon E5-2680v3	2.5 GHz	128GB	2014
3	24	6	dual 12-core Xeon E5-2680v3	2.5 GHz	128GB	2015
4	28	7	dual 14-core Xeon E5-2680v4	2.4 GHz	128GB	2016

Figure 185. *Current hardware setup TU Delft Architecture BK Renderfarm (internal publication by Freeke & Balci (2018))*

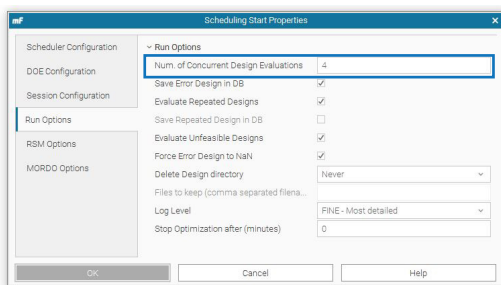


Figure 186. *Number of concurrent processes Scheduler node (by author)*

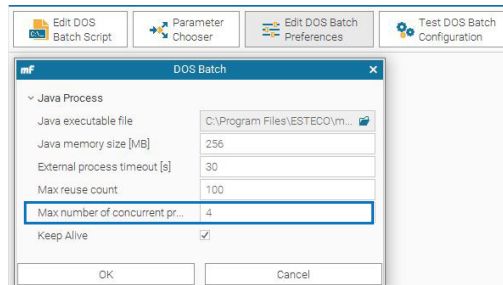


Figure 187. *Number of concurrent processes DOS node (by author)*

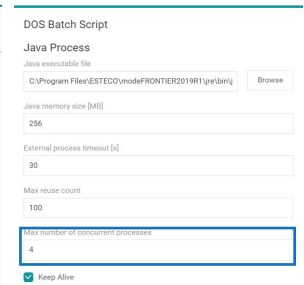


Figure 188. *Number of concurrent processes Volta player (by author)*

Unfortunately, due to restrictions in use of the BK Renderfarm for running ModeFRONTIER projects and nearing final deadlines for this research, it was not possible to run the complete optimisation for the example case on the BK Renderfarm using the next generation workflow. However, the first tests proved that the BK Renderfarm is able to theoretically execute a relatively large number of multiple visual and thermal simulations in parallel when using the next generation workflow. Since this was not possible before all developments discussed previously in this chapter, it will drastically reduce the time needed to complete the optimisation phase of the PCA framework. Using a render farm environment in conjunction with the next generation workflow will be a very interesting direction for further research.

All knowledge generated during this research has been passed on the university staff members in charge of the BK Renderfarm. They will continue to run tests on the BK Renderfarm using the next generation workflow, so that hopefully future research and projects are able to utilize the computational power of the BK Renderfarm.

3.7.10 - Testing in the VR lab

In addition to the tests on the BK Renderfarm, there were test conducted on the computers in the VR lab as well. This are the same machines used for generating the results based on the contemporary workflow discussed earlier in this research. In total, four different computers where used to conduct the tests. Based on the individual specifications, an appropriate number of concurrent processes was set. A higher number will result in overloading the CPU at a constant utilisation of 100%. This will slow down the computer, and will make the system unstable when ModeFRONTIER opens a Rhinoceros/Grasshopper session to prepare the simulation or interpret the results for a new design. This action causes a spike in CPU load, which can not be handled by a processor which is already overloaded. Based on preliminary tests, the CPU load should be around 70% when steadily running the Radiance and Energyplus simulations in order to process the spikes caused by starting a Rhino/Grasshopper session. An overview of the hardware specifications of the used VR-lab computers and the predetermined number of concurrent processes is given below.

	<i>Cores</i>	<i>Memory</i>	<i>Number of concurrent processes</i>
Computer 1:	8 @ 3.4 Ghz	8 Gb	10
Computer 2:	6 @ 3.3 Ghz	16 Gb	8
Computer 3:	4 @ 4,0 Ghz	8 Gb	6
Computer 4:	4 @ 4,0 Ghz	8 Gb	4

In order to assess to what extend the next generation workflow is capable of overcoming the identified challenges in chapter 3.6, the projects on the four VR-lab computers where left running for approximately 72 hours; the same amount of time as the optimisations using the contemporary workflow in chapter 3.4. The results of these optimisation runs will be evaluated in the next chapter.

3.8 - Analysing the next generation workflow

3.8.1 - Comparing the feasibility to the conventional workflow

The tests in the VR lab were left running during a weekend, but unfortunately none of the four managed to keep running the entire 72 hours. The second computer failed to stay powered on for the entire weekend, causing these results to be lost. The other three failed due to different errors related to Rhino/Grasshopper. These errors come in the form of a pop-up which requires user input to be closed. Due to these error pop-ups the entire optimisation process comes to a stall and will not continue evaluating designs. The first computer stalled on a generic Rhino error report (see figure 189). The third computer failed due to 'expired Honeybee components' in the Grasshopper script. This resulted in an error pop-up for each of the components present on the Grasshopper canvas. Figure 191 shows a few of these error pop-ups, but all included the same message. The fourth computer stalled on an error produced by an exception in the python script used by ModeFRONTIER to open a new Grasshopper session (see figure 190).

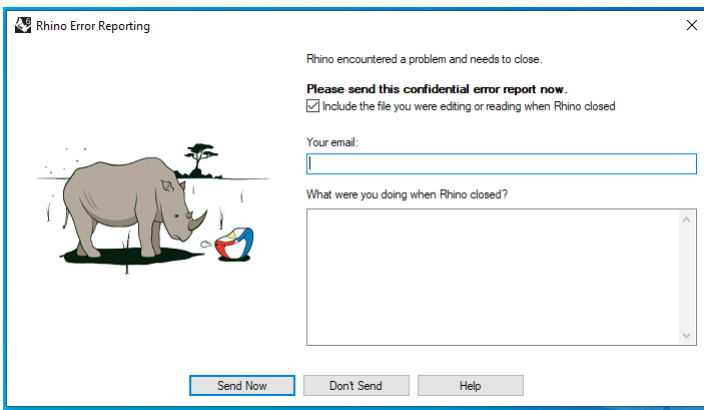
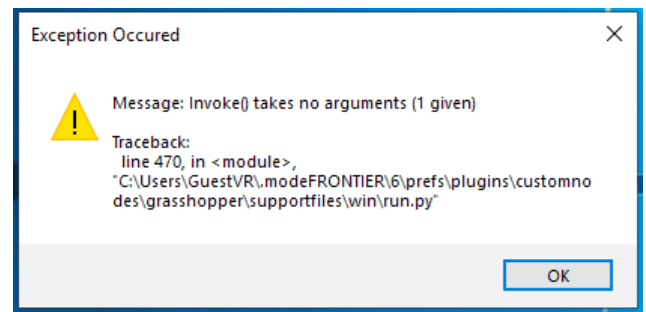


Figure 189. Error pop-up computer 1 (by author)



The most important property on which the feasibility can be compared to the contemporary workflow is the amount of calculations over time. Even though there are some slight differences between the simulations conducted using each of the two workflows, like the lighting schedule discussed in paragraph 3.7.2 and the changes in input parameters discussed in paragraph 3.4.7, the time required per simulation is relatively equal. The difference in total calculation time needed is grounded in the ability to run multiple processes in parallel. The reference for the contemporary workflow will be the optimisation for the climate of Abu Dhabi, since this one has the most evaluations; a total of 261 in a time spawn of 72 hours. Even though the optimisation using the next generation workflow did not manage to keep running for the complete 72 hours, the evaluations over time can be calculated based on the amount of time the computer manager to stay on (see the table below). Based on the test optimisation in the VR-lab and the calculated evaluations per hour it can be stated that the next generation workflow is capable of generating data about 2.5 to 3 times faster compared to the contemporary workflow.

	<i>Total running time</i>	<i>Total evaluations</i>	<i>Evaluations / hour</i>
Contemporary workflow (Ran on PC 2)	72:00 h	261	3.6
Next generation PC 1	05:00 h	46	9.2
Next generation PC 2	02:40 h	36	13.5
Next generation PC 3	01:10 h	6	5.1
Next generation PC 4	09:30 h	86	9.1

3.8.2 - Comparing the results to the conventional workflow

The main challenge within analyzing the contemporary workflow was the lack of data. This caused the Pareto front to not properly form. Even though the next generation workflow has proven do be significantly faster than the contemporary workflow, it is also less stable, resulting once again in a lack of data. Unfortunately, time restrictions regarding this research prevented to rerun the optimisation and generate more data. Nevertheless, the results of the two workflows can be compared. There is however one main difference; the choice of algorithm. In the optimisations using the contemporary workflow, the PilOpt algorithm was used in combination with a Uniform Latin Hypercube DOE of 50. In the optimisation using the next generation workflow, the PilOpt algorithm was used in self-initializing mode, because research of fellow graduate students indicated the Pareto front will form more quickly using this setting. For the comparison the results of computer 4 are used, because these include the most evaluations, a total of 86. The Pareto front graph is given in figure 192, but the Pareto front has not formed yet. Since this is the case, it does not make sense to apply the other post-processing analysis techniques to these results. The distribution of PMV and UDI scores seems very similar to the simulations ran using the contemporary workflow, validating that the individual simulations are ran correctly using the next generation workflow as well.

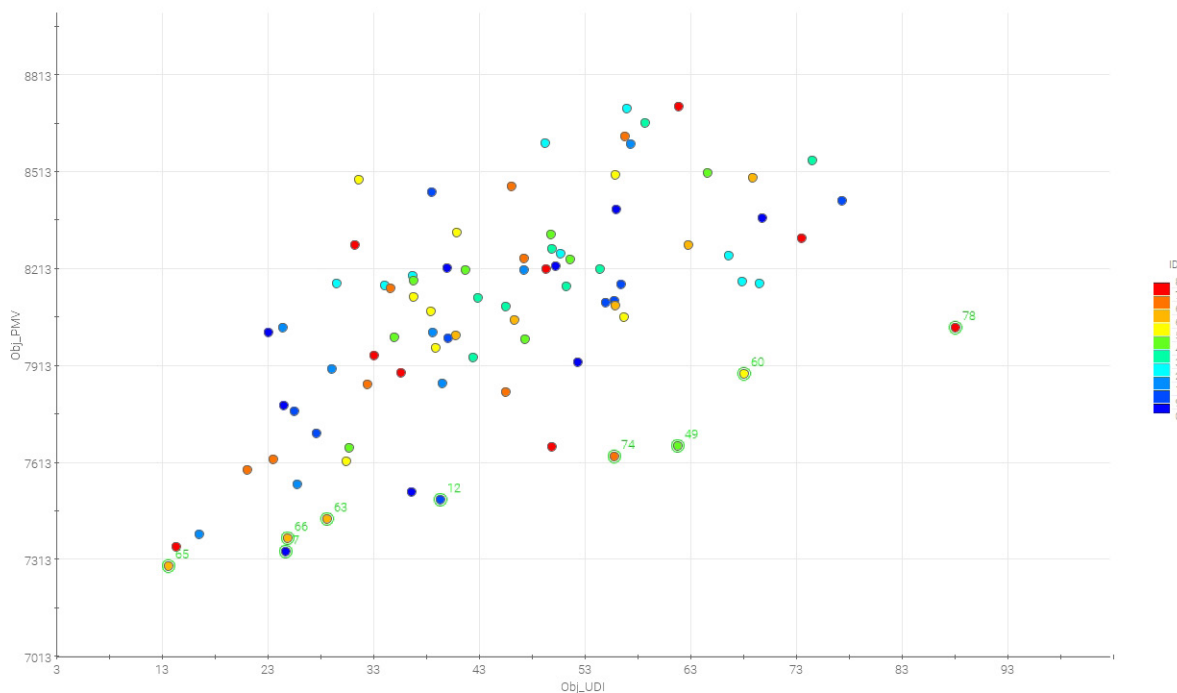


Figure 192. Pareto front results of the next generation workflow on PC 4, containing 86 design evaluations (by author)

3.8.3 - Conclusions on the next generation workflow

The most important conclusion regarding the next generation workflow is the fact the designs can be evaluated faster, but the workflow is not yet fully stable. This is due to some random errors, caused by Rhino/Grasshopper and Ladybug/Honeybee. During the testing in the VR-lab this was unanticipated for, because these errors did not show up in preliminary tests containing just a few evaluations, which were used to test the concept of the next generation workflow. As a result, all conducted tests failed to continue running over the weekend, as the errors mentioned earlier require user input for the process to continue. So, when the process is left to run for a longer period without supervision, this will stall the optimisation process.

At this point the hypothesis is these errors are produced when both Grasshopper scripts are opened simultaneously. This behaviour is expected in the workflow and ModeFRONTIER functioned correctly, as the queue nodes only control the portion of workflow in between the queue start and end node. This means there are no elements in the workflow preventing the first and second Grasshopper custom myNodes from starting a Grasshopper instance for different design evaluations simultaneously. Since the plug-ins of Ladybug and Honeybee are not intended to operate in multiple Grasshopper instances simultaneously, this still forms a challenge for the next generation workflow. The next two paragraphs will discuss a workaround and conceptual solutions for this challenge.

There is an option in ModeFRONTIER which could serve as a workaround for this problem; the timeout function (see fig. 193). This option controls the maximum amount of time a node is allowed to run before the process will be terminated. This will result in generating one failed design, but will ensure the ModeFRONTIER optimisation run will continue afterwards. However, in order to verify whether the timeout option will work as intended for the next generation workflow, further research is needed.

At this moment, no definitive solution was found to prevent both Grasshopper custom myNodes from starting a Grasshopper instance simultaneously. In terms of conceptual solutions, two directions would be desirable. The first being an option to limit the global option for the number of concurrent processes conducted by external software. Such an option could be used to limit the global amount of Grasshopper instances to only one. The second conceptual solution would be some sort of link between the queue nodes would be desired solutions. This link should prevent ModeFRONTIER from starting a Grasshopper script, while the other Grasshopper node is active (see fig. 194).

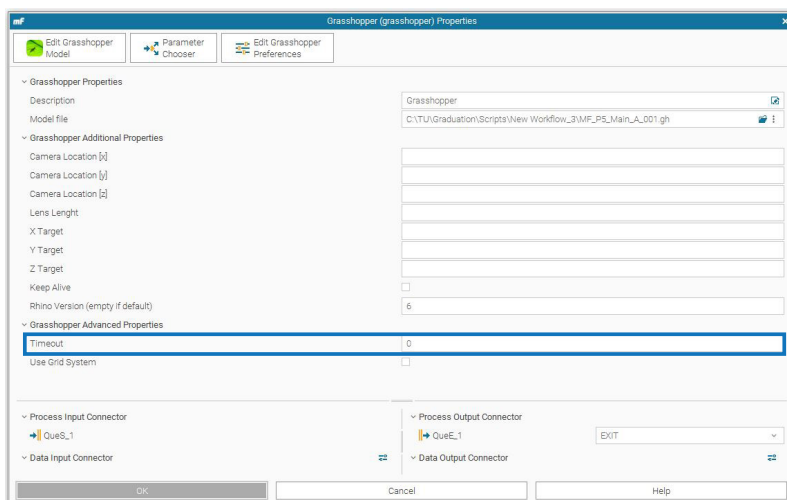


Figure 193. *The timeout option for the Grasshopper node (by author)*

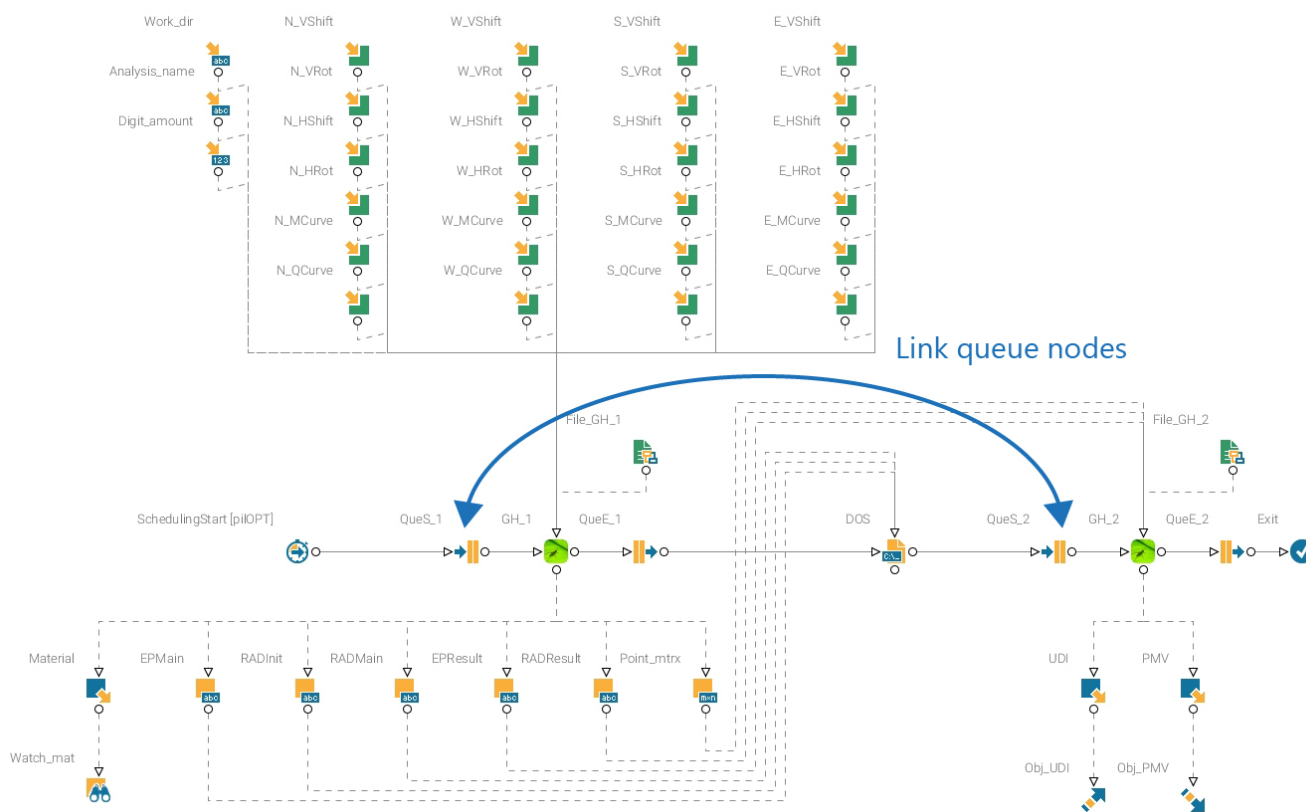


Figure 194. *Interlinking the queue nodes (by author)*

3.9 - Automated physical models

3.9.1 - Automatized workflow

The optimisation results in a set of optimal solutions, making up the Pareto-front. The final step within the PCA process, making the final assessment, allows for human interpretation. The choice for the desirable solution out of the optimal solutions can be made based upon the performance metrics. However, since the process is related to an architectural project, aesthetic quality of the solutions can be used in the assessment process as well. One common tool for assessing the aesthetic quality is by making physical models. Since 3D models of the solution are already present due to the nature of the form-finding phase, this can serve as a direct input for creating physical model using an automated methodology.

Developing this methodology is a reversed engineering process, starting with selecting the proper manufacturing technique. Since the geometry is made up of 2D elements, but includes lots of unique curvature, the technique chosen for this research is wood laser cutting. This technique requires 2D vector files, which will serve as cutting paths for the machine. These files can be generated automatically by Grasshopper. Since this research is conducted at the TU Delft, the files are generated according to the requirements of the faculty's laser cutting machines. These machines require a DWG file with the outlines for the wooden plate included. This paragraph will continue describing the automatized workflow.

Step 1

The first step in generating the DWG files is generating the wood surface outline based upon the standard available sizes. In case of a 1:10 scale model, a plate of 600x300 will be sufficient.

Step 2

Next are the intersection cut-outs for the shading elements will be generated. The width of the cut-out is based on the material thickness and the angle between the shading elements.

Step 3

The next step involves the connections with the side panels of the double skin façade. These are made by introducing a new cutting-box, accounting for the material thickness of the geometry side panels, but leaving a left-over width for the connections.

Step 4

After generating the connections on the shading elements, the holes in the side panels can be generated by projecting the intersecting geometry onto the plane of the side panels.

Step 5

In this step, all geometry is 3D rotated in order to align to the world XY plane.

Step 6

After 3D rotation, all geometry is placed on the world XY plane in order to fit the wood surface outline.

Step 7

In order to simplify the process of assembling the physical model after last cutting, marking are added to the geometry. These marking contain either the letter H (for horizontal element) or V (for vertical element) and a number. The markings will be engraved into the wood and use a special single line font which is intended for engraving purposes.

Step 8

This step involves deleting overlapping line parts, so the laser cutter can do the job as efficient as possible.

Step 9

After checking for overlapping lines, all geometry can be baked into layers. The names and colours of the layers correspond with the file requirements for the laser cutters at the architecture faculty of the TU Delft.

Step 10

The final step is to export the file as a DWG file and send it to the laser cutter. When finished, the physical model can be assembled by hand, resulting in model like shown in the next paragraph.

3.9.2 - Physical test models

These are two of the physical models created during the research. They were made to assess the aesthetics of two different cut-off shapes. Since the research is more aimed towards the methodology of the next generation workflow, the models were not used for the final assessment like shown in the methodology scheme in paragraph 1.6. However, when the PCA methodology would be applied in practice, this automated physical model workflow might be valuable to the designers to assess differences in aesthetic quality in this phase of the project as well.



Figure 195. *Frontside photographs of the two physical models (by author)*



Figure 196. *Backside photographs of the two physical models and connection detail photograph (by author)*

3.9.3 - Relation to the commercial design process

The primary goal of this automated physical model workflow is to serve the final assessment of selecting the desirable solution from the Pareto front. Over the past few decades, many architecture offices have invested in new modelling production techniques such as 3D printers, foam carvers and laser cutting machines. This allows them to produce architectural scale models faster, resulting in a more efficient business model. Implementing a production script in the PCA process is in line with this trend, further increasing the overall value of the PCA process for contemporary architecture offices.

Secondary, the physical models can also serve a role in assessing the aesthetic quality of shading geometry. This quality is obtained in the parametrization of the shading geometry within the form-finding phase of the PCA process. The ability to make preliminary scale models, enables the designer to assess the aesthetic quality or spot possible challenges and change the parametric set-up of the shading geometry according to the findings.

Thirdly, the methodology developed for making the physical models can serve as a starting point for the production process. Since the shading of the example case contains lots of unique geometry, the technique of laser cutting might be feasible to use for the actual production process as well. When this methodology is further developed, it offers an opportunity to automatically produce the input drawings for the actual production laser cutter machines, resulting in a time-efficient production process.

3.10 - Automated VR rendering

3.10.1 - Automatized workflow

Another methodology for aiding the final assessment is the automatized production of VR renderings. The exact workflow for producing these VR rendering is open to interpretation, but the workflow used for this research will be elaborated below.

There are many software solutions for producing renderings. Rhinoceros even offers built-in rendering capabilities. However, the workflow used in the research is based on a connection with Autodesk Revit. This software is used in the architectural field for creating building information models (BIM) and has become the standard for the industry over the last few decades. Revit offers a built-in tool for parametric modeling; Dynamo. Dynamo offers functions to import geometry into Revit and assign materials. This will be used to directly import the shading geometry from Grasshopper into Revit.

In contrast to other rendering solutions, Autodesk offers the ability to use their cloud for producing and storing renderings. The connection to the cloud is fully integrated in Revit and offers used to send a view for rendering relatively easily. After completing the ray-tracing calculations, the rendered image is stored on the cloud and can be downloaded or linked via a QR-code. When working with VR rendering, the storage section of the cloud offers a built-in viewer. If people where to scan the QR-code using their phone, they can view the VR rendering by rotating their phone or placing it in a set of VR-glasses.

Step 1

The first step is to collect all shading and building geometry in Grasshopper and properly name/sort them for exporting.

Step 2

The next step is importing the geometry to Revit via Dynamo. The methodology for this is based on the Dynamo plug-in Rhynamo, which features a direct link between an open Rhinoceros file and the Dynamo file. This way, baking the shading and façade geometry in Grasshopper will result in a direct transfer of the geometry to Dynamo.

Step 3

Dynamo is used to assign materials to the geometry. The materials themselves can be created using the regular Revit material editor.

Step 4

This step only has to be taken once, and can be skipped every new iteration of the VR rendering workflow. Standard Revit modelling techniques are used to recreate office interior, by placing furniture, equipment, people, etc. The goal is to create a Revit model in which only the shading itself has to be replaced in order to quickly compare different designs of the Pareto front. The level of detail of this model is depending on the designer and materials can be assigned using standard Revit modelling techniques.

Step 5

The next step is to use Dynamo to place the shading geometry in a 'design options', an entity in Revit intended for this purpose.

Step 6

The next step is to set an appropriate view for the VR render to be made. The direction of the view is irrelevant, since a 360-degree image will be rendered.

Step 7

This step involves sending the render scene to the Autodesk cloud. Before sending the scene, a resolution and other settings have to be supplied. It is advised to first to first run a free Draft rendering before uploading the final version in high-resolution. These final versions in high resolution may a relatively small payment.

Step 8

After waiting for the rendering to be completed, is image can be downloaded from the cloud or be viewed on any device by scanning the QR-code. This enables the designer to experience the shading design in virtual reality.

Step 9

The final step in the VR rendering workflow is the post processing. This step in not necessary within the design process, but might be valuable for preparing the final renders for a presentation. In the case of the VR renders for the example case sun shading, post processing is done by adding a high resolution photograph of a high-rise skyline into the render to give the impression of a building surrounding.

3.10.2 - VR renderings

This paragraph shows the still image render versions of the VR renders as well as the flat box image that represents the VR render when opened in a proper viewer. In addition, the QR codes for viewing the non-postprocessed VR rendering directly in the Autodesk storage cloud are given as well. Due to the limited storage time allowed on the Autodesk cloud, these QR links may become invalid over time.



Figure 197. *Day-time VR render flat box image & QR code for non-post-processed VR rendering (by author)*



Figure 198. *Night-time VR render flat box image & QR code for non-post-processed VR rendering (by author)*



Figure 199. *Still image version of day-time VR rendering (by author)*



Figure 200. *Still image version of night-time VR rendering (by author)*

3.10.3 - Relation to the commercial design process

Over the recent years, many commercial architectural offices have invested in VR technology, enabling them to use VR as a powerful presentation technique. However, this methodology allows to quickly make VR renderings during the design process as well and use the VR rendering as a tool for assessing the architectural quality of the optimisation results. A big advantage of the described workflow is the elimination of the need for special equipment. Since the cloud is used to produce the renderings, no high-end computers are needed. In addition, the cloud storage with integrated viewer and the QR-code system allows to easily view the renderings on mobile phones instead of dedicated VR glasses.

4. Conclusions





4.1 - Literature review conclusions

This chapter will briefly summarize and conclude on all the matter discussed previously according to the answered research questions stated in the introduction.

4.1.1 - Conclusions on visual comfort

Q1: How is visual comfort defined?

Visual comfort is defined as a “subjective condition of visual well-being induced by the luminous environment” (CEN, 2018, p.9). Due to its subjective nature visual comfort is hard to quantify and impossible to quantify in a single number, visual comfort will always be described using multiple quantities. (Carlucci, 2015)

Q2: What factors are responsible for the level of visual comfort?

The four main contributing factors are as following (Carlucci, 2015):

1. The amount of light
2. The uniformity of light
3. The quality of light in rendering colors
4. The prediction of the risk of glare for occupants

Q3: How can visual comfort be calculated?

One calculation method by Dubois (2001) is based on various international standards (AFNOR, 1990; ISO, 2000; IES, 1993; CIE, 1986; CIBSE, 1994; NUTEK, 1994). This method focuses especially on the first two contributing factors; the amount and uniformity of light, as they are normative for the perceived visual comfort. The method by Dubois (2001) describes 5 performance indicators and suited requirements for an office building: daylight factor, work plane illuminance, illuminance uniformity, absolute luminance and luminance ratios.

International European calculation methods and requirements can be found in NEN-EN-12665. (CEN, 2018)

Q4: How are visual comfort related to shading systems?

Sun shading is primarily needed to reduce glare. The most common source for this glare is the direct sun light. Shading can be used to block this direct light for the occupant, improving the level of visual comfort regarding glare. The secondary goal of the shading is to allow indirect daylight to enter the room in order to keep absolute illuminance levels within the requirement boundaries as well. The absolute illumination levels are needed as well to experience visual comfort while executing tasks

4.1.2 - Conclusions on thermal comfort

Q1: How is thermal comfort defined?

Thermal comfort is defined as “that condition of mind which expresses satisfaction with the thermal environment” (ISO, 2005). This condition of mind is influenced by various aspects, including physiological, psychological, medical, climatological and engineering aspects. (Carlucci, 2013)

Q2: What factors are responsible for the level of thermal comfort?

A commonly used index for thermal comfort is the PMV index. This index is based on six contributing factors:

1. Clothing
2. Activity
3. Air temperature
4. Mean radiant temperature (MRT)
5. Air velocity
6. Humidity

Q3: How can thermal comfort be calculated?

According to CEN standard NEN-EN-15251 (CEN, 2007), the PMV and PPD indices should be used for calculating thermal comfort in HVAC controlled building and the adaptive comfort index for naturally ventilated buildings. All three indexes can be calculated using various formula's given in International standard NEN-EN-ISO-7730 (ISO, 2005). Another method is by using the CBE thermal comfort tool by Tyler et al. (2017). This tool is based on the same formula's and can be used to calculate thermal comfort and compare it to the requirements of NEN-EN-15251 or ASHRAE 55

Q4: How are thermal comfort related to shading systems?

A prominent contributing factor to thermal comfort is the mean radiant temperature. This quantity is influenced by the sun as a result of solar gain. The radiation energy from the sun will heat up the room, which can result in overheating, causing thermal discomfort. Sun shading can be used to partly block this solar radiation from entering the room and thereby controlling the amount of solar gain and influencing the level of thermal comfort.

4.1.3 - Conclusions on performative computational architecture

Q5: What are the principles of the performative computational architecture method?

The principle of performative computational architecture is based on a three-phase cycle which is iteratively looped until the best solution is found. The three phases are as following: (Ekici et al., 2019)

1. The form-finding phase; generating geometry using a parametric approach
2. The performance evaluation phase; a digital simulation evaluating the performance of the geometry
3. The optimization phase; using a search method to find the best configuration of input parameters based on their performance criteria.

Q6: How can the form-finding phase of the performative computational architecture method be used to design sun shading systems?

Parametric modelling can be used to generate geometry, based on parameters. (Barrios, 2005). These parameters define certain key values describing the geometrical shape. Since sun shading consists of geometrical shapes, parametric modelling can be used for this application as well. All geometry generated by the parametric script is derived from these input parameters using mathematical alterations, often implemented by using some kind of scripting or coding. This way, altering the input parameters influences the geometry, allowing to relatively quickly explore design alternatives. Commonly used software for the form-finding phase is Grasshopper.

Q7: How can the performance evaluation phase of the performative computational architecture method be used to design sun shading systems?

Performance evaluation can be used to determine the performance of the geometry generated in the form-finding phase, using a digital simulation. For designing solar shading, this means the visual and thermal comfort can be simulated. This will determine the feasibility of a design alternative. Commonly used software is Ladybug & Honeybee, two plug-ins for Grasshopper. The software mimics a physical test set-up as illustrated by Dubois (2001), simulates the visual comfort using Radiance/Daysim and simulates thermal comfort using Energyplus/Open studio.

Q8: How can the optimization phase of the performative computational architecture method be used to design sun shading systems?

The optimization phase uses a search method to find the best set of input parameters based on the performance evaluation. This is done using (evolutionary) search algorithms. Since designing sun shading often involves a multi-objective optimization, the algorithm of choice is the NSGA-II method. (Ekici et al., 2019). Commonly used software to execute these search algorithms are Octopus, another plug-in for Grasshopper, and ModeFRONTIER, a stand-alone software solution dedicated to evolutionary optimization.

4.1.4 - Conclusions on sun shading in contemporary high-rise

Q9: What is the relevance of sun shading in contemporary high-rise buildings?

A common building type of contemporary architecture is the high-rise office building with an all-glass exterior. (Chow & Lin, 2010; Nicholson-Cole, 2016; MacErlean, 2018; CTBUH, 2019). However, buildings with all-glass exteriors are at increased risk to visual and thermal discomfort and a well-designed sun shading system is essential to increase the levels of visual and thermal comfort. (Evola, Gullo, & Marletta, 2017).

Q10: What are the technical requirements for sun shading systems in high rise office buildings with all-glass exteriors?

The seven standard requirements for sun shading are given in the list below: (Kuhn, Bühler and Platzer, 2001).

1. Thermal comfort
2. Visual comfort
3. Low costs
4. High reliability
5. Aesthetic requirements
6. Compliance with technical boundary conditions
7. Protection against fire, noise, weather and burglary

The scope of high-rise buildings introduces two requirements within the technical boundary category; the resistance to the effects of windload and the access aspects for façade maintenance. The all-glass exterior introduces a requirement within the aesthetic requirements category; the unfeasibility of external shading elements. Since high-rise office buildings are often built with double skin facades, the shading could be integrated in between the two glazing panes as well. However, the ventilation capacities of the double skin façade should not be obstructed. Additional requirements for the office function regarding visual and thermal comfort can be found in the international standards NEN-EN-12464, NEN-EN-ISO-7730 and NEN-EN-15251.

Q11: How does the local climate influence sun shading design in contemporary high-rise office buildings with all-glass exteriors?

The local climate influences the sun shading strategy because in locations with a hot climate, solar radiation is undesirable the entire year, while in regions with more temperate climates, solar radiation is often desirable in winter time, but undesirable in summer time. (O'Brien et al., 2013; Al-Obaidi et al., 2016).

In the tropic climate, sun shading is especially relevant, because as a result of relatively high levels of solar radiation, overheating and glare can become serious risks in this region. (Al-Tamimi & Fadzil, 2011).

Q12: How can PCA be used to improve sun shading systems in contemporary high-rise office buildings in extreme climates with all-glass exteriors?

Many studies have been conducted to research the application of PCA methods in architectural design. The applications for sun shading have been proven. (Ekici et al., 2019; Eltaweel and Yuehong, 2017). However, the application for sun shading for contemporary high-rise office buildings in tropical climates is less researched. Multiple studies concluded using PCA is a promising direction for the future of sun shading design, but more research is needed for designing sun shading systems in this specific situation. (Eltaweel and Yuehong, 2017; Evola, Gullo, & Marletta, 2017; Al-Masrani et al., 2018)

4.1.5 - Conclusions on the state of the art: PCA use in sun shading design

Q13: What projects have been important to the development of PCA methods for designing sun shading?

Over the past few decades, many projects have been important for the development of the PCA process. One of the available sources for an overview projects involving the PCA method is the literature review of Ekici et al. (2019). From this overview, six researches involved shading design. Among others, these six researches can be regarded important, because they gain insight in the development of the state of the art of applying the PCA method for sun shading design.

Q14: How would PCA methods for designing sun shading be categorized based on typology?

Based on the literature review and case studies, a new typology categorization was developed. This categorization defined 5 typologies on which the PCA methods can be grouped;

1. Number of objectives; single objective, multi-objective & many objective
2. Type of objectives; direct physical quantities, comfort metrics & energy usage
3. Type of set-up; single room, section/floor, entire building & urban scale
4. Type of tool combination; all integrated, plug-in depending & model depending
5. Type of geometry; shading only, building envelope & fully integrated

4.1.6 - Conclusions on the state of the art: Sun shading design in high-rise

Q15: What projects have been important to the development of sun shading in contemporary high-rise office buildings in extreme climates?

Over the past few decades, many projects have been important for the development of shading systems meeting the requirements of contemporary high-rise buildings in extreme climates. One of the available sources for an overview of projects involving sun shading design for high-rise buildings is the literature review of Al-Masrani et al. (2018). From this overview, 17 researches fitted the scope of this research. Among others, these can be regarded important, because they gain insight in the current state of the art on sun shading design for contemporary high-rise builds in extreme climates. In addition, some of these case studies compared shading systems on performance.

Q16: How would designs for sun shading in contemporary high-rise office buildings in extreme climates be categorized based on typology?

Sun shading designs can be categorized according to their energy involvement and the placement. Another typology categorization, proposed by Raji (2018), defines some common typologies of sun shading found in high-rise buildings, which can all be categorized according to their energy involvement and placement as well.

For energy involvement, the categorization of Al-Masrani et al. (2018) defined the following typologies:

1. Passive; fixed systems & manually adjustable systems
2. Active; mechanical systems
3. Hybrid; biomimetic systems

For the placement, three typologies can be defined:

1. Exterior shading
2. Interior shading
3. Glazing integrated shading

4.2 - Practical research conclusions

4.2.1 - Conclusions on the example case

Q17: Can the performance on visual and thermal comfort of current state-of-the-art sun shading systems with potential for high-rise office buildings be improved using the common contemporary PCA workflow?

There are many available sun shading systems for high-rise office buildings with all glass facades. Based on findings in literature and case studies, one of the standard available systems with potential has been selected for further research; the egg-crate system. This system can be categorised based on the defined sun shading typologies as following:

Energy involvement: Passive, fixed

Based on the limited annual differences in solar radiation and outdoor temperatures, and the implications of the large scale of the high-rise building, a passive, fixed shading system shows potential for a feasible system.

Placement: Integrated shading

Since exterior shading was not preferred due the scope of the all-glass exterior, and the limited performance of interior shading on overheating prevention, a façade integrated solution seems to show most potential. Hence the integrating of the egg-crate inside a double skin cavity.

High-rise shading strategy: Double skin integrated fixed shading

Although this typology is more common in combination with dynamic shading, integration of a fixed shading system shows potential due to the effects of the tropic climate.

In order to assess whether the PCA methodology can be used to improve the performance of this system, one workflow with increased potential was selected; the contemporary PCA workflow. This specific workflow, applied to the example case can be defined by the developed typology categorization as following:

Number of objectives: Multi-objective

In order to asses performance on thermal and visual performance, two objectives where used.

Type of objectives: Comfort metrics

The objectives regard the minimization of the annual exceeding of the PMV comfort domain and the maximization of the UDI mod-75 metric.

Type of set-up: Section/floor

A contemporary trend in high-rise office buildings is the open office landscape floorplan typology. Based on the absence of interspace subdivisions, such as interior walls, and the vertical repetition among floors found within this type of office high-rise buildings, a test set-up for an entire floor was used. As an example, an oval floorplan was used for this research.

Type of tool combination: Model-dependent

Based on findings in literature and precedences, Grasshopper was selected for the form-finding phase and the combination of Radiance and Energyplus (via Ladybug and Honeybee) for the performance evaluation phase. Based on the advantages for post-processing and analysing optimisation results, ModeFRONTIER was selected for the optimisation phase. This combination of tools, with ModeFRONTIER as the main interface, is defined as a model-dependent workflow.

Type of geometry: only shading

Since this research is scoped on the sun shading explicitly, only the shading geometry itself is parametrized in the form-finding phase.

Research has shown that the contemporary PCA workflow, in regard to sun shading design, is capable of assessing the performance on thermal and visual comfort. Results have shown that this workflow is also capable of improving the performance when compared to other available shading systems. However, whether this workflow is also capable of finding the optimal performance for this sun shading typology is yet unclear due to insufficient data. In order to generate a proper amount of data, an unfeasible amount of calculation time is required.

Q18: How does the possibly improved sun shading system perform in comparison to currently available systems for high-rise office buildings with all glass facades?

For this comparison two reference facades without sun shading and three alternatives were compared, which are defined as following:

- Reference 1: Single façade
- Reference 2: Empty double skin
- Alternative A: Solar reflective glazing
- Alternative B: Dynamic shading
- Alternative C: Default egg-crate

Comparison showed that the eggcrate performs best for all three climates. Due to the lack of data, no actual optimized shading systems can be compared yet. However, some conclusions can be made based on the available data. The optimization with most evaluations, for the climate of Abu Dhabi, implied a Pareto-front was forming. The available dataset supplied one design that stood out and did indeed perform better on both objectives in regard to the default egg-crate. For the climate of Singapore the results did not include a design performance better than the default eggcrate alternative, and for Brisbane the results only included designs improving performance on one of the objectives.

Q19: How do the possibly improved sun shading system perform for different façade orientations of the building envelope?

Based on the test set-up, which includes an open office floorplan layout and an ellipse-shaped perimeter, the interpolation principle was developed. This allowed for each orientation to have different sun shading geometry. The geometry of the optimized egg-crate shading system showed that the shading system is more closed on orientations with more solar radiation (East and west for Singapore, South for Abu Dhabi and North for Brisbane). This indicates the shading system will perform differently for each façade orientation, based on the annual solar path of the specific location.

Q20: How do the possibly improved sun shading system perform in various tropic climates around the world?

This research is scoped on the tropic climate, but in reality this includes a group of different climates. Based on the climate classification map (1980-2016) of Köppen-Geiger, three different climates have been selected for comparison.

Singapore: The tropical rainforest climate
Abu Dhabi: Hot desert climate
Brisbane: Humid sub-tropical climate

Based on the results, it can be stated the optimized egg-crate sun shading system does perform similar in these climates when compared to alternative systems. The geometry of the shading is very different. In Brisbane, the orientation with most radiation is very closed and others very open, whereas the other two show a more even distribution. However, since the optimizations lack sufficient data, some of the values controlling the shape of the geometry might be arbitrary and not describing an optimal design.

4.2.2 - Conclusions on the next generation workflow

Q21: What are the challenges of the of the contemporary PCA workflow in regard to sun shading design?

The main challenge regarding the contemporary PCA workflow is to generate more data in a smaller amount of time. In order to do so, the research proposed two approaches to overcome this challenge; the stepped approach and the grid-based approach. The grid-based approach is the one with the most potential. Using the contemporary workflow, it is not possible to harvest the full power of the grid, because the plug-ins of Ladybug and Honeybee are not intended to operate in such environment. In addition, the contemporary workflow would require a Rhinoceros license for each computer in the grid. In a corporate environment this is very unfeasible because Rhino licenses are relatively expensive.

Q22: How can the workflow be altered in order to overcome these challenges?

The contemporary workflow can be altered to overcome this main challenge by separating it into three core phases; preparation, execution and interpretation. This core concept of the next generation workflow divides the Grasshopper script in two parts, one for the preparation phase and one for the interpretation phase. These two phases are the least time consuming and can be conducted on one local machine. The execution phase is conducted using a DOS script node and only requires the installation of freely available software. Therefore, only this time-consuming step is executed using the grid. Executing the simulations outside the Grasshopper interface also result in decreased CPU loads on the computer, allowing for more concurrent processes. The distribution of parallel and sequential processes in the next generation workflow is controlled using queue nodes and concurrent processes settings. Even though this alteration did help to generate more data in a smaller amount of time, the next generation workflow is not yet fully stable, as there are still some more challenges to be overcome. The paragraph on recommendations and further development will further address these issues.

4.2.3 - Conclusion on the main research question

The main research question:

How can the contemporary Performative Computational Architecture (PCA) workflow for optimising sun shading designs on visual and thermal comfort in high-rise office buildings with all-glass exteriors be advanced to the next generation?

In order to answer this question, a relatively complex example case was set-up and optimised using the contemporary PCA workflow. The contemporary PCA workflow for sun shading design can be categorized as a model-depending workflow, where ModeFRONTIER is responsible for the optimisation phase and depends on a Grasshopper model for the form-finding and performance evaluation phase. The visual and thermal comfort simulations are conducted using Radiance & Energyplus via Honeybee.

The sun shading in the example case is based on the yet existing egg-crate system. This system has arguable potential for a fictive building resembling common trends within the specified scope of high-rise office buildings with all-glass exteriors in tropical climates. Results have shown that the contemporary PCA workflow is capable of assessing the performance on visual and thermal comfort of the selected sun shading system. Whether it is capable of improving this performance by finding optimal design solutions, is not yet fully understood, because more data is needed to give a comprehensive answer.

The research has identified the main challenge to generate more data in a smaller amount time. The main bottle-neck within the contemporary PCA workflow for doing so is the disability to properly utilize the full potential of the grid, resulting in impractical calculation times or insufficient data. This disability is mainly caused by the plug-ins of Ladybug and Honeybee not being intended for use in a grid or render farm environment and the fact that executing the Grasshopper script on multiple cloud nodes would require the installation of relatively expensive software on each node. This will drastically limit the feasibility of the using the PCA framework for sun shading in a corporate environment.

The research resulted in two proposals to advance the workflow, the cloud-based approach having the most potential to overcome the main challenge of generating more data in a smaller amount of time. Further development of this cloud-based approach has resulted in the birth of the next generation workflow. This workflow is conceptually based on splitting the optimisation workflow in three phases; preparation, execution & interpretation. The preparation phase is about generating the geometry and preparing the visual and thermal performance simulations. This first phase is conducted using Grasshopper and will give the file directories of the analyses batch files as the main outputs. By using the queue nodes in ModeFRONTIER, it is ensured that this phase is conducted sequentially and only on the host computer of the cloud network. The second phase, the execution, is conducted using a simple DOS script which will execute the visual and thermal simulations, which is by far the most time-consuming task within the PCA framework. By executing the analyses outside the interface of Grasshopper, these tasks can be divided among the nodes in the grid and ran in parallel, because the simulations themselves only rely on freely available software; Radiance and Energyplus. In addition, bypassing the Grasshopper interface for

the execution will also reduce the total amount of computational power needed per evaluation. The total amount of parallel executable processes depends on the hardware specifications of the computers. The final phase, interpretation, is also conducted using Grasshopper and will transform to raw output data of the visual and thermal comfort simulations into comfort metrics, serving as the objectives in the PCA framework. An overview of the currently finalized version of the next generation is given in figure 201.

The development of the next generation workflow would not have been possible without this research, as the needs for this specific case required an updated version of the ModeFRONTIER Grasshopper myNode. This fact emphasizes the novelty of the next generation workflow. In order to properly assess the feasibility of this new workflow, more research is needed. The first tests, which are part of this research, indicated the next generation workflow is capable of running in a render farm environment and has proven to be about 2.5 to 3 times faster when running on a regular high-end computer. However, the next generation workflow is not fully stable yet. Some of the issues still present will be addressed in the next chapter. Further research on these issues and the next generation workflow in general is highly recommended, as it will drastically increase the power of the PCA methodology in relation to sun shading design by advancing the workflow to the next generation.

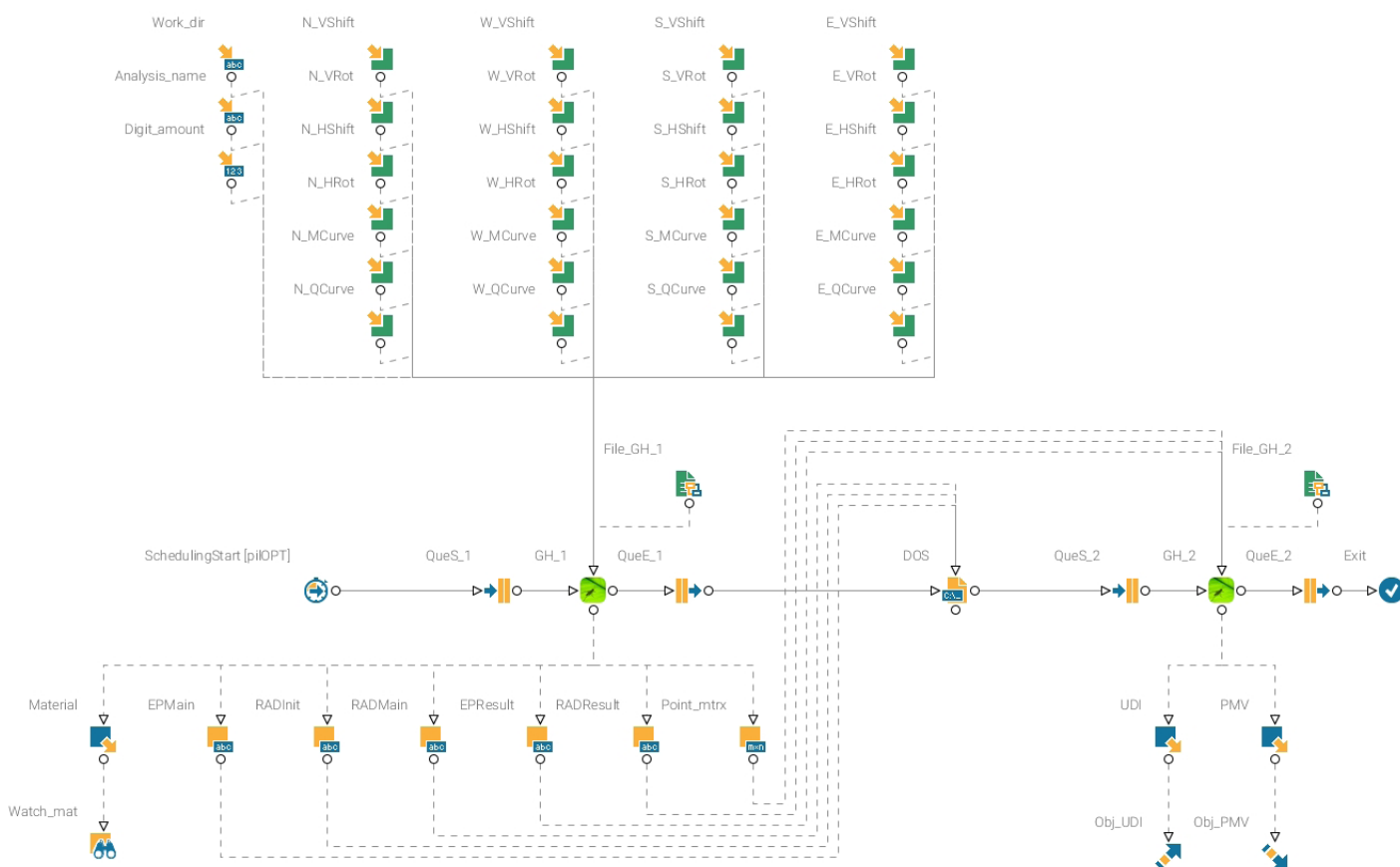


Figure 201. Currently finalized version of the net generation workflow (by author)

4.3 - Recommendations & further development

4.3.1 - Broadening future research

This research has focused on the example case, which regards one particular shading system which was found to have potential for high-rise office buildings with all-glass exteriors. However, there are more shading systems with potential to be found in literature. Since the implementation of the PCA method varies depending on the specific shading system, these other systems with potential could be interesting topics for further research as it would help to validate the next generation workflow as a standardized workflow for optimising sun shading designs on visual and thermal comfort. In addition, further research could also be extended outside the realm of sun shading design. Grasshopper is a common tool in architectural design nowadays, so the challenge of harvesting the computational force of a grid- or render farm environment might also be of interest for other architectural design processes.

4.3.2 - Deepening future research

Like stated before, the next generation workflow offers great potential for the application of the PCA framework to sun shading design. However, this research is just the start of the development of this new workflow and further research is highly recommended. This paragraph will continue by listing some of the issues that are still present within the next generation workflow.

Linking the queues

As stated before in paragraph 3.8, the next generation workflow is not completely stable yet. The hypothesis is that the system is likely to crash when the two Grasshopper scripts are opened simultaneously, causing the entire optimisation process to stall. If this can be prevented by somehow linking the two queues and only allowing one instance of Grasshopper to be started at a time, this issue might be resolved. A workaround for this issue could be the time-out limitation options within ModeFRONTIER, which will force kill processes that take over a set amount of time to complete. Both methods are advised to be explored in further research as this stalling action caused by random errors is currently the biggest challenge, limiting the feasibility of the next generation workflow.

Suppressing the multi-save Grasshopper pop-up

The multi-save pop-up is a native feature of Grasshopper acting as a safety feature when the software is shut down. However, it has proven to be unfeasible in regard to the next generation workflow. In this research a custom VB script was used to suppress this pop-up using Rhinoceros API, but finding a more elegant solution is recommended for further research. This will also limit the possibility of random errors, which could cause the optimisation process to stall, as this custom component did show some problems in earlier research phases.

The lighting schedule issue

Paragraph 3.7.2 discusses the lighting schedule issue. In the contemporary workflow, the lighting schedule used for the thermal comfort simulation is derived from the results of the visual comfort analysis. For the next generation workflow however, this is not feasible because it would be preferred to execute the visual and thermal comfort simulations simultaneously. With regard to the development of the next generation workflow it was for this research chosen to not include artificial lighting at all, because it is not very relevant to the example case. The alternative options discussed in paragraph 3.7.2 and other solutions for the lighting schedule can all be interesting directions for further research.

Further testing on the BK Renderfarm

The first test with the next generation workflow indicated to be compatible with the BK Renderfarm present on the TU Delft architecture faculty. However, limitations in time availability prevented to extensively explore this compatibility. When some of the issues listed above are resolved and the next generation workflow is more stable, it is highly recommended to test the limitations of the BK Renderfarm. Running the optimisation on high-end regular computers in the VR-lab showed the next generation workflow is already 2.5 to 3 times faster. In theory, much higher speeds could be achieved when using a render farm environment.

4.4 - Reflection

4.4.1 - Relationship between research & design

In order to design the sun shading of the future, it is important to gain insight in what defines the performance of the sun shading. Ultimately, the main purpose of shading systems in building design is to enhance the comfort of the occupants. When this is done as efficient as possible, the use of energy consuming HVAC systems to artificially achieve a state of comfort can be limited as much as possible, resulting in more sustainable buildings.

In the first phase of the graduation, leading up to the P2 presentation, lots of literature research was done to define metrics qualifying the levels of thermal and visual comfort. These metrics will be used in the design process to evaluate the performance of various shading systems. Based on the findings of this research two design tasks were to be completed.

The first design task involved selecting and adapting a sun shading system. This was done based on typologies defined by literature sources in combination with their suitability for the specific scope of this research. This resulted in selecting a fixed shading system; the egg-crate system, and placing it within the cavity of a double skin façade, in order to adapt it to fit the requirements of the scope. The next step within this design task was the parametrization of the concept, in order to be integrated in the PCA method. After applying this sun shading system to an example building floorplan, this will serve as an example case to explore how the PCA method can contribute to improving the performance of the selected shading system

The second design task involved developing a specific PCA methodology. Firstly, the fundamentals of the PCA method in general were researched in literature. Thereafter, based on literature findings and case studies, a typology categorization for PCA processes was developed. This helped designing the PCA workflow for the performance evaluation and optimization phase. The workflow is tested using the example case defined in the first design task. Based on these results, various questions about the performance of the optimized version of the selected example can be answered. In addition, the results for the example case can be used to assess the feasibility of the developed PCA methodology itself as well. This resulted in two proposals for further improvement of the researched PCA methodology itself.

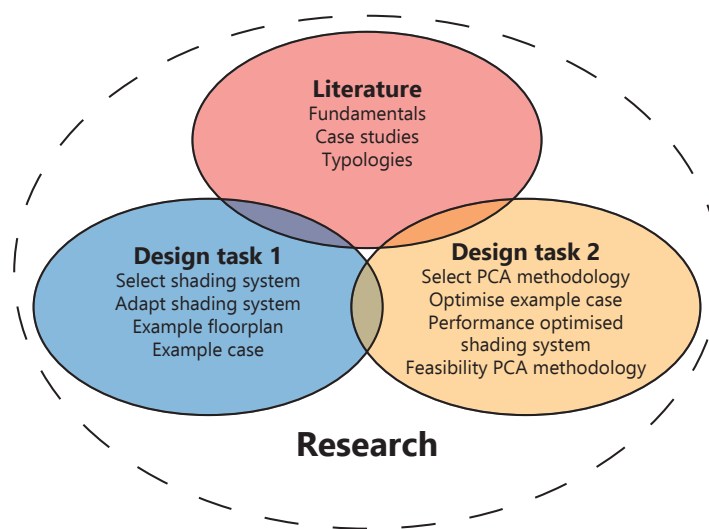


Figure 202. *Diagram: relation between research & design (by author)*

4.4.2 - Relationship between the topic, building technology track & Msc program

In my opinion, this graduation topic covers the core of the building technology master track; Using technology to design better buildings. In this case, better means more comfortable visual and thermal indoor environments achieved in a more sustainable way. The technology used in this case to achieve this improvement on comfort is the PCA method.

I think one of the main purpose of graduates of this master track is to form a bridge between the novelty developments of the scientific research realm and the architectural practice realm. Before graduating, I gained some practical experience working in multiple architecture offices. During these experiences I noticed there is a lot of interest in the development of these parametric design tools in relation to healthier buildings. However, there also appears to be a lack of knowledge about how to properly use these tools to create architecture. This research has shown the current methodology for implementing the PCA method can still be improved. As a future graduate, I hope be a part of this development and to be able to use it's potential to help designing the buildings of the future.

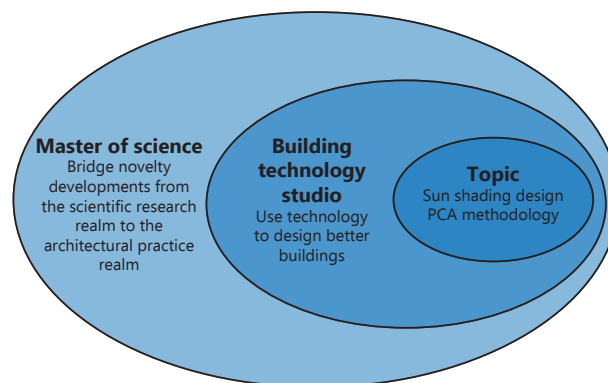


Figure 203. *Diagram: relation between topic, studio & master program (by author)*

4.4.3 - Research method & approach in relation to BT inquiry & scientific relevance

In my graduation plan I described multiple methods used for this project in chronological order. The first one is the literature research method. This consisted of two parts, the first being the fundamental theory part (about visual comfort, thermal comfort, the PCA process and shading requirements for high-rise.) And the second part, the state-of-the-art review (about case studies and typology on PCA use in sun shading and sun shading in high-rise. The relevance of this method is to assemble all required information for the design tasks.

The second selection method is the selection method, with the goal of selecting the most promising sun shading concept for buildings within the scope. At the time of writing the graduation plan, this method was envisioned to use three steps;

1. Cross-referencing typologies; building two databases, one with parametrically design shading systems, the other with shading systems used in high-rise. The two databases would be cross-referenced with the other scopes of this graduating project
2. Out-of-the-box brainstorm; thinking about possibilities for adapting other shading systems to fit the criteria.
3. Literature review findings; reflect the finding to literature reviews

However, after reconsideration, the order of those three steps was changed to better fit the building technology studio methodical line of inquiry; start at findings in literature findings and work from there. Although the selected shading system is still open for interpretation, the findings in literature helped to substantiate the choice for the egg-crate system in a double skin cavity, by proving its potential for the specific scope of the high-rise office building with all-glass exterior in tropic climates.

The third method is the PCA method, also consisting of three steps; form-finding, performance evaluation and optimization. I did have some previous knowledge about this method, but researching the literature on this topic definitely put things better in perspective. Within the building physics track, a common part of the methodical line of inquiry is to base the specific choice of PCA workflow on precedences. The specific PCA workflow was developed to meet the requirements of this specific case study. As a concluding part, the research gives two proposals to further improve this workflow itself as well.

The fourth method used in this research is the comparison method. This method is used to assess the performance of the selected shading system, optimized using the PCA method, in relation to different alternatives and climates. The graphic representation of the methodology has been changed in between P2 and P4, but the methodology itself remained the same; define shading alternatives, run simulations and compare the presentation on comfort metrics.

The fifth and final method is the exploration method. Originally this phase of the research was envisioned as rerunning the PCA cycle in order to make sure the selected option is actually the best option. However, during the research, the completion of this phase was revised, based on new insights. Being open to adapt the research methodology when preliminary results indicate this might lead to better results is also in line with the studio's methodical line of inquiry. During the research, multiple analysis techniques for optimization techniques were discovered, which have shown to be of value in precedences. Therefore, the step of interpretation and analysis was added to the exploration method. Conclusions derived from these analyses have also resulted in a feedback loop to the PCA methodology itself. In addition, steps for assessing the architectural performance were added as well. Originally this step was neglected in the exploration method, but precedences showed the importance of this assessment in making the final selection for a desirable design. In order to do so, two steps were added to the methodology scheme; automated physical model making and automated VR rendering.

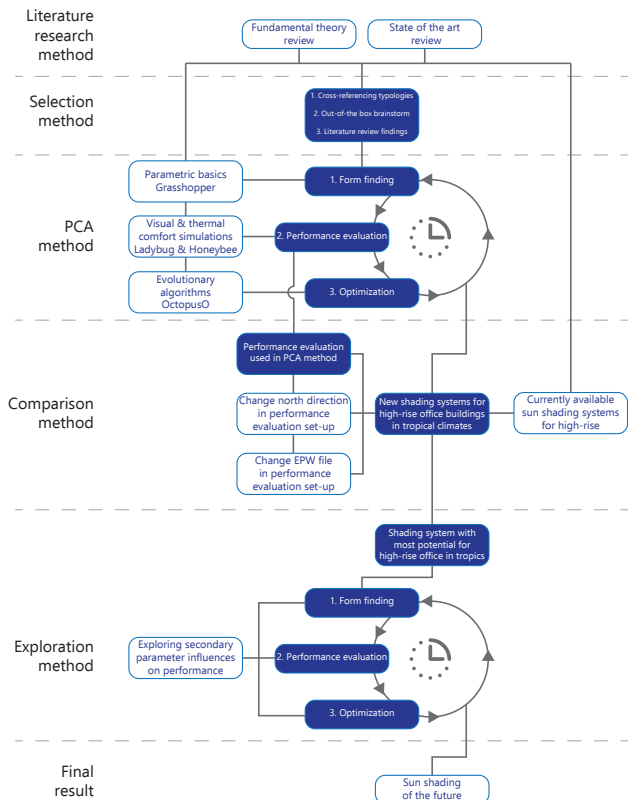


Figure 204. Diagram: research methodology at P2 (by author)

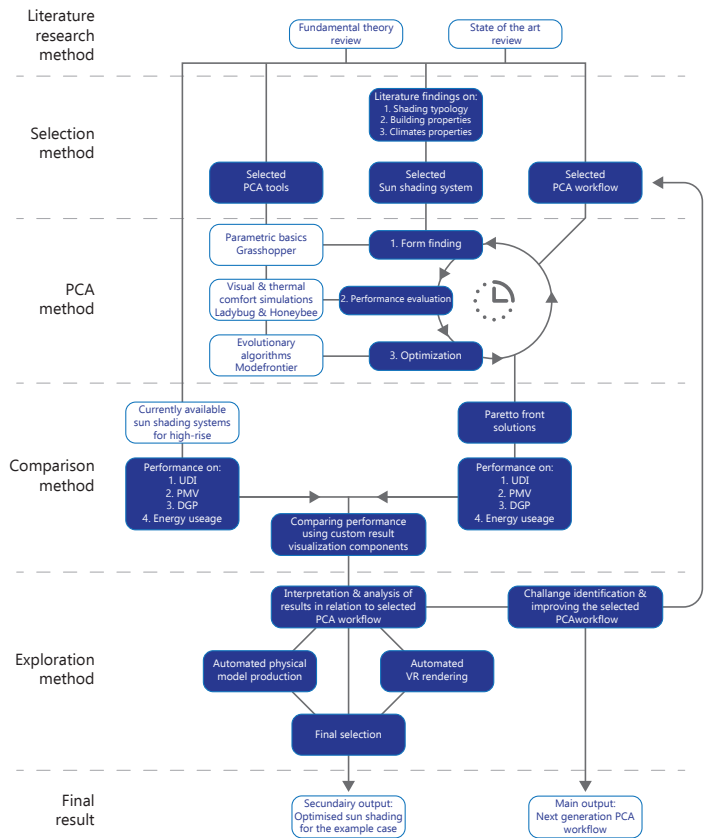


Figure 205. Diagram: research methodology at P4 (by author)

4.4.4 - The research in wider frameworks & transferability

As stated previously, I noticed an increasing demand for the use of parametric design tools in the professional field. In combination with the observed lack of knowledge within the professional framework, the graduation project fits neatly in a wider professional framework.

Secondly, this graduation project contributes to the design of more healthy and sustainable buildings. With phenomena such as global warming and fossil fuels running out, the need for more healthy and sustainable buildings will become ever larger over time. In the meantime, the demands for visual and thermal comforts will most likely increase in the future, because people have a tendency to become accustomed to luxury. In addition, contemporary trends in architecture such as the all-glass exterior makes the challenge of realizing these comfortable buildings in a tropic climate even harder. Since this research offers a potential solution to the challenges resulting from these trends, it fits in the wider social framework.

With regard to the scientific framework, the topic links to an ongoing scientific field with is currently increasing in popularity due to its high potential for architectural designers. Within the boundaries of the contemporary PCA workflow, the research identified the main bottle neck to be the disability to utilize the full potential of the grid. In addition, the research proposed an improvement of the selected workflow. When this challenge can be overcome, it might result in a big leap forward in the state-of-the-art on implementing the PCA process for sun shading design. The secondary goal of this graduation project would be a system that will be actually applicable in practice. In this context, that means the parametric script will be able to generate an optimal sun shading geometry for every building perimeter shape, across different locations with tropical climates. Since the comparison method showed the egg-crate shading does perform better than some alternatives, the concept might have potential to be implied in practice. Multiple design decisions have been made based on current trends in architecture and the constructibility of the shading system, further increasing the transferability to actual architectural practice.

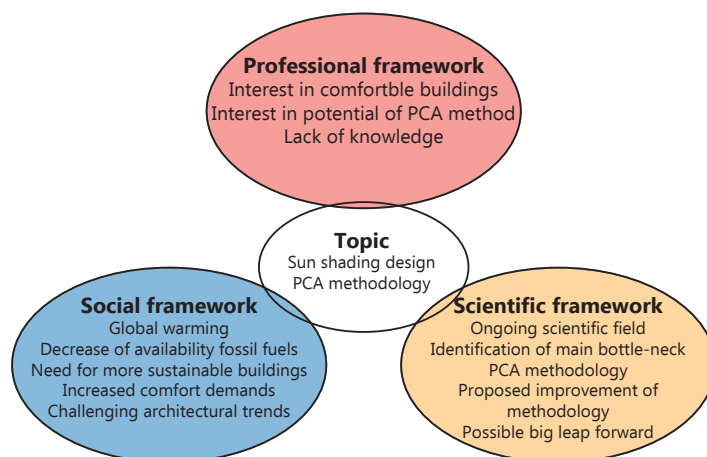


Figure 206. *Diagram: relation between topic, professional, social & scientific framework (by author)*

4.4.5 - Ethical issues & dilemmas

The first encountered issue was involving the argumentation for the selection of a shading system. Unsuccessfully, the research tried to identify the best shading system. After reconsideration this goal was classified as unfeasible and the research shifted focus to selecting a shading system with proved potential. After this was found in the form of the egg-crate system, the shading served as a valid example. This still resulted in valuable research results, but due to scoping the research on the egg-crate system, these results cannot be interpreted as comprehensive for all available sun shading systems.

Another issue involved translating the comfort metrics to objectives. With regard to the PCA workflow, it is preferred to combine comfort metrics into a single annual value. For the UDI this was completed relatively easily, by using the UDI (mod-75). However, the PMV score refers to an hourly result by definition. Literature showed no predefined methodology for combining this to an annual data. First an approach similar to the UDI was proposed, but based on preliminary results this was later changed to a sum of the annual exceedance of the PMV comfort domain. Even though this combined PMV score proved to give insight in the performance on thermal comfort, the methodology for combining the hourly values to the annual score is not supported by literature.

Perhaps the biggest dilemma in this research was how to deal with the limitations running ModeFRONTIER in combination with Ladybug and Honeybee. This semester, the faculty's ICT staff tried to integrate ModeFRONTIER in the BK Renderfarm. This was successful for other integrations such as Matlab, but unfortunately without success for the case of Ladybug and Honeybee integration, due to technical limitations. After losing some valuable time by awaiting these developments in vain, the decision was made to run the simulations over the weekend on three computers in the VR lab. Like stated before various times, this resulted in insufficient data to actually identify the Pareto front optimal solutions. The big dilemma at this stage involved the choice of continuing with the current workflow and reserving more time for the computational process, or to try and speed up the workflow by improving the workflow. Since an improved workflow seemed of bigger scientific relevance, the research shifted focus towards developing the next generation workflow.

The last issue involves implementing the final result in practice would be the validation of the performance simulations. The tools found within Grasshopper for assessing visual and thermal comfort; Radiance and Energyplus (via Ladybug and Honeybee) are well suited for architectural design exploration. However, most countries have strict legal requirements on the used methods for validating the climatological performance of a building as part of building standards. Unfortunately, the used PCA methodology would not fit these requirements for many cases. This would cause the need for yet another software to validate the design and obtain the required building permits.

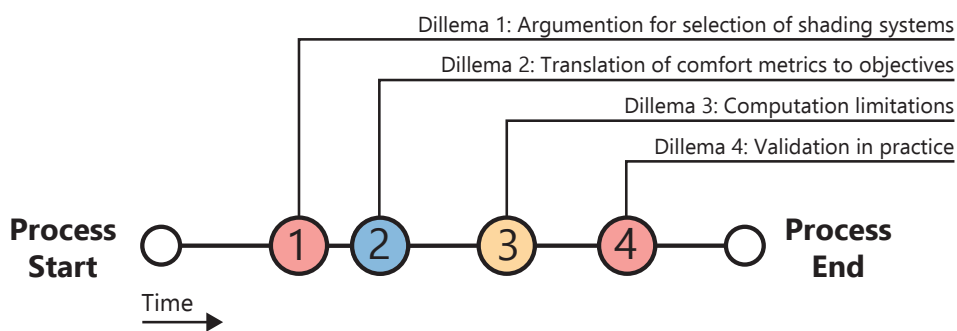


Figure 207. *Diagram: ethical issues & dilemmas (by author)*

5. Appendices

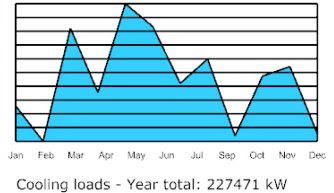
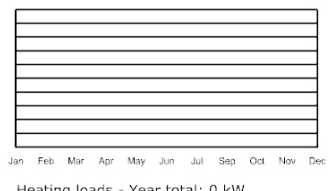
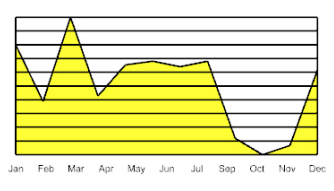
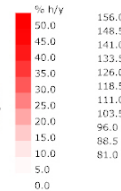
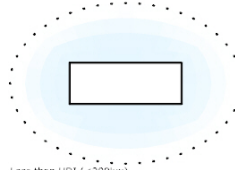
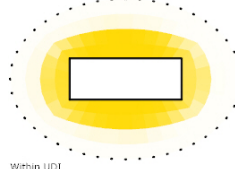
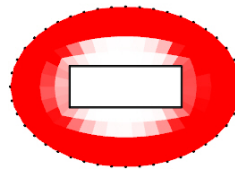




5.1 - Appendix I: Complete results of compared evaluations

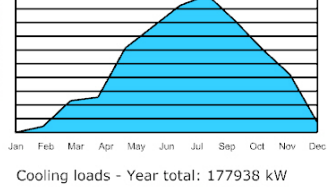
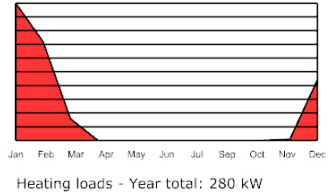
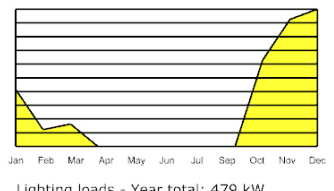
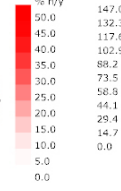
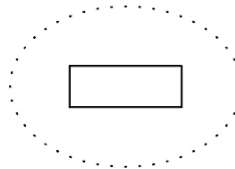
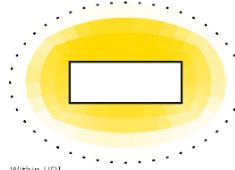
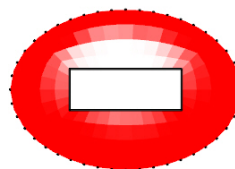
Analysis name: Sim1 Single skin facade
 Location: Singapore
 PMV result: 11587
 UDI result: 19.2 %

	Jan	Feb	Mar	Apr	May	Jun	Jul	Aug	Sep	Oct	Nov	Dec
00:00	0.95	1.03	1.16	1.38	1.48	1.48	1.32	1.31	1.15	1.13	0.96	0.91
23:00	1.03	1.07	1.19	1.4	1.51	1.5	1.37	1.36	1.17	1.17	1.02	0.97
22:00	1.13	1.16	1.26	1.46	1.55	1.55	1.41	1.42	1.22	1.21	1.06	1.02
21:00	1.29	1.33	1.41	1.56	1.64	1.71	1.52	1.54	1.29	1.29	1.14	1.12
20:00	1.78	1.92	1.94	1.96	1.95	2.13	2.02	1.93	1.55	1.55	1.42	1.43
19:00	2.99	3.3	3.23	3.14	2.97	3.34	3.26	2.97	2.56	2.46	2.34	2.48
18:00	4.46	4.76	4.68	4.62	4.4	4.99	4.74	4.36	3.94	3.84	3.8	3.97
17:00	5.27	5.59	5.34	5.49	5.18	5.84	5.46	5.17	4.73	4.77	4.73	4.82
16:00	5.74	6.01	5.6	5.85	5.64	6.16	5.8	5.56	5.09	5.35	5.28	5.24
15:00	5.85	5.97	5.55	5.78	5.72	6.12	5.74	5.51	4.95	5.42	5.42	5.36
14:00	5.74	5.85	5.44	5.76	5.7	5.96	5.6	5.5	4.89	5.33	5.4	5.34
13:00	5.69	5.77	5.42	5.9	5.81	5.95	5.69	5.53	4.87	5.39	5.54	5.27
12:00	5.43	5.6	5.34	5.96	5.85	5.74	5.68	5.38	4.88	5.42	5.57	5.06
11:00	4.79	4.97	5.0	5.59	5.44	5.14	5.25	4.8	4.6	5.16	5.14	4.61
10:00	3.84	4.04	4.19	4.7	4.55	4.3	4.46	3.91	3.91	4.41	4.33	3.92
09:00	2.83	2.87	3.12	3.5	3.47	3.38	3.36	2.93	3.12	3.38	3.29	2.97
08:00	1.75	1.76	1.86	2.15	2.29	2.2	2.13	1.86	1.9	2.07	1.96	1.74
07:00	0.77	0.81	0.9	1.08	1.25	1.24	1.12	0.95	0.87	0.99	0.82	0.65
06:00	0.72	0.82	0.93	1.08	1.22	1.28	1.1	1.02	0.91	0.96	0.78	0.65
05:00	0.74	0.88	0.95	1.13	1.24	1.31	1.12	1.04	0.96	0.98	0.8	0.67
04:00	0.77	0.91	0.99	1.16	1.29	1.35	1.16	1.06	0.98	1.02	0.85	0.72
03:00	0.8	0.95	1.03	1.19	1.33	1.38	1.21	1.08	1.02	1.05	0.9	0.76
02:00	0.84	1.01	1.06	1.26	1.37	1.43	1.25	1.12	1.08	1.08	0.93	0.79
01:00	0.87	1.04	1.11	1.32	1.4	1.49	1.3	1.18	1.11	1.11	0.97	0.83



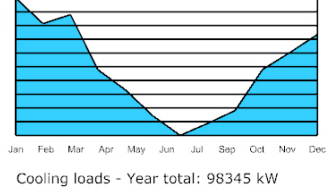
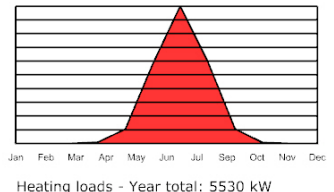
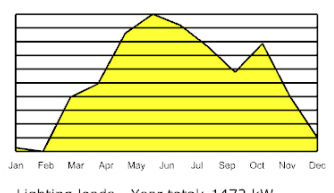
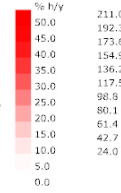
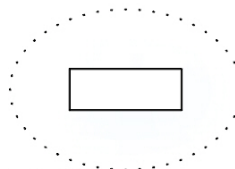
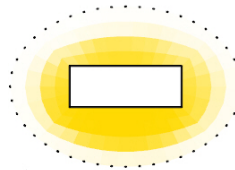
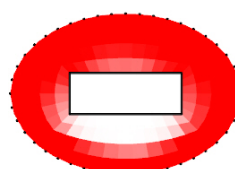
Analysis name: Sim1 Single skin facade
 Location: Abu Dhabi
 PMV result: 14031
 UDI result: 16.3 %

	Jan	Feb	Mar	Apr	May	Jun	Jul	Aug	Sep	Oct	Nov	Dec
00:00	-1.72	-1.38	-0.66	0.45	1.3	1.98	2.66	2.63	2.14	0.97	0.06	-1.16
23:00	-1.53	-1.18	-0.49	0.6	1.53	2.16	2.85	2.79	2.3	1.17	0.22	-0.98
22:00	-1.34	-0.92	-0.29	0.75	1.75	2.36	3.04	2.97	2.49	1.36	0.34	-0.82
21:00	-1.12	-0.61	-0.08	0.98	2.03	2.65	3.34	3.26	2.7	1.59	0.53	-0.63
20:00	-0.74	-0.1	0.39	1.41	2.59	3.31	3.96	3.78	3.09	1.96	0.91	-0.23
19:00	0.28	1.21	1.77	2.68	4.16	5.04	5.48	5.19	4.11	2.87	1.85	0.79
18:00	2.33	3.69	3.86	4.61	6.45	7.28	7.67	7.39	6.12	4.6	3.36	2.38
17:00	4.14	5.31	5.04	5.73	7.41	8.17	8.73	8.65	7.93	6.54	5.13	4.0
16:00	5.11	5.85	5.38	6.04	7.31	8.02	8.65	8.75	8.56	7.72	6.49	5.18
15:00	5.44	5.86	5.28	5.96	6.83	7.37	8.05	8.23	8.27	7.96	7.01	5.77
14:00	5.48	5.6	4.96	5.76	6.54	6.91	7.58	7.71	7.66	7.74	7.04	5.95
13:00	5.25	5.28	4.72	5.56	6.45	6.7	7.38	7.51	7.29	7.5	6.85	5.83
12:00	4.84	4.93	4.6	5.43	6.47	6.76	7.38	7.4	7.14	7.25	6.55	5.39
11:00	4.08	4.23	4.27	5.32	6.49	6.93	7.46	7.36	7.06	6.88	5.94	4.56
10:00	2.72	3.03	3.57	4.89	6.34	6.89	7.2	6.97	6.58	6.08	4.83	3.34
09:00	0.81	1.31	2.39	3.85	5.36	6.0	6.15	5.7	5.27	4.47	3.22	1.61
08:00	-1.32	-0.82	0.52	1.92	3.41	4.11	4.22	3.71	3.27	2.13	0.98	-0.49
07:00	-2.54	-2.26	-1.1	-0.02	1.32	2.09	2.44	1.98	1.54	0.24	-0.75	-1.83
06:00	-2.48	-2.15	-1.17	-0.3	0.54	1.33	1.97	1.7	1.35	0.1	-0.81	-1.75
05:00	-2.4	-2.0	-1.11	-0.23	0.53	1.31	2.01	1.79	1.46	0.23	-0.69	-1.65
04:00	-2.25	-1.92	-1.05	-0.13	0.64	1.42	2.09	1.94	1.59	0.4	-0.53	-1.59
03:00	-2.08	-1.81	-0.97	-0.02	0.78	1.54	2.22	2.13	1.7	0.58	-0.39	-1.51
02:00	-1.95	-1.68	-0.89	0.11	0.9	1.71	2.37	2.28	1.84	0.72	-0.25	-1.4
01:00	-1.82	-1.54	-0.79	0.29	1.05	1.87	2.53	2.4	2.0	0.84	-0.07	-1.27



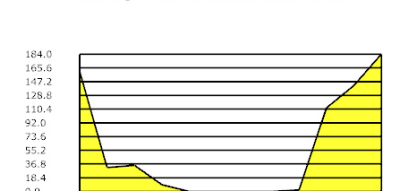
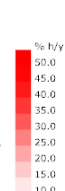
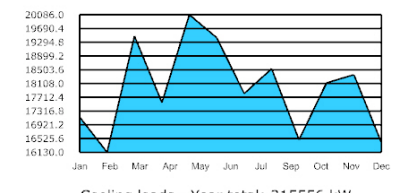
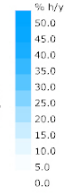
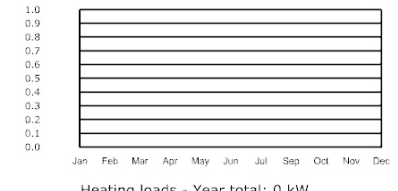
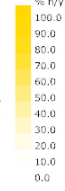
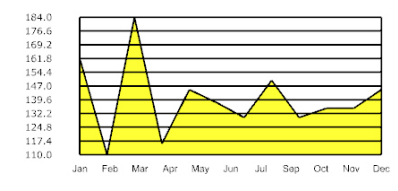
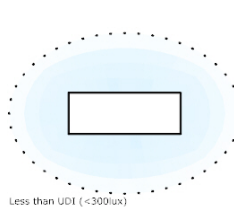
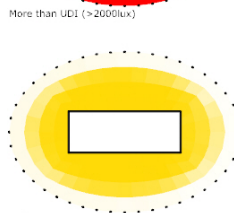
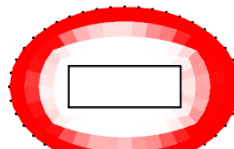
Analysis name: Sim1 Single skin facade
 Location: Brisbane
 PMV result: 9072
 UDI result: 14.2 %

	Jan	Feb	Mar	Apr	May	Jun	Jul	Aug	Sep	Oct	Nov	Dec
00:00	0.11	-0.09	-0.44	-1.42	-2.58	-3.18	-4.03	-3.29	-2.57	-1.33	-0.95	-0.53
23:00	0.28	0.12	-0.25	-1.19	-2.32	-3.0	-3.81	-2.99	-2.32	-1.07	-0.77	-0.34
22:00	0.46	0.31	-0.07	-0.97	-2.03	-2.8	-3.54	-2.7	-2.08	-0.81	-0.58	-0.14
21:00	0.74	0.54	0.14	-0.73	-1.7	-2.57	-3.14	-2.4	-1.78	-0.5	-0.31	0.11
20:00	1.21	0.91	0.5	-0.34	-1.17	-2.1	-2.51	-1.89	-1.29	-0.05	0.12	0.52
19:00	2.32	1.78	1.38	0.61	-0.05	-0.98	-1.26	-0.78	-0.21	0.92	1.07	1.53
18:00	4.08	3.28	2.74	1.87	1.18	0.34	0.13	0.52	1.09	2.17	2.41	3.2
17:00	5.29	4.7	4.18	3.21	2.4	1.43	1.26	1.61	2.27	3.26	3.62	4.52
16:00	5.74	5.39	5.27	4.99	4.45	3.51	3.21	3.23	3.82	4.35	4.5	4.96
15:00	5.62	5.43	5.48	5.53	5.36	5.0	4.27	3.91	4.3	4.57	4.7	4.8
14:00	5.39	5.26	5.31	5.49	5.49	5.22	4.36	3.98	4.21	4.36	4.58	4.51
13:00	5.16	5.08	5.07	5.22	5.22	4.95	4.03	3.76	3.9	4.09	4.42	4.32
12:00	5.06	4.99	5.0	5.01	4.84	4.52	3.55	3.45	3.71	3.96	4.33	4.24
11:00	5.0	4.87	4.93	4.74	4.33	3.98	2.95	3.01	3.53	3.86	4.23	4.2
10:00	4.97	4.71	4.75	4.31	3.64	3.2	2.11	2.36	3.26	3.75	4.13	4.22
09:00	4.59	4.16	4.04	3.32	2.37	1.59	0.65	1.15	2.47	3.3	3.83	4.13
08:00	3.65	3.01	2.58	1.34	-0.02	-1.27	-1.96	-1.02	0.85	2.23	3.0	3.51
07:00	2.1	1.22	0.34	-1.36	-2.68	-3.68	-4.57	-3.68	-1.6	0.41	1.59	2.21
06:00	0.5	-0.46	-1.16	-2.42	-3.99	-4.14	-4.84	-4.36	-3.26	-1.38	0.25	0.63
05:00	-0.44	-0.86	-1.23	-2.43	-3.39	-4.07	-4.79	-4.35	-3.37	-2.2	-1.25	-0.9
04:00	-0.43	-0.76	-1.09	-2.31	-3.25	-3.86	-4.63	-4.19	-3.23	-2.18	-1.36	-1.02
03:00	-0.36	-0.65	-0.99	-2.23	-3.12	-3.69	-4.47	-4.07	-3.13	-2.13	-1.32	-0.93
02:00	-0.22	-0.49	-0.85	-2.08	-2.95	-3.51	-4.3	-3.9	2.98	-2.01	-1.21	-0.8
01:00	-0.04	-0.29	-0.66	-1.88	-2.74	-3.34	-4.13	-3.7	-2.77	-1.81	-1.07	-0.62



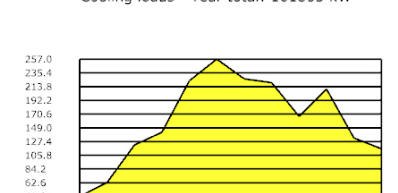
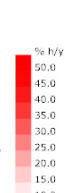
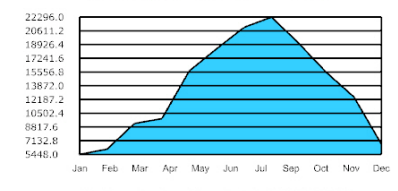
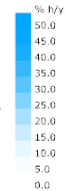
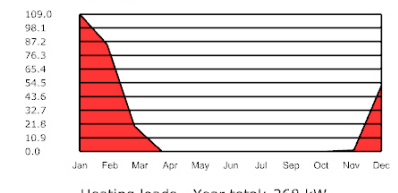
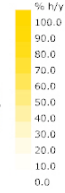
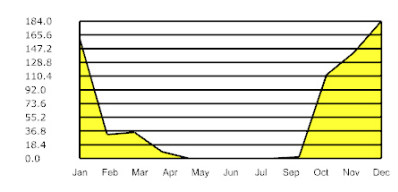
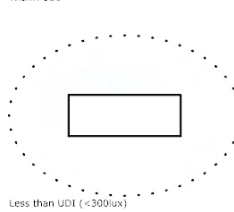
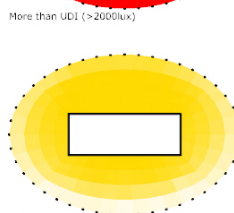
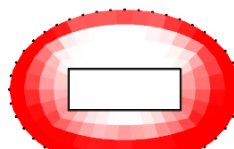
Analysis name: Sim2 Empty DSF
 Location: Singapore
 PMV result: 9833
 UDI result: 39.9 %

Time	Jan	Feb	Mar	Apr	May	Jun	Jul	Aug	Sep	Oct	Nov	Dec
00:00	0.98	1.06	1.19	1.41	1.51	1.51	1.36	1.34	1.18	1.16	1.01	0.94
23:00	1.05	1.1	1.22	1.43	1.55	1.53	1.4	1.39	1.2	1.2	1.05	1.0
22:00	1.15	1.18	1.29	1.48	1.58	1.58	1.44	1.45	1.25	1.24	1.09	1.04
21:00	1.28	1.33	1.42	1.57	1.65	1.71	1.54	1.56	1.31	1.32	1.17	1.13
20:00	1.7	1.84	1.87	1.91	1.94	2.07	1.96	1.9	1.53	1.56	1.41	1.42
19:00	2.71	2.94	2.95	2.88	2.8	3.08	2.99	2.78	2.41	2.36	2.23	2.32
18:00	3.89	4.12	4.13	4.06	3.93	4.4	4.16	3.87	3.53	3.46	3.42	3.53
17:00	4.46	4.73	4.59	4.71	4.47	5.0	4.67	4.43	4.06	4.11	4.06	4.12
16:00	4.8	5.05	4.79	4.97	4.78	5.21	4.9	4.71	4.35	4.54	4.46	4.42
15:00	4.87	5.02	4.78	4.91	4.84	5.16	4.83	4.65	4.26	4.58	4.55	4.5
14:00	4.78	4.92	4.73	4.91	4.82	5.04	4.72	4.63	4.23	4.51	4.53	4.47
13:00	4.73	4.83	4.66	5.03	4.9	5.03	4.78	4.64	4.2	4.56	4.63	4.4
12:00	4.56	4.69	4.56	5.06	4.93	4.87	4.78	4.53	4.16	4.59	4.67	4.25
11:00	4.1	4.25	4.3	4.79	4.64	4.42	4.5	4.11	3.95	4.41	4.37	3.93
10:00	3.42	3.55	3.72	4.14	3.99	3.82	3.94	3.48	3.47	3.86	3.78	3.43
09:00	2.67	2.66	2.93	3.23	3.21	3.15	3.11	2.77	2.91	3.16	3.07	2.74
08:00	1.74	1.74	1.85	2.11	2.25	2.17	2.1	1.85	1.86	2.09	2.0	1.69
07:00	0.8	0.84	0.93	1.11	1.27	1.27	1.15	0.98	0.89	1.01	0.85	0.68
06:00	0.75	0.85	0.96	1.11	1.25	1.31	1.13	1.05	0.94	0.99	0.81	0.68
05:00	0.76	0.91	0.98	1.16	1.27	1.34	1.15	1.07	0.99	1.01	0.83	0.7
04:00	0.8	0.94	1.02	1.19	1.32	1.38	1.19	1.09	1.01	1.05	0.88	0.75
03:00	0.83	0.98	1.06	1.23	1.36	1.41	1.24	1.12	1.05	1.08	0.93	0.79
02:00	0.86	1.04	1.11	1.29	1.4	1.46	1.28	1.15	1.11	1.11	0.96	0.82
01:00	0.9	1.07	1.14	1.35	1.43	1.52	1.34	1.21	1.14	1.14	1.0	0.85



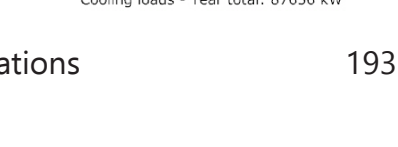
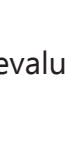
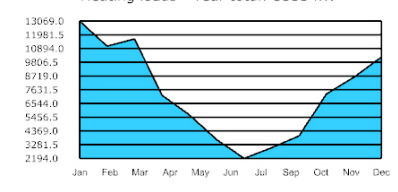
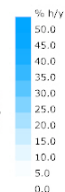
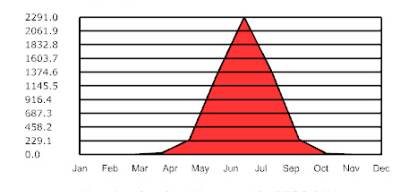
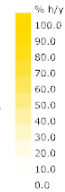
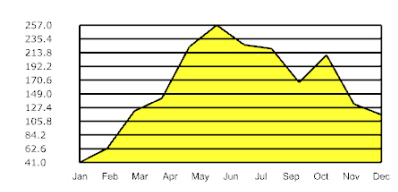
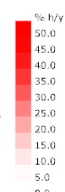
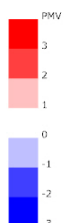
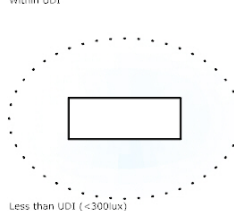
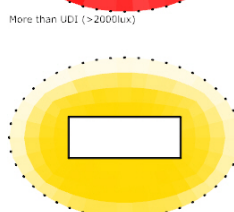
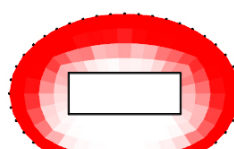
Analysis name: Sim2 Empty DSF
 Location: Abu Dhabi
 PMV result: 11890
 UDI result: 41.8 %

Time	Jan	Feb	Mar	Apr	May	Jun	Jul	Aug	Sep	Oct	Nov	Dec
00:00	-1.68	-1.35	-0.63	0.49	1.33	2.01	2.71	2.66	2.17	1.01	0.09	-1.13
23:00	-1.5	-1.14	-0.46	0.63	1.56	2.19	2.88	2.82	2.33	1.2	0.26	-0.95
22:00	-1.31	-0.89	-0.26	0.78	1.78	2.39	3.07	3.01	2.52	1.39	0.37	-0.78
21:00	-1.09	-0.58	-0.05	1.0	2.05	2.66	3.36	3.28	2.73	1.62	0.57	-0.6
20:00	-0.7	-0.09	0.37	1.4	2.56	3.25	3.89	3.74	3.09	1.99	0.94	-0.21
19:00	0.33	1.07	1.57	2.5	3.87	4.68	5.16	4.92	3.95	2.85	1.83	0.78
18:00	2.13	3.12	3.32	4.09	5.74	6.52	6.94	6.71	5.59	4.32	3.13	2.18
17:00	3.39	4.36	4.2	4.92	6.46	7.21	7.77	7.7	7.03	5.74	4.48	3.4
16:00	4.11	4.74	4.44	5.15	6.38	7.1	7.71	7.78	7.52	6.65	5.51	4.29
15:00	4.33	4.7	4.33	5.11	6.05	6.63	7.27	7.4	7.28	6.82	5.89	4.72
14:00	4.34	4.47	4.06	4.99	5.86	6.31	6.94	6.99	6.79	6.61	5.89	4.84
13:00	4.14	4.19	3.86	4.79	5.79	6.16	6.76	6.78	6.46	6.4	5.7	4.74
12:00	3.81	3.87	3.72	4.62	5.72	6.08	6.62	6.61	6.24	6.15	5.42	4.35
11:00	3.17	3.28	3.42	4.47	5.62	6.07	6.56	6.43	6.07	5.79	4.91	3.67
10:00	2.02	2.3	2.85	4.08	5.42	5.95	6.27	6.05	5.64	5.13	4.01	2.65
09:00	0.49	0.88	1.89	3.23	4.59	5.19	5.4	5.01	4.6	3.83	2.67	1.25
08:00	-1.26	-0.92	0.31	1.59	2.95	3.62	3.84	3.39	2.97	1.85	0.75	-0.49
07:00	-2.51	-2.24	-1.1	-0.07	1.17	1.94	2.35	1.93	1.51	0.23	-0.75	-1.8
06:00	-2.45	-2.12	-1.14	-0.27	0.56	1.34	2.0	1.73	1.38	0.14	-0.78	-1.72
05:00	-2.37	-1.96	-1.08	-0.19	0.57	1.34	2.04	1.82	1.49	0.26	-0.66	-1.61
04:00	-2.21	-1.89	-1.02	-0.09	0.68	1.45	2.13	1.97	1.62	0.43	-0.5	-1.55
03:00	-2.05	-1.78	-0.94	0.01	0.81	1.57	2.25	2.17	1.73	0.61	-0.36	-1.48
02:00	-1.92	-1.64	-0.86	0.14	0.94	1.74	2.4	2.31	1.87	0.75	-0.21	-1.36
01:00	-1.78	-1.5	-0.75	0.32	1.09	1.9	2.56	2.44	2.03	0.88	-0.04	-1.24



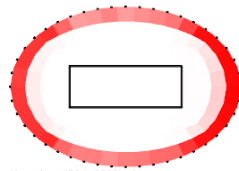
Analysis name: Sim2 Empty DSF
 Location: Brisbane
 PMV result: 7251
 UDI result: 40.0 %

Time	Jan	Feb	Mar	Apr	May	Jun	Jul	Aug	Sep	Oct	Nov	Dec
00:00	0.13	-0.06	-0.41	-1.4	-2.55	-3.16	-4.0	-3.26	-2.55	-1.3	-0.92	-0.51
23:00	0.31	0.14	-0.22	-1.16	-2.29	-2.97	-3.78	-2.97	-2.29	-1.05	-0.75	-0.32
22:00	0.49	0.33	-0.05	-0.94	-2.0	-2.77	-3.51	-2.67	-2.05	-0.78	-0.55	-0.12
21:00	0.77	0.56	0.16	-0.71	-1.67	-2.54	-3.14	-2.37	-1.75	-0.48	-0.28	0.13
20:00	1.21	0.94	0.52	-0.31	-1.14	-2.07	-2.48	-1.87	-1.26	-0.03	0.16	0.53
19:00	2.21	1.8	1.39	0.62	-0.04	-0.95	-1.23	-0.76	-0.19	0.94	1.08	1.5
18:00	3.69	3.09	2.59	1.79	1.19	0.37	0.16	0.5	1.05	2.04	2.28	2.95
17:00	4.63	4.1	3.62	2.82	2.18	1.29	1.1	1.38	1.95	2.86	3.17	3.94
16:00	4.96	4.61	4.45	4.16	3.72	2.91	2.58	2.6	3.09	3.71	3.81	4.29
15:00	4.87	4.63	4.59	4.57	4.42	4.08	3.4	3.09	3.45	3.88	3.97	4.2
14:00	4.68	4.48	4.44	4.49	4.48	4.2	3.44	3.13	3.35	3.66	3.88	3.95
13:00	4.46	4.29	4.21	4.22	4.23	3.94	3.14	2.91	3.06	3.39	3.71	3.74
12:00	4.33	4.17	4.11	4.02	3.87	3.56	2.66	2.6	2.85	3.24	3.6	3.62
11:00	4.21	4.03	4.01	3.78	3.41	3.06	2.07	2.17	2.65	3.1	3.47	3.51
10:00	4.14	3.87	3.87	3.42	2.79	2.35	1.3	1.58	2.38	2.96	3.34	3.46
09:00	3.8	3.4	3.26	2.55	1.66	0.94	0.02	0.52	1.65	2.54	3.03	3.34
08:00	2.97	2.39	2.01	0.81	-0.47	-1.57	-2.28	-1.4	0.22	1.56	2.26	2.77
07:00	1.6	0.82	0.04	-1.53	-2.92	-3.88	-4.58	-3.78	-1.93	-0.07	1.02	1.63
06:00	0.34	-0.53	-1.15	-2.39	-3.36	-4.11	-4.81	-4.32	-3.26	-1.52	-0.05	0.35
05:00	-0.41	-0.83	-1.2	-2.41	-3.36	-4.04	-4.76	-4.32	-3.34	-2.17	-1.24	-0.89
04:00	-0.41	-0.73	-1.06	-2.29	-3.22	-3.83	-4.6	-4.18	-3.2	-2.15	-1.33	-0.99
03:00	-0.33	-0.62	-0.97	-2.2	-3.09	-3.66	-4.44	-4.04	-3.11	-2.11	-1.29	-0.91
02:00	-0.2	-0.46	-0.82	-2.05	-2.92	-3.48	-4.27	-3.87	-2.95	-1.98	-1.19	-0.77
01:00	-0.01	-0.26	-0.63	-1.85	-2.71	-3.31	-4.1	-3.67	-2.74	-1.78	-1.04	-0.59

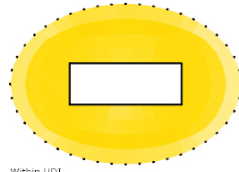


Analysis name: Sim3 solar reflective
 Location: Singapore
 PMV result: 8417
 UDI result: 63.3 %

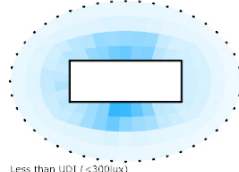
	Jan	Feb	Mar	Apr	May	Jun	Jul	Aug	Sep	Oct	Nov	Dec
00:00	0.98	1.06	1.19	1.41	1.51	1.51	1.36	1.18	1.16	1.01	0.94	
23:00	1.05	1.1	1.22	1.43	1.54	1.53	1.4	1.39	1.2	1.05	1.0	
22:00	1.15	1.18	1.28	1.48	1.58	1.58	1.44	1.45	1.25	1.24	1.09	1.04
21:00	1.27	1.31	1.4	1.56	1.64	1.71	1.52	1.55	1.3	1.32	1.17	1.13
20:00	1.63	1.71	1.76	1.84	1.89	2.02	1.87	1.85	1.49	1.55	1.41	1.38
19:00	2.52	2.63	2.67	2.66	2.67	2.9	2.77	2.65	2.29	2.34	2.21	2.18
18:00	3.47	3.59	3.66	3.63	3.62	3.92	3.73	3.52	3.24	3.3	3.22	3.19
17:00	3.77	4.02	4.03	4.11	3.9	4.23	4.02	3.85	3.59	3.62	3.53	3.54
16:00	4.0	4.27	4.18	4.3	4.11	4.4	4.17	4.03	3.8	3.89	3.77	3.73
15:00	4.08	4.26	4.16	4.23	4.15	4.4	4.13	3.97	3.74	3.92	3.85	3.84
14:00	4.01	4.17	4.13	4.23	4.13	4.33	4.02	3.94	3.67	3.84	3.84	3.79
13:00	3.97	4.08	4.08	4.33	4.17	4.31	4.05	3.93	3.66	3.9	3.91	3.72
12:00	3.83	3.94	3.98	4.33	4.18	4.14	4.03	3.83	3.63	3.95	3.95	3.6
11:00	3.53	3.6	3.76	4.09	3.94	3.81	3.84	3.52	3.5	3.81	3.72	3.36
10:00	3.11	3.17	3.34	3.64	3.52	3.42	3.52	3.14	3.16	3.38	3.29	3.04
09:00	2.6	2.59	2.7	3.01	3.01	2.97	2.99	2.66	2.69	2.85	2.81	2.55
08:00	1.69	1.7	1.8	2.06	2.16	2.11	2.03	1.81	1.84	2.01	1.92	1.61
07:00	0.8	0.84	0.93	1.11	1.27	1.27	1.15	0.98	0.89	1.0	0.84	0.67
06:00	0.75	0.85	0.96	1.11	1.25	1.31	1.13	1.05	0.94	0.99	0.81	0.68
05:00	0.76	0.91	0.98	1.16	1.27	1.34	1.15	1.07	0.99	1.01	0.83	0.7
04:00	0.8	0.94	1.02	1.19	1.32	1.38	1.19	1.09	1.01	1.05	0.88	0.75
03:00	0.83	0.98	1.06	1.23	1.36	1.41	1.24	1.12	1.05	1.08	0.93	0.79
02:00	0.86	1.04	1.11	1.29	1.4	1.46	1.28	1.15	1.11	1.11	0.96	0.82
01:00	0.9	1.07	1.14	1.35	1.43	1.52	1.34	1.21	1.14	1.14	1.0	0.85



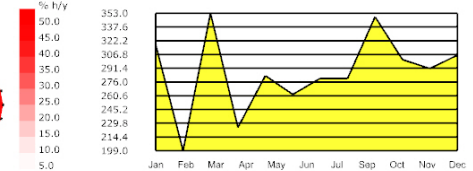
More than UDI (>2000lux)



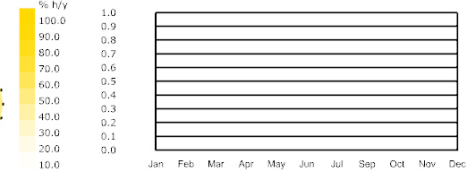
Within UDI



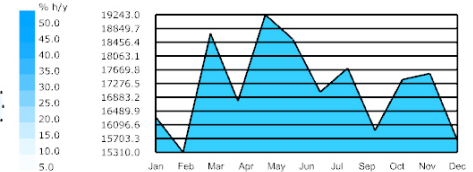
Less than UDI (<300lux)



Lighting loads - Year total: 3447 kW



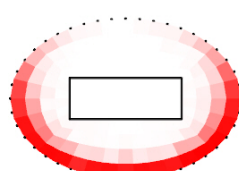
Heating loads - Year total: 0 kW



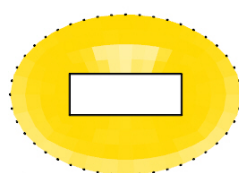
Cooling loads - Year total: 206193 kW

Analysis name: Sim3 solar reflective
 Location: Abu Dhabi
 PMV result: 10063
 UDI result: 69.1 %

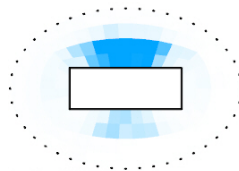
	Jan	Feb	Mar	Apr	May	Jun	Jul	Aug	Sep	Oct	Nov	Dec
00:00	-1.68	-1.35	-0.63	0.49	1.33	2.01	2.71	2.66	2.17	1.01	0.09	-1.13
23:00	-1.5	-1.14	-0.46	0.63	1.56	2.19	2.88	2.82	2.33	1.2	0.26	-0.95
22:00	-1.31	-0.89	-0.26	0.78	1.78	2.39	3.07	3.0	2.52	1.39	0.37	-0.78
21:00	-1.09	-0.59	-0.06	1.0	2.04	2.65	3.34	3.27	2.73	1.62	0.57	-0.6
20:00	-0.72	-0.12	0.35	1.38	2.51	3.17	3.81	3.69	3.09	1.97	0.93	-0.23
19:00	0.28	0.98	1.47	2.41	3.67	4.37	4.83	4.69	3.99	2.8	1.8	0.74
18:00	1.76	2.64	2.91	3.7	5.11	5.78	6.22	6.07	5.34	4.04	2.95	2.01
17:00	2.6	3.41	3.44	4.19	5.54	6.25	6.83	6.74	6.14	5.03	3.88	2.84
16:00	3.04	3.69	3.63	4.45	5.7	6.45	6.99	7.01	6.62	5.66	4.48	3.32
15:00	3.17	3.7	3.63	4.54	5.71	6.39	6.86	6.96	6.65	5.86	4.73	3.57
14:00	3.18	3.55	3.46	4.5	5.63	6.16	6.6	6.68	6.38	5.79	4.72	3.63
13:00	3.02	3.28	3.3	4.3	5.53	6.0	6.41	6.46	6.07	5.65	4.56	3.55
12:00	2.73	2.9	3.07	4.1	5.29	5.76	6.13	6.14	5.73	5.34	4.31	3.24
11:00	2.21	2.34	2.69	3.82	4.97	5.45	5.82	5.7	5.27	4.83	3.86	2.66
10:00	1.3	1.52	2.14	3.37	4.56	5.06	5.39	5.16	4.69	4.14	3.17	1.87
09:00	0.1	0.44	1.37	2.6	3.79	4.35	4.63	4.28	3.67	3.13	2.15	0.81
08:00	-0.37	-1.0	0.14	1.22	2.41	3.09	3.41	2.99	2.61	1.59	0.61	-0.6
07:00	-2.51	-2.24	-1.14	-0.16	0.96	1.72	2.21	1.85	1.45	0.17	-0.77	-1.81
06:00	-2.45	-2.12	-1.14	-0.27	0.54	1.32	1.99	1.73	1.38	0.14	-0.78	-1.72
05:00	-2.37	-1.96	-1.08	-0.19	0.57	1.34	2.04	1.82	1.49	0.26	-0.66	-1.61
04:00	-2.21	-1.89	-1.02	-0.09	0.68	1.45	2.13	1.97	1.62	0.43	-0.5	-1.55
03:00	-2.05	-1.78	-0.94	0.01	0.81	1.57	2.25	2.17	1.73	0.61	-0.36	-1.48
02:00	-1.92	-1.64	-0.86	0.14	0.94	1.74	2.4	2.31	1.87	0.75	-0.21	-1.36
01:00	-1.78	-1.5	-0.75	0.32	1.09	1.9	2.56	2.44	2.03	0.88	-0.04	-1.24



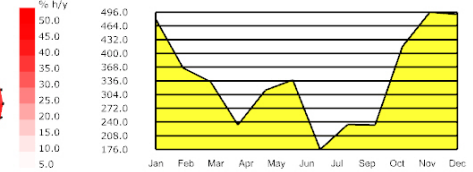
More than UDI (>2000lux)



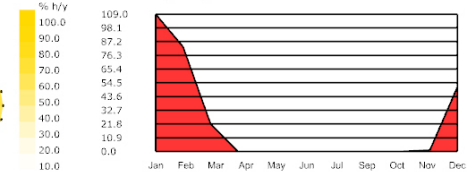
Within UDI



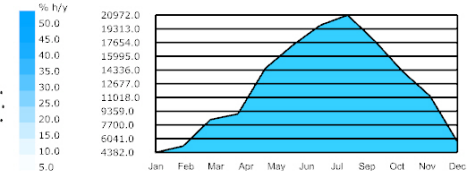
Less than UDI (<300lux)



Lighting loads - Year total: 4109 kW



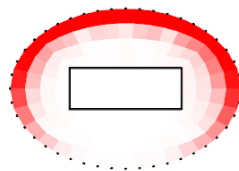
Heating loads - Year total: 267 kW



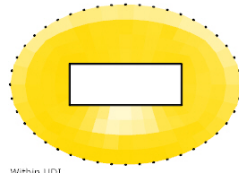
Cooling loads - Year total: 148341 kW

Analysis name: Sim3 solar reflective
 Location: Brisbane
 PMV result: 5761
 UDI result: 54.4 %

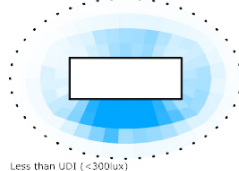
	Jan	Feb	Mar	Apr	May	Jun	Jul	Aug	Sep	Oct	Nov	Dec
00:00	0.13	-0.06	-0.41	-1.4	-2.55	-3.16	-4.0	-3.26	-2.55	-1.3	-0.92	-0.51
23:00	0.31	0.14	-0.22	-1.16	-2.29	-2.97	-3.78	-2.97	-2.29	-1.05	-0.75	-0.32
22:00	0.49	0.33	-0.05	-0.94	-2.0	-2.77	-3.51	-2.67	-2.05	-0.78	-0.55	-0.12
21:00	0.77	0.56	0.16	-0.71	-1.67	-2.54	-3.11	-2.36	-1.75	-0.48	-0.28	0.13
20:00	1.21	0.94	0.52	-0.32	-1.14	-2.07	-2.48	-1.86	-1.27	-0.02	0.15	0.52
19:00	2.18	1.81	1.4	0.61	-0.05	-0.95	-1.22	-0.77	-0.2	0.94	1.1	1.45
18:00	3.44	2.92	2.49	1.76	1.19	0.37	0.17	0.5	1.04	2.05	2.23	2.73
17:00	4.13	3.62	3.22	2.52	1.99	1.16	0.97	1.21	1.74	2.68	2.87	3.5
16:00	4.52	4.07	3.79	3.4	3.01	2.24	2.0	2.04	2.49	3.17	3.35	3.87
15:00	4.49	4.13	3.94	3.66	3.46	3.0	2.52	2.39	2.76	3.35	3.51	3.86
14:00	4.3	3.98	3.84	3.62	3.46	3.08	2.46	2.38	2.71	3.25	3.44	3.7
13:00	4.02	3.74	3.61	3.39	3.22	2.83	2.15	2.16	2.44	2.98	3.25	3.47
12:00	3.85	3.6	3.47	3.19	2.87	2.47	1.67	1.82	2.2	2.77	3.09	3.31
11:00	3.72	3.43	3.33	2.92	2.43	1.97	1.07	1.37	1.91	2.6	2.93	3.19
10:00	3.58	3.21	3.13	2.54	1.88	1.33	0.37	0.82	1.57	2.38	2.76	3.08
09:00	3.16	2.7	2.51	1.76	0.93	0.19	-0.69	-0.1	0.84	1.67	2.37	2.8
08:00	2.28	1.72	1.3	0.23	-0.86	-1.85	-2.57	-1.81	-0.52	0.82	1.55	2.06
07:00	1.01	0.33	-0.34	-1.75	-3.0	-3.92	-4.61	-3.89	-2.35	-0.67	0.35	0.86
06:00	0.12	-0.62	-1.18	-2.39	-3.36	-4.11	-4.81	-4.32	-3.29	-1.7	-0.41	-0.04
05:00	-0.41	-0.83	-1.2	-2.41	-3.36	-4.04	-4.76	-4.32	-3.34	-2.17	-1.26	-0.91
04:00	-0.41	-0.73	-1.06	-2.29	-3.22	-3.83	-4.6	-4.18	-3.2	-2.15	-1.33	-0.99
03:00	-0.33	-0.62	-0.97	-2.2	-3.09	-3.66	-4.44	-4.04	-3.11	-2.11	-1.29	-0.91
02:00	-0.2	-0.46	-0.82	-2.05	-2.92	-3.48	-4.27	-3.87	-2.95	-1.98	-1.19	-0.77
01:00	-0.01	-0.26	-0.63	-1.85	-2.71	-3.31	-4.1	-3.67	-2.74	-1.78	-1.04	-0.59



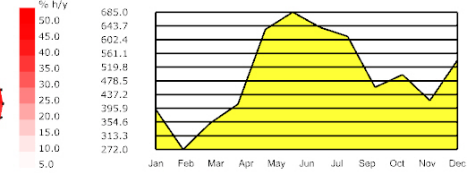
More than UDI (>2000lux)



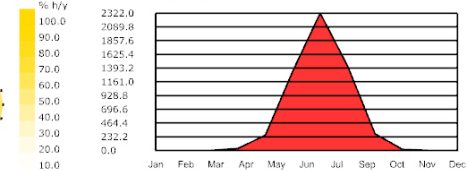
Within UDI



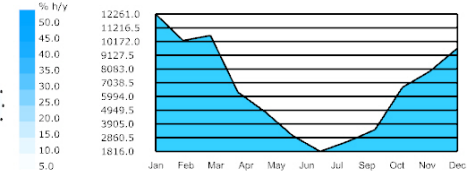
Less than UDI (<300lux)



Lighting loads - Year total: 5911 kW



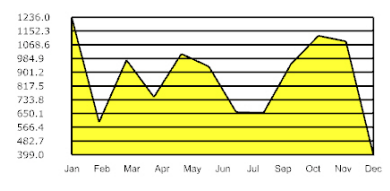
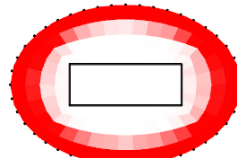
Heating loads - Year total: 5678 kW



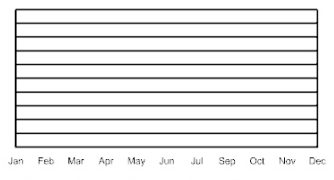
Cooling loads - Year total: 79384 kW

Analysis name: Sim4 dynamic
 Location: Singapore
 PMV result: 9865
 UDI result: 31.9 %

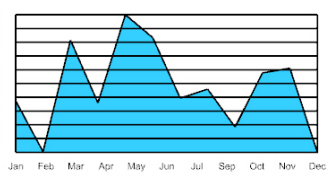
00:00	0.95	1.03	1.16	1.38	1.48	1.48	1.32	1.31	1.15	1.13	0.96	0.91
23:00	1.03	1.07	1.19	1.4	1.51	1.5	1.37	1.36	1.17	1.17	1.02	0.97
22:00	1.12	1.15	1.26	1.46	1.55	1.55	1.41	1.42	1.22	1.21	1.06	1.02
21:00	1.26	1.3	1.4	1.54	1.63	1.69	1.52	1.54	1.28	1.29	1.14	1.11
20:00	1.71	1.8	1.89	1.89	1.91	2.09	1.98	1.92	1.52	1.55	1.42	1.41
19:00	2.89	2.91	3.16	2.95	2.85	3.24	3.22	3.0	2.47	2.4	2.36	2.38
18:00	4.23	4.02	4.56	4.22	4.07	4.74	4.6	4.24	3.69	3.67	3.66	3.6
17:00	4.68	4.47	4.9	4.8	4.57	5.28	4.94	4.39	4.19	4.44	4.33	4.0
16:00	4.95	4.67	4.9	5.01	4.9	5.43	4.99	3.85	4.39	4.79	4.74	4.17
15:00	4.99	4.57	4.69	4.72	4.94	5.25	4.76	3.76	4.16	4.73	4.8	4.21
14:00	4.9	4.52	4.49	4.53	4.87	4.99	4.54	4.18	4.05	4.5	4.75	4.19
13:00	4.92	4.7	4.51	4.69	4.97	4.94	4.51	4.24	4.19	4.54	4.84	4.14
12:00	4.83	4.85	4.56	4.98	5.09	4.87	4.51	4.25	4.33	4.74	4.81	4.03
11:00	4.43	4.55	4.37	4.91	4.9	4.51	4.35	3.96	4.2	4.66	4.41	3.78
10:00	3.73	3.93	3.77	4.37	4.29	3.95	3.89	3.41	3.77	4.15	3.79	3.34
09:00	2.76	2.84	2.77	3.34	3.32	3.12	2.94	2.57	3.14	3.29	2.94	2.65
08:00	1.62	1.65	1.59	2.0	2.1	1.98	1.81	1.57	1.88	1.99	1.72	1.46
07:00	0.77	0.81	0.9	1.08	1.24	1.24	1.12	0.95	0.86	0.98	0.81	0.65
06:00	0.72	0.82	0.93	1.08	1.22	1.28	1.1	1.02	0.91	0.96	0.78	0.65
05:00	0.74	0.88	0.95	1.13	1.24	1.31	1.12	1.04	0.96	0.98	0.8	0.67
04:00	0.77	0.91	0.99	1.16	1.29	1.35	1.16	1.08	0.98	1.02	0.85	0.72
03:00	0.8	0.95	1.03	1.19	1.33	1.38	1.21	1.08	1.02	1.05	0.9	0.76
02:00	0.84	1.01	1.06	1.26	1.37	1.43	1.25	1.12	1.08	1.08	0.93	0.79
01:00	0.87	1.04	1.11	1.32	1.4	1.49	1.3	1.18	1.11	1.11	0.97	0.83
	Jan	Feb	Mar	Apr	May	Jun	Jul	Aug	Sep	Oct	Nov	Dec



Lighting loads - Year total: 10381 kW



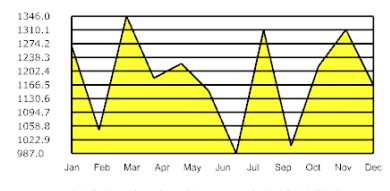
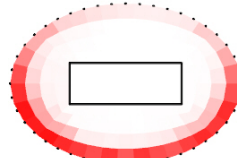
Heating loads - Year total: 0 kW



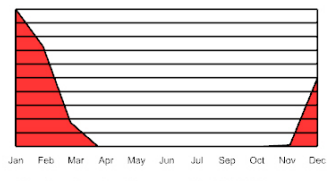
Cooling loads - Year total: 217731 kW

Analysis name: Sim4 dynamic
 Location: Abu Dhabi
 PMV result: 9650
 UDI result: 0.0 %

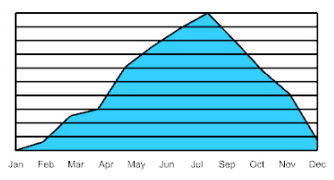
00:00	-1.72	-1.38	-0.66	0.45	1.3	1.98	2.66	2.63	2.14	0.97	0.06	-1.16
23:00	-1.53	-1.17	-0.49	0.6	1.53	2.16	2.85	2.79	2.3	1.17	0.22	-0.98
22:00	-1.34	-0.92	-0.29	0.75	1.75	2.36	3.04	2.97	2.49	1.36	0.34	-0.82
21:00	-1.12	-0.6	-0.07	0.98	2.03	2.64	3.31	3.25	2.71	1.56	0.53	-0.63
20:00	-0.73	-0.05	0.39	1.41	2.57	3.25	3.81	3.75	3.09	1.93	0.9	-0.27
19:00	0.35	1.35	1.78	2.68	4.06	4.81	4.9	5.09	4.12	2.78	1.76	0.65
18:00	1.92	3.43	3.33	4.11	5.69	6.34	6.12	6.64	5.58	4.03	2.93	1.94
17:00	2.33	3.89	3.22	4.06	5.41	6.03	6.11	6.58	5.94	4.66	3.59	2.6
16:00	2.64	3.16	3.28	4.2	5.4	6.09	6.63	6.7	6.25	5.22	4.09	2.99
15:00	2.8	3.13	3.24	4.22	5.21	5.82	6.37	6.53	6.18	5.42	4.3	3.18
14:00	2.83	3.02	3.07	4.13	4.97	5.48	6.0	6.21	5.97	5.33	4.3	3.26
13:00	2.69	2.85	2.94	3.95	4.83	5.23	5.75	5.93	5.72	5.26	4.23	3.17
12:00	2.42	2.58	2.81	3.81	4.78	5.14	5.7	5.74	5.42	5.01	4.1	2.87
11:00	1.98	2.17	2.55	3.62	4.7	5.09	5.63	5.55	5.15	4.56	3.71	2.41
10:00	1.51	1.91	2.16	3.28	4.5	4.89	5.29	5.21	4.73	4.1	3.07	1.79
09:00	0.86	1.47	1.65	2.88	4.1	4.31	4.59	4.65	4.16	3.44	2.34	1.0
08:00	-0.16	-0.63	0.59	1.91	3.16	3.15	3.45	3.64	3.22	2.15	1.09	-0.34
07:00	-2.54	-2.26	-1.13	-0.11	1.12	1.88	2.29	1.88	1.47	0.19	-0.76	-1.83
06:00	-2.48	-2.15	-1.17	-0.3	0.52	1.31	1.96	1.69	1.35	0.1	-0.81	-1.75
05:00	-2.4	-2.0	-1.11	-0.23	0.53	1.31	2.01	1.79	1.46	0.23	-0.69	-1.65
04:00	-2.25	-1.92	-1.05	-0.13	0.64	1.42	2.09	1.94	1.59	0.4	-0.53	-1.59
03:00	-2.08	-1.81	-0.97	-0.02	0.78	1.54	2.22	2.13	1.7	0.58	-0.39	-1.51
02:00	-1.95	-1.68	-0.89	0.11	0.9	1.71	2.37	2.28	1.84	0.72	-0.25	-1.4
01:00	-1.82	-1.54	-0.79	0.29	1.05	1.87	2.53	2.4	2.0	0.84	-0.07	-1.27
	Jan	Feb	Mar	Apr	May	Jun	Jul	Aug	Sep	Oct	Nov	Dec



Lighting loads - Year total: 14214 kW



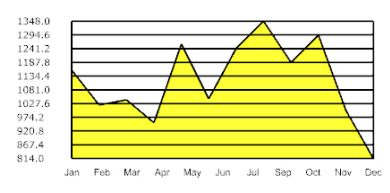
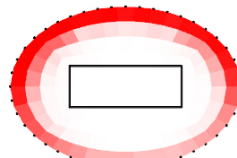
Heating loads - Year total: 248 kW



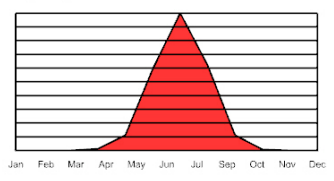
Cooling loads - Year total: 147623 kW

Analysis name: Sim4 dynamic
 Location: Brisbane
 PMV result: 5696
 UDI result: 0.0 %

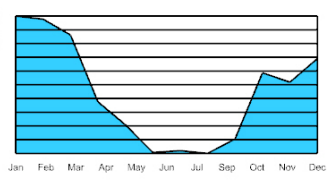
00:00	0.11	-0.09	-0.44	-1.42	-2.58	-3.18	-4.03	-3.29	-2.57	-1.33	-0.95	-0.53
23:00	0.28	0.12	-0.25	-1.19	-2.32	-3.0	-3.81	-2.99	-2.32	-1.07	-0.77	-0.34
22:00	0.46	0.31	-0.07	-0.97	-2.03	-2.8	-3.54	-2.7	-2.08	-0.81	-0.58	-0.14
21:00	0.75	0.55	0.14	-0.74	-1.7	-2.57	-3.14	-2.4	-1.78	-0.51	-0.31	0.11
20:00	1.22	0.95	0.5	-0.34	-1.17	-2.13	-2.51	-1.9	-1.31	-0.07	0.1	0.51
19:00	2.34	1.92	1.37	0.55	-0.11	-1.06	-1.28	-0.8	-0.32	0.88	0.97	1.48
18:00	3.66	3.41	2.66	1.8	1.13	0.19	0.21	0.55	0.99	2.14	2.09	2.72
17:00	3.86	4.59	3.52	2.67	1.98	1.01	1.38	1.38	1.9	3.29	2.6	3.06
16:00	4.12	5.09	3.48	2.94	2.54	1.82	2.95	1.8	2.27	4.22	2.97	3.34
15:00	4.12	4.99	3.6	3.16	2.88	2.4	3.6	2.06	2.5	4.34	3.05	3.33
14:00	3.95	4.63	3.51	3.13	2.89	2.43	3.48	2.03	2.44	4.01	2.97	3.17
13:00	3.67	4.22	3.27	2.93	2.67	2.18	3.09	1.76	2.19	3.55	2.78	2.92
12:00	3.54	4.09	3.12	2.75	2.39	1.88	2.82	1.41	1.97	3.32	2.64	2.8
11:00	3.41	4.12	2.99	2.53	2.03	1.51	2.14	1.02	1.76	3.26	2.55	2.72
10:00	3.27	4.18	2.87	2.27	1.58	0.96	1.56	0.55	1.52	3.28	2.43	2.68
09:00	2.95	3.83	2.45	1.6	0.75	-0.06	0.41	-0.26	0.94	2.96	2.06	2.51
08:00	2.08	2.71	1.55	0.33	-0.88	-1.91	-1.98	-1.78	-1.07	1.86	1.18	1.74
07:00	0.91	0.86	0.08	-1.52	-2.94	-3.9	-4.58	-3.78	-1.85	-0.03	0.09	0.49
06:00	0.34	-0.54	-1.17	-2.42	-3.99	-4.14	-4.84	-4.36	-3.28	-1.54	-0.64	-0.21
05:00	-0.44	-0.86	-1.23	-2.43	-3.39	-4.07	-4.79	-4.35	-3.37	-2.2	-1.26	-0.91
04:00	-0.43	-0.76	-1.09	-2.31	-3.25	-3.86	-4.63	-4.19	-3.23	-2.18	-1.36	-1.02
03:00	-0.36	-0.65	-0.99	-2.23	-3.12	-3.69	-4.47	-4.07	-3.13	-2.13	-1.32	-0.93
02:00	-0.22	-0.49	-0.85	-2.08	-2.95	-3.51	-4.3	-3.9	-2.98	-2.01	-1.21	-0.8
01:00	-0.04	-0.29	-0.66	-1.88	-2.74	-3.34	-4.13	-3.7	-2.77	-1.81	-1.07	-0.62
	Jan	Feb	Mar	Apr	May	Jun	Jul	Aug	Sep	Oct	Nov	Dec



Lighting loads - Year total: 13365 kW



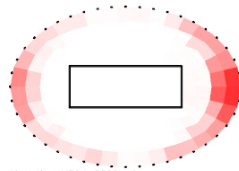
Heating loads - Year total: 5615 kW



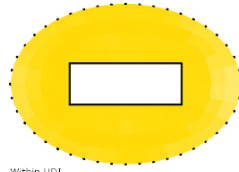
Cooling loads - Year total: 81433 kW

Analysis name: Sim5 Default Eggcrate
Location: Singapore
PMV result: 7375
UDI result: 82.1 %

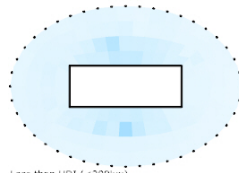
	Jan	Feb	Mar	Apr	May	Jun	Jul	Aug	Sep	Oct	Nov	Dec
00:00	1.02	1.1	1.23	1.44	1.55	1.55	1.4	1.38	1.22	1.2	1.05	0.97
23:00	1.09	1.14	1.26	1.47	1.59	1.57	1.44	1.42	1.24	1.24	1.09	1.03
22:00	1.18	1.21	1.32	1.52	1.62	1.62	1.48	1.48	1.29	1.28	1.13	1.07
21:00	1.29	1.34	1.43	1.59	1.68	1.74	1.55	1.58	1.34	1.35	1.19	1.15
20:00	1.59	1.68	1.76	1.84	1.9	2.02	1.87	1.85	1.5	1.55	1.4	1.36
19:00	2.32	2.45	2.54	2.55	2.57	2.77	2.63	2.54	2.17	2.18	2.05	2.03
18:00	3.1	3.22	3.33	3.33	3.31	3.59	3.38	3.26	2.94	2.95	2.86	2.86
17:00	3.31	3.53	3.54	3.61	3.45	3.73	3.5	3.43	3.15	3.24	3.14	3.11
16:00	3.44	3.71	3.67	3.72	3.58	3.78	3.57	3.56	3.31	3.43	3.29	3.2
15:00	3.51	3.79	3.77	3.8	3.66	3.8	3.58	3.55	3.34	3.49	3.34	3.24
14:00	3.48	3.75	3.77	3.87	3.68	3.79	3.54	3.56	3.36	3.5	3.36	3.25
13:00	3.41	3.61	3.66	3.92	3.69	3.74	3.53	3.54	3.32	3.52	3.42	3.18
12:00	3.28	3.42	3.47	3.82	3.63	3.59	3.48	3.39	3.21	3.48	3.43	3.07
11:00	3.08	3.16	3.28	3.61	3.46	3.36	3.38	3.12	3.07	3.34	3.25	2.91
10:00	2.76	2.78	3.01	3.31	3.2	3.13	3.18	2.86	2.83	3.04	2.92	2.68
09:00	2.39	2.34	2.57	2.87	2.88	2.84	2.82	2.53	2.56	2.68	2.58	2.34
08:00	1.71	1.72	1.82	2.07	2.17	2.12	2.05	1.83	1.83	1.98	1.88	1.61
07:00	0.83	0.88	0.97	1.16	1.31	1.31	1.19	1.02	0.93	1.04	0.88	0.71
06:00	0.79	0.89	1.0	1.16	1.29	1.35	1.17	1.09	0.98	1.02	0.85	0.71
05:00	0.8	0.95	1.03	1.21	1.31	1.38	1.19	1.12	1.03	1.05	0.87	0.74
04:00	0.83	0.98	1.06	1.24	1.36	1.41	1.23	1.14	1.05	1.09	0.91	0.79
03:00	0.87	1.02	1.1	1.27	1.4	1.44	1.28	1.16	1.09	1.12	0.96	0.83
02:00	0.9	1.08	1.15	1.33	1.44	1.5	1.32	1.19	1.15	1.15	1.0	0.86
01:00	0.94	1.11	1.18	1.39	1.47	1.56	1.38	1.25	1.17	1.18	1.04	0.89



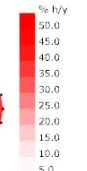
More than UDI (>2000lux)



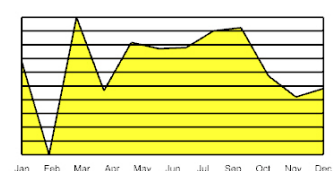
Within UDI



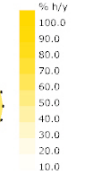
Less than UDI (<300lux)



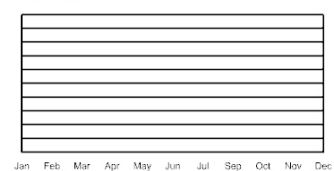
% h/y



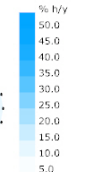
Lighting loads - Year total: 2437 kW



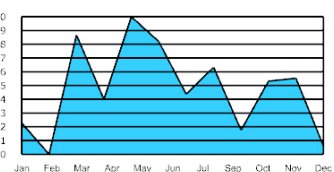
% h/y



Heating loads - Year total: 0 kW



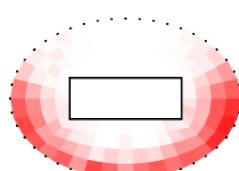
% h/y



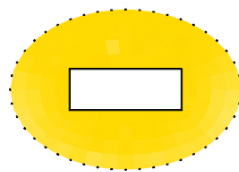
Cooling loads - Year total: 198032 kW

Analysis name: Sim5 Default Eggcrate
Location: Abu Dhabi
PMV result: 8311
UDI result: 77.8 %

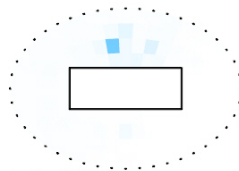
	Jan	Feb	Mar	Apr	May	Jun	Jul	Aug	Sep	Oct	Nov	Dec
00:00	-1.64	-1.3	-0.59	0.53	1.38	2.06	2.75	2.7	2.21	1.05	0.14	-1.09
23:00	-1.46	-1.09	-0.42	0.68	1.61	2.24	2.92	2.86	2.37	1.24	0.3	-0.91
22:00	-1.27	-0.84	-0.22	0.83	1.82	2.44	3.11	3.04	2.56	1.44	0.42	-0.74
21:00	-1.05	-0.53	-0.03	1.04	2.08	2.69	3.38	3.3	2.77	1.66	0.61	-0.56
20:00	-0.68	-0.08	0.34	1.39	2.51	3.17	3.81	3.7	3.11	2.01	0.97	-0.18
19:00	0.27	0.95	1.3	2.26	3.5	4.21	4.7	4.57	3.91	2.78	1.81	0.75
18:00	1.63	2.38	2.5	3.34	4.67	5.37	5.83	5.72	5.02	3.79	2.83	1.92
17:00	2.18	2.79	2.86	3.67	4.89	5.58	6.18	6.12	5.55	4.41	3.46	2.5
16:00	2.35	2.81	2.85	3.76	4.83	5.58	6.17	6.16	5.74	4.74	3.76	2.73
15:00	2.3	2.59	2.72	3.83	4.85	5.54	6.11	6.07	5.58	4.66	3.78	2.79
14:00	2.17	2.29	2.6	3.92	4.93	5.5	6.03	5.93	5.37	4.41	3.62	2.73
13:00	2.0	2.04	2.47	3.76	4.87	5.37	5.85	5.77	5.14	4.24	3.42	2.61
12:00	1.81	1.85	2.23	3.5	4.66	5.11	5.54	5.43	4.76	3.99	3.26	2.37
11:00	1.43	1.53	1.94	3.14	4.28	4.72	5.15	4.94	4.35	3.76	3.03	1.93
10:00	0.76	0.97	1.6	2.79	3.88	4.38	4.74	4.51	4.04	3.47	2.53	1.33
09:00	-0.17	0.19	1.03	2.22	3.33	3.87	4.21	3.88	3.5	2.72	1.76	0.55
08:00	-1.38	-1.01	-0.03	1.07	2.2	2.86	3.23	2.85	2.48	1.37	0.5	-0.61
07:00	-2.47	-2.2	-1.11	-0.15	0.94	1.69	2.2	1.86	1.46	0.21	-0.74	-1.77
06:00	-2.41	-2.09	-1.1	-0.23	0.58	1.36	2.03	1.77	1.42	0.19	-0.74	-1.68
05:00	-2.33	-1.92	-1.04	-0.15	0.61	1.39	2.08	1.86	1.53	0.31	-0.62	-1.57
04:00	-2.18	-1.85	-0.99	-0.05	0.72	1.5	2.17	2.01	1.66	0.48	-0.46	-1.51
03:00	-2.01	-1.74	-0.91	0.05	0.86	1.62	2.3	2.21	1.77	0.66	-0.31	-1.44
02:00	-1.88	-1.6	-0.82	0.19	0.98	1.79	2.45	2.35	1.91	0.8	-0.17	-1.32
01:00	-1.74	-1.46	-0.72	0.36	1.13	1.95	2.6	2.48	2.08	0.92	0.01	-1.2



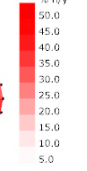
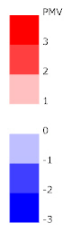
More than UDI (>2000lux)



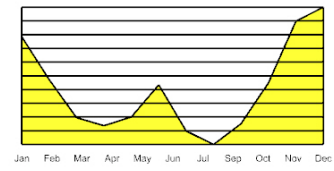
Within UDI



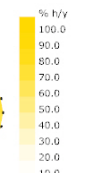
Less than UDI (<300lux)



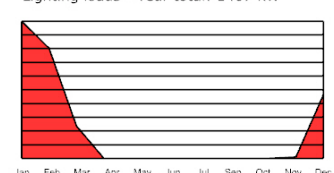
% h/y



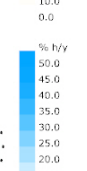
Lighting loads - Year total: 1407 kW



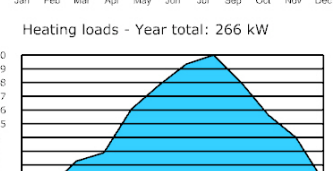
% h/y



Heating loads - Year total: 266 kW



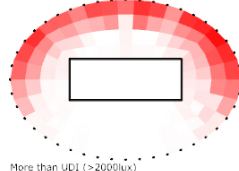
% h/y



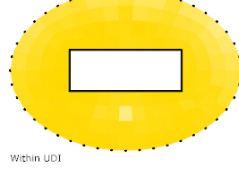
Cooling loads - Year total: 134865 kW

Analysis name: Sim5 Default Eggcrate
Location: Brisbane
PMV result: 4460
UDI result: 70.1 %

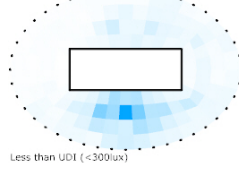
	Jan	Feb	Mar	Apr	May	Jun	Jul	Aug	Sep	Oct	Nov	Dec
00:00	0.17	-0.03	-0.38	-1.37	-2.51	-3.11	-3.96	-3.23	-2.51	-1.27	-0.88	-0.48
23:00	0.34	0.18	-0.19	-1.13	-2.25	-2.94	-3.74	-2.93	-2.26	-1.01	-0.71	-0.29
22:00	0.53	0.37	-0.02	-0.91	-1.96	-2.74	-3.47	-2.63	-2.02	-0.74	-0.51	-0.09
21:00	0.8	0.6	0.19	-0.67	-1.62	-2.5	-3.07	-2.32	-1.71	-0.43	-0.24	0.16
20:00	1.22	0.97	0.55	-0.28	-1.09	-2.03	-2.45	-1.83	-1.23	0.02	0.19	0.54
19:00	2.08	1.78	1.39	0.63	-0.01	-0.93	-1.23	-0.75	-0.18	0.96	1.1	1.4
18:00	3.14	2.76	2.35	1.69	1.16	0.35	0.14	0.45	0.98	1.93	2.07	2.5
17:00	3.81	3.19	2.83	2.26	1.78	1.01	0.8	1.01	1.49	2.33	2.47	2.99
16:00	3.83	3.46	3.19	2.87	2.59	1.93	1.61	1.62	1.98	2.67	2.83	3.21
15:00	3.84	3.48	3.2	2.93	2.83	2.45	1.93	1.75	2.05	2.72	2.92	3.15
14:00	3.8	3.48	3.11	2.76	2.71	2.37	1.79	1.61	1.87	2.61	2.94	3.14
13:00	3.6	3.33	2.97	2.48	2.42	2.07	1.39	1.3	1.59	2.46	2.84	3.0
12:00	3.43	3.15	2.83	2.3	2.08	1.72	0.91	0.98	1.34	2.3	2.7	2.85
11:00	3.17	2.86	2.62	2.12	1.72	1.32	0.42	0.63	1.09	2.02	2.46	2.65
10:00	2.9	2.59	2.46	1.89	1.29	0.83	-0.12	0.24	0.86	1.73	2.16	2.41
09:00	2.55	2.18	2.0	1.31	0.54	-0.08	-0.98	-0.5	0.3	1.29	1.78	2.15
08:00	1.86	1.39	1.03	0.06	-1.03	-1.92	-2.67	-1.96	-0.81	0.44	1.1	1.56
07:00	0.85	0.21	-0.4	-1.76	-2.98	-3.88	-4.58	-3.87	-2.42	-0.83	0.13	0.63
06:00	0.11	-0.6	-1.14	-2.35	-3.32	-4.07	-4.77	-4.28	-3.26	-1.7	-0.47	-0.09
05:00	-0.37	-0.79	-1.17	-2.37	-3.32	-4.0	-4.72	-4.28	-3.31	-2.14	-1.22	-0.88
04:00	-0.97	-0.7	-1.03	-2.25	-3.18	-3.8	-4.56	-4.12	-3.17	-2.12	-1.29	-0.95
03:00	-0.29	-0.59	-0.93	-2.17	-3.05	-3.63	-4.4	-4.01	-3.07	-2.07	-1.25	-0.87
02:00	-0.16	-0.43	-0.79	-2.01	-2.88	-3.45	-4.23	-3.84	-2.91	-1.94	-1.15	-0.73
01:00	0.02	-0.23	-0.6	-1.82	-2.68	-3.28	-4.05	-3.63	-2.71	-1.74	-1.0	-0.56



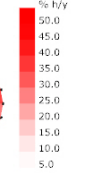
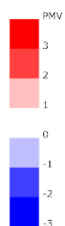
More than UDI (>2000lux)



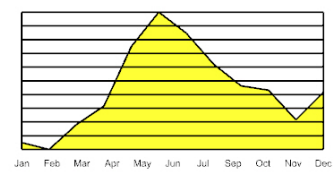
Within UDI



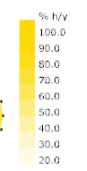
Less than UDI (<300lux)



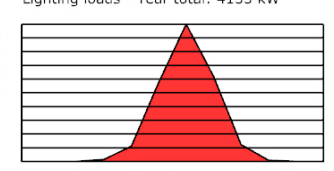
% h/y



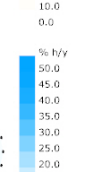
Lighting loads - Year total: 4135 kW



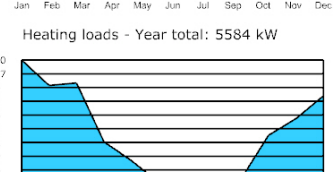
% h/y



Heating loads - Year total: 5584 kW



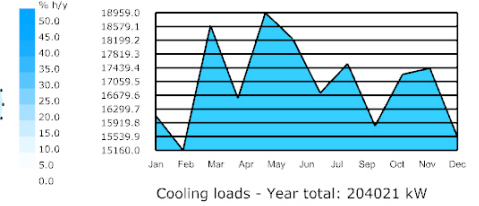
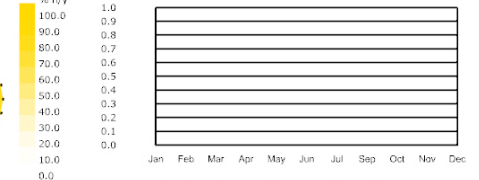
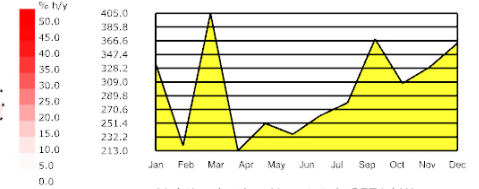
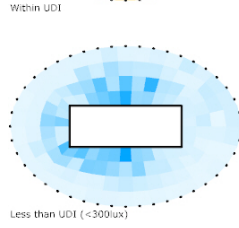
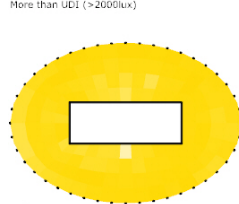
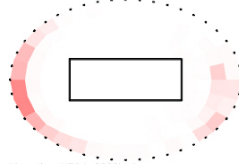
% h/y



Cooling loads - Year total: 70335 kW

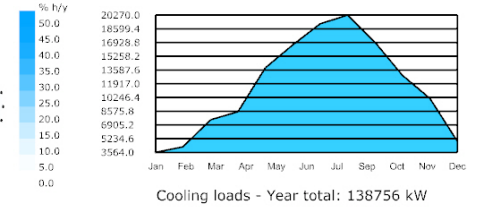
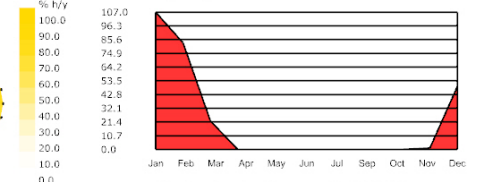
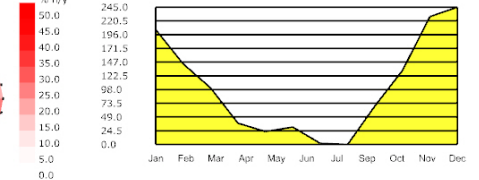
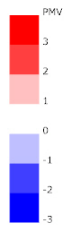
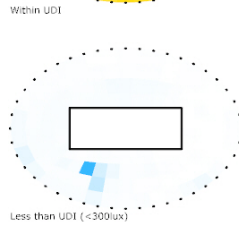
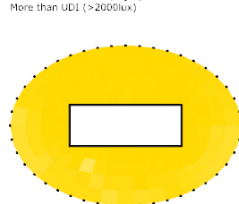
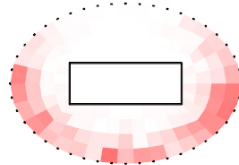
Analysis name: Sim6 Optimised Eggcrate
 Location: Singapore
 PMV result: 8086
 UDI result: 85.0 %

	Jan	Feb	Mar	Apr	May	Jun	Jul	Aug	Sep	Oct	Nov	Dec
00:00	1.01	1.09	1.22	1.43	1.54	1.54	1.39	1.37	1.21	1.19	1.04	0.96
23:00	1.08	1.13	1.25	1.46	1.58	1.56	1.43	1.42	1.23	1.23	1.08	1.03
22:00	1.17	1.21	1.31	1.51	1.61	1.61	1.47	1.47	1.28	1.27	1.12	1.07
21:00	1.3	1.35	1.44	1.58	1.67	1.73	1.55	1.58	1.34	1.35	1.19	1.15
20:00	1.67	1.78	1.84	1.86	1.9	2.02	1.89	1.86	1.55	1.59	1.43	1.42
19:00	2.57	2.73	2.8	2.65	2.62	2.83	2.75	2.58	2.35	2.34	2.21	2.23
18:00	3.48	3.62	3.73	3.57	3.52	3.81	3.64	3.44	3.27	3.25	3.24	3.27
17:00	3.67	3.89	3.9	3.94	3.78	4.08	3.83	3.75	3.5	3.56	3.54	3.55
16:00	3.79	4.06	4.0	4.04	3.89	4.1	3.86	3.86	3.62	3.74	3.62	3.57
15:00	3.84	4.11	4.08	4.1	3.94	4.08	3.84	3.85	3.63	3.8	3.66	3.59
14:00	3.78	4.07	4.09	4.18	3.96	4.05	3.8	3.86	3.65	3.81	3.67	3.59
13:00	3.72	3.91	3.99	4.22	3.95	4.01	3.78	3.82	3.62	3.82	3.73	3.51
12:00	3.6	3.71	3.77	4.1	3.89	3.85	3.72	3.66	3.5	3.77	3.73	3.39
11:00	3.36	3.41	3.53	3.83	3.65	3.56	3.57	3.35	3.32	3.59	3.53	3.22
10:00	3.05	3.06	3.23	3.5	3.37	3.33	3.39	3.08	3.05	3.27	3.23	3.0
09:00	2.6	2.58	2.74	3.02	3.01	3.0	3.01	2.72	2.71	2.85	2.83	2.59
08:00	1.72	1.72	1.82	2.07	2.18	2.13	2.06	1.83	1.86	2.02	1.91	1.63
07:00	0.83	0.87	0.96	1.15	1.3	1.3	1.18	1.01	0.92	1.03	0.87	0.7
06:00	0.78	0.88	0.99	1.15	1.28	1.34	1.16	1.08	0.97	1.01	0.84	0.7
05:00	0.79	0.94	1.02	1.2	1.3	1.37	1.18	1.11	1.02	1.04	0.86	0.73
04:00	0.82	0.97	1.05	1.23	1.35	1.41	1.22	1.13	1.04	1.08	0.9	0.78
03:00	0.86	1.01	1.09	1.26	1.39	1.43	1.27	1.15	1.08	1.11	0.95	0.82
02:00	0.89	1.07	1.14	1.32	1.43	1.49	1.31	1.18	1.14	1.14	0.99	0.85
01:00	0.93	1.1	1.17	1.38	1.46	1.55	1.37	1.24	1.16	1.17	1.03	0.88



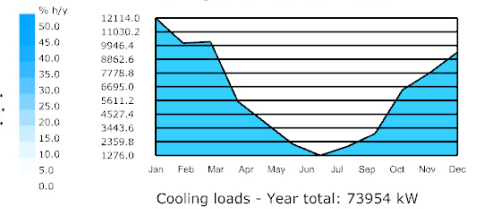
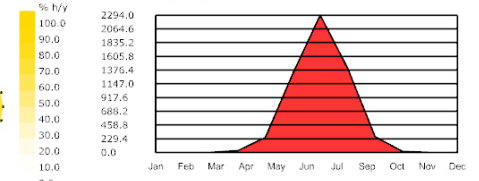
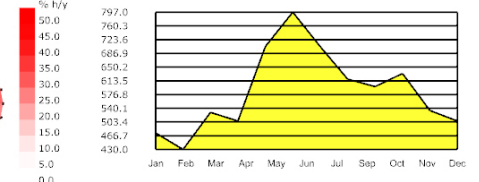
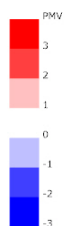
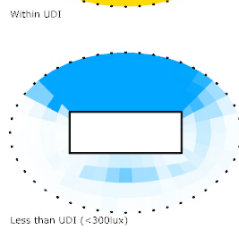
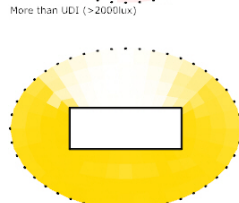
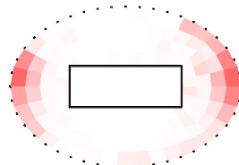
Analysis name: Sim6 Optimised Eggcrate
 Location: Abu Dhabi
 PMV result: 8791
 UDI result: 89.6 %

	Jan	Feb	Mar	Apr	May	Jun	Jul	Aug	Sep	Oct	Nov	Dec
00:00	-1.65	-1.31	-0.6	0.52	1.37	2.05	2.74	2.69	2.2	1.04	0.13	-1.1
23:00	-1.47	-1.1	-0.43	0.67	1.6	2.23	2.91	2.85	2.36	1.24	0.29	-0.92
22:00	-1.28	-0.85	-0.23	0.81	1.81	2.42	3.1	3.03	2.55	1.43	0.41	-0.75
21:00	-1.06	-0.55	-0.03	1.03	2.08	2.68	3.38	3.3	2.76	1.65	0.6	-0.57
20:00	-0.68	-0.07	0.37	1.4	2.52	3.18	3.83	3.71	3.12	2.0	0.96	-0.19
19:00	0.33	1.05	1.42	2.32	3.66	4.3	4.79	4.62	3.98	2.79	1.82	0.75
18:00	1.77	2.61	2.75	3.5	4.87	5.6	6.06	5.89	5.23	3.9	2.91	2.0
17:00	2.39	3.04	3.08	3.91	5.2	5.92	6.51	6.43	5.82	4.65	3.67	2.71
16:00	2.55	3.0	3.06	4.0	5.11	5.86	6.48	6.44	5.99	4.98	3.98	2.93
15:00	2.42	2.72	2.95	4.1	5.13	5.77	6.39	6.38	5.84	4.86	3.94	2.95
14:00	2.23	2.39	2.84	4.19	5.23	5.72	6.28	6.25	5.64	4.62	3.71	2.81
13:00	2.01	2.11	2.7	4.03	5.19	5.6	6.11	6.07	5.41	4.44	3.45	2.63
12:00	1.79	1.88	2.44	3.75	4.96	5.35	5.82	5.71	5.01	4.14	3.25	2.34
11:00	1.42	1.56	2.09	3.36	4.53	4.96	5.43	5.18	4.54	3.63	3.01	1.9
10:00	0.8	1.04	1.74	2.95	4.1	4.63	4.99	4.71	4.18	3.53	2.56	1.34
09:00	-0.1	0.29	1.19	2.41	3.55	4.13	4.44	4.07	3.65	2.86	1.85	0.6
08:00	-1.36	-0.97	0.07	1.19	2.39	3.08	3.38	2.97	2.58	1.49	0.58	-0.59
07:00	-2.48	-2.21	-1.11	-0.12	1.02	1.78	2.25	1.88	1.48	0.21	-0.74	-1.78
06:00	-2.42	-2.1	-1.11	-0.24	0.58	1.36	2.02	1.76	1.42	0.17	-0.75	-1.69
05:00	-2.34	-1.93	-1.05	-0.16	0.6	1.38	2.07	1.85	1.52	0.3	-0.63	-1.58
04:00	-2.18	-1.86	-1.0	-0.06	0.71	1.49	2.16	2.0	1.65	0.47	-0.47	-1.52
03:00	-2.02	-1.75	-0.91	0.04	0.85	1.61	2.29	2.2	1.76	0.65	-0.32	-1.45
02:00	-1.89	-1.61	-0.83	0.18	0.97	1.78	2.44	2.34	1.9	0.79	-0.18	-1.33
01:00	-1.75	-1.47	-0.72	0.35	1.12	1.94	2.59	2.47	2.07	0.91	0.0	-1.21



Analysis name: Sim6 Optimised Eggcrate
 Location: Brisbane
 PMV result: 4856
 UDI result: 54.2 %

	Jan	Feb	Mar	Apr	May	Jun	Jul	Aug	Sep	Oct	Nov	Dec
00:00	0.16	-0.03	-0.38	-1.38	-2.52	-3.12	-3.97	-3.23	-2.52	-1.27	-0.89	-0.48
23:00	0.34	0.17	-0.2	-1.14	-2.26	-2.94	-3.75	-2.94	-2.27	-1.02	-0.71	-0.29
22:00	0.52	0.36	-0.02	-0.91	-1.97	-2.74	-3.48	-2.64	-2.02	-0.75	-0.52	-0.09
21:00	0.8	0.6	0.19	-0.68	-1.63	-2.5	-3.07	-2.33	-1.72	-0.44	-0.25	0.16
20:00	1.25	0.97	0.55	-0.29	-1.11	-2.03	-2.45	-1.83	-1.23	0.01	0.18	0.56
19:00	2.24	1.83	1.39	0.63	-0.02	-0.93	-1.2	-0.74	-0.18	0.97	1.1	1.49
18:00	3.56	2.97	2.49	1.8	1.19	0.38	0.18	0.51	1.08	2.06	2.22	2.79
17:00	4.17	3.63	3.18	2.49	1.9	1.11	0.91	1.14	1.74	2.67	2.88	3.55
16:00	4.38	3.91	3.56	3.04	2.64	1.89	1.64	1.67	2.27	3.1	3.31	3.78
15:00	4.28	3.89	3.52	3.03	2.67	2.09	1.66	1.72	2.31	3.11	3.35	3.6
14:00	4.14	3.8	3.39	2.81	2.42	1.84	1.32	1.55	2.11	2.95	3.29	3.46
13:00	3.92	3.64	3.22	2.54	2.08	1.44	0.9	1.29	1.81	2.74	3.18	3.32
12:00	3.73	3.45	3.08	2.33	1.71	1.04	0.42	0.95	1.53	2.55	3.03	3.16
11:00	3.47	3.16	2.85	2.06	1.32	0.64	-0.1	0.52	1.21	2.28	2.78	2.94
10:00	3.26	2.92	2.67	1.81	0.96	0.27	-0.54	0.09	0.94	2.0	2.52	2.73
09:00	3.02	2.59	2.3	1.31	0.34	-0.4	-1.19	-0.68	0.44	1.62	2.2	2.58
08:00	2.4	1.83	1.39	0.14	-1.04	-1.94	-2.7	-1.93	-0.6	0.81	1.56	2.1
07:00	1.23	0.5	-0.19	-1.69	-2.98	-3.89	-4.58	-3.85	-2.24	-0.51	0.53	1.13
06:00	0.23	-0.55	-1.13	-2.36	-3.33	-4.06	-4.77	-4.29	-3.25	-1.59	-0.26	0.15
05:00	-0.38	-0.8	-1.17	-2.38	-3.33	-4.01	-4.72	-4.29	-3.31	-2.14	-1.22	-0.87
04:00	-0.88	-0.71	-1.03	-2.26	-3.18	-3.8	-4.56	-4.13	-3.17	-2.12	-1.3	-0.96
03:00	-0.3	-0.59	-0.94	-2.17	-3.06	-3.63	-4.41	-4.01	-3.07	-2.08	-1.26	-0.88
02:00	-0.17	-0.43	-0.8	-2.02	-2.88	-3.45	-4.24	-3.85	-2.92	-1.95	-1.16	-0.74
01:00	0.02	-0.23	-0.6	-1.83	-2.68	-3.28	-4.07	-3.64	-2.71	-1.75	-1.01	-0.56



5.2 - Appendix II: GH scripts contemporary workflow

Overview of inputs

Radiance material parameters

- RAD_mat_walls**: Reflectance 0.8
- RAD_mat_floor**: Reflectance 0.4
- RAD_mat_ceiling**: Reflectance 0.7
- RAD_mat_window trims**: Reflectance 0.5
- RAD_mat_inner facade**: Visual transmittance 0.9
- RAD_mat_outer facade**: Visual transmittance 0.8
- RAD_mat_shading**: Visual transmittance 0.5

Energy Plus material parameters

- EP_con_inner glazing**: U-value 1, g-value inner glazing 0.7, g-value outer glazing 0.7
- EP_mat_inner glazing**
- EP_con_walls**: R-value 5
- EP_mat_walls**
- EP_con_window trims**: R-value 1
- EP_mat_window trims**
- EP_con_floor**: R-value 5
- EP_mat_floor**
- EP_con_ceiling**: R-value 5
- EP_mat_ceiling**

General building input

- Enable Perimeter optimization mode: False
- Perimeter curve:
- Core curve:
- Desired panel width: 2050
- Offset: 27
- Start parameter: 0.00
- Floor height: 3200
- Window trim width: 50
- Total cavity width: 500

General Shading Input

- Amount Vertical: 4
- Amount Horizontal: 8
- Gaus curve precision: 100
- Cut-off shape selector: Gaus curve

Specific shading input - North

- MF_N_Vert_Shift: 0
- MF_N_Vert_Rot: 0
- MF_N_Hor_Shift: 0
- MF_N_Hor_Rot: 0
- MF_N_Depth: 250
- MF_N_MCurve: 0.80
- MF_N_QCurve: 0.10

Specific shading input - West

- MF_W_Vert_Shift: 0
- MF_W_Vert_Rot: 0
- MF_W_Hor_Shift: 0
- MF_W_Hor_Rot: 0
- MF_W_Depth: 250
- MF_W_MCurve: 0.80
- MF_W_QCurve: 0.10

Specific shading input - South

- MF_S_Vert_Shift: 0
- MF_S_Vert_Rot: 0
- MF_S_Hor_Shift: 0
- MF_S_Hor_Rot: 0
- MF_S_Depth: 250
- MF_S_MCurve: 0.80
- MF_S_QCurve: 0.10

Specific shading input - East

- MF_E_Vert_Shift: 0
- MF_E_Vert_Rot: 0
- MF_E_Hor_Shift: 0
- MF_E_Hor_Rot: 0
- MF_E_Depth: 250
- MF_E_MCurve: 0.80
- MF_E_QCurve: 0.10

HB_Dynamic shading

- RAD_mat_DYN_sh: LTA 0.05, ZTA 0.1
- Include dynamic shading:

Toggles

- Start all: True
- Render DPG images: False
- Include DSF in calculation: False
- Include shading in calculation: False
- Include dynamic shading: False
- Enable HVAC systems: True
- Enable custom analysis grid: True
- Create Schedules: True

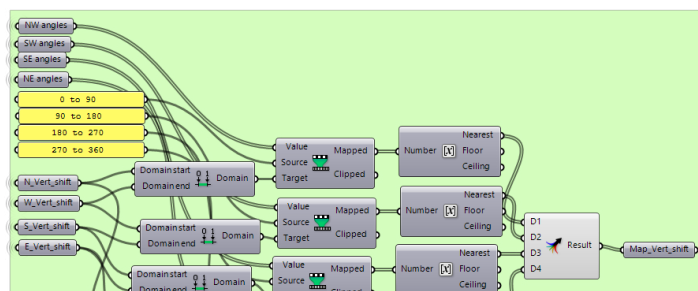
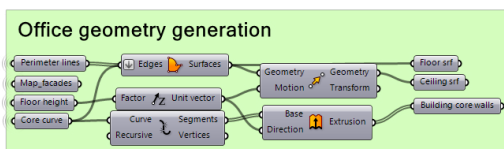
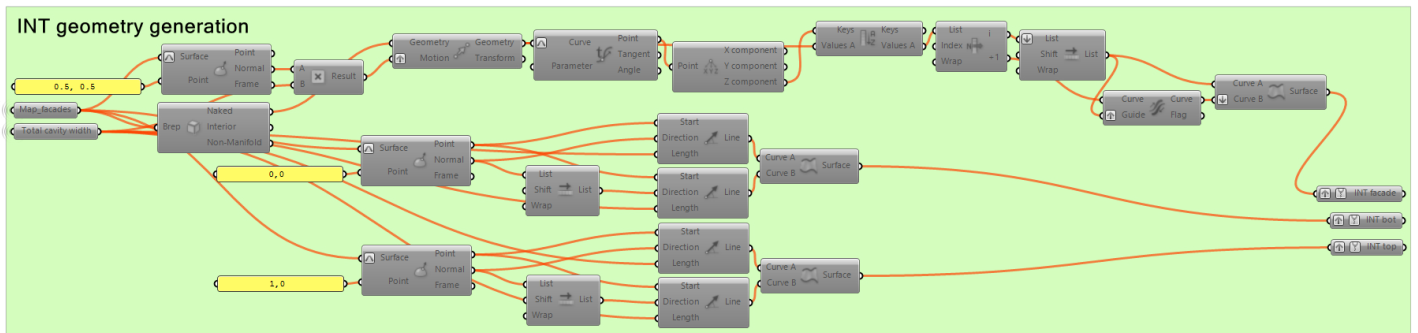
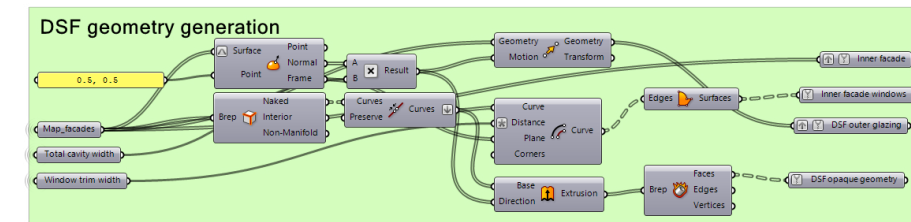
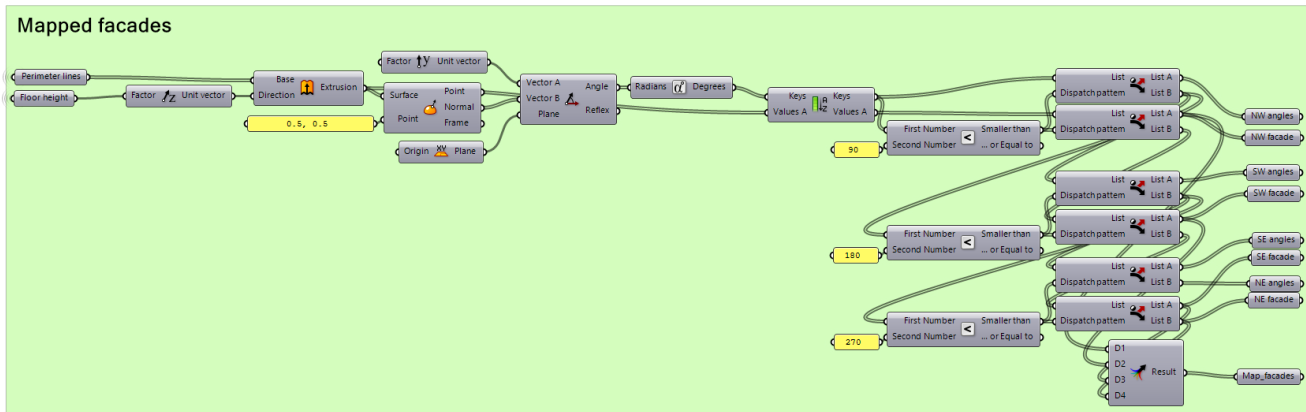
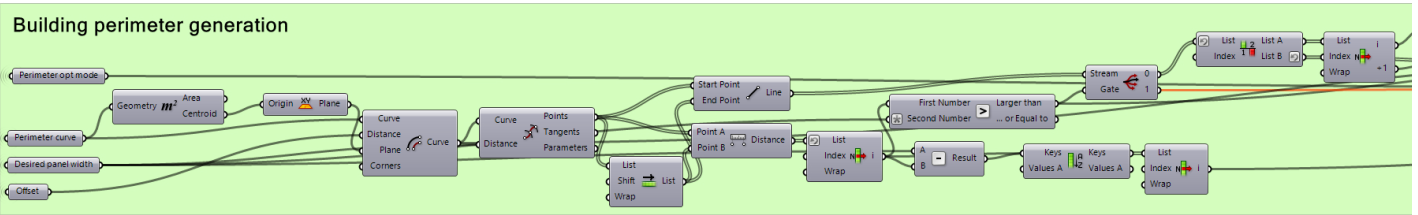
Analysis input

- General**: Analysis name, Analysis center point
- Climate**: EPW file path, True North angle
- Analysis period**: fromMonth, fromDay, fromHour, toMonth, toDay, toHour
- Resolution**: Grid size (mm), Analysis height (mm), Time step

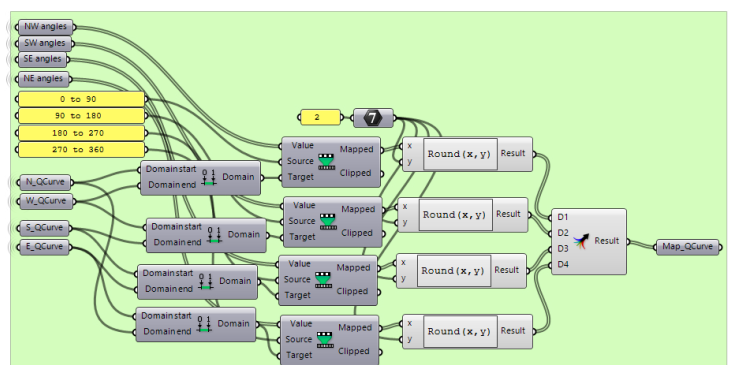
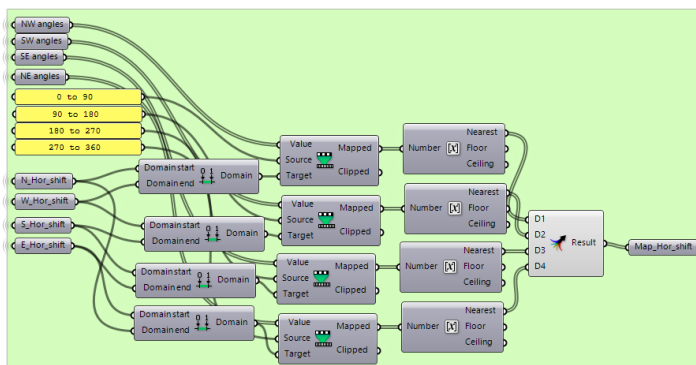
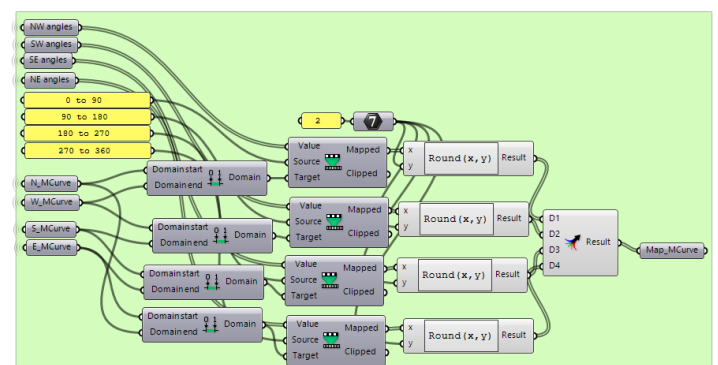
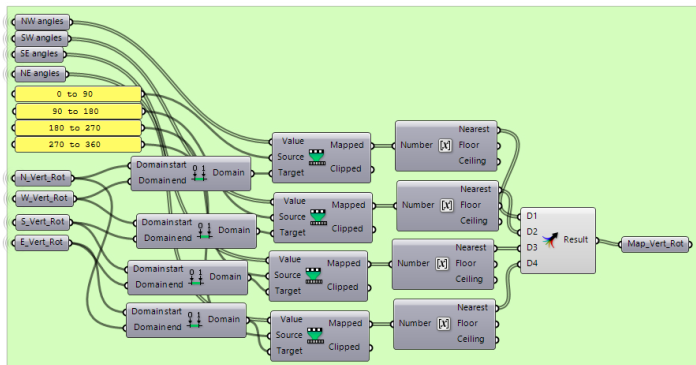
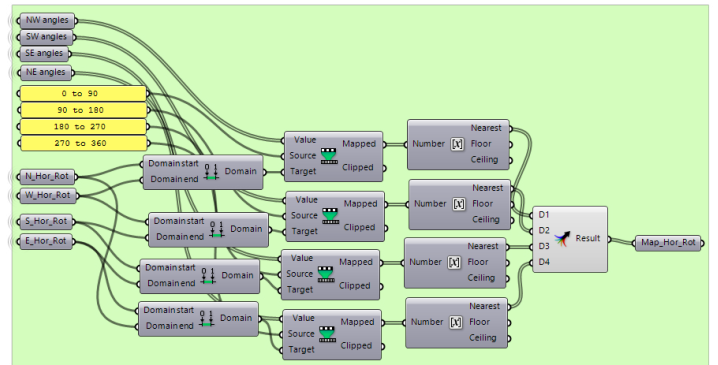
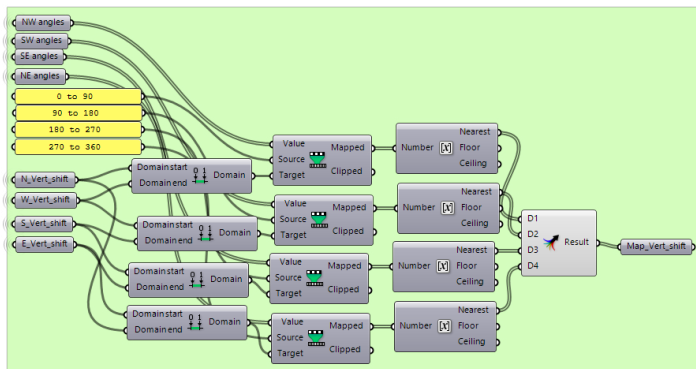
Office Zone input

- Occupancy**: Workhours start [h], Workhours end [h]
- HVAC systems**: Cooling setPt Occupied, Cooling setPt Unoccupied, Heating setPt Occupied, Heating setPt Unoccupied
- Internal loads**: Equipment Load [W/m2], Number of people [pp/m2], Lighting Load [W/m2]
- Ventilation**: Ventilation [m3/s/m2], Recirculation [m3/s/m2]

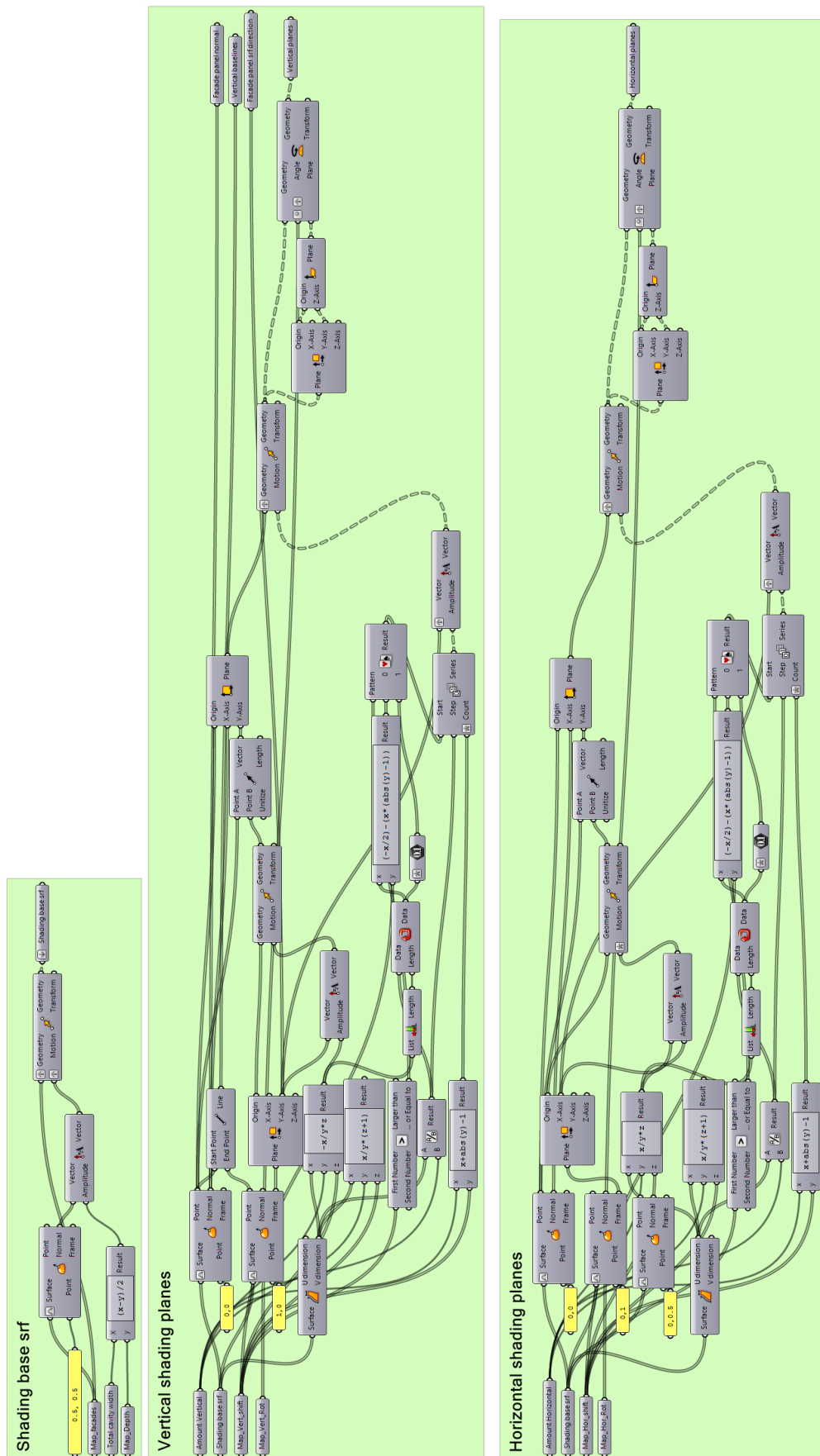
Overview of perimeter optimisation, facade mapping to orientation & geometry generation



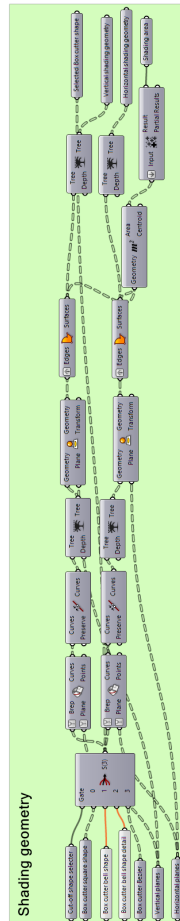
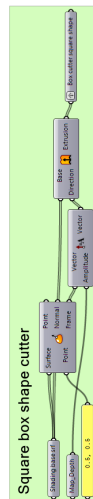
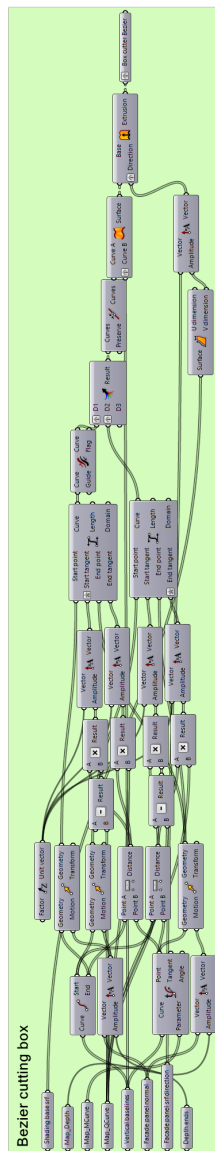
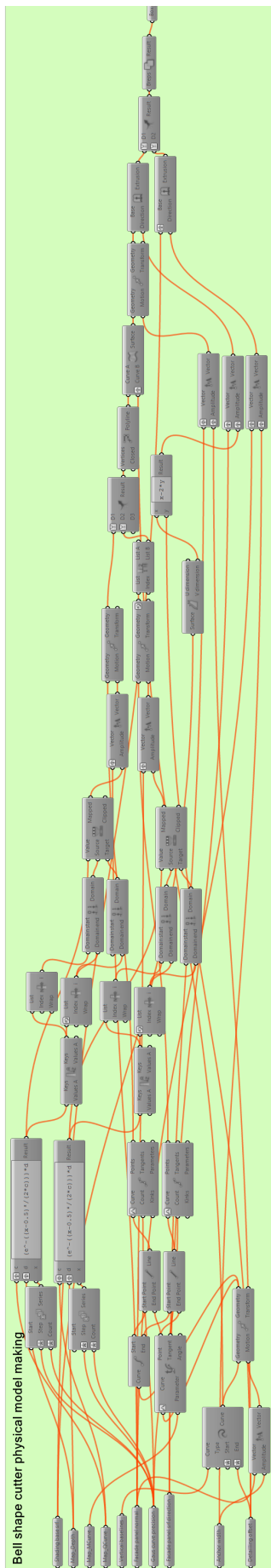
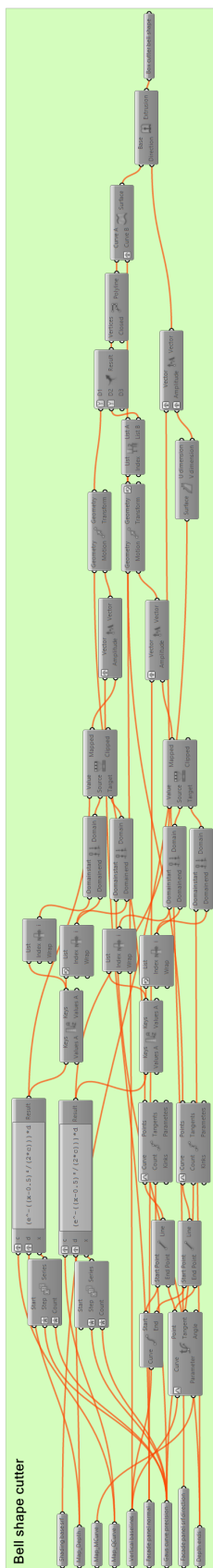
Overview of mapping the input parameters for the interpolation concept



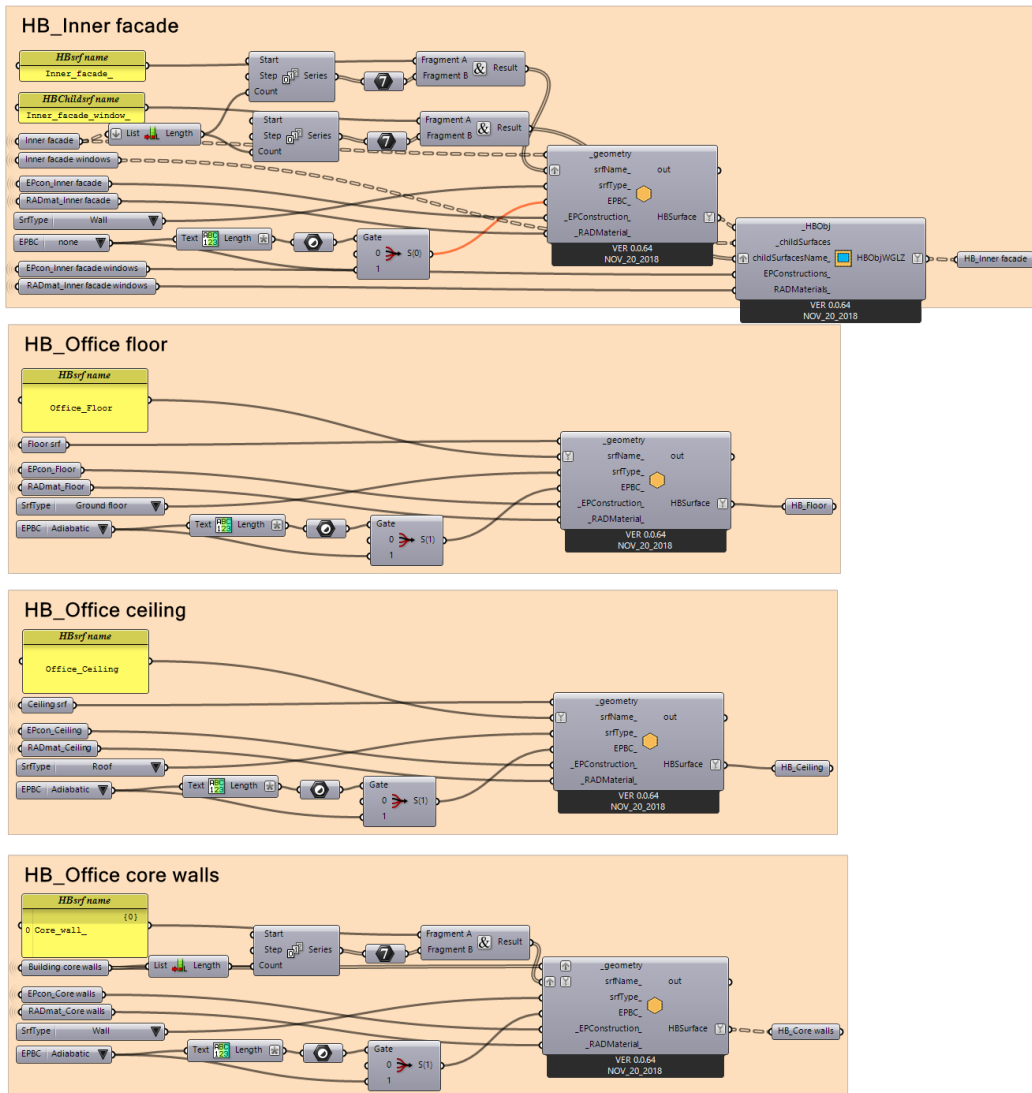
Overview of shading planes generation



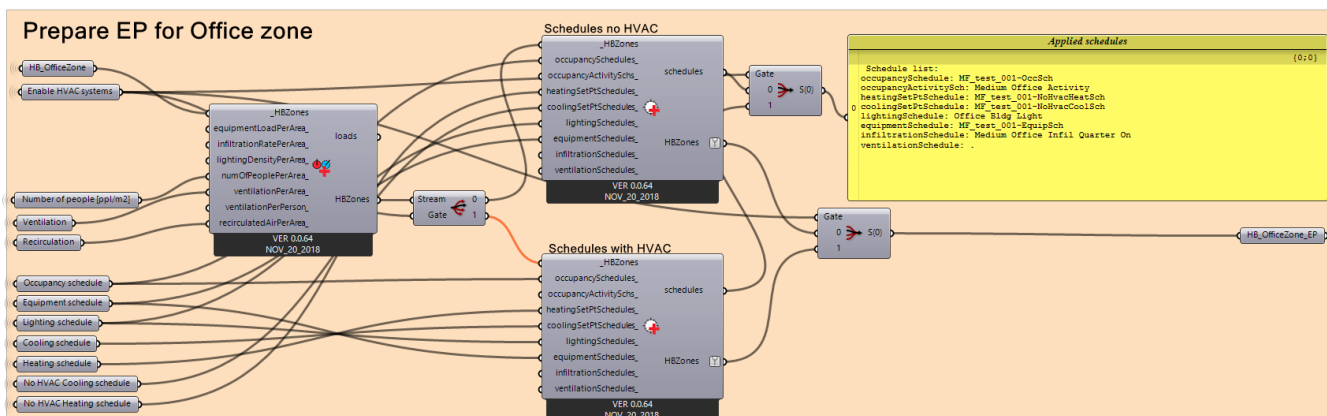
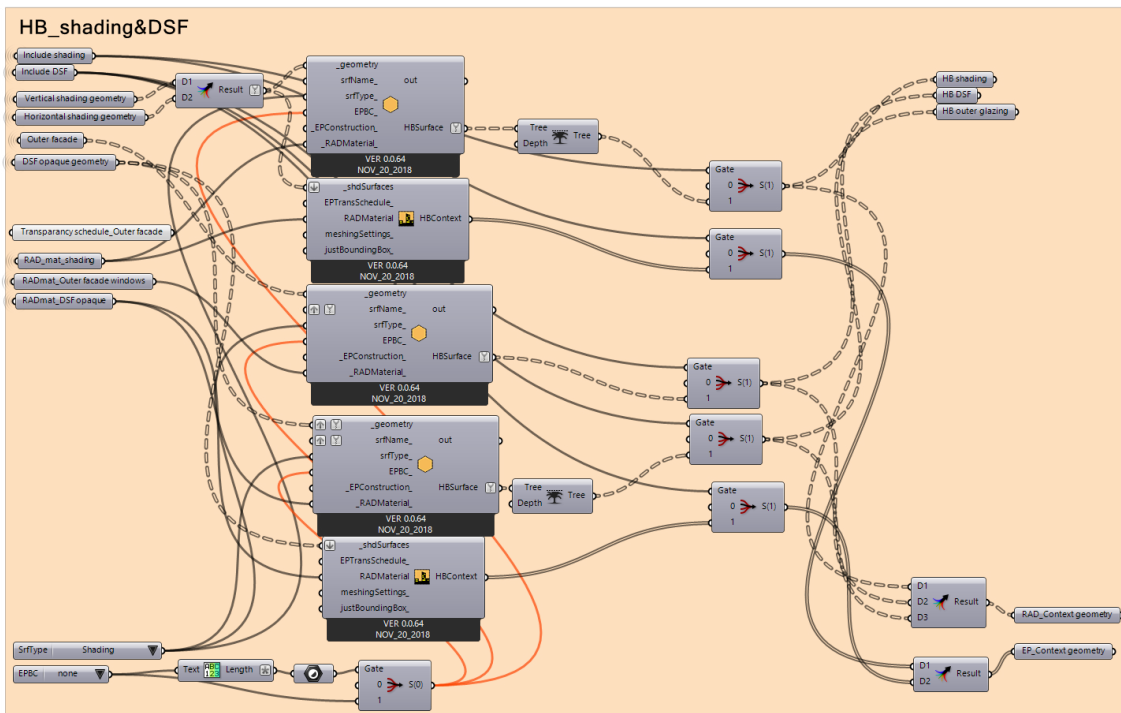
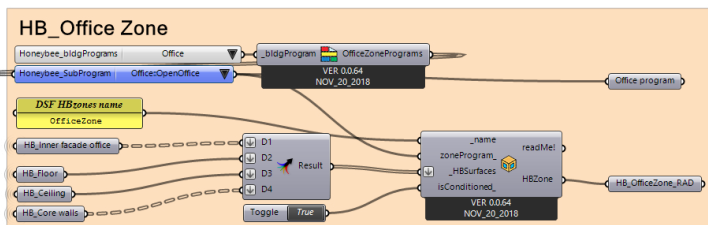
Overview of cutting-box generation and shading geometry



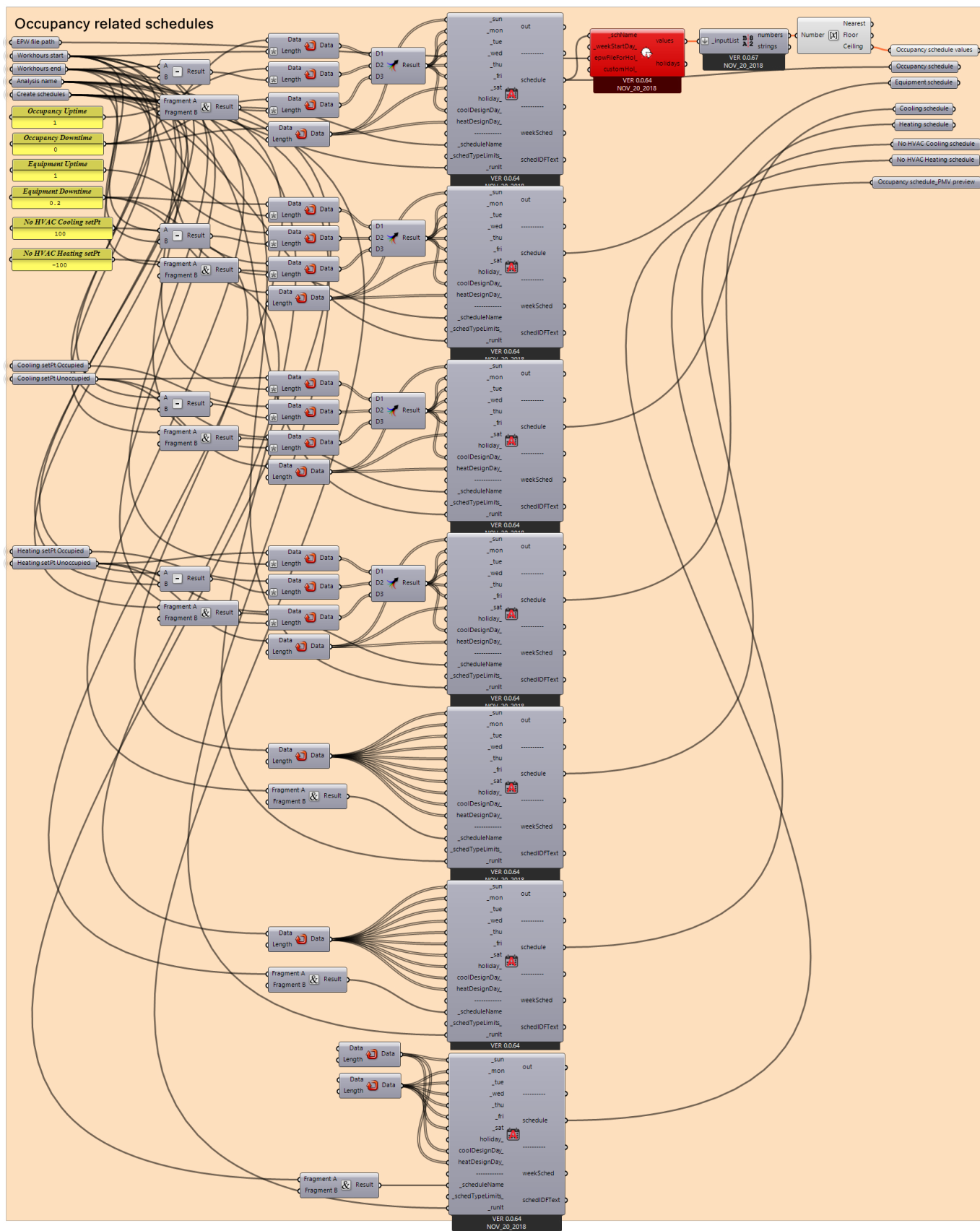
Overview of Honeybee surface elements



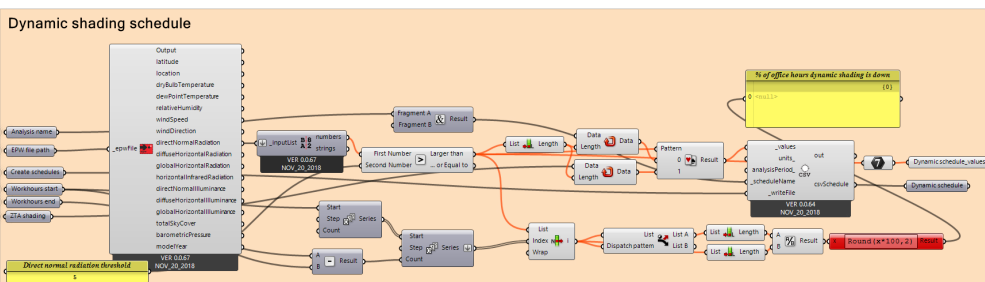
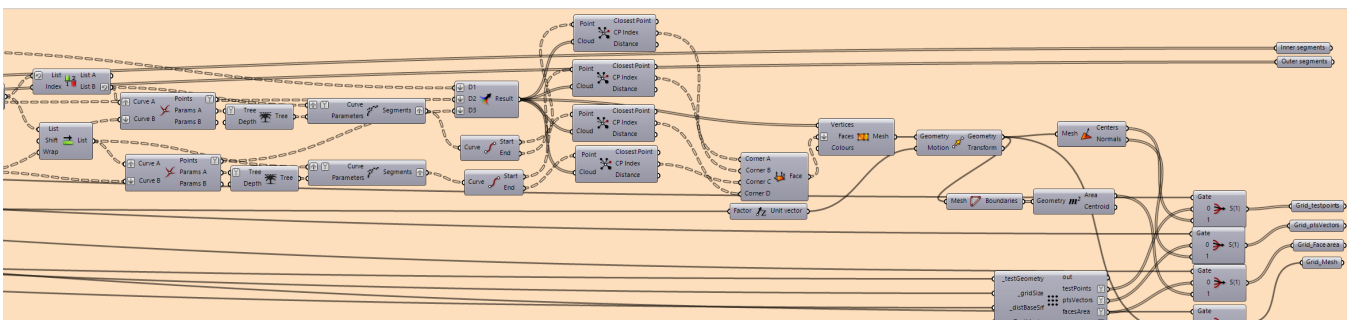
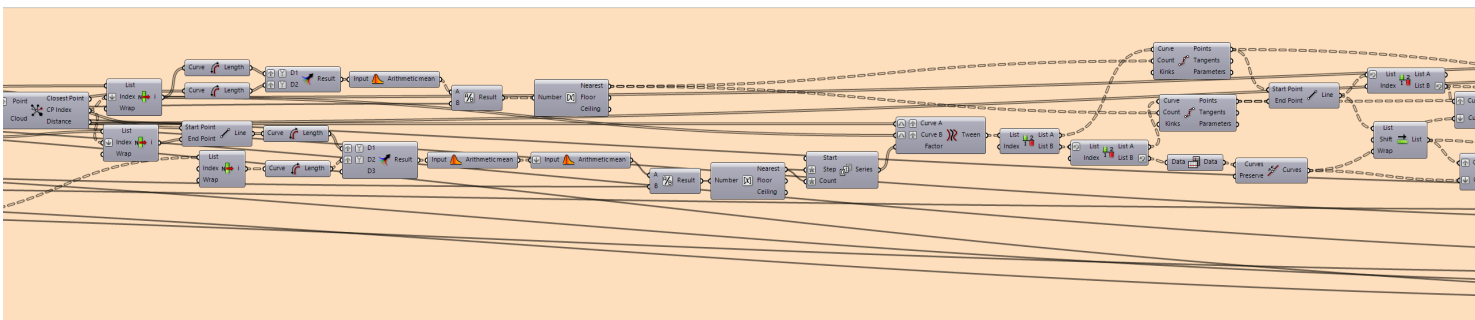
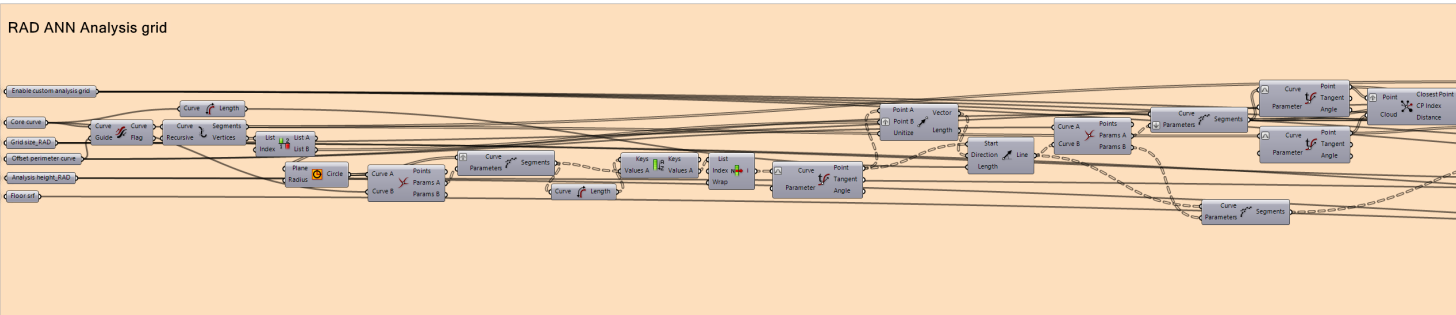
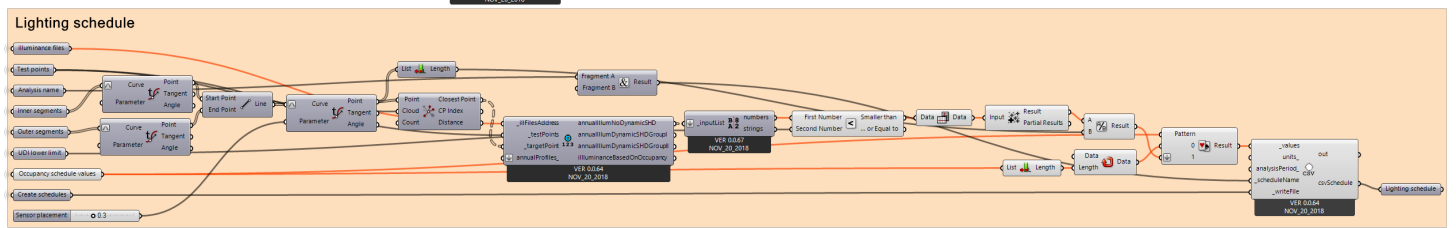
Overview of Honeybee zone and shading preparations



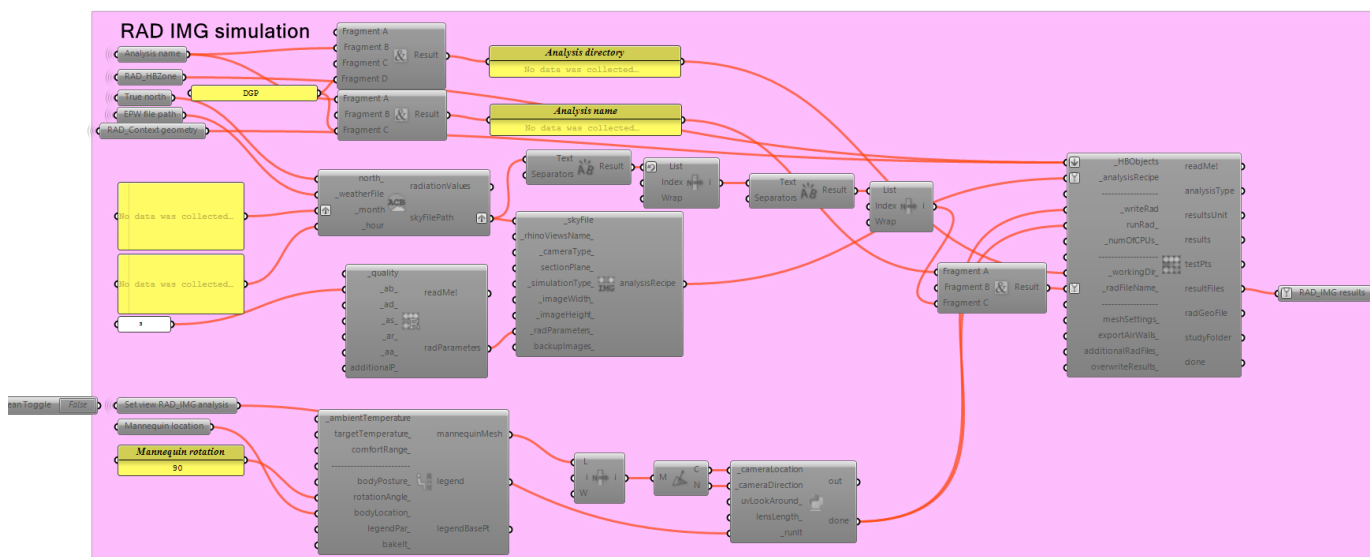
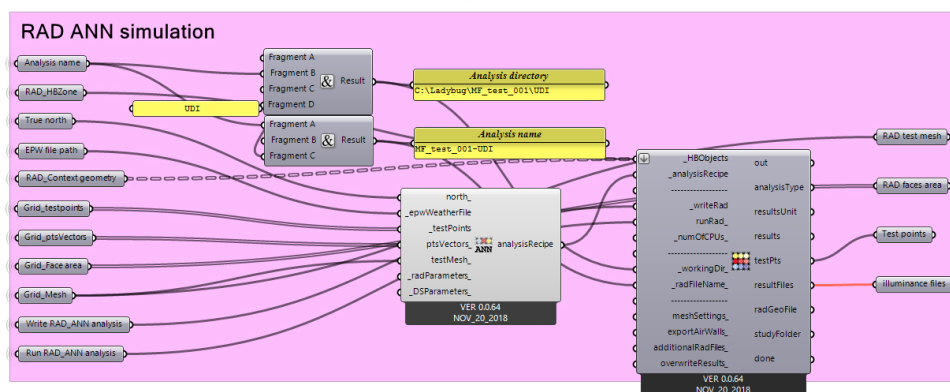
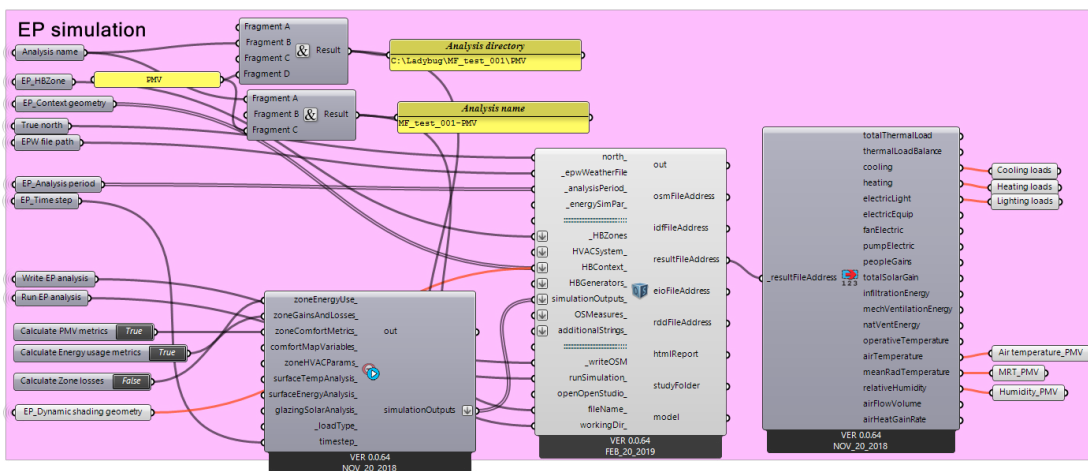
Overview of Honeybee occupancy related schedules



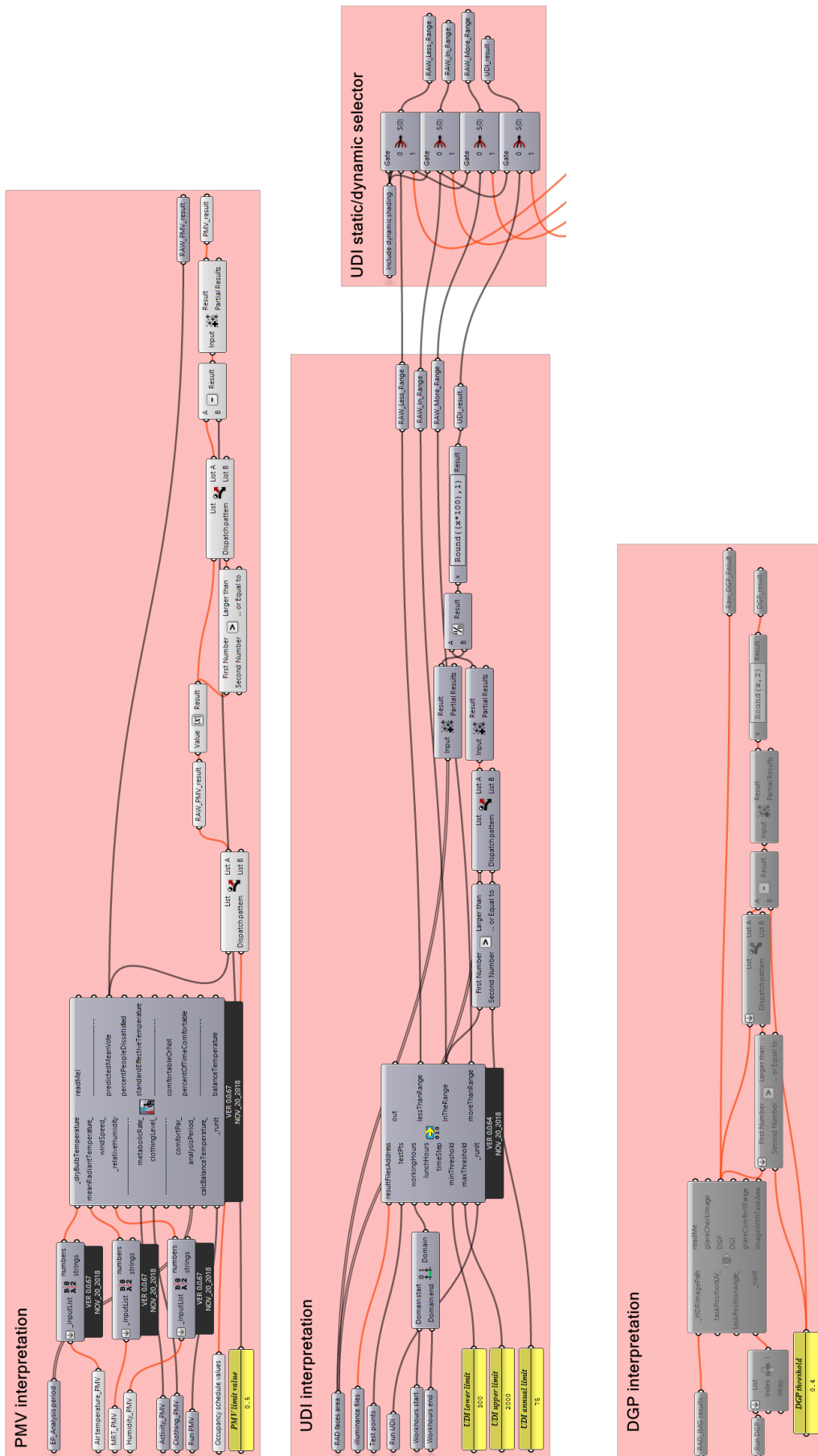
Overview of Honeybee other schedules and custom radiance analysis grid



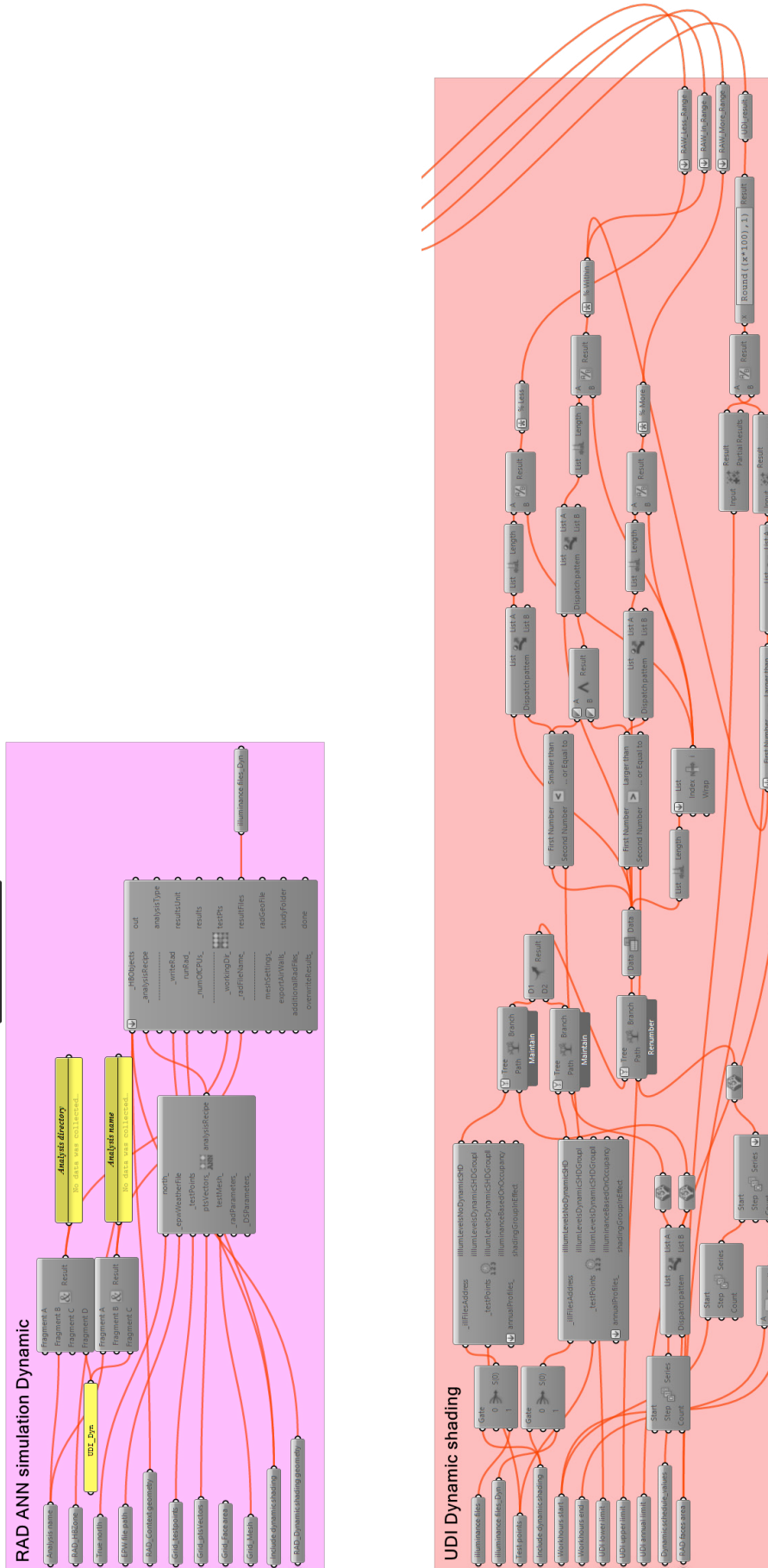
Overview of Energyplus, Daysim and Radiance engines



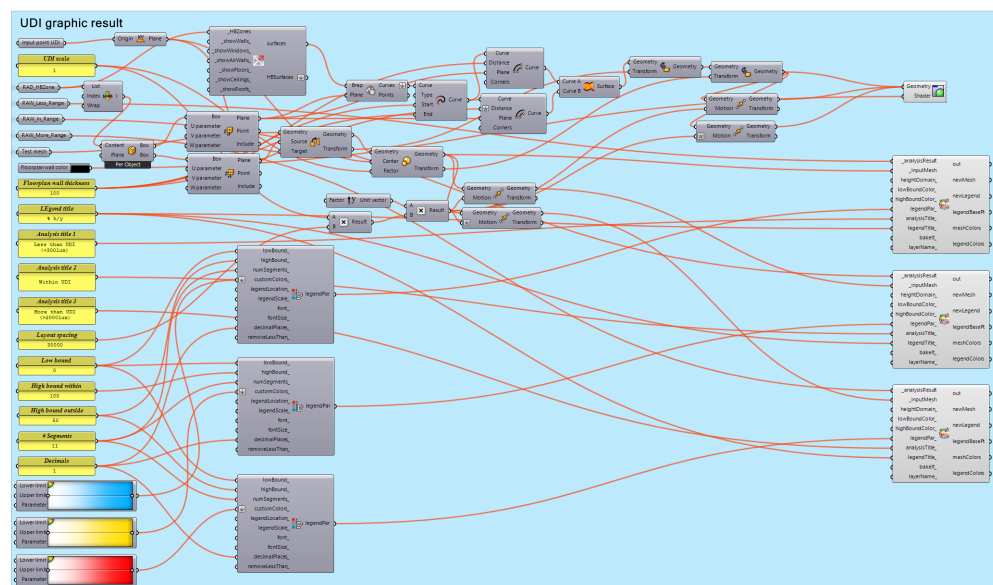
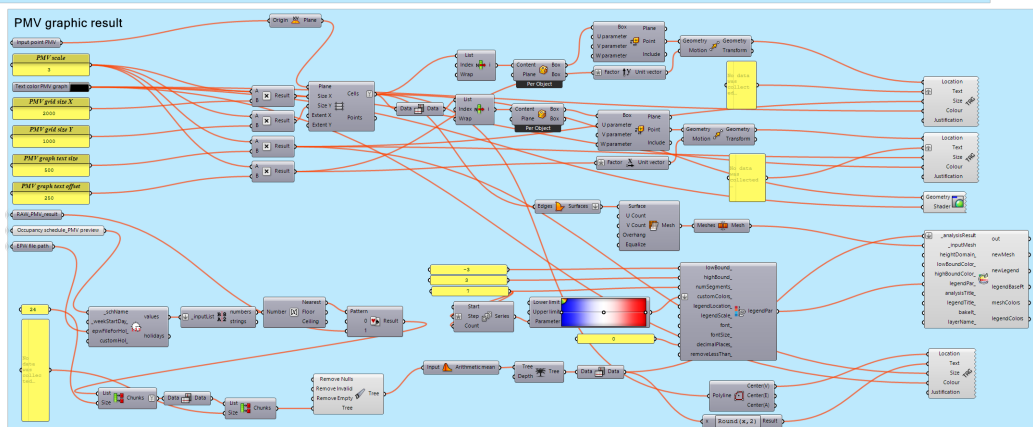
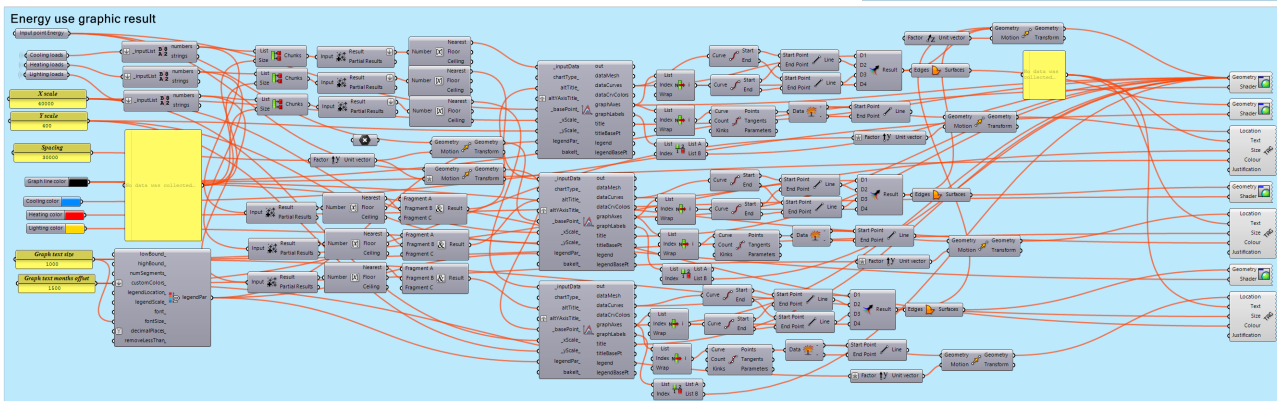
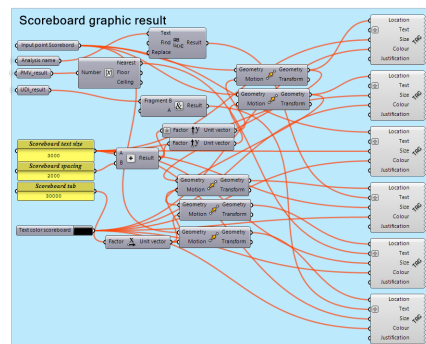
Overview of comfort metric interpretations



Overview of modules for dynamic shading alternatives



Overview of modules for graphic result output



Overview of modules for physical model laser cutting

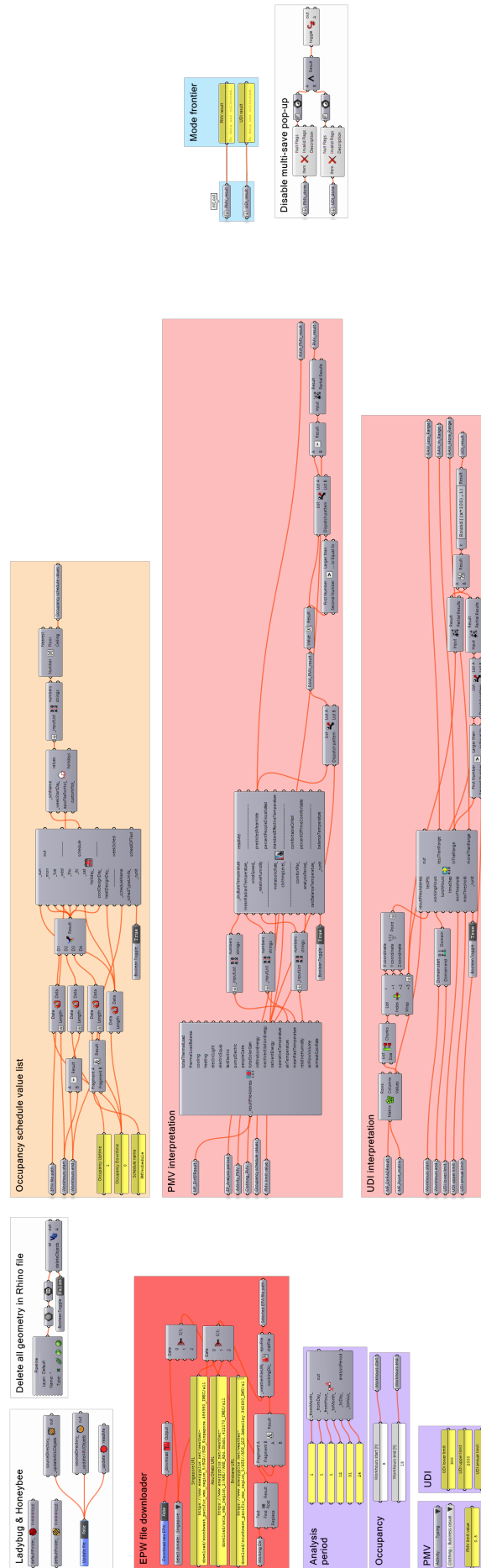


5.3 - Appendix III: GH scripts next generation workflow

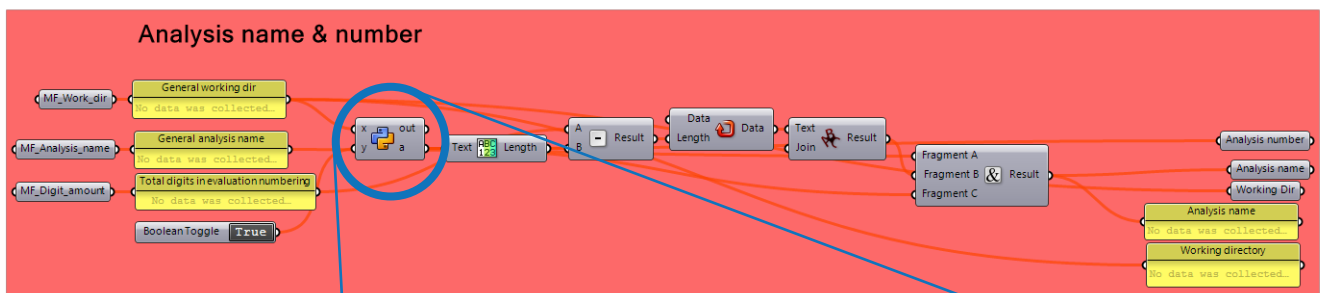
Overview of first Grasshopper script in next generation workflow



Overview of second Grasshopper script in next generation workflow



Analysis numbering (custom node)

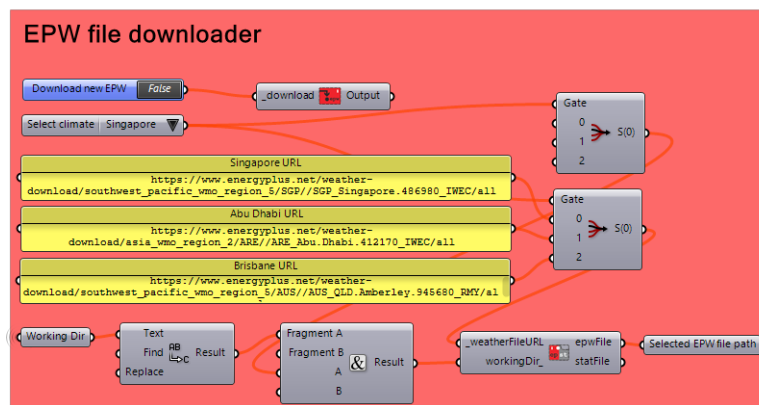


```

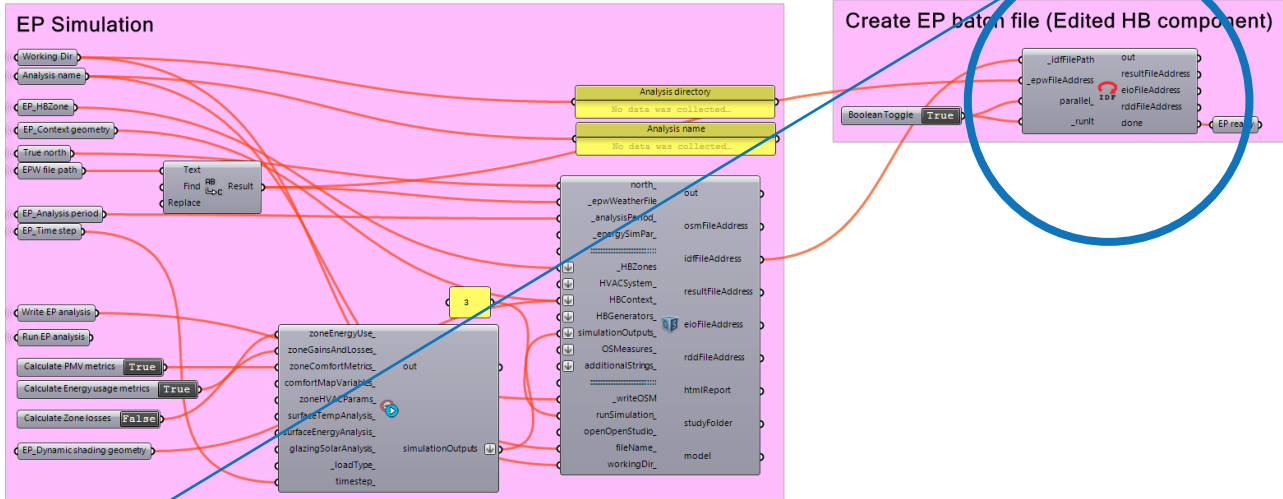
1  """Provides a scripting component.
2  ....Inputs:
3  .....x:Working Directory
4  .....y:Input changer
5  ....Output:
6  .....a:Amount of sub folders"""
7
8  __author__ = "Shane"
9  __version__ = "2019.06.19"
10
11 import rhinoscriptsyntax as rs
12 from os import walk
13
14 path = x
15 f = []
16
17 if y:
18     ....for (dirpath, dirnames, filenames) in walk(path):
19         .....f.extend(dirnames)
20         .....break
21
22 a = len(dirnames)

```

Delocalized EPW file



Preparing the Energyplus batch file (custom node)

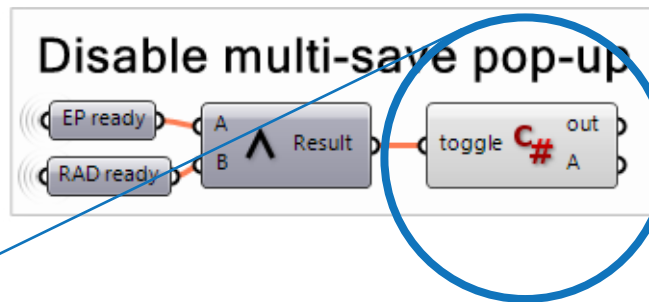


```

183 #Honeybee check.
184 initCheck = True
185 if not sc.sticky.has_key('honeybee_release') == True:
186     ....initCheck = False
187     ....print "You should first let Honeybee fly..."
188     ....ghenv.Component.AddRuntimeMessage(w, "You should first let Honeybee fly...")
189 else:
190     ....try:
191     ....if not sc.sticky['honeybee_release'].isCompatible(ghenv.Component): initCheck = False
192     ....if sc.sticky['honeybee_release'].isInputMissing(ghenv.Component): initCheck = False
193     ....hb_hvacProperties = sc.sticky['honeybee_hvacProperties']()
194     ....hb_airDetail = sc.sticky["honeybee_hvacAirDetails"]
195     ....hb_heatingDetail = sc.sticky["honeybee_hvacHeatingDetails"]
196     ....hb_coolingDetail = sc.sticky["honeybee_hvacCoolingDetails"]
197     ....except:
198     ....initCheck = False
199     ....warning = "You need a newer version of Honeybee to use this component." + \
200     ...."Use updateHoneybee component to update userObjects.\n" + \
201     ...."If you have already updated userObjects drag Honeybee_Honeybee component " + \
202     ...."into canvas and try again."
203     ....ghenv.Component.AddRuntimeMessage(w, warning)
204
205
206 if initCheck and _runIt > 0:
207     ....if len(_idFilePath) == 1:
208     ....epPath = checkTheInputs(_idFilePath[0], _epwFileAddress)
209     ....if epPath != -1:
210     ....workingDir = "\\".join(_idFilePath[0].split('\\')[:-1])
211     ....batchFileAddress, newIDFPath, idfFileName = writeBatchFile(workingDir, _idFilePath[0], _epwFileAddress, epPath)
212     ....print "The file is written to %s"%batchFileAddress
213     ....try:
214     ....os.remove(newIDFPath)
215     ....except:
216     ....pass
217     ....
218     ....print '...'
219     ....print 'RUNNING SIMULATION'
220     ....print '...'
221     ....
222     ....try:
223     ....errorFileFullName = (str(workingDir)+ '\\'+str(idfFileName)).replace('.idf', '.err')
224     ....errFile = open(errorFileFullName, 'r')
225     ....for line in errFile:
226     ....print line
227     ....if "*** Fatal ***" in line:
228     ....warning = "The simulation has failed because of this fatal error: \n" + str(line)
229     ....w = gh.GH_RuntimeMessageLevel.Warning
230     ....ghenv.Component.AddRuntimeMessage(w, warning)
231     ....resultFile = None
232     ....elif "*** Severe ***" in line and 'CheckControllerListOrder' not in line:
233     ....comment = "The simulation has not run correctly because of this severe error: \n" + str(line)
234     ....c = gh.GH_RuntimeMessageLevel.Warning
235     ....ghenv.Component.AddRuntimeMessage(c, comment)
236     ....errFile.close()
237     ....except:
238     ....pass
239     ....
240     ....shIdfFileName = idfFileName.replace('.idf', '')
241     ....resultFileAddress = str(workingDir) + '\\'+str(shIdfFileName) + '.csv'
242     ....eioFileAddress = resultFileAddress.replace('.csv', '.eio')
243     ....rddFileAddress = resultFileAddress.replace('.csv', '.rdd')
244     ....print 'EnergyPlus file '+ str(shIdfFileName)+'.idf' + 're-run successful!'
245     ....done = True
246     ....else:
247     ....resultFileAddress, eioFileAddress, rddFileAddress = runParallelIDFs(_idFilePath, _epwFileAddress, _runIt, parallel_)
248     ....done = False

```

Analysis numbering (custom node)



```
1 using System;
2 using System.Collections;
3 using System.Collections.Generic;
4
5 using Rhino;
6 using Rhino.Geometry;
7
8 using Grasshopper;
9 using Grasshopper.Kernel;
10 using Grasshopper.Kernel.Data;
11 using Grasshopper.Kernel.Types;
12
13 using System.IO;
14 using System.Linq;
15 using System.Data;
16 using System.Drawing;
17 using System.Reflection;
18 using System.Windows.Forms;
19 using System.Xml;
20 using System.Xml.Linq;
21 using System.Runtime.InteropServices;
22
23 using Rhino.DocObjects;
24 using Rhino.Collections;
25 using GH_IO;
26 using GH_IO.Serialization;
27
28 /// <summary>
29 /// This class will be instantiated on demand by the Script component.
30 /// </summary>
31 public class Script_Instance : GH_ScriptInstance
32 {
33     Utility functions
34
35     Members
36
37     /**/
38     private void RunScript(bool toggle, ref object A)
39     {
40         if(toggle && !alreadyAttached){
41             alreadyAttached = true;
42             GrasshopperDocument.SolutionEnd += OnSolutionEndHandler;
43         }
44     }
45
46     /**/
47     bool alreadyAttached;
48
49     private void OnSolutionEndHandler(Object sender, GH_SolutionEventArgs e){
50         GrasshopperDocument.IsModified = false;
51     }
52
53     /**/
54 }
```